



UNIVERSITÀ DEGLI STUDI ROMA TRE

DOTTORATO IN FISICA – XXX CICLO

**Anomalies in $b \rightarrow s$ transitions
and metastability of the two Higgs
doublet model: two global analyses**

Dottorando: Antonio Coutinho
Docente guida: Prof. Marco Ciuchini
Coordinatore: Prof. Giuseppe Degrassi

Ottobre 2017

Louco, sim, louco, porque quiz grandeza
Qual a Sorte a não dá.

Fernando Pessoa, *D. Sebastião Rei de Portugal*, in *Mensagem*

They all talked at once, their voices insistent and contradictory and impatient, making of unreality a possibility, then a probability, then an incontrovertible fact, as people will when their desires become words.

William Faulkner, in *The Sound and the Fury*

È tutto sedimentato sotto il chiacchiericcio e il rumore. Il silenzio e il sentimento. L'emozione e la paura. Gli sparuti incostanti sprazzi di bellezza.

Jep Gambardella, in Paolo Sorrentino's *La grande bellezza*

Contents

List of Acronyms	vii
1 Introduction	1
2 Flavour in the Standard Model	5
2.1 Spontaneous Symmetry Breaking	5
2.2 Gauge Sector	7
2.3 Fermion Sector	9
2.4 Flavour-changing Currents and CP Violation	11
3 The $b \rightarrow s$ Transition	15
3.1 Weak Decays and Effective Hamiltonians: A Tale of Two Scales	15
3.1.1 Operator Product Expansion	15
3.1.2 QCD Effects and Operator Renormalization	16
3.1.3 Summation of Large Logarithms	20
3.2 The $\Delta B = 1$ Effective Hamiltonian	22
3.2.1 Operator Basis	22
3.2.2 Matching Conditions for Wilson Coefficients	24
3.2.3 The Anomalous Dimension Matrix	28
3.2.4 Renormalization Group Evolution	36
3.3 The Exclusive Sector	39
3.3.1 Definition of Observables	39
3.3.2 Treatment of the Hadronic Uncertainties	43
4 HEPfit and the Bayesian Analysis Framework	46
4.1 Bayesian Interlude	46
4.2 Structure and Usage	48
5 Global Analysis of $b \rightarrow s$ Transitions	52
5.1 Scenarios and Approaches	52
5.2 Experimental Information and Input Parameters	55
5.3 Results of the Global Fit	56

6	The Two Higgs Doublet Model	66
6.1	The Higgs Basis and the Scalar Mass Terms	66
6.2	The Yukawa Sector	70
6.3	The 2HDM with a Softly-broken Z_2 Symmetry	71
6.3.1	Types I, II, X, Y	72
6.4	The Coleman-Weinberg Potential	75
6.4.1	One-loop Effective Potentials	77
6.4.2	Field-dependent Effective Mass Terms	79
7	Vacuum Stability and Other Constraints	83
7.1	Positivity, or: Boundedness from Below	83
7.2	The Tree-level Global Minimum	85
7.3	Vacuum Decay in Field Theory	86
7.3.1	Instantons in Particle Mechanics	87
7.3.2	The $O(4)$ Bounce Formalism	91
7.3.3	Numerical Solutions of Tunnelling Rates	93
7.4	Further Theoretical Constrains	94
7.4.1	Unitarity	94
7.4.2	Perturbativity	97
7.5	Experimental Constraints	97
7.5.1	Oblique Parameters	98
7.5.2	Flavour Observables	98
8	On the Metastability of the 2HDM	100
8.1	Procedure and Samples	100
8.2	Inputs and Experimental Values	101
8.3	Numerical Results	102
9	Conclusions	108
A	Beta Functions	111
A.1	Coefficients of the QCD Beta Function	111
A.2	Coefficients of Beta Functions with QED Corrections	111
B	Loop Functions	112
B.1	Functions Used in M Matchings	112
B.2	Functions Used in L Matchings	113
C	Form Factors	114
C.1	Form Factors in the Transversality Basis	114
C.2	Auxiliary Functions in Charm-loop Contributions	115

Acknowledgements	117
Bibliography	119

List of Acronyms

$\overline{\text{MS}}$	Modified Minimal Subtraction
1PI	One-Particle Irreducible
2HDM	Two Higgs Doublet Model
CKM	Cabibbo-Kobayashi-Maskawa
CP	Charge Conjugation and Parity Symmetry
FCNC	Flavour Changing Neutral Current
LCSR	Light-Cone Sum Rules
LFU(V)	Lepton Flavour Universality (Violation)
MSSM	Minimal Supersymmetric Standard Model
N^nLO	(Next-to-) n Leading Order
NFC	Natural Flavour Conservation
NP	New Physics
OPE	Operator Product Expansion
QCD	Quantum Chromodynamics
QCDF	QCD Factorization
QED	Quantum Electrodynamics
QFT	Quantum Field Theory
RGE	Renormalization Group Equation
SM	Standard Model
SSB	Spontaneous Symmetry Breaking
VEV	Vacuum Expectation Value
WC	Wilson Coefficient

Chapter 1

Introduction

It is a truth universally acknowledged, that the Standard Model (SM) must be considered one of the greatest achievements of modern science. If the discovery of the Z and W bosons in 1983 at CERN [1–4], had firmly cemented the status of gauge theories among competitor formalisms, the observation of the Higgs boson in 2012, by ATLAS and CMS at the LHC [5, 6], was the triumphant closing statement to a story that had began to be told a long time ago, and in which a succession of characters had played their parts with determination and flair. But aren't there any more stories to tell? Is the SM the final story to be written? Most certainly not. Almost as famous as its ability to meet experimental results, and its prowess in predicting them as well, are now all the shortcomings of the SM, of which the following shine brighter: it fails to include gravity; there is no viable dark matter candidate in the SM; it cannot generate the matter-antimatter asymmetry in the universe; it cannot explain the pattern of fermion masses and mixing, in particular the SM keeps neutrinos massless, and when it adds mass terms it is not able to explain their verified smallness; the SM appears to demand the fine tuning of some quantities, in both the hierarchy and strong CP problems.

Many of the aforementioned shortcomings of the SM can be addressed introducing new particles at the TeV scale. It only takes the direct discovery of those extra particles – whether it be the axion, or a superpartner, or a heavy neutrino – to point to the exact solution of the problem. There is, however, another way to point to physics beyond the SM: indirect evidence induced by virtual effects of new heavy particles beyond the discovery reach of the present experiments. A mismatch between the prediction of an observable and the measurement of that observable is an indirect signal of New Physics (NP), a clear indication that the SM does not, in fact, explain that phenomenon; and although it may not provide the exact source of the mismatch, it can nevertheless hint at the shape of physics to come. Moreover, given the lack of detection of any supersymmetric particle, any weakly interacting massive particle, or any new particle for that matter, indirect evidence seems more and more likely to be the first to arrive.

We are, thus, advancing further into the precision era of particle physics. In order to properly compare results, and because deviations are not expected to be large, theory and experiment must aim at putting out the most precise number possible. That, for sure, has been the case of flavour physics, where, indeed, the tremendous progress of the experimental facilities has probed the flavour of the SM to an

exquisite level of precision [7], and there has been a substantial effort on the part of the theoretical community to go well beyond leading order computations [8]. Among all precision tests, radiative and (semi)leptonic $\Delta B = 1$ processes, related at the partonic level to $b \rightarrow s\gamma, s\ell\ell$ transitions, appear as one of the frontrunners in probing the SM and its NP possible extensions [9, 10]. First, because these are rare B meson decays, mediated by flavour changing neutral currents (FCNCs), which, as a consequence of the Glashow-Iliopoulos-Maiani mechanism [11], arise in the SM only at the loop level. This allows significant room for sizeable contributions to this type of process from heavy new degrees of freedom. Furthermore, an exclusive mode such as $B \rightarrow K^*\ell\ell$ permits a detailed analysis of the angular distribution of the four final state particles, yielding rich experimental information that ranges from the full kinematic coverage of the dilepton invariant mass [12], to – starting from Ref. [13] – experimental correlations among the angular observables.

And it does look as if the tree is beginning to bear fruit. Recent years in B physics have witnessed the emergence of a conspicuous pattern of flavour anomalies, arriving from multiple independent sources of data on these rare $b \rightarrow s$ transitions. Of singular importance are: the measurement of the angular observable denoted as P'_5 [14–17], the measurement of the ratio of branching fractions [18]:

$$R_K \equiv \frac{\text{BR}(B^+ \rightarrow K^+\mu^+\mu^-)}{\text{BR}(B^+ \rightarrow K^+e^+e^-)}, \quad (1.1)$$

and, piling on top of the previous two, the recent measurement of another ratio [19]:

$$R_{K^*} \equiv \frac{\text{BR}(B \rightarrow K^*\mu^+\mu^-)}{\text{BR}(B \rightarrow K^*e^+e^-)}. \quad (1.2)$$

First realized by the LHCb collaboration [20, 21] and later on by the Belle collaboration as well [22], the experimental analysis of P'_5 in the large recoil region of the decay points to a deviation of about 3σ with respect to the SM prediction presented in Ref. [23]. However, there is the possibility that the theory suffers from hadronic uncertainties whose very estimation may currently be out of reach [24–27]. This assertion has, in fact, been the fuel of a debate in the theoretical community over the size of QCD power corrections to the amplitude of this process, beyond the infinite mass limit [28–31]. Extending this stalemate regarding the “ P'_5 anomaly”, two new independent measurements of this angular observable have been recently released by ATLAS [32] and CMS [33], showing, respectively, an appreciable increase and a reduction of the tension between data and the prediction of Ref. [23].

Already in 2014, the LHCb collaboration presented for the first time the measurement of R_K , in a dilepton mass (henceforth q^2) range going from 1 to 6 GeV²:

$$R_{K_{[1,6]}} = 0.745^{+0.090}_{-0.074} \pm 0.036. \quad (1.3)$$

This experimental value represents a deviation of about 2.6σ with respect to the SM prediction, which in the bin provided by LHCb is expected to be equal to 1 beyond the percent level of accuracy [34, 35]. Additionally, and unlike observables such as P'_5 , one must note that R_K may be, in general, regarded as insensitive to QCD effects [34]. On a similar footing, the measurement of the ratio of branching fractions in the K^* channel was done in two regions of q^2 , the results being:

$$R_{K^*_{[0.045,1.1]}} = 0.660^{+0.110}_{-0.070} \pm 0.024, \quad (1.4)$$

$$R_{K^*_{[1.1,6]}} = 0.685^{+0.113}_{-0.069} \pm 0.047. \quad (1.5)$$

Given the expected SM prediction is, to a very good accuracy, again equal to 1 in the central- q^2 bin, and close to 0.9 in the low- q^2 one, this indicates once more a discrepancy of about 2σ between theory and experiment.

Other smaller tensions have been around, concerning the measurement of differential branching fractions of $B \rightarrow K\mu\mu$ [36, 37] and $B_s \rightarrow \phi\mu\mu$ [38]. It is worth noting that, while for the latter mode an explanation in terms of hadronic physics may be easily conceivable, the theoretical computation of the former seems to be better under control [39]. Still, all these are suggestions enough that, in order to assess the true impact of the anomalies in the pull away from the SM, and to quantify the actual size of the combined deviations, global fits to data are in order. Indeed, several global analyses have already been produced, and they hint at a correlation of R_K with the P'_5 anomaly [9, 40–44], which has triggered different proposals of measurements of lepton flavour universality violation (LFUV) in the angular analysis of the $K^*\ell\ell$ channel [45, 46]. The idea of NP in LFUV currents has been further lead on by the new R_{K^*} result. An analysis by the Belle collaboration, which, aiming at separating the leptonic flavours in $B \rightarrow K^*\ell\ell$ [47], showed a deviation in the dimuon leptonic final state consistent with $\sim 2.6\sigma$ deviation reported in Ref. [23], has also contributed to the excitement that is felt nowadays in this field. In this thesis, we develop and make use of the publicly available package `HEFfit`[48] to perform a global fit to possible shifts in SM currents due to NP contributions, taking into account state-of-the-art theoretical predictions and experimental information, including the LHCb measurements of R_K and, for the first time ever, R_{K^*} .

Global analyses are such a powerful tool, that when all the machinery is at hand it is quite natural that one will apply it to many different scenarios. For a more “bottom-up” approach, one can perform a global fit to an actual realization of physics beyond the SM, constraining not the generic shape of what NP may be, but rather the feasibility of the model itself. One of the simplest extensions to the SM is the two Higgs doublet model (2HDM) [49, 50]. Barring the sheer simplicity of adding a second Higgs doublet to the theory, motivations to the 2HDM include: Gell Mann’s Totalitarian Principle, which states that “Everything not forbidden is compulsory.” [51] – if the scalar sector is enlarged with a particle whose quantum numbers do not break any of the symmetries of nature, the study of such a model must be a worthwhile endeavour; perhaps the best known and most recited motivation is the fact that supersymmetry contains two Higgs doublets, thus making the 2HDM, if not for anything else, significant by proxy; the augmented parameter space that comes with a second scalar is another strong selling point for this model, due to all the possible new phenomena it allows. However, as any other extension of the SM, the 2HDM has its share of uninvited problems. Among these, stands out the fact that it yields the presence of FCNCs at tree level, mediated by the new neutral heavy bosons. Interestingly enough, one of the versions of the model that cures these contributions is the very version that shares its scalar structure with the Minimal Supersymmetric Standard Model (MSSM), and, as such, it is the most studied implementation of the 2HDM in literature: the Z_2 -symmetric 2HDM.

Still, for all the attention it receives, the 2HDM seems to be always one step behind supersymmetric models. One case where it is undeniably so, is in the study of vacuum stability beyond the leading order. In the SM, there is only one quartic coupling in the potential, which makes the calculations not

too cumbersome enough for the analysis of the stability of the vacuum to be performed at a very high precision level [52, 53]. With two Higgs doublets, on the other hand, the number of degrees of freedom in the quartic sector of the scalar potential can go from five, up to ten: this means that analyticity is out of question, and even numerical minimization has its difficulties when it encounters such a parameter space. Nevertheless, in the last years numerical methods have been used to discover extra minima in supersymmetric models competing for stability with the minimum we live in, taking loop corrections, and in some cases even thermal effects, into account [54–59]. In the 2HDM, output has come out very recently concerning loop vacuum stability in the Inert Doublet Model [60, 61], but that had not been the case with the Z_2 -symmetric 2HDM. At least not until early this year, when the author of Ref. [62] set out to perform the first analysis of vacuum stability with radiative corrections included, and at times being the sole drivers of points from apparent instability at tree-level into actual stability at loop-level, and vice-versa. This issue of false negatives was stressed by the author of Ref. [62], who claimed the reopening of regions of parameter space. Regions which, we point out, higher order constraints, or other constraints not used by the author, may keep closed. We set out to use the capabilities of `HEPfit` to offer, not only a second look, which is always obligatory in science, but also a more polished and, in agreement with the theme of this thesis, more globally informed analysis.

This thesis is organized as follows: to set notation and tone, in Chapter 2 we review the SM, with an emphasis in the flavour sector; in Chapter 3 we address weak decays within the framework of the Operator Product Expansion (OPE) and effective Hamiltonians, which is followed by a description of the weak transition under analysis, touching upon the ingredients needed to compute observables and on the theoretical uncertainties associated; after a brief overview of the software used and the underlying Bayesian framework, given in Chapter 4, we present in Chapter 5 the results of the global analysis to $b \rightarrow s$ transitions; in Chapter 6 we provide a description of the 2HDM, focusing on its Z_2 -symmetric implementation and on the form of the scalar potential beyond tree-level; Chapter 7 is reserved to an exposition of the constraints used in the second global analysis, elaborating more in the issue of vacuum stability; in Chapter 8, the results of the global analysis to stability in the 2HDM are provided; finally, our conclusions are summarized in Chapter 9.

Chapter 2

Flavour in the Standard Model

In 1971, a PhD student from Utrecht University published two papers that would form the basis of his dissertation [63, 64]. This student, Gerard 't Hooft, was, however, no ordinary PhD student, for in these papers he provided the seminal proof that Yang Mills theories could be made compatible with renormalizability and unitarity, a problem that had been puzzling physicists for many years – models with local gauge invariance being deemed mere intellectual fodder at the time. One of these models was Stephen Weinberg's *Model of Leptons* from 1967 [65], which immediately resurfaced to the forefront of the theoretical stage with 't Hooft's proof, and was in the years that followed developed into what we now know as the SM.

Renormalization in quantum field theory (QFT) comprises the techniques used to remove the infinities that arise in the calculation of observable quantities. When the demand of renormalizability is relaxed, one can work with effective theories, a powerful tool for the treatment of multi-scale problems and the subject of the first half of this thesis. Unitarity is, as Matthew D. Schwartz puts it, “a fancy way of saying probabilities add up to 1” [66]. Requiring unitarity in QFT can impose strong constraints in the parameters of a given model, as we shall see later on in the chapters dedicated to the 2HDM. For now, we shall simply set the tone and the notation that henceforth will be employed. We do this by making a brief overview of the SM and the flavour properties that arise once fermions enter the picture.

2.1 Spontaneous Symmetry Breaking

A key ingredient in Weinberg's model is the spontaneous breaking of the non-Abelian local symmetry that characterizes the electromagnetic and weak interactions; spontaneous symmetry breaking (SSB) is also a central element in 't Hooft's second paper, regarding massive Yang-Mills fields. It is thus reasonable for any description of the SM to start from its gauge group and its SSB mechanism.

The gauge group of the SM is

$$\mathcal{G}_{\text{local}} = SU(3)_c \times SU(2)_L \times U(1)_Y. \quad (2.1)$$

This local symmetry yields a covariant derivative equal to

$$D_\mu = \partial_\mu - ig_s G_\mu^a L^a - ig W_\mu^a T^a - ig' B_\mu Y, \quad (2.2)$$

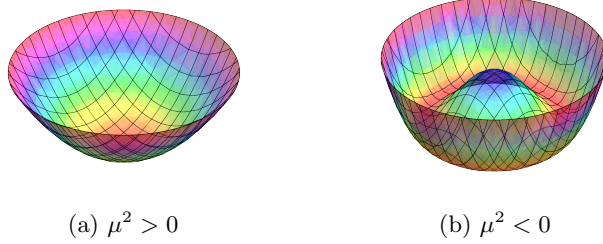


Figure 2.1: Depiction of the two possible shapes of the scalar potential: (a) a potential with a symmetry-conserving VEV; (b) a potential with an infinite number of symmetry-breaking minima, often called the *Mexican Hat potential*.

where G_μ^a , W_μ^a , and B_μ are, respectively, the gauge bosons of $SU(3)_c$, $SU(2)_L$, and $U(1)_Y$, with g_s , g , and g' being the corresponding coupling constants; $L^a = \frac{\lambda^a}{2}$ are the generators of $SU(3)$, where λ^a are the Gell-Mann matrices, and $T^a = \frac{\tau^a}{2}$ are the generators of $SU(2)$, where τ^a are the Pauli matrices; the $U(1)_Y$ charge is termed weak hypercharge and is a real multiple of the identity matrix.

SSB in the SM is accomplished via the so called Englert-Brout-Higgs mechanism [67–70], *i.e.* with the introduction of a complex scalar field invariant under $SU(3)$, in the spinor representation of $SU(2)_L$, and with hypercharge 1/2:

$$\phi(\mathbf{1}, \mathbf{2}, 1/2). \quad (2.3)$$

This scalar field, the Higgs doublet, written with charged and neutral components,

$$\phi = \begin{pmatrix} \varphi^+ \\ \varphi^0 \end{pmatrix}, \quad (2.4)$$

couple to itself through the most general renormalizable *Higgs potential*, which together with the kinetic term of a Klein-Gordon field makes up the *Higgs Lagrangian*:

$$\mathcal{L}_H = (D_\mu \phi)^\dagger (D^\mu \phi) - V(\phi^\dagger \phi) = (D_\mu \phi)^\dagger (D^\mu \phi) - \mu^2 \phi^\dagger \phi - \frac{\lambda}{2} (\phi^\dagger \phi)^2. \quad (2.5)$$

Depending on the sign of the parameter μ^2 , the potential assumes two different shapes, as depicted in Fig. 2.1. Without loss of generality, one can make use of the freedom of $SU(2)_L$ rotations to write the scalar field in a basis of isospin where only the neutral component acquires a vacuum expectation value (VEV):

$$\langle \phi \rangle_0 = \langle 0 | \phi | 0 \rangle = \frac{1}{\sqrt{2}} \begin{pmatrix} 0 \\ v \end{pmatrix}. \quad (2.6)$$

When $\mu^2 < 0$, v may have a non-zero value and, from the minimization of the Higgs potential, we get a VEV with

$$v = \sqrt{-\frac{2\mu^2}{\lambda}}. \quad (2.7)$$

Due to the rephasing invariance of the Higgs field, this situation yields an infinity of non-null vacua that no longer preserve the gauge symmetry of the electroweak sector:

$$e^{i\alpha\mathcal{X}} \langle \phi \rangle_0 \simeq (1 + i\alpha\mathcal{X}) \langle \phi \rangle_0 \neq \langle \phi \rangle_0, \quad \text{for } \mathcal{X} = T^1, T^2, T^3, Y. \quad (2.8)$$

Still, an abelian subgroup of $SU(2)_L \times U(1)_Y$ exists under which the vacuum remains invariant: for the combination

$$Q = T^3 + Y(\phi) = T^3 + \frac{1}{2} \quad (2.9)$$

one has

$$Q\langle\phi\rangle_0 = \begin{pmatrix} 1 & 0 \\ 0 & 0 \end{pmatrix} \begin{pmatrix} 0 \\ v \end{pmatrix} = \begin{pmatrix} 0 \\ 0 \end{pmatrix}, \quad (2.10)$$

and the conclusion is that the vacuum state of the Higgs field breaks the electroweak part of Eq. (2.1) into a residual $U(1)$ symmetry which has Q as generator.

2.2 Gauge Sector

After SSB, the Higgs doublet would be most generally parametrized around the vacuum as:

$$\phi = \begin{pmatrix} G^+ \\ (v + h + iG^0)/\sqrt{2} \end{pmatrix}, \quad (2.11)$$

where h , is a real scalar field, G^0 is a real pseudoscalar field, and G^+ is a complex scalar field. From Goldstone's Theorem, we know that by breaking a $SU(2) \times U(1)$ symmetry with four generators into a residual $U(1)$ there will be $4 - 1 = 3$ Goldstone bosons arising in the theory, one for each of the broken generators [71, 72]. These degrees of freedom, G^0 , G^+ , and G^- are dependent on the choice of gauge fixing, and may be *gauged away* into the longitudinal polarization of three of the gauge bosons, generating their masses in the process. This gauge boson mass generation is the *Higgs mechanism* and, in order to inspect the mass spectrum of the SM, it's easier to work in unitary gauge, where

$$\phi = \begin{pmatrix} 0 \\ (v + h)/\sqrt{2} \end{pmatrix}. \quad (2.12)$$

The field h , which persists even in the unitary gauge, is known as the *Higgs boson* and its mass is $M_h = \sqrt{\lambda}v$.

The pure gauge interactions, which include the bilinear terms that yield the boson propagators, and higher order couplings, are described by

$$\mathcal{L}_{\text{gauge}} = -\frac{1}{4}G_{\mu\nu}^a G^{a\mu\nu} - \frac{1}{4}W_{\mu\nu}^a W^{a\mu\nu} - \frac{1}{4}B_{\mu\nu} B^{\mu\nu}, \quad (2.13)$$

where the field strength tensors are defined as

$$G_{\mu\nu}^a = \partial_\mu G_\nu^a - \partial_\nu G_\mu^a + g_s f^{abc} G_\mu^b G_\nu^c, \quad (2.14)$$

$$W_{\mu\nu}^a = \partial_\mu W_\nu^a - \partial_\nu W_\mu^a + g \epsilon^{abc} W_\mu^b W_\nu^c, \quad (2.15)$$

$$B_{\mu\nu} = \partial_\mu B_\nu - \partial_\nu B_\mu. \quad (2.16)$$

The mass terms of the gauge bosons W_μ^a and B_μ , on the other hand, come from the kinetic term of \mathcal{L}_H :

$$\begin{aligned} (D_\mu\phi)^\dagger (D^\mu\phi) &= \frac{1}{2}\partial_\mu h\partial^\mu h \\ &+ g^2 \frac{(v+h)^2}{8} (W_\mu^1 + iW_\mu^2)(W^{1\mu} - iW^{2\mu}) \\ &+ \frac{(v+h)^2}{8} (g^2 W_\mu^3 W^{3\mu} - gg' W_\mu^3 B^\mu - gg' B_\mu W^{3\mu} - g'^2 B_\mu B^\mu). \end{aligned} \quad (2.17)$$

Instead of the fields W_μ^1 and W_μ^2 , it is customary to introduce two complex fields

$$W_\mu^\pm = \frac{W_\mu^1 \mp iW_\mu^2}{\sqrt{2}}, \quad (2.18)$$

whose mass Lagrangian,

$$\mathcal{L}_{\text{mass}}^W = g^2 \frac{v^2}{4} W_\mu^- W^{+\mu}, \quad (2.19)$$

yields immediately the W^\pm bosons' mass:

$$M_W = \frac{1}{2}gv. \quad (2.20)$$

Regarding W_μ^3 and B_μ , their mass terms may be suitably written as

$$\mathcal{L}_{\text{mass}}^{W^3, B} = \frac{v^2}{8} \begin{pmatrix} W_\mu^3 & B_\mu \end{pmatrix} \begin{pmatrix} g^2 & -gg' \\ -gg' & g'^2 \end{pmatrix} \begin{pmatrix} W^{3\mu} \\ B^\mu \end{pmatrix}. \quad (2.21)$$

Introducing the Weinberg angle, θ_W , these bosons are rotated into their mass eigenstates,

$$\begin{pmatrix} Z_\mu \\ A_\mu \end{pmatrix} = \begin{pmatrix} \cos \theta_W & -\sin \theta_W \\ \sin \theta_W & \cos \theta_W \end{pmatrix} \begin{pmatrix} W_\mu^3 \\ B_\mu \end{pmatrix} \quad (2.22)$$

and we get

$$\begin{aligned} \mathcal{L}_{\text{mass}}^{A, Z} &= \frac{v^2}{8} \begin{pmatrix} Z_\mu & A_\mu \end{pmatrix} \begin{pmatrix} \cos \theta_W & -\sin \theta_W \\ \sin \theta_W & \cos \theta_W \end{pmatrix} \begin{pmatrix} g^2 & -gg' \\ -gg' & g'^2 \end{pmatrix} \begin{pmatrix} \cos \theta_W & \sin \theta_W \\ -\sin \theta_W & \cos \theta_W \end{pmatrix} \begin{pmatrix} Z^\mu \\ A^\mu \end{pmatrix} \\ &= \frac{v^2}{8} \begin{pmatrix} Z_\mu & A_\mu \end{pmatrix} \begin{pmatrix} g^2 + g'^2 & 0 \\ 0 & 0 \end{pmatrix} \begin{pmatrix} Z^\mu \\ A^\mu \end{pmatrix}. \end{aligned} \quad (2.23)$$

This produces the following relations between coupling constants and Weinberg angle:

$$\cos \theta_W = \frac{g}{\sqrt{g^2 + g'^2}}, \quad \sin \theta_W = \frac{g'}{\sqrt{g^2 + g'^2}}; \quad (2.24)$$

the masses of the neutral bosons Z and A come to be

$$M_Z = \frac{v}{2} \sqrt{g^2 + g'^2}, \quad (2.25)$$

$$M_A = 0. \quad (2.26)$$

The last boson, given its null mass, is identified as the photon.

One is now able to write the covariant derivative of the gauge group of electroweak theory in terms of the physical fields. To do so, it is convenient to consider one further definition,

$$T^\pm = \frac{T^1 \pm iT^2}{\sqrt{2}}, \quad (2.27)$$

which leaves Eq. (2.2) in the form:

$$D_\mu = \partial_\mu - ig_s G_\mu^a L^a - i \frac{g}{\sqrt{2}} (W_\mu^+ T^+ + W_\mu^- T^-) - i \frac{1}{\sqrt{g^2 + g'^2}} Z_\mu (g^2 T^3 - g'^2 Y) - i \frac{gg'}{\sqrt{g^2 + g'^2}} A_\mu (T^3 + Y). \quad (2.28)$$

Recognizing the last term as the electromagnetic interaction, mediated by the photon, one identifies its coefficient as the electron charge,

$$e = \frac{gg'}{\sqrt{g^2 + g'^2}} = g \sin \theta_W, \quad (2.29)$$

and $T^3 + Y$ as the electric charge quantum number. This is, in fact, the combination we saw in Eq. (2.9): it becomes clear, then, that it is the electromagnetic symmetry that is preserved after SSB, and one thus confirms that electric charge is conserved in the SM. Finally, we put the covariant derivative in a even more suitable form, which better expresses the nature of the couplings:

$$D_\mu = \partial_\mu - ig_s G_\mu^a L^a - i \frac{g}{\sqrt{2}} (W_\mu^+ T^+ + W_\mu^- T^-) - i \frac{g}{\cos \theta_W} Z_\mu (T^3 - \sin^2 \theta_W Q) - ie A_\mu Q \quad (2.30)$$

2.3 Fermion Sector

With flavour in mind, in this section we focus on the coupling of the electroweak gauge bosons to fermions. The structure of the electroweak theory was deduced from the 4-Fermi effective theory, whose $V - A$ interaction pointed towards a chiral theory [73, 74],

$$V - A = \gamma^\mu - \gamma^\mu \gamma^5 = 2\gamma^\mu \frac{1 - \gamma^5}{2}, \quad (2.31)$$

where fermion fields would enter through their left- and right-handed components:

$$\psi_L = \frac{1 - \gamma^5}{2} \psi = P_L \psi, \quad (2.32)$$

$$\psi_R = \frac{1 + \gamma^5}{2} \psi = P_R \psi. \quad (2.33)$$

In the SM, the left-handed leptons $(e, \nu_e, \mu, \nu_\mu, \tau, \nu_\tau)_L$ pair up to form $SU(2)_L$ doublets, as do the left-handed quarks $(d, u, s, c, b, t)_L$. In turn, the right-handed fermions happen to transform as singlets of $SU(2)_L$, and we have the following fermion content:

$$Q_L^i (\mathbf{3}, \mathbf{2}, 1/6), \quad u_R^i (\mathbf{3}, \mathbf{1}, 2/3), \quad d_R^i (\mathbf{3}, \mathbf{1}, -1/3), \quad L_L^i (\mathbf{1}, \mathbf{2}, -1/2), \quad \ell_R^i (\mathbf{1}, \mathbf{1}, -1), \quad (2.34)$$

where $i = 1, 2, 3$ indexes the generation. Here, we have omitted right-handed neutrinos, since they have not yet been observed, and also because the subject of neutrino masses, whether their nature is Majorana or Dirac, is beyond the scope of this work.¹ In the SM they are strictly massless, and we will leave them as such.

The interactions of quark and lepton matter fields with the electroweak gauge boson follow directly from the Dirac Lagrangian, with the partial derivative dropped in favour of the $SU(2)_L \times U(1)_Y$ part of covariant derivative in Eq. (2.2):

$$\mathcal{L}_{\text{matter}} = \bar{Q}_L^i (i\not{D}) Q_L^i + \bar{u}_R^i (i\not{D}) u_R^i + \bar{d}_R^i (i\not{D}) d_R^i + \bar{L}_L^i (i\not{D}) L_L^i + \bar{\ell}_R^i (i\not{D}) \ell_R^i, \quad (2.35)$$

¹We direct the reader towards the book in Ref. [75], the reviews in Refs. [76, 77], and references therein, for further information on models of neutrino masses and mixing.

where summation over the generation index is implied. In terms of the gauge boson mass eigenstates, $\mathcal{L}_{\text{matter}}$ becomes

$$\begin{aligned} \mathcal{L}_{\text{matter}} = & \bar{Q}_L^i(i\cancel{\partial})Q_L^i + \bar{u}_R^i(i\cancel{\partial})u_R^i + \bar{d}_R^i(i\cancel{\partial})d_R^i + \bar{L}_L^i(i\cancel{\partial})L_L^i + \bar{\ell}_R^i(i\cancel{\partial})\ell_R^i \\ & + g(W_\mu^+ J_W^{\mu+} + W_\mu^- J_W^{\mu-} + Z_\mu J_Z^\mu) + eA_\mu J_{\text{EM}}^\mu, \end{aligned} \quad (2.36)$$

where the vector currents are written as follows:

$$J_W^{\mu+} = \frac{1}{\sqrt{2}}(\bar{u}_L^i \gamma^\mu d_L^i + \bar{\nu}_L^i \gamma^\mu \ell_L^i), \quad (2.37)$$

$$J_W^{\mu-} = \frac{1}{\sqrt{2}}(\bar{d}_L^i \gamma^\mu u_L^i + \bar{\ell}_L^i \gamma^\mu \nu_L^i), \quad (2.38)$$

$$\begin{aligned} J_Z^\mu = & \frac{1}{\cos\theta_W} [\bar{u}_L^i \gamma^\mu (\frac{1}{2} - \frac{2}{3} \sin^2\theta_W) u_L^i + \bar{u}_R^i \gamma^\mu (-\frac{2}{3} \sin^2\theta_W) u_R^i \\ & + \bar{d}_L^i \gamma^\mu (-\frac{1}{2} + \frac{1}{3} \sin^2\theta_W) d_L^i + \bar{d}_R^i \gamma^\mu (\frac{1}{3} \sin^2\theta_W) d_R^i \\ & + \bar{\nu}_L^i \gamma^\mu (\frac{1}{2}) \nu_L^i + \bar{\ell}_L^i \gamma^\mu (-\frac{1}{2} + \sin^2\theta_W) \ell_L^i + \bar{\ell}_R^i \gamma^\mu (\sin^2\theta_W) \ell_R^i], \end{aligned} \quad (2.39)$$

$$J_{\text{EM}}^\mu = \bar{u}^i \gamma^\mu (\frac{2}{3}) u^i + \bar{d}^i \gamma^\mu (-\frac{1}{3}) d^i + \bar{\ell}^i \gamma^\mu (-1) \ell^i. \quad (2.40)$$

Regarding fermion masses, it is often useful to think of the chiral projections of each fermion as different particles which live in different representations of the fundamental gauge group and mix through mass terms like

$$\mathcal{L}_{\text{mass}} = -m_f (\bar{f}_L f_R + \bar{f}_R f_L). \quad (2.41)$$

However, the very fact that these fields belong to different $SU(2)_L$ representations and have different $U(1)_Y$ charges indicates that this Lagrangian is not invariant under the gauge symmetry, and one is thus forbidden to write such terms in the theory prior to SSB. Nevertheless, our model contains a scalar field whose VEV already endows the gauge bosons with their masses, and, as it happens, this field's quantum numbers allow the addition of one further gauge-invariant Lagrangian, which indeed mixes the left- and right-handed projections of the fermion fields via scalar currents:

$$\mathcal{L}_Y = -\bar{Q}_L^i Y_{ij}^u \tilde{\phi} u_R^j - \bar{Q}_L^i Y_{ij}^d \phi d_R^j - \bar{L}_L^i Y_{ij}^\ell \phi \ell_R^j + \text{h.c.}, \quad (2.42)$$

where $\tilde{\phi} = i\tau_2 \phi^*$, and 'h.c.' denotes the Hermitian conjugate of all of the preceding terms. These terms are the Yukawa couplings, and each Y^f is an arbitrary complex matrix. After SSB, the Higgs doublet acquires a non-null VEV and, as designed, \mathcal{L}_Y generates the terms of $\mathcal{L}_{\text{mass}}$, now of the form:

$$\mathcal{L}_{\text{mass}} = -\bar{u}_L^i M_u^{ij} u_R^j - \bar{d}_L^i M_d^{ij} d_R^j - \bar{\ell}_L^i M_\ell^{ij} \ell_R^j + \text{h.c.}, \quad (2.43)$$

with each fermion mass matrix defined as

$$M_f = \frac{v}{\sqrt{2}} Y^f, \quad \text{for } f = u, d, \ell. \quad (2.44)$$

With every ingredient in place, we bring this section to an end by finally writing the full Lagrangian of the SM, which, schematically, is

$$\mathcal{L}_{\text{SM}} = \mathcal{L}_H + \mathcal{L}_{\text{gauge}} + \mathcal{L}_{\text{matter}} + \mathcal{L}_Y, \quad (2.45)$$

where, taking into account trivial $SU(3)_c$ additions to $\mathcal{L}_{\text{matter}}$, each individual Lagrangian is to be found, respectively, in Eq. (2.5), Eq. (2.13), Eq. (2.35), and Eq. (2.42).

2.4 Flavour-changing Currents and CP Violation

In the previous section we saw the generation of fermion masses in the Yukawa couplings after SSB. The resulting mass matrices, in Eq. (2.44), are, however, arbitrary complex matrices. This is because we have been working in a *flavour basis* that needs not be the basis of mass eigenstates. We have the possibility, though, to transform the fermion fields into a basis which diagonalizes the Yukawa couplings and, as a result, all M_f . Denoting the mass basis as that of the primed states given, by convention, by the unitary transformations

$$u_L^i = V_{ij}^u u_L^{\prime j}, \quad u_R^i = U_{ij}^u u_R^{\prime j}, \quad (2.46)$$

$$d_L^i = V_{ij}^d d_L^{\prime j}, \quad d_R^i = U_{ij}^d d_R^{\prime j}, \quad (2.47)$$

$$\ell_L^i = V_{ij}^\ell \ell_L^{\prime j}, \quad \ell_R^i = U_{ij}^\ell \ell_R^{\prime j}, \quad (2.48)$$

$$\nu_L^i = V_{ij}^\nu \nu_L^{\prime j}, \quad (2.49)$$

we obtain the bi-diagonalization of the mass matrices

$$V^{u\dagger} M_u U^u = \text{diag}(m_u, m_c, m_t), \quad (2.50)$$

$$V^{d\dagger} M_d U^d = \text{diag}(m_d, m_s, m_b), \quad (2.51)$$

$$V^{\ell\dagger} M_\ell U^\ell = \text{diag}(m_e, m_\mu, m_\tau). \quad (2.52)$$

By definition, the diagonal elements above, being the masses of the physical fermions, are real and non-negative. The V^f matrices, given the left-handedness of the weak interactions, have an effect on the charged currents: written in terms of the mass eigenstates, the positive-charged current becomes

$$J_W^{\mu+} = \frac{1}{\sqrt{2}} (\bar{u}_L^i \gamma^\mu (V^{u\dagger} V^d)_{ij} d_L^{\prime j} + \bar{\nu}_L^i \gamma^\mu (V^{\ell\dagger} V^\ell)_{ij} \ell_L^{\prime j}); \quad (2.53)$$

while for the leptons we simply get the identity matrix, in the case of the quarks a non diagonal unitary matrix arises:

$$V = V^{u\dagger} V^d = \begin{pmatrix} V_{ud} & V_{us} & V_{ub} \\ V_{cd} & V_{cs} & V_{cb} \\ V_{td} & V_{ts} & V_{tb} \end{pmatrix}. \quad (2.54)$$

This matrix is the Cabibbo-Kobayashi-Maskawa (CKM) matrix [78, 79], and is an unavoidable presence in the theory.

One encounters the CKM again if one looks at mass diagonalization from a different angle. Before the addition of the Yukawa Lagrangian, it happens that there is a large global symmetry in the SM which arises without being imposed. This symmetry is a $U(3)^5$ group, which can be decomposed as

$$\mathcal{G}_{\text{flavour}} = U(1)^5 \times \mathcal{G}_{\text{quark}} \times \mathcal{G}_{\text{lepton}}, \quad (2.55)$$

where

$$\mathcal{G}_{\text{quark}} = SU(3)_{Q_L} \times SU(3)_{u_R} \times SU(3)_{d_R} \quad (2.56)$$

$$\mathcal{G}_{\text{lepton}} = SU(3)_{L_L} \times SU(3)_{\ell_R}. \quad (2.57)$$

Three of the five $U(1)$ can be identified with the total baryon and lepton number, both not broken by the Yukawa couplings, and the weak hypercharge, which is gauged. $\mathcal{G}_{\text{quark}}$ and $\mathcal{G}_{\text{lepton}}$ are the subgroups controlling flavour-changing dynamics and flavour non-universality in the theory, and they are explicitly broken by the Yukawa matrices not being proportional to the identity matrix. In the lepton sector, because of the invariance of $\mathcal{L}_{\text{matter}}$ under $\mathcal{G}_{\text{lepton}}$, one has all the freedom to choose the two matrices required to diagonalize Y^ℓ without breaking gauge invariance or any observable consequence. On the other hand, $\mathcal{G}_{\text{quark}}$ only allows us to choose three of the four matrices necessary to diagonalize simultaneously Y^d and Y^u , meaning there will be a leftover mixing matrix in the Yukawa terms if we opt to leave the remaining SM Lagrangian untouched. If we use the flavour symmetry to choose, for example, a basis where Y^d is diagonal, we are left with one unitary transformation to eliminate either the left- or the right-handed diagonalization matrix in the up-sector, but not both. Eliminating, for convenience, the right-handed diagonalization matrix, one gets

$$Y_d = \lambda_d, \quad Y_u = V^\dagger \lambda_u, \quad (2.58)$$

where

$$\lambda_d = \text{diag}(y_d, y_s, y_b), \quad \lambda_u = \text{diag}(y_u, y_c, y_t), \quad \text{with } y_q = \frac{m_q}{v}. \quad (2.59)$$

In principle, the CKM is a general complex unitary matrix. Still, not all the phases are physical, given some of them may be removed by rephasing the quark fields. For a $n_g \times n_g$ complex matrix, there are $2n_g^2$ real parameters. By imposing unitarity one gets n_g^2 conditions; the number of phases which can be removed by rephasings is $2n_g - 1$. One is left, therefore, with $2n_g^2 - n_g^2 - (2n_g - 1) = (n_g - 1)^2$ independent real parameters. To parametrize a $n_g \times n_g$ orthogonal matrix one needs $n_g(n_g - 1)/2$ Euler angles. Since an unitary matrix is a complex extension of an orthogonal matrix, out of the $(n_g - 1)^2$ independent parameters, $n_g(n_g - 1)/2$ must be identified as rotation angles, the number of physical phases amounting to the remaining $(n_g - 1)^2 - n_g(n_g - 1)/2 = (n_g - 1)(n_g - 2)/2$ parameters. For the 3 generations of the SM, the CKM matrix has thus 4 parameters, 3 of which are mixing angles and 1 is a phase that can't be eliminated by rephasing the quark fields. A common parametrization, championed by the Particle Data Group [80], is

$$V = \begin{pmatrix} c_{12}c_{13} & s_{12}c_{13} & s_{13}e^{-i\delta} \\ -s_{12}c_{23} - c_{12}s_{23}s_{13}e^{i\delta} & c_{12}c_{23} - s_{12}s_{23}s_{13}e^{i\delta} & s_{23}c_{13} \\ s_{12}s_{23} - c_{12}c_{23}s_{13}e^{i\delta} & -c_{12}s_{23} - s_{12}c_{23}s_{13}e^{i\delta} & c_{23}c_{13} \end{pmatrix} \quad (2.60)$$

where $s_{ij} = \sin \theta_{ij}$ and $c_{ij} = \cos \theta_{ij}$. The angles θ_{ij} can be chosen to lie in the first quadrant and are, in fact, relatively small. This means the CKM is nearly diagonal, thus the mass and flavour bases are nearly identical. This is often used to write the CKM matrix in a different parametrization, named after Lincoln Wolfenstein, its first proponent [81]. To a good approximation, θ_{23} and θ_{13} are negligible, leaving θ_{12} , known as the *Cabibbo angle*, in charge of all flavour mixing. Defining $\lambda \equiv \sin \theta_{12}$,

$$V = \begin{pmatrix} 1 - \lambda^2/2 & \lambda & A\lambda^3(\rho - i\eta) \\ -\lambda & 1 - \lambda^2/2 & A\lambda^2 \\ A\lambda^3(1 - \rho - i\eta) & -A\lambda^2 & 1 \end{pmatrix} + \mathcal{O}(\lambda^4), \quad (2.61)$$

where $A \sim 1$, and the parameters ρ and η should be smaller than one because $|V_{ub}|/|V_{cb}| \sim \lambda/2$.

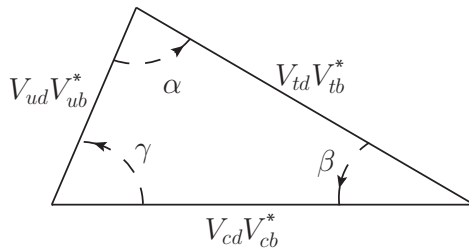


Figure 2.2: Representation of the unitarity triangle.

The phase δ , or the phase in any given parametrization which remains after imposing the invariance of V under the rephasing of fields, is the source of CP violation phenomena in the SM. Moreover, we have that physically meaningful, and therefore measurable, functions of V must be invariant under such rephasing. The simplest of these invariants are the moduli of the matrix elements, $|V_{\alpha i}|^2$. The next-simplest rephasing-invariant functions of V are the ‘quartets’:

$$Q_{\alpha i \beta j} \equiv V_{\alpha i} V_{\beta j} V_{\alpha j}^* V_{\beta i}^*, \quad \alpha \neq \beta \quad \text{and} \quad i \neq j. \quad (2.62)$$

Thus, if the complex phase of the CKM were to disappear in all rephasing-invariant functions of V , any observable sensitive to δ would be real, and the theory would be CP-converging. Turning it around, *there is only CP violation in the SM if and only if any of the rephasing-invariant functions of the CKM matrix is not real* [82].

Now, the CKM matrix is unitary by construction, all of its the rows orthogonal to each other, the same being also true to the columns. The orthogonality relation for the first and third columns of V is

$$V_{ud}V_{ub}^* + V_{cd}V_{cb}^* + V_{td}V_{tb}^* = 0. \quad (2.63)$$

If we multiply the whole equation by $V_{cb}V_{cd}^*$ and take the imaginary part, we obtain

$$\text{Im}(Q_{udcb}) + \text{Im}(Q_{cbtd}) = 0. \quad (2.64)$$

In fact, proceeding the same way for the remaining orthogonality relations, one easily shows that the imaginary parts of all quartets are equal up to their sign. One may, therefore, define a rephasing invariant quantity which flags the existence of CP violation in the SM:

$$J \equiv \text{Im}(Q_{uscb}) = \text{Im}(V_{us}V_{cb}V_{ub}^*V_{cs}^*), \quad (2.65)$$

here chosen with respect to the quartet Q_{uscb} . This quantity is known as the *Jarlskog invariant* [83].

Any orthogonality condition of the CKM matrix can be interpreted as representing a triangle in the complex plane. One of these triangles, the one we wrote in Eq. (2.63), is of particular phenomenological interest because all its sides are of the same order of magnitude. Since it is the conventional triangle, it is often termed simply as *the unitarity triangle*. The unitarity triangle is represented in Fig. 2.2. Its

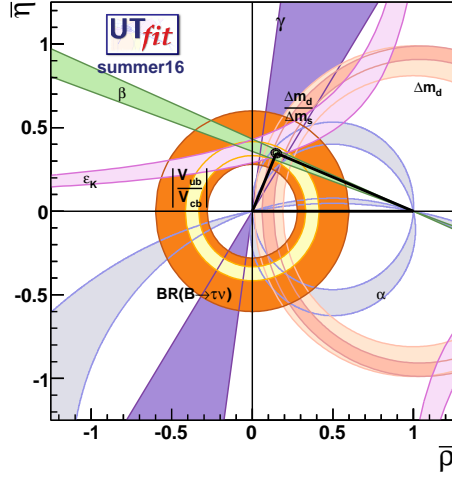


Figure 2.3: The unitarity triangle with precision measurements mapped to the $\bar{\rho} - \bar{\eta}$ plane, where $\bar{\rho} \equiv \rho(1 - \lambda^2/2)$ and $\bar{\eta} \equiv \eta(1 - \lambda^2/2)$. The bottom length is normalized to 1, when comparing with Fig. 2.2, by dividing all sides by $V_{cd}V_{cb}^*$.

inner angles are rephasing invariants as well, constructed from the elements of the CKM matrix as

$$\alpha \equiv \arg\left(-\frac{V_{td}V_{tb}^*}{V_{ud}V_{ub}^*}\right), \quad (2.66)$$

$$\beta \equiv \arg\left(-\frac{V_{cd}V_{cb}^*}{V_{td}V_{tb}^*}\right), \quad (2.67)$$

$$\gamma \equiv \arg\left(-\frac{V_{ud}V_{ub}^*}{V_{cd}V_{cb}^*}\right). \quad (2.68)$$

A particularity of these triangles arising from the orthogonality relations is that, despite having different shapes, all have the same area:

$$\text{Area} = \frac{|J|}{2}, \quad (2.69)$$

which grants some geometrical meaning to the Jarlskog invariant. This follows from the unique character of $|J|$ as being the absolute value of the imaginary parts of all the quartets, which itself follows from the number of physical phases being just one when there are three quark generations. In the ‘standard parametrization’,

$$|J| = s_{12} s_{13} s_{23} c_{12} c_{13}^2 c_{23} \sin \delta, \quad (2.70)$$

fleshing the dependence of $|J|$ on δ , and further evidencing it as the measure of the strength of CP violation in the SM.

In practice, since the theory does not provide the elements of the CKM, the unitarity triangle itself is fitted from experimental data, combining different measurements to constrain its sides lengths and angles. This procedure has been an enterprise of a few collaborations, one of which is the UTfit Collaboration [84], whose latest unitarity triangle fit results are shown in Fig. 2.3. The fit to the unitarity triangle is a landmark in the phenomenological analysis of the SM, and an inspiration to all global fits in the era of precision measurements, including those we will present in this work.

Chapter 3

The $b \rightarrow s$ Transition

Motivated by the anomalies that permeate the semileptonic $\Delta B = 1$ processes, we move now towards the first object of our global analysis machinery: the decays related at the partonic level to $b \rightarrow s\gamma, s\ell\ell$ transitions. In the present chapter, we introduce all the elements necessary to produce the results we present in a later chapter, starting by briefly surveying the formalism that underlies the weak decays of mesons.

3.1 Weak Decays and Effective Hamiltonians: A Tale of Two Scales

The weak decays of hadrons are mediated through the weak interactions of quarks, which are bound into hadrons via strong interactions. This frames these phenomena as belonging to two energy scales widely separated in magnitude: whereas weak interactions live in a scale $\mathcal{O}(M_W, M_Z)$, the typical hadronic energy sits at a much lower $\mathcal{O}(1 \text{ GeV})$: one is, thus, prompted to derive a framework that transcribes the weak interactions into an effective low energy theory. This is achieved with the language of effective Hamiltonians and the OPE, a pedagogical introduction of which can be found in three works by Andrzej J. Buras: a landmark review with Gerhard Buchalla and Markus E. Lautenbacher [85], the massive compilation of his Les Houches lectures [86], and a recent enlightening historical account [8].

3.1.1 Operator Product Expansion

It is instructive to delineate the basic ideas of the effective theory for the case of a simple process that occurs at tree level in the SM. Let us take the transition $b \rightarrow c\bar{c}s$, for example. As we have seen in the previous chapter, this flavour changing interaction is described by a charged current Lagrangian that we rewrite here as:

$$\mathcal{L}_{cc} = \frac{g}{\sqrt{2}} \left(W_\mu^+ \bar{u}_L^i \gamma^\mu V_{ij} d_L^j + \text{h.c.} \right). \quad (3.1)$$

The amplitude of the full theory diagram, on the left in Fig. 3.1, is thus:

$$\mathcal{A} = i \frac{g^2}{2} V_{cs}^* V_{cb} (\bar{s}_L \gamma^\mu c_L) \frac{g_{\mu\nu} - \frac{k_\mu k_\nu}{M_W^2}}{k^2 - M_W^2} (\bar{c}_L \gamma^\nu b_L), \quad (3.2)$$

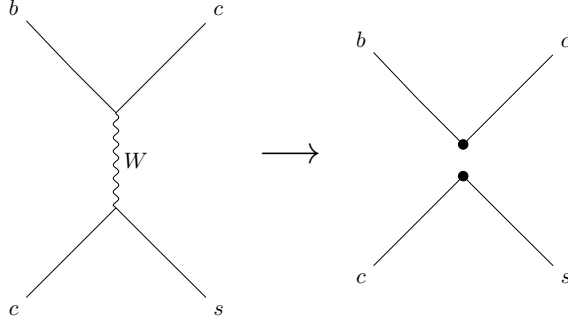


Figure 3.1: The transition $b \rightarrow c\bar{c}s$ at tree-level in the full theory, on the left, and in the effective theory, on the right, emphasizing the “integration out” of the heavy degree of freedom.

which, expanding the W propagator in terms of k^2/M_W^2 , can be turned into:

$$\mathcal{A} = -i \frac{4G_F}{\sqrt{2}} V_{cs}^* V_{cb} (\bar{s}_L \gamma^\mu c_L) (\bar{c}_L \gamma_\mu b_L) + \mathcal{O}\left(\frac{k^2}{M_W^2}\right), \quad (3.3)$$

where

$$G_F = \frac{\sqrt{2} g^2}{8 M_W^2} \quad (3.4)$$

is the *Fermi coupling constant*. If the momentum transfer through the W propagator is much smaller than the boson mass, one may neglect the terms $\mathcal{O}(k^2/M_W^2)$, and the amplitude is approximated to the first term on the right-hand side of Eq. (3.3). This is, in fact, compatible with what one would obtain from an effective Hamiltonian

$$\mathcal{H}_{\text{eff}} = \frac{4G_F}{\sqrt{2}} V_{cs}^* V_{cb} (\bar{s}_L \gamma^\mu c_L) (\bar{c}_L \gamma_\mu b_L) + \text{higher dimensional operators}, \quad (3.5)$$

where neglecting the higher dimensional operators in the expansion, these typically involving derivatives of the fields, indeed corresponds to neglecting terms $\mathcal{O}(k^2/M_W^2)$. We have, therefore, found an approximation of the weak interaction term which consists in the procedure of going to an effective theory by “integrating out” heavy degrees of freedom, here the W boson, and expand on the ensuing products of local operators, here the product in the leading term being:

$$\mathcal{H}_{\text{eff}} = \frac{4G_F}{\sqrt{2}} J_{W,\mu}^- J_W^{\mu+}. \quad (3.6)$$

This is just a rough sketch of the formal framework of the OPE [87–89], but the main features have surfaced: the dominant contributions in the expansion will be those from the operators with lowest dimension, six in this example – for weak decays, higher dimensions provide faint contributions and are usually neglected; regarding low energy dynamics, the effects of the force mediated by the heavy boson correspond, to good approximation, to a point interaction *à la* Fermi. The effective theory below any quark mass requires that field to be integrated out as well, yielding an *effective n_f -flavour theory*, where n_f denotes the number of remaining dynamical quark fields.

3.1.2 QCD Effects and Operator Renormalization

The current-current operator in Eq. (3.6) is usually labelled Q_2 ; factorizing CKM matrix elements:

$$Q_2 = (\bar{s}_L \gamma^\mu c_L) (\bar{c}_L \gamma_\mu b_L). \quad (3.7)$$

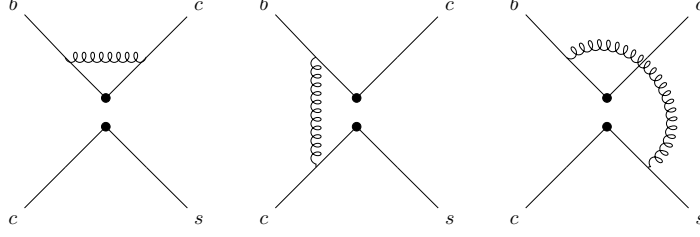


Figure 3.2: One-loop current-current Feynman diagrams in the effective theory.

The LO QCD corrections to this operator come from gluon exchanges between the fermion legs, as shown in Fig. 3.2, where each diagram carries a factor of 2 due to gluon exchange between the other pair of legs. The computation of these diagrams gives rise to a second operator with a different flavour structure. In the so-called ‘standard basis’, the form of this new operator is achieved upon reduction of triple gamma matrices,

$$\gamma^\mu \gamma^\alpha \gamma^\rho = g^{\mu\alpha} \gamma^\rho - g^{\mu\rho} \gamma^\alpha + g^{\alpha\rho} \gamma^\mu - i\gamma_\sigma \gamma_5 \varepsilon^{\mu\alpha\rho\sigma}, \quad (3.8)$$

removal of $SU(3)$ generators, here T^a instead of the L^a of Eq. (2.2) due to no ambiguity with the $SU(2)_L$ sector,

$$T_{ij}^a T_{kl}^a = \frac{1}{2} \delta_{il} \delta_{kj} - \frac{1}{2N} \delta_{ij} \delta_{kl}, \quad (3.9)$$

where N is the number of active colours in the theory, and Fierz reordering of the quark content of the object that ensue, producing for the case under consideration:

$$Q_1 = (\bar{s}_L \gamma^\mu b_L) (\bar{c}_L \gamma_\mu c_L). \quad (3.10)$$

The divergent integrals related with the loops of each diagram are regulated with dimensional regularization [90, 91], where one takes the integral at D dimensions,

$$\int \frac{d^4 k}{(2\pi)^4} \longrightarrow \mu^{2\epsilon} \int \frac{d^D k}{(2\pi)^D}, \quad (3.11)$$

with $2\epsilon = 4 - D$. We will come back to this issue later in the section.

Additional operators are present if the transition contains a quark-antiquark pair, as in our case. As seen in Fig. 3.3, there is an extra one-loop diagram which renormalizes the effective theory, referred to as a *penguin diagram*, which induces effective penguins with four different flavour structures, written in the standard basis as

$$Q_3 = (\bar{s}_L \gamma^\mu b_L) \sum_{q=u,d,s,c,b} (\bar{q}_L \gamma_\mu q_L), \quad (3.12)$$

$$Q_4 = (\bar{s}_L^i \gamma^\mu b_L^j) \sum_{q=u,d,s,c,b} (\bar{q}_L^j \gamma_\mu q_L^i), \quad (3.13)$$

$$Q_5 = (\bar{s}_L \gamma^\mu b_L) \sum_{q=u,d,s,c,b} (\bar{q}_R \gamma_\mu q_R), \quad (3.14)$$

$$Q_6 = (\bar{s}_L^i \gamma^\mu b_L^j) \sum_{q=u,d,s,c,b} (\bar{q}_R^j \gamma_\mu q_R^i), \quad (3.15)$$

together with a *chromomagnetic dipole operator* for when there is the emission of an on-shell gluon,

$$Q_{8g} = \frac{g_s}{16\pi^2} m_b \bar{s}_L \sigma_{\mu\nu} G^{a,\mu\nu} T^a b_R, \quad (3.16)$$

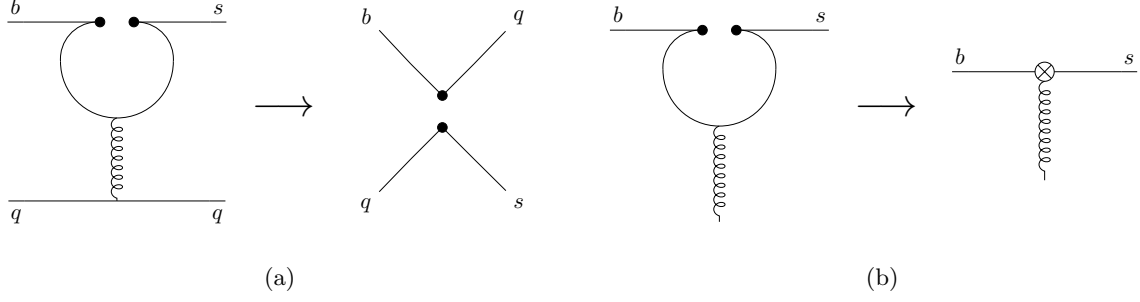


Figure 3.3: The penguin diagram introduces: a) additional four-fermion operators; b) the gluon dipole operator.

where the mass of the strange is neglected. If renormalization due to photon exchange is considered, it is straightforward to see that further operators have to be included: *QED penguin operators*,

$$Q_7 = \frac{3}{2} (\bar{s}_L \gamma^\mu b_L) \sum_{q=u,d,s,c,b} Q_q (\bar{q}_R \gamma_\mu q_R), \quad (3.17)$$

$$Q_8 = \frac{3}{2} (\bar{s}_L^i \gamma^\mu b_L^j) \sum_{q=u,d,s,c,b} Q_q (\bar{q}_R^j \gamma_\mu q_R^i), \quad (3.18)$$

$$Q_9 = \frac{3}{2} (\bar{s}_L \gamma^\mu b_L) \sum_{q=u,d,s,c,b} Q_q (\bar{q}_L \gamma_\mu q_L), \quad (3.19)$$

$$Q_{10} = \frac{3}{2} (\bar{s}_L^i \gamma^\mu b_L^j) \sum_{q=u,d,s,c,b} Q_q (\bar{q}_L^j \gamma_\mu q_L^i), \quad (3.20)$$

and the *electromagnetic dipole operator*,

$$Q_{7\gamma} = \frac{g_s}{16\pi^2} m_b \bar{s}_L \sigma_{\mu\nu} F^{\mu\nu} b_R. \quad (3.21)$$

What pertains, then, to the QCD renormalization of the effective theory? Renormalization concerns the reabsorption of the of the divergencies which occur in the limit of a vanishing regulator – the ϵ poles in dimensional regularization. Let us take a generic Lagrangian written in terms of an unrenormalized, or bare, fermion field, and a bare gluon field:

$$\mathcal{L}^{(0)} = \bar{\psi}_0^i (i\not{\partial} - m_0) \psi_0^i + g_{s,0} \bar{\psi}_0^i \not{G}_0^a T_{ij}^a \psi_0^j, \quad (3.22)$$

where m_0 and $g_{s,0}$ are, respectively, the bare mass and the bare coupling constant. One may introduce the renormalized fields, mass, and coupling, defined as

$$\psi_0 = Z_\psi^{1/2} \psi, \quad G_{\mu,0}^a = Z_G^{1/2} G_\mu^a, \quad m_0 = Z_m m, \quad g_{s,0} = Z_g g_s, \quad (3.23)$$

with which the Lagrangian becomes

$$\mathcal{L} = Z_\psi \bar{\psi}^i (i\not{\partial}) \psi^i - Z_\psi Z_m m \bar{\psi}^i \psi^i + Z_\psi Z_G Z_g g_s \bar{\psi}^i \not{G}^a T_{ij}^a \psi^j. \quad (3.24)$$

This is, in turn, often split into a free Lagrangian plus counterterms, a shape that is better suited for renormalized perturbation theory:

$$\begin{aligned} \mathcal{L} = & \bar{\psi}^i (i\not{\partial} - m) \psi^i + g_s \bar{\psi}^i \not{G}^a T_{ij}^a \psi^j \\ & + (Z_\psi - 1) \bar{\psi}^i (i\not{\partial}) \psi^i - (Z_\psi Z_m - 1) m \bar{\psi}^i \psi^i + (Z_\psi Z_G Z_g - 1) g_s \bar{\psi}^i \not{G}^a T_{ij}^a \psi^j. \end{aligned} \quad (3.25)$$

The renormalization constants are expanded in powers of the coupling constant,

$$Z = 1 + \sum_{k=1}^{\infty} \left(\frac{\alpha_s}{4\pi} \right)^k Z^{(k)}, \quad (3.26)$$

where $\alpha_s = g_s^2/(4\pi)$, each order being further expanded in powers of its ϵ poles:

$$Z^{(k)} = \sum_{l=0}^{\infty} \frac{1}{\epsilon^l} Z^{(k,l)}. \quad (3.27)$$

It must be noted, however, that the coupling is only dimensionless if $D = 4$; for it to be a number we expand in, it is rescaled following the prescription

$$g_{s,0} = Z_g \mu^\epsilon g_s. \quad (3.28)$$

Out of the many arbitrary ways to define the $Z^{(k)}$ factors, the *modified minimal subtraction scheme* ($\overline{\text{MS}}$) [92] is the renormalization scheme that, as the name suggests, subtracts the pole parts and, on its way, redefines μ so as to absorb the universal constants that always appear in dimensional regularization calculations:

$$\mu^2 \rightarrow \frac{e^{-\gamma_E}}{4\pi} \mu^2, \quad (3.29)$$

where γ_E is the Euler-Mascheroni constant. We shall be employing the $\overline{\text{MS}}$ scheme in this work.

Going back to the effective weak decays, while quark field renormalization can deal with the divergences of the first diagram in Fig. 3.2, an additional renormalization is needed to remove the remaining divergent terms: *operator renormalization*, which consists in the elimination of the singularity in the bare operator by way of a renormalization constant,

$$Z^{-1}(\mu, \epsilon, \alpha_s) Q^{(0)}(\epsilon, \alpha_s) \equiv Q(\mu, \alpha_s). \quad (3.30)$$

This constant is, in general, a non-diagonal matrix, such that the operators are said to *mix under renormalization*. It is worth noting that Eq. (3.8) is not valid in D dimensions; the Dirac algebra is no longer closed, and γ_5 is ill-defined. There are many ways, or schemes, to treat γ_5 in D dimensions which make the manipulation of Dirac matrices not so straightforward beyond the LO. In particular, renormalization requires the introduction of extra operators that vanish in four dimensions, thus named *evanescent operators* [93–95]. The choice of these operators is part of the definition of the renormalization scheme of the effective theory. For an introduction to effective theory renormalization beyond the LO see Ref. [85].

The μ -dependence of the operators implies that the effective Hamiltonian, which we write as a sum of all possible operators, requires the introduction of scale-dependent coefficients as a compensation:

$$\mathcal{H}_{\text{eff}} = \frac{4G_F}{\sqrt{2}} V_{cs}^* V_{cb} \sum_i C_i(\mu) Q_i(\mu). \quad (3.31)$$

These coefficients are termed *Wilson coefficients* (WCs). Their relevance is immediately made transparent in the process of matching, *i.e.* when, in accordance to the formal systematization of the treatment of short-distance effects in weak decays [96], we demand that the physical amplitudes produced by the full

theory, $\mathcal{A}_{\text{full}}$, and the effective theory, $\mathcal{A}_{\text{eff}} = \langle \mathcal{H}_{\text{eff}} \rangle$, are the same at a given matching scale. At the LO, this typically produces coefficients that look like

$$C_i(\mu) = \Omega_i \frac{\alpha_s}{4\pi} \ln \frac{M_W^2}{\mu^2} + \mathcal{O}(\alpha_s), \quad \text{for } i \neq 2, \quad (3.32)$$

$$C_2(\mu) = 1 + \Omega_2 \frac{\alpha_s}{4\pi} \ln \frac{M_W^2}{\mu^2} + \mathcal{O}(\alpha_s). \quad (3.33)$$

where the Ω_i are basis-dependent factors. A prompt observation that can be made is that removing the QCD effects returns us to the case of only one operator, Q_2 , as expected. Moreover, the effective theory has the property that short-distance and long-distance contributions get factorized, respectively, into the WCs and the operator matrix elements. At the LO matching level, this is testified by the split of the logarithms present in the full amplitudes, which span the full band between the participating energies – the ultraviolet scale M_W and the infrared scale p^2 –, into a high scale, that goes into the WCs, and a low scale part, which pertains to the matrix elements:

$$\ln \frac{M_W^2}{-p^2} = \ln \frac{M_W^2}{\mu^2} + \ln \frac{\mu^2}{-p^2}, \quad (3.34)$$

where $-p^2$ stands in for the external momenta of participating particles in the decay, and μ is the renormalization scale, acting also as the scale separating short- and long-distance contributions. The fact that full and effective theories share the same infrared behaviour makes the matching possible. Another facet of WCs is that the renormalization of the effective Hamiltonian can be traded from a renormalization of the operators, to the equivalent renormalization of coefficients. One can define

$$C_i^{(0)} = Z_{ij}^c C_j, \quad (3.35)$$

which, again up to quark field renormalization and omitting pre-factors, is related to the matrix Z as:

$$\left. \begin{aligned} \mathcal{A}_{\text{eff}} &= Z_{ij}^c C_j \langle Q_i \rangle^{(0)} \\ \mathcal{A}_{\text{eff}} &= C_j \langle Q_j \rangle = C_j Z_{ji}^{-1} \langle Q_i \rangle^{(0)} \end{aligned} \right\} Z_{ij}^c = Z_{ji}^{-1}. \quad (3.36)$$

3.1.3 Summation of Large Logarithms

It is perfectly graspable from Eq. (3.32) that, if the matching scale μ is chosen near M_W , the logarithms in the coefficients are small and the matching is allowed to be done in fixed order perturbation theory. Yet, the matrix elements involve scales which are typically much lower – in our case of decaying B mesons these are of $\mathcal{O}(m_b)$. This means that by choosing $\mu = \mu_b \approx m_b$ to make the matrix element logarithms small, one turns $\alpha_s \ln(M_W/\mu)$ into $\mathcal{O}(1)$ and thus spoils the fixed order perturbativity of the WCs. This situation can be improved, however, if we take the relation in Eq. (3.36) to treat the C_i as renormalized ‘coupling constants’ of the effective Hamiltonian, and use their RGEs to sum up all the terms of the form

$$\left[\alpha_s(\mu) \ln \frac{M_W}{\mu} \right]^n \quad (3.37)$$

in the LO – or leading logarithmic – approximation, all the terms

$$\alpha_s(\mu) \left[\alpha_s(\mu) \ln \frac{M_W}{\mu} \right]^n \quad (3.38)$$

in the NLO approximation, and so on and so forth.

As our choice of renormalization scheme corresponds to a redefinition of μ , infinitesimal changes of the scale will result in infinitesimal tweaks of the renormalized quantities to still render all physical observables invariant; in the continuous limit these changes translate to differential equations, the RGEs [97, 98]. It is a well known fact that the RGE of the coupling constant is related to its β function as

$$\mu \frac{dg_s}{d\mu} = \beta(g_s, \epsilon), \quad (3.39)$$

where, given Eq. (3.28),

$$\beta(g_s, \epsilon) = -\epsilon g_s - Z_g^{-1} \left(\mu \frac{d}{d\mu} Z_g \right) g_s \equiv -\epsilon g_s - \beta(g_s). \quad (3.40)$$

The function $\beta(g_s)$, traceable order by order from Eq. (3.26) and Eq. (3.27), is known at the four-loop level [99, 100], and follows, in the $\overline{\text{MS}}$ scheme, the expansion:

$$\beta(g_s) = -\beta_0 \frac{g_s^3}{(4\pi)^2} - \beta_1 \frac{g_s^5}{(4\pi)^4} - \beta_2 \frac{g_s^7}{(4\pi)^6} - \beta_3 \frac{g_s^9}{(4\pi)^8} + \mathcal{O}(g_s^{11}). \quad (3.41)$$

The coefficients of the expansion are written, in full dependence on the number of active flavours, and on the index and quadratic Casimirs of $SU(3)$, in Appendix A.1.

By the same token, the RGE of the mass operator is governed by the mass anomalous dimension,

$$\mu \frac{dm}{d\mu} = -\gamma_m m \quad (3.42)$$

which bears a relation with the corresponding renormalization constant:

$$\gamma_m = Z_m^{-1} \left(\mu \frac{d}{d\mu} Z_m \right). \quad (3.43)$$

Interestingly, up to a difference in sign, μ -independence of the bare WCs leads to a matrix RGE that has the same shape as that of the running fermion mass:

$$\mu \frac{d}{d\mu} \vec{C}(\mu) = \gamma^T(g_s) \vec{C}(\mu). \quad (3.44)$$

where \vec{C} is a column vector of WCs, and γ , here transposed due to Eq. (3.36), is the *anomalous dimension matrix* corresponding to the column vector of effective operators. That being said, and upon defining as usual

$$\gamma(g_s) = \frac{g_s^2}{16\pi^2} \gamma^{(0)} + \left(\frac{g_s^2}{16\pi^2} \right)^2 \gamma^{(1)} + \left(\frac{g_s^2}{16\pi^2} \right)^3 \gamma^{(2)} + \dots, \quad (3.45)$$

the solution of Eq. (3.44) mirrors, of course, the equation of the running mass:

$$\vec{C}(\mu) = U(\mu, \mu_W) \vec{C}(\mu_W), \quad (3.46)$$

where μ_W is the high energy matching scale, and $U(\mu, \mu_W)$ is the the evolution function

$$U(\mu, \mu_W) = T_g \exp \left[\int_{g_s(\mu_W)}^{g_s(\mu)} dg \frac{\gamma^T(g)}{\beta(g)} \right], \quad (3.47)$$

T_g denoting the ordering of the coupling constants $g_s(\mu)$ with increasing value from right to left.

The result at LO is easily obtained, and relevant for future use. First, the evolution matrix comes to be

$$U^{(0)}(\mu, \mu_W) = \exp \left[\frac{\gamma^{(0)T}}{\beta_0} \int_{g_s(\mu_W)}^{g_s(\mu)} dg \left(-\frac{1}{g} \right) \right]. \quad (3.48)$$

If one introduces

$$\eta = \frac{\alpha_s(\mu_W)}{\alpha_s(\mu)} = \left(\frac{g_s(\mu_W)}{g_s(\mu)} \right)^2, \quad (3.49)$$

and denotes $\gamma_D^{(0)}$ as the diagonal matrix that contains the eigenvalues of the anomalous dimension matrix,

$$\gamma_D^{(0)} = V^{-1} \gamma^{(0)T} V, \quad (3.50)$$

the evolver that takes WCs from a scale $\mu_W \approx M_W$, where there are no large logarithms, down to the renormalization scale μ ,

$$\vec{C}^{(0)}(\mu) = U^{(0)}(\mu, \mu_W) \vec{C}^{(0)}(\mu_W) \quad (3.51)$$

is simply

$$U^{(0)}(\mu, \mu_W) = V \left(\eta^{\frac{\gamma_D^{(0)}}{2\beta_0}} \right) V^{-1}, \quad (3.52)$$

where η to the power of a diagonal matrix is algebraically equivalent to a matrix with diagonal entries that consist of η to the power of the corresponding eigenvalue. Running beyond the LO will be sketched in the next sections.

3.2 The $\Delta B = 1$ Effective Hamiltonian

In the previous section we managed to provide the basics of the formalism. In what follows we will list the complete basis of operators needed for our analysis, the state-of-the-art of their matching conditions and anomalous dimensions, and the form of the evolver in the presence of both QCD and QED corrections. We point the reader towards Refs. [101, 102] for recent reviews that address this subject.

3.2.1 Operator Basis

Our illustration of the OPE for weak decays was done in the so-called ‘standard basis’, where, as we said there, triple products of Dirac matrices are reduced with the help of the identity in Eq. (3.8), and the generators T^a are removed into Kronecker deltas according to Eq. (3.9). However, proceeding in the same manner in the calculations at the two-loop level and beyond requires, as identified by Chetyrkin, Misiak, and Münz [103, 104], the introduction of several more evanescent operators and leads to problematic traces with γ_5 . It is thus customary to work in the basis put forward by those authors, which, aiming at the least convoluted definition of evanescent operators possible, leaves gamma products in penguins as they stand, and, for convenience, keeps the colour structure as it is. This choice of basis allows the convenient use of fully anticommuting γ_5 at any number of loops, at the leading order in the Fermi coupling.

In the Chetyrkin-Misiak-Münz basis, the effective Hamiltonian that is relevant to $b \rightarrow s\gamma, sll$ transitions involves the following set of dimension six operators within the SM:

- **Current-current operators (C)**

$$Q_1^p = (\bar{s}_L \gamma_\mu T^a p_L) (\bar{p}_L \gamma^\mu T^a b_L), \quad (3.53)$$

$$Q_2^p = (\bar{s}_L \gamma_\mu p_L) (\bar{p}_L \gamma^\mu b_L), \quad (3.54)$$

- **QCD penguin operators (P)**

$$P_3 = (\bar{s}_L \gamma_\mu b_L) \sum_q (\bar{q} \gamma^\mu q), \quad (3.55)$$

$$P_4 = (\bar{s}_L \gamma_\mu T^a b_L) \sum_q (\bar{q} \gamma^\mu T^a q), \quad (3.56)$$

$$P_5 = (\bar{s}_L \gamma_{\mu 1} \gamma_{\mu 2} \gamma_{\mu 3} b_L) \sum_q (\bar{q} \gamma^{\mu 1} \gamma^{\mu 2} \gamma^{\mu 3} q), \quad (3.57)$$

$$P_6 = (\bar{s}_L \gamma_{\mu 1} \gamma_{\mu 2} \gamma_{\mu 3} T^a b_L) \sum_q (\bar{q} \gamma^{\mu 1} \gamma^{\mu 2} \gamma^{\mu 3} T^a q), \quad (3.58)$$

- **Chromo- and Electromagnetic dipole operators (M)**

$$Q_{8g} = \frac{g_s}{16\pi^2} m_b \bar{s}_L \sigma_{\mu\nu} G^{a,\mu\nu} T^a b_R, \quad (3.59)$$

$$Q_{7\gamma} = \frac{e}{16\pi^2} m_b \bar{s}_L \sigma_{\mu\nu} F^{\mu\nu} b_R, \quad (3.60)$$

where $F_{\mu\nu} = \partial_\mu A_\nu - \partial_\nu A_\mu$,

- **Semileptonic operators (L)**

$$Q_{9V} = \frac{\alpha_e}{4\pi} (\bar{s}_L \gamma_\mu b_L) (\bar{\ell} \gamma^\mu \ell), \quad (3.61)$$

$$Q_{10A} = \frac{\alpha_e}{4\pi} (\bar{s}_L \gamma_\mu b_L) (\bar{\ell} \gamma^\mu \gamma^5 \ell), \quad (3.62)$$

which occur only in the semileptonic mode,

- **Electroweak penguin operators (Q)**

$$P_{3Q} = (\bar{s}_L \gamma_\mu b_L) \sum_q Q_q (\bar{q} \gamma^\mu q), \quad (3.63)$$

$$P_{4Q} = (\bar{s}_L \gamma_\mu T^a b_L) \sum_q Q_q (\bar{q} \gamma^\mu T^a q), \quad (3.64)$$

$$P_{5Q} = (\bar{s}_L \gamma_{\mu 1} \gamma_{\mu 2} \gamma_{\mu 3} b_L) \sum_q Q_q (\bar{q} \gamma^{\mu 1} \gamma^{\mu 2} \gamma^{\mu 3} q), \quad (3.65)$$

$$P_{6Q} = (\bar{s}_L \gamma_{\mu 1} \gamma_{\mu 2} \gamma_{\mu 3} T^a b_L) \sum_q Q_q (\bar{q} \gamma^{\mu 1} \gamma^{\mu 2} \gamma^{\mu 3} T^a q), \quad (3.66)$$

when QED corrections are taken into account, and penguins with the exchange of a photon are non-negligible. Above, $p = u, c$, since top is integrated out in an effective 5-flavour theory, $\ell = e, \mu, \tau$, α_e is the electromagnetic counterpart of α_s , Q_q is the electric charge of a corresponding quark q , and we have neglected the chirally suppressed SM dipoles. If higher order electroweak effects are considered, one further, “evanescent-like”, operator is required:

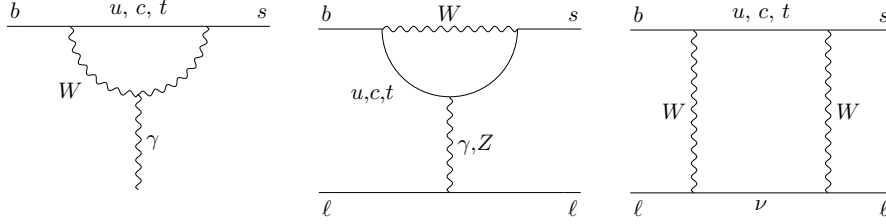


Figure 3.4: Examples of typical radiative and semileptonic channels of the $b \rightarrow s$ transition within the SM.

- **The operator Q_b (B)**

$$Q_b = \frac{1}{12} [(\bar{s}_L \gamma_{\mu 1} \gamma_{\mu 2} \gamma_{\mu 3} b_L) (\bar{b} \gamma^{\mu 1} \gamma^{\mu 2} \gamma^{\mu 3} b) - 4(\bar{s}_L \gamma_{\mu} b_L) (\bar{b} \gamma^{\mu} b)], \quad (3.67)$$

which corresponds in four dimensions to $(\bar{s}_L \gamma_{\mu} b_L) (\bar{b} \gamma^{\mu} b_L)$, and receives contributions from electroweak boxes [105, 106].

The removal of the top allows for the CKM pre-factors of sums over quark-blind operators to be simplified using one of the unitarity conditions of the CKM matrix:

$$V_{us}^* V_{ub} + V_{cs}^* V_{cb} = -V_{ts}^* V_{tb}. \quad (3.68)$$

Writing each combination $V_{is}^* V_{ib}$ as λ_i , the $\Delta B = 1$ effective Hamiltonian is cast, in full generality, as a combination of two distinct parts:

$$\mathcal{H}_{\text{eff}}^{\Delta B=1} = \mathcal{H}_{\text{eff}}^{\text{had}} + \mathcal{H}_{\text{eff}}^{\text{sl}+\gamma}, \quad (3.69)$$

where the hadronic term involves the usual first seven operators – current-current operators, QCD penguins, and the chromomagnetic dipole operator – together with the QED-related P_{iQ} and Q_b ,

$$\mathcal{H}_{\text{eff}}^{\text{had}} = \frac{4G_F}{\sqrt{2}} \left[\sum_{p=u,c} \lambda_p (C_1 Q_1^p + C_2 Q_2^p) - \lambda_t \left(\sum_{i=3}^6 C_i P_i + C_8 Q_{8g} + \sum_{i=3}^6 C_{iQ} P_{iQ} + C_b Q_b \right) \right], \quad (3.70)$$

while the second piece includes the electromagnetic dipole and semileptonic operators:

$$\mathcal{H}_{\text{eff}}^{\text{sl}+\gamma} = -\frac{4G_F}{\sqrt{2}} \lambda_t \left(C_7 Q_{7\gamma} + C_9 Q_{9V} + C_{10} Q_{10A} \right). \quad (3.71)$$

3.2.2 Matching Conditions for Wilson Coefficients

Ever since the work of Inami and Lim [107], the calculation of penguin and box diagrams has been systematized, with each possible type of FCNC process having its own loop described by a given function of $x_t = m_t^2/M_W^2$. In Fig. 3.4, we display some examples of the lowest order penguin and box diagrams contributing to the matching conditions. The Inami-Lim functions and the matchings that follow come, unless specifically said otherwise, from the QCD calculations of Ref. [108] and the QED conditions added in Ref. [109]. Due to their large expressions, we collect in Appendix B the functions not provided in either of those two references.

Given the prevalence of factors 4π in matching conditions and anomalous dimensions, we introduce the modified couplings $\tilde{\alpha}_{s,e} = \alpha_{s,e}/(4\pi)$, and define the ratio $\kappa = \tilde{\alpha}_e/\tilde{\alpha}_s$. Although the orders in QED

Order label	$\tilde{\alpha}_s^n \kappa^m$	$e - s$ relation
LO _{QED}	κ	$\tilde{\alpha}_e / \tilde{\alpha}_s$
NLO _{QED,11}	$\tilde{\alpha}_s \kappa$	$\tilde{\alpha}_e$
NLO _{QED,21}	$\tilde{\alpha}_s^2 \kappa$	$\tilde{\alpha}_e \tilde{\alpha}_s$
NLO _{QED,02}	κ^2	$\tilde{\alpha}_e^2 / \tilde{\alpha}_s^2$
NLO _{QED,12}	$\tilde{\alpha}_s \kappa^2$	$\tilde{\alpha}_e^2 / \tilde{\alpha}_s$
NLO _{QED,22}	$\tilde{\alpha}_s^2 \kappa^2$	$\tilde{\alpha}_e^2$

Table 3.1: Structure and labelling of the orders in QED. How each order translates to powers of $\tilde{\alpha}_e$ and $\tilde{\alpha}_s$ is given for clarity in the last column.

will mainly be given in numeric form, with two indices (n, m) that represent the power of, respectively, $\tilde{\alpha}_s$ and κ , the labelling in Table 3.1 is also used throughout the work. We can, therefore, organize the expansion in terms of coupling constants of a WC at the matching scale as follows [109]:

$$C_i(\mu_W) = C_i^{00}(\mu_W) + \tilde{\alpha}_s(\mu_W) C_i^{10}(\mu_W) + \tilde{\alpha}_s^2(\mu_W) C_i^{20}(\mu_W) + \tilde{\alpha}_s(\mu_W) \kappa(\mu_W) C_i^{11}(\mu_W) + \tilde{\alpha}_s^2(\mu_W) \kappa(\mu_W) C_i^{21}(\mu_W) + \mathcal{O}(\tilde{\alpha}_s^3, \tilde{\alpha}_s^2 \kappa^2), \quad (3.72)$$

where C_i^{00} , C_i^{10} , and C_i^{20} are, respectively, the QCD LO, NLO and NNLO terms of the WC, while matchings at LO_{QED}, C_i^{01} , and at NLO_{QED,02} and NLO_{QED,12} are absent at high energy. For C_9 and C_{10} , contributions at NLO_{QED,22} are also implemented.

As with the list of operators in the previous subsection, we go here block by block, each block moniker being the suitably chosen letter that we put in between parenthesis for each type of operator [108, 109]:

- **Matching conditions for C**

$$C_2^{00}(\mu_W) = 1, \quad (3.73)$$

$$C_1^{10}(\mu_W) = 15 + 6L, \quad (3.74)$$

$$C_1^{20}(\mu_W) = -T(x_t) + \frac{7987}{72} + \frac{17}{3}\pi^2 + \frac{475}{6}L + 17L^2, \quad (3.75)$$

$$C_2^{20}(\mu_W) = \frac{127}{18} + \frac{4}{3}\pi^2 + \frac{46}{3}L + 4L^2, \quad (3.76)$$

$$C_2^{11}(\mu_W) = -\frac{22}{9} - \frac{4}{3}L_z + \frac{1}{9}, \quad (3.77)$$

where $L = \ln(\mu_W^2/M_W^2)$, $L_z = \ln(\mu_W^2/M_Z^2)$, and the NLO_{QED,11} matching of C_2 is as given in Ref. [110].

- **Matching conditions for P**

$$C_4^{10}(\mu_W) = E_0(x_t) - \frac{7}{9} + \frac{2}{3}L, \quad (3.78)$$

$$C_3^{20}(\mu_W) = G_1^t(x_t) - \frac{680}{243} - \frac{20}{81}\pi^2 - \frac{68}{81}L - \frac{20}{27}L^2, \quad (3.79)$$

$$C_4^{20}(\mu_W) = E_1^t(x_t) + \frac{950}{243} + \frac{10}{81}\pi^2 + \frac{124}{27}L + \frac{10}{27}L^2, \quad (3.80)$$

$$C_5^{20}(\mu_W) = -\frac{1}{10}G_1^t(x_t) + \frac{2}{15}E_0(x_t) + \frac{68}{243} + \frac{2}{81}\pi^2 + \frac{14}{81}L + \frac{2}{27}L^2, \quad (3.81)$$

$$C_6^{20}(\mu_W) = -\frac{3}{16}G_1^t(x_t) + \frac{1}{4}E_0(x_t) + \frac{85}{162} + \frac{5}{108}\pi^2 + \frac{35}{108}L + \frac{5}{36}L^2, \quad (3.82)$$

$$C_3^{11}(\mu_W) = -\frac{2}{9s_W^2} \left(2B_0(x_t) + C_0(x_t) \right), \quad (3.83)$$

$$C_5^{11}(\mu_W) = \frac{1}{9s_W^2} \left(B_0(x_t) + \frac{1}{2}C_0(x_t) \right), \quad (3.84)$$

$$C_3^{21}(\mu_W) = \frac{1}{s_W^2} \left(\frac{4}{9}B_1^d(x_t) + \frac{4}{27}\tilde{B}_1^d(x_t) + \frac{2}{9}B_1^u(x_t) + \frac{2}{27}\tilde{B}_1^u(x_t) - \frac{2}{9}C_1(x_t) \right. \\ \left. + \frac{320}{27}B_0(x_t) + \frac{160}{27}C_0(x_t) \right), \quad (3.85)$$

$$C_4^{21}(\mu_W) = \frac{16}{27}C_0(x_t) + \frac{1}{s_W^2} \left(\frac{8}{9}\tilde{B}_1^d(x_t) + \frac{4}{9}\tilde{B}_1^u(x_t) - \frac{2}{9}G(x_t, x_z) - \frac{88}{9}B_0(x_t) - \frac{184}{27}C_0(x_t) \right), \quad (3.86)$$

$$C_5^{21}(\mu_W) = \frac{1}{s_W^2} \left(-\frac{1}{9}B_1^d(x_t) - \frac{1}{27}\tilde{B}_1^d(x_t) - \frac{1}{18}B_1^u(x_t) - \frac{1}{54}\tilde{B}_1^u(x_t) + \frac{1}{18}C_1(x_t) \right. \\ \left. - \frac{32}{27}B_0(x_t) - \frac{16}{27}C_0(x_t) \right), \quad (3.87)$$

$$C_6^{21}(\mu_W) = \frac{1}{s_W^2} \left(-\frac{2}{9}\tilde{B}_1^d(x_t) - \frac{1}{9}\tilde{B}_1^u(x_t) + \frac{1}{18}G(x_t, x_z) + \frac{4}{3}B_0(x_t) + \frac{2}{3}C_0(x_t) \right), \quad (3.88)$$

where $s_w^2 = \sin^2 \theta_W$, $x_z = M_Z^2/M_W^2$, and the contributions C_i^{21} , calculated in the ‘standard basis’ in Ref. [111], were kindly provided to us by Mikolaj Misiak and Ulrich Haisch.

- **Matching conditions for M**

$$C_7^{00}(\mu_W) = -\frac{1}{2}A_0(x_t) - \frac{23}{36}, \quad (3.89)$$

$$C_8^{00}(\mu_W) = -\frac{1}{2}F_0(x_t) - \frac{1}{3}, \quad (3.90)$$

$$C_7^{10}(\mu_W) = -\frac{1}{2}A_1^t(x_t) + \frac{713}{243} + \frac{4}{81}L - \frac{4}{9}C_4^{10}(\mu_W), \quad (3.91)$$

$$C_8^{10}(\mu_W) = -\frac{1}{2}F_1^t(x_t) + \frac{91}{324} - \frac{4}{27}L - \frac{1}{6}C_4^{10}(\mu_W), \quad (3.92)$$

$$C_7^{20}(\mu_W) = C_{7,m_t}^{t,(3)}(x_t) + C_{7,\text{loop}}^{t,(3)}(x_t) - \left(C_{7,M_W}^{c,(3)}(x_t) + \frac{13763}{2187}L + \frac{814}{729}L^2 \right) \\ - \frac{1}{3}C_3^{20}(\mu_W) - \frac{4}{9}C_4^{20}(\mu_W) - \frac{20}{3}C_5^{20}(\mu_W) - \frac{80}{9}C_6^{20}(\mu_W), \quad (3.93)$$

$$C_8^{20}(\mu_W) = C_{8,m_t}^{t,(3)}(x_t) + C_{8,\text{loop}}^{t,(3)}(x_t) - \left(C_{8,M_W}^{c,(3)}(x_t) + \frac{16607}{5832}L + \frac{397}{486}L^2 \right) \\ + C_3^{20}(\mu_W) - \frac{1}{6}C_4^{20}(\mu_W) - 20C_5^{20}(\mu_W) - \frac{10}{3}C_6^{20}(\mu_W), \quad (3.94)$$

$$C_7^{11}(\mu_W) = \frac{1}{s_W^2} \left[1.11 - 1.15 \left(1 - \frac{m_t^2}{170^2} \right) - 0.444 \ln \frac{M_h}{100} - 0.21 \ln^2 \frac{M_h}{100} - 0.513 \ln \frac{M_h}{100} \ln \frac{m_t}{170} \right] \\ + \left(\frac{8}{9}C_7^{00}(\mu_W) - \frac{104}{243} \right) L, \quad (3.95)$$

$$C_8^{11}(\mu_W) = \frac{1}{s_W^2} \left[-0.143 + 0.156 \left(1 - \frac{m_t^2}{170^2} \right) - 0.129 \ln \frac{M_h}{100} - 0.0244 \ln^2 \frac{M_H}{100} \right. \\ \left. - 0.037 \ln \frac{M_h}{100} \ln \frac{m_t}{170} \right] + \left(\frac{4}{9}C_8^{00}(\mu_W) - \frac{4}{3}C_7^{00}(\mu_W) - \frac{58}{81} \right) L. \quad (3.96)$$

It cannot go without remark that these matching conditions are not those of the plain dipole operators, but of effective operators which are given by the combinations that actually enter the calculation of

physical observables [103, 112]:

$$C_7(\mu) \longrightarrow C_7(\mu) + \sum_{i=3}^6 y_i \left[C_i(\mu) - \frac{1}{3} C_{iQ}(\mu) \right], \quad (3.97)$$

$$C_8(\mu) \longrightarrow C_8(\mu) + \sum_{i=3}^6 z_i \left[C_i(\mu) - \frac{1}{3} C_{iQ}(\mu) \right], \quad (3.98)$$

where $y = (-1/3, -4/9, -20/3, -80/9)$, $z = (1, -16, 20, -10/3)$. Unlike C_7 and C_8 alone, the effective coefficients are regularization scheme independent at LO [113, 114], and do not depend on the basis of physical operators. $C_{i,m_t}^{t,(3)}$, $C_{i,M_W}^{c,(3)}$, and $C_{i,\text{loop}}^{t,(3)}$ correspond to power expansions and a loop function appearing in the 3-loop matching calculated in Ref. [115], all given in Appendix B.1. The QED contributions, only known up to $\text{NLO}_{\text{QED},11}$, were provided in Ref. [110] in the accurate approximate formulas above.

- **Matching conditions for L**

$$C_{9V}^{11}(\mu_W) = \frac{1}{s_W^2} Y_0(x_t) + W_0(x_t) + \frac{4}{9} - \frac{4}{9} L_t, \quad (3.99)$$

$$C_{10A}^{11}(\mu_W) = -\frac{1}{s_W^2} Y_0(x_t), \quad (3.100)$$

$$C_{9V}^{21}(\mu_W) = \frac{1 - 4s_W^2}{s_W^2} C_1^t(x_t) - \frac{1}{s_W^2} B_1^t(x_t) - D_1^t(x_t) + \frac{1}{s_W^2} + \frac{524}{729} - \frac{128}{243} \pi^2 - \frac{16}{3} L - \frac{128}{81} L^2, \quad (3.101)$$

$$C_{10A}^{21}(\mu_W) = \frac{1}{s_W^2} [B_1^t(x_t) - C_1^t(x_t)] - \frac{1}{s_W^2}, \quad (3.102)$$

$$C_{9V}^{22}(\mu_W) = -\frac{x_t^2}{32s_W^2} (4s_W^2 - 1) \left[3 + \tau_b^{(2)}(x_{ht}) - \Delta_t(\mu_W, x_{ht}) \right], \quad (3.103)$$

$$C_{10A}^{22}(\mu_W) = -\frac{x_t^2}{32s_W^2} \left[3 + \tau_b^{(2)}(x_{ht}) - \Delta_t(\mu_W, x_{ht}) \right], \quad (3.104)$$

where $L_t = \ln(\mu_W^2/m_t^2)$, and $\tau_b^{(2)}$ and Δ_t , with $x_{ht} = M_h^2/m_t^2$, are auxiliary functions from Ref. [116], written here in Appendix B.2. For C_{10} , the expression of the $\text{NLO}_{\text{QED},22}$ matching refers to the large- m_t expansion of Ref. [116]. We have used, however, the full m_t dependence found in Ref. [117], which is attached to the paper on arXiv as a Mathematica package.

- **Matching conditions for Q**

$$C_{3Q}^{11}(\mu_W) = 4C_0(x_t) + \tilde{D}_0(x_t) + \frac{4}{9} L - \frac{1}{s_W^2} \left(\frac{10}{3} B_0(x_t) - \frac{4}{3} C_0(x_t) \right), \quad (3.105)$$

$$C_{5Q}^{11}(\mu_W) = \frac{1}{s_W^2} \left(\frac{5}{6} B_0(x_t) - \frac{1}{3} C_0(x_t) \right), \quad (3.106)$$

$$C_{3Q}^{21}(\mu_W) = 4C_1(x_t) + 4D_1^t(x_t) + \frac{320}{9} C_0(x_t) + \frac{1}{s_W^2} \left(-\frac{2}{3} B_1^d(x_t) - \frac{2}{9} \tilde{B}_1^d(x_t) + \frac{2}{3} B_1^u(x_t) \right. \\ \left. + \frac{2}{9} \tilde{B}_1^u(x_t) + \frac{4}{3} C_1(x_t) + \frac{800}{9} B_0(x_t) - \frac{640}{9} C_0(x_t) \right), \quad (3.107)$$

$$C_{4Q}^{21}(\mu_W) = -\frac{4}{3} G(x_t, x_z) - \frac{16}{3} H(x_t, x_z) - 32C_0(x_t) + \frac{1}{s_W^2} \left(-\frac{4}{3} \tilde{B}_1^d(x_t) + \frac{4}{3} \tilde{B}_1^u(x_t) \right. \\ \left. + \frac{4}{3} G(x_t, x_z) - 80B_0(x_t) + \frac{112}{3} C_0(x_t) \right), \quad (3.108)$$

$$C_{5Q}^{21}(\mu_W) = -\frac{32}{9}C_0(x_t) + \frac{1}{s_W^2} \left(\frac{1}{6}B_1^d(x_t) + \frac{1}{18}\tilde{B}_1^d(x_t) - \frac{1}{6}B_1^u(x_t) - \frac{1}{18}\tilde{B}_1^u(x_t) - \frac{1}{3}C_1(x_t) - \frac{80}{9}B_0(x_t) + \frac{64}{9}C_0(x_t) \right), \quad (3.109)$$

$$C_{6Q}^{21}(\mu_W) = \frac{1}{3}G(x_t, x_z) + \frac{1}{3}H(x_t, x_z) + 4C_0(x_t) + \frac{1}{s_W^2} \left(\frac{1}{3}\tilde{B}_1^d(x_t) - \frac{1}{3}\tilde{B}_1^u(x_t) - \frac{1}{3}G(x_t, x_z) + 10B_0(x_t) - \frac{16}{3}C_0(x_t) \right), \quad (3.110)$$

where the matchings for C_{iQ}^{21} were, as with the case of the QCD penguins, obtained from personal notes of Mikolaj Misiak and Ulrich Haisch.

- **Matching condition for B**

$$C_b^{11}(\mu_W) = -\frac{1}{2s_W^2}S_0(x_t). \quad (3.111)$$

Coding in `HEPfit`, whose structure shall be overviewed in the next chapter, all QED contributions and the totality of the Q and B blocks, putting all blocks together in a coherent set of SM matchings, was an integral part of the student's work.

3.2.3 The Anomalous Dimension Matrix

In this subsection we survey the QCD and QED anomalous dimension matrices of our operator basis. By QCD, we mean the matrices γ^{n0} in the augmented expansion we now make in powers of $\tilde{\alpha}_s$ and $\tilde{\alpha}_e$:

$$\gamma(\mu) = \sum_{\substack{n,m=0 \\ n+m \geq 1}} \gamma^{(nm)} \tilde{\alpha}_s^n(\mu) \tilde{\alpha}_e^m(\mu). \quad (3.112)$$

Ordering the operators by block, with the same order as was used to list the operators, only with a slight swap in M to follow convention – such that $Q_{7\gamma}$ precedes Q_{8g} –, we mimic Ref. [109] in dividing the matrix at any given order n, m into combinations of blocks, its generic structure being

$$\gamma^{(nm)} = \begin{pmatrix} [\gamma_{CC}^{(nm)}]_{2 \times 2} & [\gamma_{CP}^{(nm)}]_{2 \times 4} & [\gamma_{CM}^{(nm)}]_{2 \times 2} & [\gamma_{CL}^{(nm)}]_{2 \times 2} & [\gamma_{CQ}^{(nm)}]_{2 \times 4} \\ & [\gamma_{PP}^{(nm)}]_{4 \times 4} & [\gamma_{PM}^{(nm)}]_{4 \times 2} & [\gamma_{PL}^{(nm)}]_{4 \times 2} & [\gamma_{PQ}^{(nm)}]_{4 \times 4} \\ & & [\gamma_{MM}^{(nm)}]_{2 \times 2} & & \\ & & & [\gamma_{LL}^{(nm)}]_{2 \times 2} & \\ & [\gamma_{QP}^{(nm)}]_{4 \times 4} & [\gamma_{QM}^{(nm)}]_{4 \times 2} & [\gamma_{QL}^{(nm)}]_{4 \times 2} & [\gamma_{QQ}^{(nm)}]_{4 \times 4} \\ [\gamma_{BP}^{(nm)}]_{1 \times 4} & & & [\gamma_{BL}^{(nm)}]_{1 \times 2} & [\gamma_{BQ}^{(nm)}]_{1 \times 4} & [\gamma_{BB}^{(nm)}]_{1 \times 1} \end{pmatrix} \quad (3.113)$$

where the vanishing elements were left blank so as to optimize readability.

Before presenting the state-of-the-art of each combination in Eq. (3.113), a few general issues may be addressed. First there is the issue of n_f -dependence: while most QCD matrices are known from literature with number of active flavours unfixed, all QED matrices, and the QCD matrices associated with the Q and B blocks, have been provided in Refs. [106, 109] only for $n_f = 5$. Moreover, on that first reference one encounters also the predicament that the operators are written in the so-called *rescaled basis*, where dipole and semileptonic operators are divided by powers of the strong coupling constant, which has the

effect of moving some QCD contributions around, and some QED anomalous dimensions get mixed into their QCD counterparts. For the combinations of blocks that are blind to the rescaling, we still managed to salvage many elements that were omitted in Ref. [109].

Let us proceed, then, one by one, through all the known non-vanishing sub-matrices of Eq. (3.113), writing only the orders that either were not present in Ref. [109], or for which we found an n_f -dependent formulation, referencing at every step whence they were obtained. For all the remaining parts, we refer the reader to that paper. We present $n_f = 5$ cases in matrix form, expanding the n_f -dependent matrices element by element; in order to avoid writing too many zeros, we stick to the non-null matrix elements. Notice that for the C, P, and Q blocks, n_f dependence of the QED anomalous dimension is known in the standard basis [118–120], but n_f -dependent rotation matrices for the three blocks is not available at NLO. The exercise of deriving an n_f -dependent matrix falls from the scope of the present thesis, and is thus left for the future.

CC: The QCD anomalous dimension matrix is known at NNLO, with n_f -dependence [121]:

- $\gamma^{(20)}$

$$\gamma_{\text{CC}}(0,0) = -\frac{145}{3} + n_f \frac{16}{9}, \quad (3.114)$$

$$\gamma_{\text{CC}}(0,1) = -26 + n_f \frac{40}{27}, \quad (3.115)$$

$$\gamma_{\text{CC}}(1,0) = -45 + n_f \frac{20}{3}, \quad (3.116)$$

$$\gamma_{\text{CC}}(1,1) = -\frac{28}{3}, \quad (3.117)$$

- $\gamma^{(30)}$

$$\gamma_{\text{CC}}(0,0) = -\frac{1927}{2} + n_f \frac{257}{9} + n_f^2 \frac{40}{9} + \zeta(3) \left(224 + n_f \frac{160}{3} \right), \quad (3.118)$$

$$\gamma_{\text{CC}}(0,1) = \frac{475}{9} + n_f \frac{362}{27} - n_f^2 \frac{40}{27} - \zeta(3) \left(\frac{896}{3} + n_f \frac{320}{9} \right), \quad (3.119)$$

$$\gamma_{\text{CC}}(1,0) = \frac{475}{9} + n_f \frac{362}{27} - n_f^2 \frac{40}{27} - \zeta(3) \left(\frac{896}{3} + n_f \frac{320}{9} \right), \quad (3.120)$$

$$\gamma_{\text{CC}}(1,1) = \frac{1298}{3} - n_f \frac{76}{3} - \zeta(3) 224, \quad (3.121)$$

where $\zeta(3)$ is Apéry's constant.

CP: Again from Ref. [121], this sub-matrix of Eq. (3.113) is known at NNLO in QCD, with n_f -dependence:

- $\gamma^{(30)}$

$$\gamma_{\text{CP}}(0,0) = \frac{269107}{13122} - n_f \frac{2288}{729} - \zeta(3) \frac{1360}{81}, \quad (3.122)$$

$$\gamma_{\text{CP}}(0,1) = -\frac{2425817}{13122} + n_f \frac{30815}{4374} - \zeta(3) \frac{776}{81}, \quad (3.123)$$

$$\gamma_{\text{CP}}(0,2) = -\frac{343783}{52488} + n_f \frac{392}{729} + \zeta(3) \frac{124}{81}, \quad (3.124)$$

$$\gamma_{\text{CP}}(0,3) = -\frac{37573}{69984} + n_f \frac{35}{972} + \zeta(3) \frac{100}{27}, \quad (3.125)$$

$$\gamma_{\text{CP}}(1,0) = \frac{69797}{2187} + n_f \frac{904}{243} + \zeta(3) \frac{2720}{27}, \quad (3.126)$$

$$\gamma_{\text{CP}}(1,1) = \frac{1457549}{8748} - n_f \frac{22067}{729} - \zeta(3) \frac{2768}{27}, \quad (3.127)$$

$$\gamma_{\text{CP}}(1,2) = -\frac{37889}{8748} - n_f \frac{28}{243} - \zeta(3) \frac{248}{27}, \quad (3.128)$$

$$\gamma_{\text{CP}}(1,3) = \frac{366919}{11664} - n_f \frac{35}{162} - \zeta(3) \frac{110}{9}. \quad (3.129)$$

CM: The QCD anomalous dimension matrix has been determined, in Ref. [122], at NNLO and with n_f -dependence:

- $\gamma^{(10)}$

$$\gamma_{\text{CM}}(0,0) = \frac{8}{243} - Q_u \frac{4}{3}, \quad (3.130)$$

$$\gamma_{\text{CM}}(0,1) = \frac{173}{162}, \quad (3.131)$$

$$\gamma_{\text{CM}}(1,0) = -\frac{16}{81} + Q_u 8, \quad (3.132)$$

$$\gamma_{\text{CM}}(1,1) = \frac{70}{27}, \quad (3.133)$$

- $\gamma^{(20)}$

$$\gamma_{\text{CM}}(0,0) = \frac{12614}{2187} - n_f \frac{64}{2187} - Q_u \frac{374}{27} + n_f Q_u \frac{2}{27}, \quad (3.134)$$

$$\gamma_{\text{CM}}(0,1) = \frac{65867}{5832} + n_f \frac{431}{5832}, \quad (3.135)$$

$$\gamma_{\text{CM}}(1,0) = -\frac{2332}{729} + n_f \frac{128}{729} + Q_u \frac{136}{9} - n_f Q_u \frac{4}{9}, \quad (3.136)$$

$$\gamma_{\text{CM}}(1,1) = \frac{10577}{486} - n_f \frac{917}{972}, \quad (3.137)$$

- $\gamma^{(30)}$

$$\begin{aligned} \gamma_{\text{CM}}(0,0) = & \frac{77506102}{531441} - n_f \frac{875374}{177147} + n_f^2 \frac{560}{19683} - Q_u \frac{9731}{162} + n_f Q_u \frac{11045}{729} + n_f^2 Q_u \frac{316}{729} \\ & + \bar{Q} \frac{3695}{486} + \zeta(3) \left(-\frac{112216}{6561} + n_f \frac{728}{729} + Q_u \frac{25508}{81} - n_f Q_u \frac{64}{81} - \bar{Q} \frac{100}{27} \right), \end{aligned} \quad (3.138)$$

$$\gamma_{\text{CM}}(0,1) = -\frac{421272953}{1417176} - n_f \frac{8210077}{472392} - n_f^2 \frac{1955}{6561} + \zeta(3) \left(-\frac{953042}{2187} - n_f \frac{10381}{486} \right), \quad (3.139)$$

$$\begin{aligned} \gamma_{\text{CM}}(1,0) = & -\frac{15463055}{177147} + n_f \frac{242204}{59049} - n_f^2 \frac{1120}{6561} + Q_u \frac{55748}{27} - n_f Q_u \frac{33970}{243} - n_f^2 Q_u \frac{632}{243} \\ & - \bar{Q} \frac{3695}{81} + \zeta(3) \left(\frac{365696}{2187} - n_f \frac{1168}{243} - Q_u \frac{51232}{27} - n_f Q_u \frac{1024}{27} + \bar{Q} \frac{200}{9} \right), \end{aligned} \quad (3.140)$$

$$\gamma_{\text{CM}}(1,1) = \frac{98548513}{472392} - n_f \frac{5615165}{78732} - n_f^2 \frac{2489}{2187} + \zeta(3) \left(-\frac{607103}{729} - n_f \frac{1679}{81} \right), \quad (3.141)$$

where $Q_u = 2/3$, $Q_d = -1/3$, and $\bar{Q} = n_u Q_u + n_d Q_d$, with n_u and n_d the number of, respectively, up-type and down-type quarks in a given n_f -flavour theory. In Ref. [123], the leading QED anomalous dimension matrix is found for the basis with non-rescaled dipole operators, for $n_f = 5$ only:

- $\gamma_{\text{CM}}^{(01)} = \begin{pmatrix} -\frac{832}{729} & \frac{22}{243} \\ \frac{208}{243} & -\frac{116}{81} \end{pmatrix}.$ (3.142)

PP: Like CC and CP, this sub-matrix has been given in Ref. [121], at NNLO in QCD, with n_f -dependence:

- $\gamma^{(10)}$

$$\gamma_{\text{PP}}(0,1) = -\frac{52}{3}, \quad (3.143)$$

$$\gamma_{\text{PP}}(0,3) = 2, \quad (3.144)$$

$$\gamma_{\text{PP}}(1,0) = -\frac{40}{9}, \quad (3.145)$$

$$\gamma_{\text{PP}}(1,1) = -\frac{160}{9} + n_f \frac{4}{3}, \quad (3.146)$$

$$\gamma_{\text{PP}}(1,2) = \frac{4}{9}, \quad (3.147)$$

$$\gamma_{\text{PP}}(1,3) = \frac{5}{6}, \quad (3.148)$$

$$\gamma_{\text{PP}}(2,1) = -\frac{256}{3}, \quad (3.149)$$

$$\gamma_{\text{PP}}(2,3) = 20, \quad (3.150)$$

$$\gamma_{\text{PP}}(3,0) = -\frac{256}{9}, \quad (3.151)$$

$$\gamma_{\text{PP}}(3,1) = -\frac{544}{9} + n_f \frac{40}{3}, \quad (3.152)$$

$$\gamma_{\text{PP}}(3,2) = \frac{40}{9}, \quad (3.153)$$

$$\gamma_{\text{PP}}(3,3) = \frac{2}{3}, \quad (3.154)$$

- $\gamma^{(20)}$

$$\gamma_{\text{PP}}(0,0) = -\frac{4468}{81}, \quad (3.155)$$

$$\gamma_{\text{PP}}(0,1) = -\frac{29129}{81} - n_f \frac{52}{9}, \quad (3.156)$$

$$\gamma_{\text{PP}}(0,2) = \frac{400}{81}, \quad (3.157)$$

$$\gamma_{\text{PP}}(0,3) = \frac{3493}{108} - n_f \frac{2}{9}, \quad (3.158)$$

$$\gamma_{\text{PP}}(1,0) = -\frac{13678}{243} + n_f \frac{368}{81}, \quad (3.159)$$

$$\gamma_{\text{PP}}(1,1) = -\frac{79409}{243} + n_f \frac{1334}{81}, \quad (3.160)$$

$$\gamma_{\text{PP}}(1,2) = \frac{509}{486} - n_f \frac{8}{81}, \quad (3.161)$$

$$\gamma_{\text{PP}}(1,3) = \frac{13499}{648} - n_f \frac{5}{27}, \quad (3.162)$$

$$\gamma_{\text{PP}}(2,0) = -\frac{244480}{81} - n_f \frac{160}{9}, \quad (3.163)$$

$$\gamma_{\text{PP}}(2,1) = -\frac{29648}{81} - n_f \frac{2200}{9}, \quad (3.164)$$

$$\gamma_{\text{PP}}(2,2) = \frac{23116}{81} + n_f \frac{16}{9}, \quad (3.165)$$

$$\gamma_{\text{PP}}(2,3) = \frac{3886}{27} + n_f \frac{148}{9}, \quad (3.166)$$

$$\gamma_{\text{PP}}(3,0) = \frac{77600}{243} - n_f \frac{1264}{81}, \quad (3.167)$$

$$\gamma_{\text{PP}}(3,1) = -\frac{28808}{243} + n_f \frac{164}{81}, \quad (3.168)$$

$$\gamma_{\text{PP}}(3,2) = -\frac{20324}{243} + n_f \frac{400}{81}, \quad (3.169)$$

$$\gamma_{\text{PP}}(3,3) = -\frac{21211}{162} + n_f \frac{622}{27}, \quad (3.170)$$

• $\gamma^{(30)}$

$$\gamma_{\text{PP}}(0,0) = -\frac{4203068}{2187} + n_f \frac{14012}{243} - \zeta(3) \frac{608}{27}, \quad (3.171)$$

$$\gamma_{\text{PP}}(0,1) = -\frac{18422762}{2187} + n_f \frac{888605}{2916} + n_f^2 \frac{272}{27} + \zeta(3) \left(\frac{39824}{27} + n_f 160 \right), \quad (3.172)$$

$$\gamma_{\text{PP}}(0,2) = \frac{674281}{4374} - n_f \frac{1352}{243} - \zeta(3) \frac{496}{27}, \quad (3.173)$$

$$\gamma_{\text{PP}}(0,3) = \frac{9284531}{11664} - n_f \frac{2798}{81} - n_f^2 \frac{26}{27} - \zeta(3) \left(\frac{1921}{9} + n_f 20 \right), \quad (3.174)$$

$$\gamma_{\text{PP}}(1,0) = -\frac{5875184}{6561} + n_f \frac{217892}{2187} + n_f^2 \frac{472}{81} + \zeta(3) \left(\frac{27520}{81} + n_f \frac{1360}{9} \right), \quad (3.175)$$

$$\gamma_{\text{PP}}(1,1) = -\frac{70274587}{13122} + n_f \frac{8860733}{17496} - n_f^2 \frac{4010}{729} + \zeta(3) \left(\frac{16592}{81} + n_f \frac{2512}{27} \right), \quad (3.176)$$

$$\gamma_{\text{PP}}(1,2) = \frac{2951809}{52488} - n_f \frac{31175}{8748} - n_f^2 \frac{52}{81} - \zeta(3) \left(\frac{3154}{81} + n_f \frac{136}{9} \right), \quad (3.177)$$

$$\gamma_{\text{PP}}(1,3) = \frac{3227801}{8748} - n_f \frac{105293}{11664} - n_f^2 \frac{65}{54} + \zeta(3) \left(\frac{200}{27} - n_f \frac{220}{9} \right), \quad (3.178)$$

$$\gamma_{\text{PP}}(2,0) = -\frac{194951552}{2187} + n_f \frac{358672}{81} - n_f^2 \frac{2144}{81} + \zeta(3) \frac{87040}{27}, \quad (3.179)$$

$$\gamma_{\text{PP}}(2,1) = -\frac{130500332}{2187} - n_f \frac{2949616}{729} + n_f^2 \frac{3088}{27} + \zeta(3) \left(\frac{238016}{27} + n_f 640 \right), \quad (3.180)$$

$$\gamma_{\text{PP}}(2,2) = \frac{14732222}{2187} - n_f \frac{27428}{81} + n_f^2 \frac{272}{81} - \zeta(3) \frac{13984}{27}, \quad (3.181)$$

$$\gamma_{\text{PP}}(2,3) = \frac{16521659}{2916} + n_f \frac{8081}{54} - n_f^2 \frac{316}{27} - \zeta(3) \left(\frac{22420}{9} + n_f 200 \right), \quad (3.182)$$

$$\gamma_{\text{PP}}(3,0) = \frac{162733912}{6561} - n_f \frac{2535466}{2187} + n_f^2 \frac{17920}{243} + \zeta(3) \left(\frac{174208}{81} + n_f \frac{12160}{9} \right), \quad (3.183)$$

$$\gamma_{\text{PP}}(3,1) = \frac{13286236}{6561} - n_f \frac{1826023}{4374} - n_f^2 \frac{159548}{729} - \zeta(3) \left(\frac{24832}{81} + n_f \frac{9440}{27} \right), \quad (3.184)$$

$$\gamma_{\text{PP}}(3,2) = -\frac{22191107}{13122} + n_f \frac{395783}{4374} - n_f^2 \frac{1720}{243} - \zeta(3) \left(\frac{33832}{81} + n_f \frac{1360}{9} \right), \quad (3.185)$$

$$\gamma_{\text{PP}}(3,3) = -\frac{32043361}{8748} + n_f \frac{3353393}{5832} - n_f^2 \frac{533}{81} + \zeta(3) \left(\frac{9248}{27} - n_f \frac{1120}{9} \right). \quad (3.186)$$

PM: The QCD anomalous dimension matrix is known at NNLO, with n_f -dependence [122]:

• $\gamma^{(10)}$

$$\gamma_{\text{PM}}(0,0) = -\frac{176}{81}, \quad (3.187)$$

$$\gamma_{\text{PM}}(0,1) = \frac{14}{27}, \quad (3.188)$$

$$\gamma_{\text{PM}}(1,0) = \frac{88}{243} - n_f \frac{16}{81}, \quad (3.189)$$

$$\gamma_{\text{PM}}(1,1) = \frac{74}{81} - n_f \frac{49}{54}, \quad (3.190)$$

$$\gamma_{\text{PM}}(2, 0) = -\frac{6272}{81}, \quad (3.191)$$

$$\gamma_{\text{PM}}(2, 1) = \frac{1736}{27} + n_f 36, \quad (3.192)$$

$$\gamma_{\text{PM}}(3, 0) = \frac{3136}{243} - n_f \frac{160}{81} + \bar{Q} 48, \quad (3.193)$$

$$\gamma_{\text{PM}}(3, 1) = \frac{2372}{81} + n_f \frac{160}{27}, \quad (3.194)$$

• $\gamma^{(20)}$

$$\gamma_{\text{PM}}(0, 0) = \frac{97876}{729} - n_f \frac{4352}{729} - \bar{Q} \frac{112}{3}, \quad (3.195)$$

$$\gamma_{\text{PM}}(0, 1) = \frac{42524}{243} - n_f \frac{2398}{243}, \quad (3.196)$$

$$\gamma_{\text{PM}}(1, 0) = -\frac{70376}{2187} - n_f \frac{15788}{2187} + n_f^2 \frac{32}{729} - \bar{Q} \frac{140}{9}, \quad (3.197)$$

$$\gamma_{\text{PM}}(1, 1) = -\frac{159718}{729} - n_f \frac{39719}{5832} - n_f^2 \frac{253}{486}, \quad (3.198)$$

$$\gamma_{\text{PM}}(2, 0) = \frac{1764752}{729} - n_f \frac{65408}{729} - \bar{Q} \frac{3136}{3}, \quad (3.199)$$

$$\gamma_{\text{PM}}(2, 1) = \frac{2281576}{243} + n_f \frac{140954}{243} - n_f^2 \frac{14}{3}, \quad (3.200)$$

$$\gamma_{\text{PM}}(3, 0) = \frac{4193840}{2187} - n_f \frac{324128}{2187} + n_f^2 \frac{896}{729} - \bar{Q} \frac{1136}{9} - n_f \bar{Q} \frac{56}{3}, \quad (3.201)$$

$$\gamma_{\text{PM}}(3, 1) = -\frac{3031517}{729} - n_f \frac{15431}{1458} - n_f^2 \frac{6031}{486}, \quad (3.202)$$

• $\gamma^{(30)}$

$$\begin{aligned} \gamma_{\text{PM}}(0, 0) = & \frac{102439553}{177147} - n_f \frac{12273398}{59049} + n_f^2 \frac{5824}{6561} + \bar{Q} \frac{26639}{81} - n_f \bar{Q} \frac{8}{27} + \zeta(3) \left(\frac{3508864}{2187} \right. \\ & \left. - n_f \frac{1904}{243} - \bar{Q} \frac{1984}{9} - n_f \bar{Q} \frac{64}{9} \right), \end{aligned} \quad (3.203)$$

$$\gamma_{\text{PM}}(0, 1) = \frac{3205172129}{472392} - n_f \frac{108963529}{314928} + n_f^2 \frac{58903}{4374} + \zeta(3) \left(-\frac{1597588}{729} + n_f \frac{13028}{81} - n_f^2 \frac{20}{9} \right), \quad (3.204)$$

$$\begin{aligned} \gamma_{\text{PM}}(1, 0) = & -\frac{2493414077}{1062882} - n_f \frac{9901031}{354294} + n_f^2 \frac{243872}{59049} - n_f^3 \frac{1184}{6561} - \bar{Q} \frac{49993}{972} + n_f \bar{Q} \frac{305}{27} \\ & + \zeta(3) \left(-\frac{1922264}{6561} + n_f \frac{308648}{2187} - n_f^2 \frac{1280}{243} + \bar{Q} \frac{1010}{9} - n_f \bar{Q} \frac{200}{27} \right), \end{aligned} \quad (3.205)$$

$$\begin{aligned} \gamma_{\text{PM}}(1, 1) = & -\frac{6678822461}{2834352} + n_f \frac{127999025}{1889568} + n_f^2 \frac{1699073}{157464} + n_f^3 \frac{505}{4374} + \zeta(3) \left(\frac{2312684}{2187} \right. \\ & \left. + n_f \frac{128347}{729} + n_f^2 \frac{920}{81} \right), \end{aligned} \quad (3.206)$$

$$\begin{aligned} \gamma_{\text{PM}}(2, 0) = & \frac{8808397748}{177147} - n_f \frac{174839456}{59049} + n_f^2 \frac{1600}{729} - \bar{Q} \frac{669694}{81} + n_f \bar{Q} \frac{10672}{27} \\ & + \zeta(3) \left(\frac{123543040}{2187} - n_f \frac{207712}{243} + n_f^2 \frac{128}{27} - \bar{Q} \frac{24880}{9} - n_f \bar{Q} \frac{640}{9} \right), \end{aligned} \quad (3.207)$$

$$\begin{aligned} \gamma_{\text{PM}}(2, 1) = & \frac{29013624461}{118098} - n_f \frac{64260772}{19683} - n_f^2 \frac{230962}{243} - n_f^3 \frac{148}{27} + \zeta(3) \left(-\frac{69359224}{729} \right. \\ & \left. - n_f \frac{885356}{81} - n_f^2 \frac{5080}{9} \right), \end{aligned} \quad (3.208)$$

$$\begin{aligned} \gamma_{\text{PM}}(3,0) = & \frac{7684242746}{531441} - n_f \frac{351775414}{177147} - n_f^2 \frac{479776}{59049} - n_f^2 \frac{11456}{6561} + \bar{Q} \frac{3950201}{243} - n_f \bar{Q} \frac{130538}{81} \\ & - n_f^2 \bar{Q} \frac{592}{81} + \zeta(3) \left(\frac{7699264}{6561} + n_f \frac{2854976}{2187} - n_f^2 \frac{12320}{243} - \bar{Q} \frac{108584}{9} - n_f \bar{Q} \frac{1136}{27} \right), \end{aligned} \quad (3.209)$$

$$\begin{aligned} \gamma_{\text{PM}}(3,1) = & -\frac{72810260309}{708588} + n_f \frac{2545824851}{472392} - n_f^2 \frac{33778271}{78732} - n_f^3 \frac{3988}{2187} + \zeta(3) \left(-\frac{61384768}{2187} \right. \\ & \left. - n_f \frac{685472}{729} + n_f^2 \frac{350}{81} \right). \end{aligned} \quad (3.210)$$

In Ref. [123], the leading QED anomalous dimension matrix is found for the basis with non-rescaled dipole operators, for $n_f = 5$ only:

$$\bullet \gamma_{\text{PM}}^{(01)} = \begin{pmatrix} -\frac{20}{243} & \frac{20}{81} \\ \frac{176}{729} & \frac{14}{243} \\ \frac{22712}{243} & \frac{1328}{81} \\ -\frac{6272}{729} & -\frac{1180}{243} \end{pmatrix}. \quad (3.211)$$

MM: For this block, we cite Ref. [124], and write the following expressions of the QCD anomalous dimension matrix up to NNLO, with n_f -dependence:

• $\gamma^{(10)}$

$$\gamma_{\text{MM}}(0,0) = \frac{32}{3}, \quad (3.212)$$

$$\gamma_{\text{MM}}(1,0) = Q_d \frac{32}{3}, \quad (3.213)$$

$$\gamma_{\text{MM}}(1,1) = \frac{28}{3}, \quad (3.214)$$

• $\gamma^{(20)}$

$$\gamma_{\text{MM}}(0,0) = \frac{1936}{9} - n_f \frac{224}{27}, \quad (3.215)$$

$$\gamma_{\text{MM}}(1,0) = Q_d \frac{368}{3} - n_f Q_d \frac{224}{27}, \quad (3.216)$$

$$\gamma_{\text{MM}}(1,1) = \frac{1456}{9} - n_f \frac{61}{27}, \quad (3.217)$$

• $\gamma^{(30)}$

$$\gamma_{\text{MM}}(0,0) = \frac{307448}{81} - n_f \frac{23776}{81} - n_f^2 \frac{352}{81} + \zeta(3) \left(-\frac{1856}{27} - n_f \frac{1280}{9} \right), \quad (3.218)$$

$$\begin{aligned} \gamma_{\text{MM}}(1,0) = & -\bar{Q} \frac{1600}{27} + Q_d \frac{159872}{81} - n_f Q_d \frac{17108}{81} - n_f^2 Q_d \frac{352}{81} + \zeta(3) \left(\bar{Q} \frac{640}{9} - Q_d \frac{1856}{27} \right. \\ & \left. - n_f Q_d \frac{1280}{9} \right), \end{aligned} \quad (3.219)$$

$$\gamma_{\text{MM}}(1,1) = \frac{268807}{81} - n_f \frac{4343}{27} - n_f^2 \frac{461}{81} + \zeta(3) \left(-\frac{28624}{27} - n_f \frac{1312}{9} \right). \quad (3.220)$$

Regarding the QED anomalous dimension matrix, we read the following contributions from Ref. [106], which has fixed $n_f = 5$:

$$\bullet \gamma_{\text{MM}}^{(01)} = \begin{pmatrix} \frac{16}{9} & 0 \\ -\frac{8}{3} & \frac{8}{9} \end{pmatrix}, \quad (3.221)$$

$$\bullet \gamma_{\text{MM}}^{(11)} = \begin{pmatrix} -\frac{256}{27} & -\frac{152}{9} \\ \frac{128}{81} & -\frac{40}{27} \end{pmatrix}. \quad (3.222)$$

QP: Once more from Ref. [106], here are this combination's QED anomalous dimensions, fixed at $n_f = 5$:

$$\bullet \gamma_{\text{QP}}^{(01)} = \begin{pmatrix} \frac{40}{27} & 0 & -\frac{4}{27} & 0 \\ 0 & \frac{40}{27} & 0 & -\frac{4}{27} \\ \frac{256}{27} & 0 & -\frac{40}{27} & 0 \\ 0 & \frac{256}{27} & 0 & -\frac{40}{27} \end{pmatrix}, \quad (3.223)$$

$$\bullet \gamma_{\text{QP}}^{(11)} = \begin{pmatrix} -\frac{2240}{81} & \frac{39392}{729} & \frac{224}{81} & -\frac{92}{27} \\ \frac{2176}{243} & \frac{84890}{2187} & -\frac{184}{243} & -\frac{224}{81} \\ -\frac{23552}{81} & \frac{399776}{729} & \frac{2240}{81} & -\frac{752}{27} \\ \frac{23296}{243} & \frac{933776}{2187} & -\frac{1504}{243} & -\frac{2030}{81} \end{pmatrix}. \quad (3.224)$$

QM: The QCD anomalous dimension matrix was derived in Ref. [123] for the non-recaled basis, at LO and with $n_f = 5$:

$$\bullet \gamma_{\text{QM}}^{(01)} = \begin{pmatrix} \frac{176}{243} & -\frac{14}{81} \\ -\frac{136}{729} & -\frac{295}{486} \\ \frac{6272}{243} & -\frac{764}{81} \\ \frac{39152}{729} & -\frac{1892}{243} \end{pmatrix}. \quad (3.225)$$

QQ: As a rescaling-blind sub-matrix of the anomalous dimension, we take its first two orders in QED from Ref. [106], given with $n_f = 5$:

$$\bullet \gamma_{\text{QQ}}^{(01)} = \begin{pmatrix} \frac{332}{27} & 0 & -\frac{2}{9} & 0 \\ \frac{32}{81} & \frac{20}{9} & 0 & -\frac{2}{9} \\ \frac{3152}{27} & 0 & -\frac{20}{9} & 0 \\ \frac{512}{81} & \frac{128}{9} & 0 & -\frac{20}{9} \end{pmatrix}, \quad (3.226)$$

$$\bullet \gamma_{\text{QQ}}^{(11)} = \begin{pmatrix} -\frac{5888}{729} & \frac{13916}{81} & \frac{112}{27} & -\frac{812}{81} \\ -\frac{2552}{2187} & \frac{15638}{243} & -\frac{176}{81} & -\frac{2881}{486} \\ -\frac{90944}{729} & \frac{90128}{81} & \frac{1120}{27} & -\frac{1748}{81} \\ \frac{1312}{2187} & \frac{102488}{243} & -\frac{1592}{81} & -\frac{6008}{243} \end{pmatrix}. \quad (3.227)$$

BP: This mixing constitutes a row vector, which has a non-zero element at NLO in QED, as given in Ref. [106], for $n_f = 5$:

$$\bullet \gamma_{\text{BP}}^{(11)} = \begin{pmatrix} 0 & -\frac{232}{81} & 0 & 0 \end{pmatrix}. \quad (3.228)$$

BQ: A row vector as well, these QED entries can be obtained from Ref. [106], for $n_f = 5$:

$$\bullet \gamma_{\text{BQ}}^{(01)} = \begin{pmatrix} -\frac{16}{9} & 0 & 0 & 0 \end{pmatrix}, \quad (3.229)$$

$$\bullet \gamma_{\text{BQ}}^{(11)} = \begin{pmatrix} 0 & \frac{580}{27} & 0 & -\frac{94}{27} \end{pmatrix}. \quad (3.230)$$

BB: Finally, the QED contributions to this matrix element read from Ref. [106], for $n_f = 5$:

$$\bullet \gamma_{\text{BB}}^{(01)} = \frac{4}{3}, \quad (3.231)$$

$$\bullet \gamma_{\text{BB}}^{(11)} = -\frac{388}{9}. \quad (3.232)$$

3.2.4 Renormalization Group Evolution

Regarding the running of WCs from the matching scale down to the typical scale of B decays, μ_b , we follow once more Ref. [109], which stands as the current last word on the evolution with both QCD and QED contributions. The system of RGEs for $\tilde{\alpha}_s$ and $\tilde{\alpha}_e$ can be written as

$$\begin{cases} \mu \frac{d\tilde{\alpha}_s}{d\mu} = -2\tilde{\alpha}_s^2 \sum_{n,m=0} \beta_{nm}^s \tilde{\alpha}_s^n \tilde{\alpha}_s^m \\ \mu \frac{d\tilde{\alpha}_e}{d\mu} = +2\tilde{\alpha}_e^2 \sum_{n,m=0} \beta_{nm}^e \tilde{\alpha}_e^n \tilde{\alpha}_s^m \end{cases}, \quad (3.233)$$

where the β_{n0} correspond to the already mentioned pure-QCD coefficients, β_n , given, in the $\overline{\text{MS}}$ scheme, in Appendix A.1. Solving for $\tilde{\alpha}_s$ with an initial condition at μ_W , perturbatively in $\tilde{\alpha}_s(\mu_W)$ and $\tilde{\alpha}_e(\mu_W)$, but exactly in the denominators of the LO solution,

$$v_s = 1 + 2\beta_{00}^s \tilde{\alpha}_s(\mu_W) \ln \frac{\mu}{\mu_W}, \quad (3.234)$$

$$v_e = 1 - 2\beta_{00}^e \tilde{\alpha}_e(\mu_W) \ln \frac{\mu}{\mu_W}, \quad (3.235)$$

one obtains, including all 3-loop contributions plus the QCD NNNLO term [109]:

$$\begin{aligned}
\tilde{\alpha}_s(\mu) = & \frac{\tilde{\alpha}_s(\mu_W)}{v_s} - \frac{\tilde{\alpha}_s^2(\mu_W)}{v_s^2} \left(\frac{\beta_{10}^s}{\beta_{00}^s} \ln v_s - \frac{\beta_{01}^s}{\beta_{00}^e} \ln v_e \right) + \frac{\tilde{\alpha}_s^3(\mu_W)}{v_s^3} \left[\frac{\beta_{20}^s}{\beta_{00}^s} (1 - v_s) \right. \\
& + \left. \left(\frac{\beta_{10}^s}{\beta_{00}^s} \right)^2 (\ln^2 v_s - \ln v_s + v_s - 1) + \left(\frac{\beta_{01}^s}{\beta_{00}^e} \right)^2 \ln^2 v_e + \frac{\beta_{01}^s \beta_{10}^s}{\beta_{00}^s \beta_{00}^e} (-2 \ln v_s \ln v_e + \rho v_e \ln v_e) \right] \\
& + \frac{\tilde{\alpha}_s^2(\mu_W) \tilde{\alpha}_e(\mu_W)}{v_s^2 v_e} \left[\frac{\beta_{02}^s}{\beta_{00}^e} (v_e - 1) + \frac{\beta_{11}^s}{\beta_{00}^s} \rho v_e \ln \frac{v_e}{v_s} + \frac{\beta_{01}^s \beta_{10}^e}{(\beta_{00}^e)^2} (\ln v_e - v_e + 1) + \frac{\beta_{01}^s \beta_{10}^s}{(\beta_{00}^s)^2} \rho \ln v_s \right. \\
& + \left. \frac{\beta_{01}^s \beta_{01}^e}{\beta_{00}^s \beta_{00}^e} \left(\rho v_e \ln \frac{v_s}{v_e} - \ln v_s \right) \right] + \frac{\tilde{\alpha}_s^4(\mu_W)}{v_s^4} \left[\frac{\beta_{30}^s}{\beta_{00}^s} \frac{1 - v_s^2}{2} + \frac{\beta_{20}^s \beta_{10}^s}{(\beta_{00}^s)^2} ((2v_s - 3) \ln v_s + v_s^2 - v_s) \right. \\
& + \left. \left(\frac{\beta_{10}^s}{\beta_{00}^s} \right)^3 \left(-\ln^3 v_s + \frac{5}{2} \ln^2 v_s + 2(1 - v_s) \ln v_s - \frac{1}{2} (v_s - 1)^2 \right) \right] + \mathcal{O}(\tilde{\alpha}_s^5, \tilde{\alpha}_s^2 \tilde{\alpha}_e^2, \tilde{\alpha}_s^3 \tilde{\alpha}_e),
\end{aligned} \tag{3.236}$$

where

$$\rho = \frac{\beta_{00}^s \tilde{\alpha}_s(\mu_W)}{\beta_{00}^s \tilde{\alpha}_s(\mu_W) + \beta_{00}^e \tilde{\alpha}_e(\mu_W)}. \tag{3.237}$$

By the same token, the solution for $\tilde{\alpha}_e$ follows much the same structure, with obvious replacements applied: $\tilde{\alpha}_s \leftrightarrow \tilde{\alpha}_e$, $v_s \leftrightarrow v_e$, and $\beta_{nm}^s \leftrightarrow -\beta_{nm}^e$. For this coupling, we keep the terms up to $\mathcal{O}(\tilde{\alpha}_e^3, \tilde{\alpha}_e^2 \tilde{\alpha}_s^2)$. As with the pure-QCD coefficients, the expressions of β_{nm}^e , and those of β_{nm}^s with $m \neq 0$ are pushed to Appendix A.2.

To solve the RGE of the WCs, in Eq. (3.44), one acknowledges that $\tilde{\alpha}_e \ll \tilde{\alpha}_s$ and defines

$$\lambda = \frac{\beta_{00}^e}{\beta_{00}^s} \kappa(\mu_W), \quad \omega = 2 \beta_{00}^s \tilde{\alpha}_s(\mu_W), \tag{3.238}$$

on which one will expand the evolver, to $\mathcal{O}(\omega^3, \lambda^3, \omega^2 \lambda^2)$. It also proves useful to define the quantities

$$\begin{aligned}
b_1 = \frac{\beta_{10}^s}{2(\beta_{00}^s)^2}, \quad b_2 = \frac{\beta_{20}^s}{2(\beta_{00}^s)^2} - b_1^2, \quad b_3 = \frac{\beta_{01}^s}{2\beta_{00}^s \beta_{00}^e}, \\
b_4 = \frac{\beta_{11}^s}{4(\beta_{00}^s)^2 \beta_{00}^e} - 2b_1 b_3, \quad b_5 = \frac{\beta_{01}^e}{2\beta_{00}^s \beta_{00}^e} - b_1
\end{aligned} \tag{3.239}$$

together with a normalized version of the anomalous dimension matrices we encountered in the previous subsection:

$$W^{(nm)} = \frac{(\gamma^{(nm)})^T}{2(\beta_{00}^s)^n (\beta_{00}^e)^m}. \tag{3.240}$$

It can be shown that, recalling $\eta = \tilde{\alpha}_s(\mu_W)/\tilde{\alpha}_e(\mu_W)$, the RGE can be cast as [109]:

$$\frac{d}{d\eta} \vec{C} = \frac{1}{\eta} \left[W^{(10)} + \sum_{k=-2}^2 B^{(k)} \eta^k + \omega \lambda^2 b_5 W^{(01)} \eta \ln \eta + \mathcal{O}(\omega^3, \lambda^3, \omega^2 \lambda^2) \right] \vec{C}, \tag{3.241}$$

where $B^{(k)}$ are η -independent matrices:

$$B^{(-2)} = \omega^2 \left(W^{(30)} - b_1 W^{(20)} - b_2 W^{(10)} \right), \tag{3.242}$$

$$B^{(-1)} = \omega \left(W^{(20)} - b_1 W^{(10)} \right) + \omega^2 \lambda \left(W^{(21)} - b_1 W^{(11)} - b_2 W^{(01)} - b_3 W^{(20)} - b_4 W^{(10)} \right), \tag{3.243}$$

$$B^{(0)} = \omega \lambda (1 - \lambda) \left(W^{(11)} - b_1 W^{(01)} - b_3 W^{(10)} \right), \tag{3.244}$$

$$B^{(1)} = \lambda (1 - \lambda) W^{(01)} + \omega \lambda^2 \left(W^{(02)} + W^{(11)} - (b_1 + b_3) W^{(01)} - b_3 W^{(10)} \right), \tag{3.245}$$

$$B^{(2)} = \lambda^2 W^{(01)}. \tag{3.246}$$

In this form, the evolution of each WC becomes

$$C_a(\mu) = V_{ai} \left\{ D_{ij}(\eta) + \sum_{k=-2}^2 E_{ij}^{(k)} f_{ij}^{(k)}(\eta) + \sum_{k,l=-2}^2 \sum_p \left[E_{ip}^{(k)} E_{pj}^{(l)} \right] g_{ipj}^{(kl)}(\eta) \right. \\ \left. + \sum_{k,l,m=-2}^2 \sum_{p,q} \left[E_{ip}^{(k)} E_{pq}^{(l)} E_{qj}^{(m)} \right] h_{ipqj}^{(klm)}(\eta) + R_{ij} r_{ij}^{(1)}(\eta) + \mathcal{O}(\omega^3, \lambda^3, \omega^2 \lambda^2) \right\} V_{ib}^{-1} C_b(\mu_W), \quad (3.247)$$

where V is the matrix that diagonalizes the LO anomalous dimension matrix,

$$\left[V^{-1} W^{(10)} V \right]_{ij} = \theta_i \delta_{ij}, \quad (3.248)$$

such that the matrices D , $E^{(k)}$, and R are equal to:

$$D_{ij} = \eta^{\theta_i} \delta_{ij}, \quad (3.249)$$

$$E_{ij}^{(k)} = \left[V^{-1} B^{(k)} V \right]_{ij}, \quad (3.250)$$

$$R_{ij} = \omega \lambda^2 b_5 \left[V^{-1} W^{(01)} V \right]_{ij}. \quad (3.251)$$

The remaining objects are tensors, which are functions of both η and the eigenvalues θ_i :

$$f_{ij}^{(k)}(\eta) = \begin{cases} \eta^{\theta_i} \ln \eta, & \text{if } \theta_j + k - \theta_i = 0, \\ \frac{1}{\theta_j + k - \theta_i}, & \text{otherwise,} \end{cases} \quad (3.252)$$

$$r_{ij}^{(k)}(\eta) = \begin{cases} \frac{1}{2} \eta^{\theta_i} \ln^2 \eta, & \text{if } \theta_j + k - \theta_i = 0, \\ \frac{1}{\theta_j + k - \theta_i} \left(\eta^{\theta_i + k} \ln \eta - f_{ij}^{(k)}(\eta) \right), & \text{otherwise,} \end{cases} \quad (3.253)$$

$$g_{ipj}^{(kl)}(\eta) = \begin{cases} r_{ip}^{(k)}(\eta), & \text{if } \theta_j + l - \theta_p = 0, \\ \frac{1}{\theta_j + l - \theta_p} \left(f_{ij}^{(k+l)}(\eta) - f_{ip}^{(k)}(\eta) \right), & \text{otherwise,} \end{cases} \quad (3.254)$$

$$h_{ipqj}^{(klm)}(\eta) = \begin{cases} \frac{1}{6} \eta^{\theta_i} \ln^3 \eta & \text{if } \theta_p + k - \theta_i = \theta_q + l - \theta_p = \\ & = \theta_j + m - \theta_q = 0, \\ \frac{1}{\theta_p + k - \theta_i} \left(\frac{1}{2} \eta^{\theta_p + k} \ln^2 \eta - r_{ip}^{(k)}(\eta) \right), & \text{if } \theta_q + l - \theta_p = \theta_j + m - \theta_q = 0, \\ \frac{1}{\theta_q + l - \theta_p} \left(r_{iq}^{(k+l)}(\eta) - g_{ipq}^{(kl)}(\eta) \right), & \text{if } \theta_j + m - \theta_q = 0, \\ \frac{1}{\theta_j + m - \theta_q} \left(g_{ipj}^{(k,l+m)}(\eta) - g_{ipq}^{(kl)}(\eta) \right), & \text{otherwise.} \end{cases} \quad (3.255)$$

This solution to the RGE has WCs at the low scale, obtained from a series written in terms of, and truncated in, couplings at the high scale. If one wants to express the low scale coefficients as

$$C_a = \sum_{n,m=0}^2 \tilde{\alpha}_s^n(\mu_b) \kappa^m(\mu_b) C_a^{(nm)}(\mu_b) + \mathcal{O}(\tilde{\alpha}_s^3, \kappa^3), \quad (3.256)$$

one must take into consideration

$$\tilde{\alpha}_s(\mu_W) = \eta \tilde{\alpha}_s(\mu_b), \quad (3.257)$$

which holds at all orders, and, obtainable from the inversion of the solution to the RGE of the coupling constant, the following relation [109]:

$$\kappa(\mu_W) = \frac{\kappa(\mu_b)}{\eta} + \frac{\beta_{00}^e}{\beta_{00}^s} \frac{1-\eta}{\eta^2} \kappa^2(\mu_b) + \left(\frac{\beta_{00}^e \beta_{10}^s}{(\beta_{00}^s)^2} - \frac{\beta_{01}^e}{\beta_{00}^s} \right) \frac{\ln \eta}{\eta} \tilde{\alpha}_s(\mu_b) \kappa^2(\mu_b) + \mathcal{O}(\kappa^2 \tilde{\alpha}_s, \kappa^3). \quad (3.258)$$

3.3 The Exclusive Sector

The inclusive decay $B \rightarrow X_s \gamma$ notwithstanding, it being the “K2 mountain” of weak decays [8], which branching fraction has been measured at percent level [125–127] and to which we reserve a brief spot in this section, experimental novelty and, more importantly, flavour anomalies lie nowadays with exclusive channels of the $b \rightarrow s$ transition. At the hadronic level, these comprehend rare semileptonic and radiative decays into vector mesons, such as $B \rightarrow K^* \ell^+ \ell^- / \gamma$, for a spectator d -quark, and $B \rightarrow \phi \ell^+ \ell^- / \gamma$, for a spectator s -quark; the rare semileptonic mode $B \rightarrow K \ell^+ \ell^- / \gamma$; and, when b and s form themselves a bound state, the leptonic B decay into muons, $B_s \rightarrow \mu^+ \mu^-$. Baryonic modes, like $\Lambda_b \rightarrow \Lambda \ell^+ \ell^-$, still have large uncertainties associated [128] and will, thus, not be considered.

We dedicate this section to the observables whose experimental information we have used in the global analysis that follows this chapter. The specifications of how we treat hadronic contributions in the semileptonic (radiative) modes, plus a comment on the ratios sensible to lepton flavour universality, are subsequently provided.

3.3.1 Definition of Observables

The K^* channel is very rich from the quantity of information standpoint. The full semileptonic decay is, in fact, $\bar{B} \rightarrow \bar{K}^* [\rightarrow \bar{K} \pi] \ell^+ \ell^-$, where $\bar{K} = \bar{K}^0$ or \bar{K}^- , and $\pi = \pi^+$ or π^0 . This allows a precise angular reconstruction of the decay, resulting in twelve different observables. Since different conventions to the kinematic variables can be found in literature, it is important to define the one we use. With an on-shell K^* , the decay is completely determined by four independent kinematic variables: the dilepton invariant mass squared, q^2 , and the three angles: ϕ , the angle between the normals to the planes defined by $K^- \pi^+$ and $\ell^+ \ell^-$, in the B meson rest frame; θ_K , the angle between the direction of flight of the \bar{B} and the ℓ^- , in the dilepton rest frame; θ_K , the angle between the direction of motion of the \bar{B} and the \bar{K} in the dimension the dimeson rest frame. Thus, the full differential decay rate can be shown to be [129, 130]:

$$\begin{aligned} \frac{d^4 \Gamma}{dq^2 d(\cos \theta_\ell) d(\cos \theta_K) d\phi} = & \frac{9}{32} \left(I_{1s} \sin^2 \theta_K + I_{1c} \cos^2 \theta_K + (I_{2s} \sin^2 \theta_K + I_{2c} \cos^2 \theta_K) \cos 2\theta_\ell \right. \\ & + I_3 \sin^2 \theta_K \sin^2 \theta_\ell \cos 2\phi + I_4 \sin 2\theta_K \sin 2\theta_\ell \cos \phi \\ & + I_5 \sin 2\theta_K \sin \theta_\ell \cos \phi + (I_{6s} \sin^2 \theta_K + I_{6c} \cos^2 \theta_K) \cos \theta_\ell \\ & + I_7 \sin 2\theta_K \sin \theta_\ell \sin \phi + I_8 \sin 2\theta_K \sin 2\theta_\ell \sin \phi \\ & \left. + I_9 \sin^2 \theta_K \sin^2 \theta_\ell \sin 2\phi \right). \end{aligned} \quad (3.259)$$

The angular coefficients I_i are functions of q^2 , and their expressions depend on the choice of basis used to describe $B \rightarrow V$ form factors. Here, we follow Ref. [24] and write these coefficients in terms of the helicity amplitudes that appear in the SM,

$$I_{1s} = F \left(\frac{1}{2} (|H_V^0|^2 + |H_A^0|^2) + |H_P|^2 + \frac{2m_\ell^2}{q^2} (|H_V^0|^2 - |H_A^0|^2) \right), \quad (3.260)$$

$$I_{1c} = F \left(\frac{\beta^2 + 2}{8} (|H_V^+|^2 + |H_V^-|^2 + |H_A^+|^2 + |H_A^-|^2) + \frac{m_\ell^2}{q^2} (|H_V^+|^2 - |H_V^-|^2 - |H_A^+|^2 + |H_A^-|^2) \right), \quad (3.261)$$

$$I_{2c} = -F \frac{\beta^2}{2} (|H_V^0|^2 + |H_A^0|^2), \quad (3.262)$$

$$I_{2s} = F \frac{\beta^2}{8} (|H_V^+|^2 + |H_V^-|^2 + |H_A^+|^2 + |H_A^-|^2), \quad (3.263)$$

$$I_3 = -\frac{F}{2} \text{Re}[H_V^+(H_V^-)^* + H_A^+(H_A^-)^*], \quad (3.264)$$

$$I_4 = F \frac{\beta^2}{4} \text{Re}[(H_V^- - H_V^+)(H_A^0)^* + (H_A^- - H_A^+)(H_V^0)^*], \quad (3.265)$$

$$I_5 = F \frac{\beta}{4} \text{Re}[(H_V^+ + H_V^-)(H_V^0)^* + (H_A^+ + H_A^-)(H_A^0)^*], \quad (3.266)$$

$$I_{6s} = F \beta \text{Re}[H_V^-(H_A^-)^* - H_V^+(H_A^+)^*], \quad (3.267)$$

$$I_{6c} = 0, \quad (3.268)$$

$$I_7 = F \frac{\beta}{2} \text{Im}[(H_A^+ + H_A^-)(H_V^0)^* + (H_V^+ + H_V^-)(H_A^0)^*], \quad (3.269)$$

$$I_8 = F \frac{\beta^2}{4} \text{Im}[(H_V^- - H_V^+)(H_V^0)^* + (H_A^- - H_A^+)(H_A^0)^*], \quad (3.270)$$

$$I_9 = F \frac{\beta^2}{4} \text{Im}[H_V^+(H_V^-)^* + H_A^+(H_A^-)^*], \quad (3.271)$$

where H_V^λ , H_A^λ , and H_P are helicity amplitudes, and

$$F = \frac{\sqrt{\lambda} \beta q^2}{3 \times 2^5 \pi^3 m_B^3} \text{BR}(K^* \rightarrow K\pi), \quad \beta = \sqrt{1 - \frac{4m_\ell^2}{q^2}}, \quad (3.272)$$

$$\lambda = m_B^4 + m_V^4 + q^4 - 2(m_B^2 m_V^2 + m_B^2 q^2 + m_V^2 q^2).$$

We shall come back to the helicity basis and the form of each helicity amplitude in the next subsection.

For the CP-conjugate decay, one uses the angles as defined in the \bar{B} decay with $K^- \rightarrow K^+$, but still referring to ℓ^- (corresponding to $\theta_l \rightarrow \theta_l - \pi$ and $\phi \rightarrow -\phi$), such that with conjugated CKM elements the angular coefficients become:

$$I_{1s(c),2s(c),3,4,7} \longrightarrow \bar{I}_{1s(c),2s(c),3,4,7}, \quad I_{5,6s(c),8,9} \longrightarrow -\bar{I}_{5,6s(c),8,9}. \quad (3.273)$$

Given both $\bar{B} \rightarrow \bar{K}^* \ell^+ \ell^-$ and its CP-conjugate decay, $B \rightarrow K^* \ell^+ \ell^-$, produce the same number of observables, it is useful to define twelve CP-averaged combinations. Two different prescriptions have been advocated in the literature: while the authors of Ref. [130] have proposed

$$S_i = \left(I_i + \bar{I}_i \right) \left/ \frac{d(\Gamma + \bar{\Gamma})}{dq^2} \right., \quad (3.274)$$

together with twelve CP asymmetries,

$$A_i = \left(I_i - \bar{I}_i \right) \left/ \frac{d(\Gamma + \bar{\Gamma})}{dq^2} \right., \quad (3.275)$$

most experiments employ the so-called ‘‘clean’’ observables championed by the authors of Ref. [14]:

$$\Sigma_i = \frac{I_i + \bar{I}_i}{2}, \quad \Delta_i = \frac{I_i - \bar{I}_i}{2}. \quad (3.276)$$

With the Σ_i in hand, one goes one step further on, and defines the following angular observables:

$$\begin{aligned} P_1 &= \frac{\Sigma_3}{2\Sigma_{2s}}, & P_2 &= \frac{\Sigma_{6s}}{8\Sigma_{2s}}, & P_3 &= \frac{\Sigma_9}{4\Sigma_{2s}}, \\ P'_4 &= \frac{\Sigma_4}{\sqrt{-\Sigma_{2s}\Sigma_{2c}}}, & P'_5 &= \frac{\Sigma_5}{2\sqrt{-\Sigma_{2s}\Sigma_{2c}}}, & P'_6 &= \frac{\Sigma_7}{2\sqrt{-\Sigma_{2s}\Sigma_{2c}}}, & P'_8 &= \frac{\Sigma_8}{\sqrt{-\Sigma_{2s}\Sigma_{2c}}}. \end{aligned} \quad (3.277)$$

The traditional observables themselves, branching fraction – here CP-averaged –, longitudinal component, and forward-backward asymmetry, can be written as functions of the angular coefficients Σ_i as well:

$$\Gamma' = \frac{1}{2} \frac{d\Gamma + d\bar{\Gamma}}{dq^2} = \frac{1}{4} [(3\Sigma_{1c} - \Sigma_{2c}) + 2(3\Sigma_{1s} - \Sigma_{2s})], \quad (3.278)$$

$$F_L = \frac{3\Sigma_{1c} - \Sigma_{2c}}{4\Gamma'}, \quad (3.279)$$

$$A_{FB} = \frac{3\Sigma_{6s}}{4\Gamma'}. \quad (3.280)$$

An aside must be reserved for the fact that there is a difference in the conventions used by the theoretical community, and at the LHCb for experimental measurements. Nevertheless, the numerical results between the two are related, that relation being [131]:

$$P_2^{\text{LHCb}} = -P_2^{\text{T}}, \quad P_4^{\text{LHCb}} = -\frac{1}{2}P_4^{\text{T}}, \quad P_6^{\text{LHCb}} = -P_6^{\text{T}}, \quad P_8^{\text{LHCb}} = \frac{1}{2}P_8^{\text{T}}, \quad (3.281)$$

where the observables marked with T correspond to theory definitions. Also concerning the experimental side of things, these observables are, in fact, measured in binned data, divided in regions of the dilepton invariant mass. The binning of the angular coefficients is done by integrating in each q^2 interval,

$$\langle \Sigma_i \rangle = \int_{q_{\text{min}}^2}^{q_{\text{max}}^2} dq^2 \Sigma_i(q^2); \quad (3.282)$$

as such, one notes that for the angular observables, relevant are the ratios of binned coefficients, rather than the direct binning of ratios [15]:

$$\begin{aligned} \langle P_1 \rangle &= \frac{\langle \Sigma_3 \rangle}{2\langle \Sigma_{2s} \rangle}, & P_2 &= \frac{\langle \Sigma_{6s} \rangle}{8\langle \Sigma_{2s} \rangle}, & P_3 &= \frac{\langle \Sigma_9 \rangle}{4\langle \Sigma_{2s} \rangle}, \\ \langle P_4' \rangle &= \frac{\langle \Sigma_4 \rangle}{\sqrt{-\langle \Sigma_{2s} \Sigma_{2c} \rangle}}, & \langle P_5' \rangle &= \frac{\langle \Sigma_5 \rangle}{2\sqrt{-\langle \Sigma_{2s} \Sigma_{2c} \rangle}}, & \langle P_6' \rangle &= \frac{\langle \Sigma_7 \rangle}{2\sqrt{-\langle \Sigma_{2s} \Sigma_{2c} \rangle}}, & \langle P_8' \rangle &= \frac{\langle \Sigma_8 \rangle}{\sqrt{-\langle \Sigma_{2s} \Sigma_{2c} \rangle}}. \end{aligned} \quad (3.283)$$

In the same vein, the binned branching fraction, F_L , and A_{FB} are defined as

$$\langle \Gamma' \rangle = \langle \Sigma_{1c} + 4\Sigma_{2s} \rangle, \quad \langle F_L \rangle = \frac{\langle 3\Sigma_{1c} - \Sigma_{2c} \rangle}{4\langle \Gamma' \rangle}, \quad \langle A_{FB} \rangle = \frac{3\langle \Sigma_{6s} \rangle}{4\langle \Gamma' \rangle}. \quad (3.284)$$

All we have been defining for K^* can be used for any $B \rightarrow V\ell^+\ell^-$ decay [24]. Therefore, for the decay with ϕ , one defines everything much in the same way. Regarding the other semileptonic decay, $B \rightarrow K\ell^+\ell^-$, the main distinction stems from its different decay form factors and different kinematics: a decay into a pseudoscalar meson, $B \rightarrow P$, whereas the previous cases were decays into vector mesons. Still, once the form factors are translated to helicity amplitudes, one proceeds in defining exactly the same kind of observables. A similar remark can be made for both of the exclusive radiative decays we're using in our global analysis, $B \rightarrow K^*\gamma$ and $B \rightarrow \phi\gamma$: their helicity amplitudes are a subset of those involved in the $B \rightarrow V\ell^+\ell^-$ decay, this meaning that, although with a reduced complexity, they follow the framework we've been addressing. We will touch upon this when we discuss the hadronic uncertainties in these channels.

For $B_s \rightarrow \mu^+\mu^-$, we have used its branching fraction. Since there is a sizeable decay width difference in the B_s system [7],

$$y_s = \frac{\Delta\Gamma_s}{2\Gamma_s} \simeq 0.065, \quad (3.285)$$

implies that there is a deviation between the branching fraction at a time $t = 0$, and the time-integrated, and CP-averaged, branching fraction. Defining the mass-eigenstate rate asymmetry by

$$A_{\mu\mu} = \frac{\Gamma(B_s^H \rightarrow \mu^+ \mu^-) - \Gamma(B_s^L \rightarrow \mu^+ \mu^-)}{\Gamma(B_s^H \rightarrow \mu^+ \mu^-) + \Gamma(B_s^L \rightarrow \mu^+ \mu^-)} \quad (3.286)$$

where B_s^H and B_s^L denote, respectively, the heavy and light eigenstates of the B_s system, the relation between both branching fractions is

$$\overline{\text{BR}}(B_s \rightarrow \mu^+ \mu^-) = \frac{1 + A_{\mu\mu} y_s}{1 - y_s^2} \text{BR}^{[t=0]}(B_s \rightarrow \mu^+ \mu^-). \quad (3.287)$$

In the SM, *i.e.* discarding NP scalar and pseudoscalar operators, $A_{\mu\mu} = 1$, and the factor above becomes just $(1 - y_s)^{-1}$. Not considering scalar currents has also the effect of making the instantaneous branching fraction solely determined by the WC C_{10} :

$$\text{BR}^{[t=0]}(B_s \rightarrow \mu^+ \mu^-) = \frac{G_F^2 \alpha_e^2}{16\pi^2} |\lambda_t|^2 f_{B_s}^2 \tau_{B_s} m_{B_s} m_\mu^2 \sqrt{1 - 4 \frac{m_\mu^2}{m_{B_s}^2}} |C_{10}|^2, \quad (3.288)$$

where f_{B_s} is the B_s decay constant,

$$\langle 0 | \bar{s} \gamma_\mu \gamma_5 b | \overline{B}_s(p) \rangle = i f_{B_s} p_\mu, \quad (3.289)$$

and τ_{B_s} is the lifetime of said meson. For this observable we evaluate the WC at NLO in QED, including NNLO QCD corrections, as sketched in the previous section. The numerical expression of the C_{10} evolution can be found in Refs. [117, 132]. For the meson decay constant we used a value from lattice QCD calculations, as discussed in the global analysis chapter.

A final word goes to $B \rightarrow X_s \gamma$, whose branching fraction is used in the analysis. A detailed explanation of the inclusive sector would require a dedicated section, with definitions of both QCD and QED contributions to the observable, bremsstrahlung corrections, and power corrections to the infinite mass limit. This is beyond the scope of this presentation, but for the reader's sake, we write here the LO expression of the decay rate:

$$\Gamma(B \rightarrow X_s \gamma) = \frac{G_F^2 m_b^5 \alpha_e}{32\pi^4} |\lambda_t|^2 C_7^2. \quad (3.290)$$

It is clear that we use the high precision measurement of this observable to constrain the contribution of the electromagnetic dipole operator, leaving little room for NP contributions to C_7 , as we shall witness in the chapter of results. For the actual analyses we perform in this thesis at NNLO in α_s and NLO in α_e , the decay rate goes by a formula with the shape

$$\Gamma(B \rightarrow X_s \gamma)_{E_\gamma > E_0} = N \sum_{i,j=1}^8 C_i(\mu_b) C_j(\mu_b) G_{ij}(E_0, m_b), \quad (3.291)$$

where N collects the pre-factor in Eq. (3.290), and E_0 is the photon energy cutoff. The functions G_{ij} , which reduce to $\delta_{i7} \delta_{j7}$ at LO, encapsulate the higher order corrections. We follow Ref. [133], and references therein.

Last but not least, one can build the binned ratios of branching fractions

$$R_{M[q_{\min}^2, q_{\max}^2]} = \frac{\int_{q_{\min}^2}^{q_{\max}^2} dq^2 \Gamma(B \rightarrow M \mu^+ \mu^-)}{\int_{q_{\min}^2}^{q_{\max}^2} dq^2 \Gamma(B \rightarrow M e^+ e^-)}, \quad \text{with } M = K, K^*, \phi. \quad (3.292)$$

which are free from most hadronic uncertainties and sensitive to the breaking of lepton flavour universality, *i.e.* to a preference of a channel with one type of leptons, over a channel with another flavour.

3.3.2 Treatment of the Hadronic Uncertainties

We turn now to form factors and the definition of the helicity amplitudes present in Eq. (3.260). With our definition of the effective Hamiltonian, in Eq. (3.69), the decay amplitudes of $B \rightarrow V \ell^+ \ell^-$ have two distinct parts:

$$\mathcal{A} = \langle M \ell^+ \ell^- | \mathcal{H}_{\text{eff}}^{\text{sl}} | \bar{B} \rangle + \langle M \ell^+ \ell^- | \mathcal{H}_{\text{eff}}^{\text{had}} | \bar{B} \rangle. \quad (3.293)$$

The contribution of the semileptonic Hamiltonian factorizes (in the “naive” sense of factorization) into a sum of leptonic currents multiplied by hadronic currents,

$$\mathcal{A}^{\text{sl}} = \langle \ell^+ \ell^- | \mathcal{H}_{\text{eff}}^{\text{sl}} | 0 \rangle \langle V | \mathcal{H}_{\text{eff}}^{\text{sl}} | \bar{B} \rangle \quad (3.294)$$

$$= L_V^\mu a_{V\mu} + L_A^\mu a_{A\mu} + L_S a_S + L_P a_P + L_{TL}^\mu a_{TL,\mu} + L_{TR}^\mu a_{TR,\mu}, \quad (3.295)$$

where we have kept vector, axial, scalar, pseudoscalar, and tensor operators. The leptonic currents are given by [24]:

$$\begin{aligned} L_V^\mu &= \langle \ell^+ \ell^- | \bar{\ell} \gamma^\mu \ell | 0 \rangle, & L_A^\mu &= \langle \ell^+ \ell^- | \bar{\ell} \gamma^\mu \gamma_5 \ell | 0 \rangle, \\ L_S^\mu &= \langle \ell^+ \ell^- | \bar{\ell} \ell | 0 \rangle, & L_P^\mu &= \langle \ell^+ \ell^- | \bar{\ell} \gamma_5 \ell | 0 \rangle, \\ L_{TL}^\mu &= \frac{i}{\sqrt{q^2}} \langle \ell^+ \ell^- | q_\nu \bar{\ell} \sigma^{\mu\nu} P_L \ell | 0 \rangle, & L_{TR}^\mu &= \frac{i}{\sqrt{q^2}} \langle \ell^+ \ell^- | q_\nu \bar{\ell} \sigma^{\mu\nu} P_L \ell | 0 \rangle. \end{aligned} \quad (3.296)$$

In turn, the hadronic currents $a_{X\mu}$ are parametrized by seven $B \rightarrow V$ form factors. The standard basis in which these form factors are presented is the transversality basis, which labels them as $V(q^2)$, $A_0(q^2)$, $A_1(q^2)$, $A_2(q^2)$, $A_3(q^2)$, $T_1(q^2)$, $T_2(q^2)$, and $T_3(q^2)$ [134].¹ We shall be working in a different basis, however, which defines seven helicity form factors appearing in the SM as follows [24]:

$$-i m_B \tilde{V}_{L\lambda}(q^2) = \langle M(\lambda) | \bar{s} \not{\epsilon}^*(\lambda) P_L b | \bar{B} \rangle, \quad (3.297)$$

$$m_B^2 \tilde{T}_{L\lambda}(q^2) = \epsilon^{*\mu}(\lambda) \langle M(\lambda) | \bar{s} q^\nu \sigma_{\mu\nu} P_R b | \bar{B} \rangle, \quad (3.298)$$

$$i m_B \tilde{S}_{L(R)}(q^2) = \langle M(\lambda = 0) | \bar{s} P_{R(L)} b | \bar{B} \rangle, \quad (3.299)$$

with M an arbitrary charmless final meson state, and $\epsilon_\mu(\lambda)$, for $\lambda = \pm 1, 0$, denoting a spin-1 helicity triplet of polarization vectors, for a vector particle of momentum q^μ and mass $\sqrt{q^2}$. In fact, taking into account the completeness relation

$$\eta_{\mu\nu} = \epsilon_{t,\mu} \epsilon_{t,\mu}^* - \sum_{\lambda=\pm 1,0} \epsilon_\mu(\lambda) \epsilon_\nu^*(\lambda) \quad (3.300)$$

where $\epsilon_t^\mu = q^\mu / \sqrt{q^2}$, one may carry out an helicity decomposition of the semileptonic matrix element, obtaining:

$$\begin{aligned} \mathcal{A}^{\text{sl}} &= - \sum_{\lambda=\pm 1,0} \epsilon_\mu(\lambda) L_V^\mu H_V^\lambda - \sum_{\lambda=\pm 1,0} \epsilon_\mu(\lambda) L_A^\mu H_A^\lambda + L_S H_S + L_P H_P \\ &\quad - \sum_{\lambda=\pm 1,0} \epsilon_\mu(\lambda) L_{TL}^\mu H_{TL}^\lambda - \sum_{\lambda=\pm 1,0} \epsilon_\mu(\lambda) L_{TR}^\mu H_{TR}^\lambda, \end{aligned} \quad (3.301)$$

¹For completeness, the transversality form factors are provided in Appendix C, together with the relation between both bases.

where the coefficients

$$H_V^\lambda = \epsilon_\mu^*(\lambda) a_V^\mu, \quad (3.302)$$

$$H_A^\lambda = \epsilon_\mu^*(\lambda) a_A^\mu, \quad (3.303)$$

$$H_S^\lambda = a_S^\mu, \quad (3.304)$$

$$H_P^\lambda = a_P^\mu + \frac{2m_\ell}{q^2} q_\mu a_A^\mu, \quad (3.305)$$

$$H_{TL}^\lambda = \epsilon_\mu^*(\lambda) a_{TL}^\mu, \quad (3.306)$$

$$H_{TR}^\lambda = \epsilon_\mu^*(\lambda) a_{TR}^\mu, \quad (3.307)$$

are the helicity amplitudes. The axial current obeys $q_\mu L_A^\mu = 2m_\ell L_P$, which allows the spin-zero axial vector amplitude to be absorbed into H_P [130]. One can immediately see that the amplitudes that receive contributions in the SM are H_V^λ , H_A^λ , and H_P .

Now, regarding the hadronic part of the Hamiltonian, $\mathcal{H}_{\text{eff}}^{\text{had}}$, it does not naively factorize, for it involves two additional insertions of the electromagnetic current, one leptonic and, the source of difficulties, one hadronic, in order to mediate the semileptonic decay:

$$\begin{aligned} \mathcal{A}^{\text{had}} &= -i \frac{e^2}{q^2} \int d^4x e^{-iq \cdot x} \langle \ell^+ \ell^- | j_{\text{em},\mu}^{\text{lept}}(x) | 0 \rangle \int d^4y e^{iq \cdot y} \langle M | T \{ j_{\text{em}}^{\text{had},\mu}(y) \mathcal{H}_{\text{eff}}^{\text{had}}(0) \} | \bar{B} \rangle \\ &\equiv \frac{e^2}{q^2} L_V^\mu a_\mu^{\text{had}}, \end{aligned} \quad (3.308)$$

where $j_{\text{em}}^{\text{had},\mu} = e \sum_q Q_q \bar{q} \gamma^\mu q$. While non-factorizable, these hadronic contributions can, nevertheless, be absorbed into $a_{V\mu}$. Sticking to the helicity amplitudes relevant for a SM computation,² one has:

$$H_V^\lambda = -i N \left\{ C_9 \tilde{V}_{L\lambda} + \frac{m_B^2}{q^2} \left[\frac{2m_b}{m_B} C_7 \tilde{T}_{L\lambda} - 16\pi^2 h_\lambda \right] \right\}, \quad (3.309)$$

$$H_A^\lambda = -i N C_{10} V_{L\lambda}, \quad (3.310)$$

$$H_P = i N \frac{2m_\ell m_b}{q^2} C_{10} \left(\tilde{S}_L - \frac{m_s}{m_B} \tilde{S}_R \right), \quad (3.311)$$

where N is a normalization factor,

$$N = -\frac{4G_F m_B}{\sqrt{2}} \frac{e^2}{16\pi^2} \lambda_t, \quad (3.312)$$

and h_λ contains all the non-factorizable hadronic effects. From the definition of H_V^λ above, one observes that the radiative decay $B \rightarrow V\gamma$ is but a mere subset of the amplitudes that describe the semileptonic counterpart, such that its decay amplitude can be written as [24]:

$$\mathcal{A}(\bar{B} \rightarrow V(\lambda)\gamma(\lambda)) = \frac{i N m_B^2}{e} \left[\frac{2m_b}{m_B} C_7 \tilde{T}_{L\lambda}(q^2 = 0) - 16\pi^2 h_\lambda(q^2 = 0) \right]. \quad (3.313)$$

In the case of $B \rightarrow P\ell^+\ell^-$, instead of seven form factors one has three instead, which, in the notation of Ref. [135], are f_+ , f_T , and f_0 . Following again Ref. [24], they are translated into the helicity basis by:

$$\tilde{V}_{L0}(q^2) = i f_+(q^2), \quad (3.314)$$

$$\tilde{T}_{L0}(q^2) = i \frac{2m_B}{m_B + m_P} f_T(q^2), \quad (3.315)$$

$$\tilde{S}_L = \tilde{S}_R = \frac{1 + \frac{m_s}{m_b} \frac{m_B^2 - m_P^2}{\sqrt{\lambda}}}{1 - \frac{m_s}{m_b}} f_0(q^2), \quad (3.316)$$

²For the full basis, we refer the reader to Ref. [24].

where $\lambda = 4 m_B^2 |\vec{k}|^2$, with \vec{k} being the 3-momentum of the recoiling meson, in the \bar{B} rest frame. These are consequently combined to make up the helicity amplitudes, and one has once more all the ingredients to define the angular coefficients I_i and all the observables that ensue.

Form factor calculation, as well as estimates of the non-factorizable corrections used in this analysis, will be discussed in Chapter 5.

Chapter 4

HEPfit and the Bayesian Analysis Framework

The two global analyses that make up this thesis are powered by `HEPfit`, a code for the combination of indirect and direct constraints on high energy physics models [48]. `HEPfit` is a publicly available package¹ that aims at performing globally correlated studies of observables in the Standard Model, or in any given realization of NP – model-independent generalizations of flavour or electroweak operators, supersymmetry, the 2HDM, *etc.* This is made possible by one of the main strengths of `HEPfit`, its modularity, which allows for any number of NP models to be seamlessly appended to the code, either as package-ready modules added by new developers, or, in the absence of some specific model from the latest release of `HEPfit`, as straightforward external user inputs.

Generically, `HEPfit` follows a simple streamlined configuration: the model is chosen, the values of the parameters are given, the desired observables are computed. If the observables have experimental input they can be used in a global fit of the model, if not, they can be predicted in the fit. The fits in this code are based on a Bayesian framework, and to explain what is meant by that, let us delve briefly into `HEPfit`'s data analysis procedure, before turning to the structure of modules and a succinct description of usage.

4.1 Bayesian Interlude

In the Bayesian approach to probability, density functions are not seen as frequency distributions, as in the frequentist approach, but rather as *degrees of belief* [136]. Our degree of belief in the set of parameters of a model $\vec{\theta}$, given existing experimental data D , can be obtained with Bayes' Theorem, which relates this $P(\vec{\theta}|D)$ with the probability that D will be the outcome of an observation once the parameters are fixed, $P(D|\vec{\theta})$:

$$P(\vec{\theta}|D) = \frac{P(D|\vec{\theta})P(\vec{\theta})}{P(D)}. \quad (4.1)$$

¹Available under the GNU General Public License from <https://github.com/silvest/HEPfit>.

The set of $P(\vec{\theta})$ constitute our initial belief in the parameters of the model, before the considered set of measurements is performed, and for this they are called *priors* and denoted as $\pi(\vec{\theta})$; $P(D|\vec{\theta})$ is known as the *likelihood*, $L(D|\vec{\theta})$, which updates our knowledge by turning the priors into the final set of probability density functions, which one terms *posteriors* and writes as $p(\vec{\theta}|D)$. Bayes' Theorem can thus be re-expressed as:

$$p(\vec{\theta}|D) = \frac{L(D|\vec{\theta}) \pi(\vec{\theta})}{\int d\vec{\theta} L(D|\vec{\theta}) \pi(\vec{\theta})}, \quad (4.2)$$

such that

$$\int d\vec{\theta} p(\vec{\theta}|D) = 1. \quad (4.3)$$

The full posterior contains all the information one could wish to know. By marginalizing the full posterior, one extracts the probability distribution of a single parameter θ_i ,

$$p(\theta_i|D) = \int d\theta_{j \neq i} p(\vec{\theta}|D), \quad (4.4)$$

upon which one can define, for example, the mean of a parameter,

$$\mu_i = \int d\theta_i \theta_i p(\theta_i|D), \quad (4.5)$$

the mode,

$$\text{Mode}(\theta_i) = \text{argmax} [p(\theta_i|D)], \quad (4.6)$$

the variance,

$$\sigma_i^2 = \int d\theta_i \theta_i^2 p(\theta_i|D) - \mu_i^2, \quad (4.7)$$

or the correlation between two parameters,

$$\rho_{ij} = \frac{\int d\theta_i d\theta_j \theta_i \theta_j p(\theta_i, \theta_j|D) - \mu_i \mu_j}{\sigma_i \sigma_j}. \quad (4.8)$$

To determine posteriors, HEPfit uses BAT [137], a Bayesian analysis toolkit that is provided as a C++ library. This software receives as inputs the priors of one model, and the likelihood, composed of a set of observables distributed according to experimental values and uncertainties; to compute the full posterior, BAT uses a Markov Chain Monte Carlo. A Markov Chain is a stochastic sequence of numbers, or vectors of numbers, whose main property is that the choice of elements in the sequence is memoryless, *i.e.* the probability distribution for the next state depends only on the current state, and not on any previous history of the chain. A Markov Chain Monte Carlo is a method that generates *ergodic* (non-dependent on the starting point) Markov Chains which have a well-defined asymptotic, or *equilibrium*, probability distribution. The algorithm implemented in BAT to sample from the desired equilibrium distribution, the full posterior of a given model in our case, is the Metropolis algorithm [138], which can be described as follows:

1. the sequence starts in a state \vec{x}_t ;
2. a random point \vec{y} is generated around \vec{x}_t via a certain symmetric ‘proposal distribution’ – *e.g.* a Breit-Wigner, or a Gaussian;
3. being Eq. (4.2) the distribution one is mapping out:

- if $f(\vec{y}) = L(\vec{y}|D)\pi(\vec{y})$ is non-zero, one sets $\vec{x}_{t+1} = \vec{y}$ with an ‘acceptance probability’

$$A(\vec{x}_t \rightarrow \vec{y}) = \min\left(1, \frac{f(\vec{y})}{f(\vec{x}_t)}\right), \quad (4.9)$$

- the sequence remains at \vec{x}_t otherwise, $\vec{x}_{t+1} = \vec{x}_t$;

4. a new random point \vec{y} is generated around \vec{x}_{t+1} , and step 3 is repeated.

To ensure convergence of the Markov Chain and to find reasonable run parameters, BAT performs a *pre-run* before doing the actual *sampling and analysis* run. The pre-run consists in a user-defined number of chains that run in parallel, starting from a random value in parameter space, and iterating over consecutive steps for each parameter. After a given number of iterations, the efficiencies for accepting or rejecting new points are evaluated, such that the proposal distributions are updated until an efficiency between 10% and 50% is found for each input parameter. The chains converge when the *R*-value [139], given by

$$R = \sqrt{\frac{V}{W}} \quad (4.10)$$

where V is the estimated variance of the equilibrium distribution, and W is the mean of variances of all chains, is approximately 1. The default criterion used in BAT is to consider convergence is reached when $R < 1.1$, simultaneously for all parameters and the full posterior density function. The sampling and analysis run is performed for a defined (large) number of iterations, using the parameters obtained in the pre-run. During sampling, the mode of the full posterior, the global mode, is compared to the current point, histograms are filled for all marginalized distributions, and the likelihood of the function being fitted is evaluated.

As the χ^2 goodness-of-fit test is not applicable to Bayesian analyses, in order to compare different scenarios we resort to the Information Criterion [140, 141], defined as

$$IC = -2\overline{\log L} + 4\sigma_{\log L}^2, \quad (4.11)$$

where $\overline{\log L}$ is the average of the log-likelihood, and $\sigma_{\log L}^2$ is its variance. The second term in Eq. (4.11) takes into account the effective number of parameters in the model, allowing for a meaningful comparison of models with different number of parameters. Preferred models are expected to be those with smaller *IC* values.

4.2 Structure and Usage

Returning to the concept of modularity, HEPfit allows the user to turn BAT on or off, such that when turned off the code runs in *Single Event Mode*, which simply computes observable predictions with the central values of parameters priors, or in *Library Mode*, which allows for using the coded models and observables for statistical analysis in different approaches. Other sectors include modules with auxiliary functions and configurations, modules for input parsing and event generation, one module for each of the available models, which can also be turned on or off depending on the analysis in course, a module for flavour observables, another focused on electroweak observables, and so on and so forth. While a full

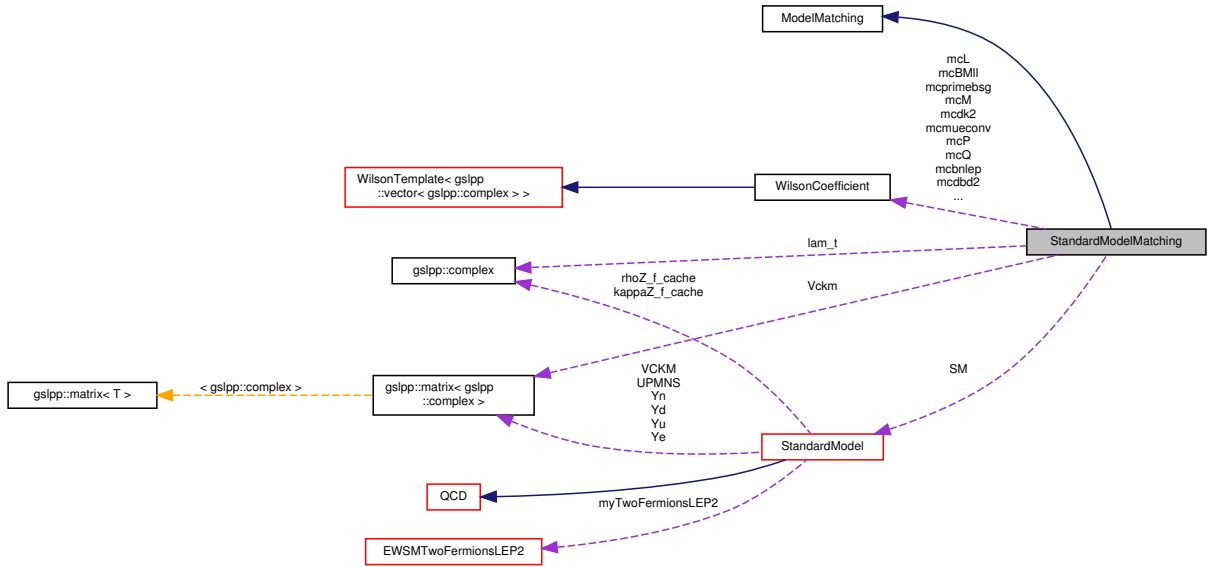


Figure 4.1: Collaboration diagram for the StandardModelMatching class.

description of the structure of the code can be found in the documentation of `HEPfit`,² here we will touch upon the modules which saw direct contribution from the student.

Let us start with the module for the SM. Here the code saw the update of WC matchings already mentioned in Chapter 3, where QED matchings were not merely updated, but fully added to the code. The class dedicated to this is `StandardModelMatching`, and a Doxygen-generated diagram of its dependencies and relations within the code is represented in Fig. 4.1. Without going into much detail, it is perceptible in the diagram how the matching sector depends on QCD definitions, Standard Model parameters and functions, and on the auxiliary modules that define WCs, generic model matching, even complex numbers and complex matrices. To account for the full QCD and QED running of WCs, a new coefficient block-dependent evolution method for $\Delta F = 1$ processes was designed inside the Flavour module, together with a new class that puts together the corresponding effective Hamiltonian, the `HeffDF1` class, depicted in Fig. 4.2. This class links to the matchings from `StandardModel`, and evolves them inside `EvolDF1` according to Eq. (3.247), thus depending on the auxiliary `RGEvolutor` class built in the code.

Participation of the student on code development also includes the building of the inclusive sector of $b \rightarrow s$ transitions, currently on a finalization stage for a subsequent global analysis [142], and the creation of a module for general 2HDMS other than just the Z_2 -symmetric realization studied in this thesis.³

Usage of `HEPfit`, our final topic of this chapter, must start with a step zero, which pertains the required installation of all the software dependencies:

- C++ compiler;
- GSL and boost, for numerical solutions to integration, algebra, differential equations, etc.;
- BAT, the aforementioned library for Bayesian analyses;

²Currently available at <http://hepfit.roma1.infn.it/doc/v1.0-RC1>.

³A full list of contributions can be found at <https://github.com/silvest/HEPfit/graphs/contributors>.

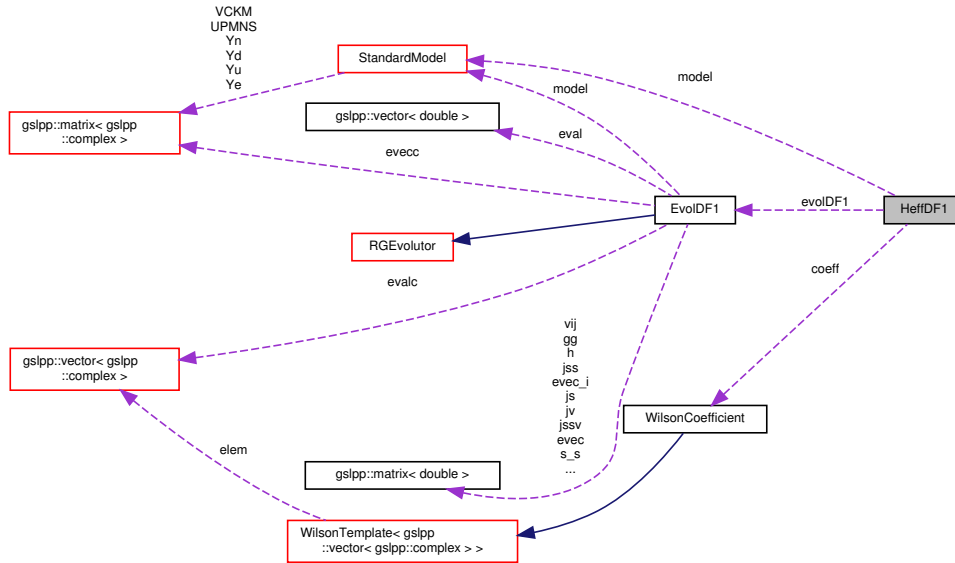


Figure 4.2: Collaboration diagram for the HeffDF1 class.

- ROOT, for graphical output of the resulting histograms;
- openMPI, in case the user opts for parallelized fits.

Then, and after downloading the HEPfit-x.x.tar.gz archive from hepfit.roma1.infn.it, a concise run of

```
tar zxvf HEPfit-x.x.tar.gz
cd HEPfit-x.x
cmake . -DLOCAL_INSTALL_ALL=ON -DMPIBAT=ON
make
make install
```

brings the user to a position where a first fit can be done with:

```
./analysis StandardModel.conf MonteCarlo.conf
```

The two configuration files contain all the information the code needs, from the user-defined number of chains, pre-run iterations, sampling and analysis run iterations, and other BAT options that one gives in MonteCarlo.conf, to the detailed listing of model parameters and observables provided in StandardModel.conf. An example of the general form of the model configuration file is presented in Fig. 4.3. The first line indicates the model name. All the model parameters have then to be given, usually in the format of lines 3 and 4,

```
ModelParameter <name> <central value> <Gaussian error> <flat error>
```

or, when applicable, in correlated form as seen from line 6 to line 10, the last two lines representing the correlation matrix. The observables which will determine the likelihood follow, from line 14 to line 33 of the sketched file. They come in the format

```
Observable <name> <obs label> <histolabel> <min> <max> MCMC weight
<central value> <Gaussian error> <flat error>
```

or in correlated form as well, and a prediction from the fit is asked by writing simply

```
Observable <name> <obs label> <histolabel> <min> <max> noMCMC noweight
```

```

1 StandardModel
2 # Model parameters:
3 ModelParameter mtop      173.2    0.9    0.
4 ModelParameter mH1      125.6    0.3    0.
5 ...
6 CorrelatedGaussianParameters V1_lattice 2
7 ModelParameter a_0V      0.496    0.067  0.
8 ModelParameter a_1V     -2.03    0.92  0.
9 1.00    0.86
10 0.86    1.00
11
12 <All the model parameters have to be listed here>
13
14 # Observables:
15 Observable Mw           Mw           M_{W}      80.3290 80.4064 MCMC weight 80.385 0.015 0.
16 Observable GammaW      GammaW      #Gamma_{W} 2.08569 2.09249 MCMC weight 2.085 0.042 0.
17 #
18 # Correlated observables:
19 CorrelatedGaussianObservables Zpole2 7
20 Observable Alepton Alepton A_{l}      0.143568 0.151850 MCMC weight 0.1513 0.0021 0.
21 Observable Rbottom Rbottom R_{b}      0.215602 0.215958 MCMC weight 0.21629 0.00066 0.
22 Observable Rcharm Rcharm R_{c}      0.172143 0.172334 MCMC weight 0.1721 0.0030 0.
23 Observable AFBbottom AFBbottom A_{FB}^{b} 0.100604 0.106484 MCMC weight 0.0992 0.0016 0.
24 Observable AFBcharm AFBcharm A_{FB}^{c} 0.071750 0.076305 MCMC weight 0.0707 0.0035 0.
25 Observable Abottom Abottom A_{b}      0.934320 0.935007 MCMC weight 0.923 0.020 0.
26 Observable Acharm Acharm A_{c}      0.666374 0.670015 MCMC weight 0.670 0.027 0.
27 1.00    0.00    0.00    0.00    0.00    0.09    0.05
28 0.00    1.00    -0.18   -0.10    0.07    -0.08   0.04
29 0.00   -0.18    1.00    0.04   -0.06    0.04   -0.06
30 0.00   -0.10    0.04    1.00    0.15    0.06    0.01
31 0.00    0.07   -0.06    0.15    1.00   -0.02    0.04
32 0.09   -0.08    0.04    0.06   -0.02    1.00    0.11
33 0.05    0.04   -0.06    0.01    0.04    0.11    1.00
34 #
35 # Output correlations:
36 Observable2D MwvsGammaW Mw M_{W} 80.3290 80.4064 noMCMC noweight GammaW #Gamma_{W} 2.08569 2.09249
37 ...
38 Observable2D Bd_Bsbar_mumu noMCMC noweight
39 Observable BR_Bdmumu BR(B_{d}#rightarrow#mu#mu) 1. -1. 1.05e-10 0. 0.
40 Observable BR_Bsrmumu BR(B_{s}#rightarrow#mu#mu) 1. -1. 3.65e-9 0. 0.
41 ...
42 Observable2D S5_P5 noMCMC noweight
43 BinnedObservable S_5 S_5 1. -1. 0. 0. 0. 4. 6.
44 BinnedObservable P_5 P_5 1. -1. 0. 0. 0. 4. 6.
45 #
46 # Including other configuration files
47 IncludeFile Flavour.conf

```

Figure 4.3: An example of a configuration file for StandardModel.

As line 35 suggests, the observables below are output 2D correlations between two observables, and can be obtained with:

```
Observable2D <name> <obs1 label> <histolabel1> <min1> <max1> noMCMC noweight
           <obs2 label> <histolabel2> <min2> <max2>
```

or

```
Observable2D <name> MCMC weight
(Binned)Observable <obs label 1> <histolabel 1> <min> <max> <central value>
                 <Gaussian error> <flat error> (<bin_min> <bin_max>)
(Binned)Observable <obs label 2> <histolabel 2> <min> <max> <central value>
                 <Gaussian error> <flat error> (<bin_min> <bin_max>)
```

The directive in the last line of the example shows how more parameters and observables can be added to the configuration, either for reasons of organization, such as having a file with the information related with a separate module, like Flavour, or to add the parameters and observables of an extension to the SM, as the is the case of the 2HDM.

Chapter 5

Global Analysis of $b \rightarrow s$ Transitions

In this chapter we present the results of the first of two global analysis that compose this thesis. These are original results, most of which have been published in Ref. [143]. The different scenarios for WCs and the approaches to hadronic uncertainties that were adopted in that reference are outlined in the first section of this chapter. After a delineation of the experimental information and all the inputs used, we present the numerical and graphical output of the fit.

5.1 Scenarios and Approaches

While a general ultraviolet completion of the SM may enter all the couplings of the effective Hamiltonian in Eq. (3.69), general NP effects in $b \rightarrow s\gamma, s\ell\ell$ can be phenomenologically parametrized as shifts of a subset of WCs, namely those of $\mathcal{H}_{\text{eff}}^{\text{sl}+\gamma}$:

$$C_i(\mu_b) \longrightarrow C_i(\mu_b) + C_i^{\text{NP}}(\mu_b), \quad i = 7, 9, 10. \quad (5.1)$$

The most general basis for NP effects in radiative and (semi)leptonic B decays is enlarged by the presence scalar, pseudo-scalar and tensorial semileptonic operators, together with right-handed counterparts of the $Q_{7\gamma}, Q_{9V}, Q_{10A}$ SM operators [24, 144]. In our work, motivated by previous literature concerning LFUV [41–43] and the recent measurements of R_K and R_{K^*} , we focus only on the contributions of the left-handed shifts described in Eq. (5.1). A comprehensive analysis with different chiral structures and a more general effective theory framework is left for a future global analysis [142]. It must also be noted that here we restrict ourselves to CP-conserving effects, thus keeping all WCs real even beyond the SM.

In order to access possible LFUV in NP, the shifts in semileptonic operators are discriminated between couplings to muon and to electron fields, both in the axial and vector leptonic currents. We characterize our phenomenological analysis through six different benchmark scenarios, studying the impact of the following combinations of NP WCs:

(I) $C_{9,\mu}^{\text{NP}}$ and $C_{9,e}^{\text{NP}}$ varied in the range $[-4, 4]$, *i.e.* adding to the SM two NP parameters;

(II) $C_{9,\mu}^{\text{NP}}$ and $C_{10,\mu}^{\text{NP}}$ varied in the range $[-4, 4]$, *i.e.* adding to the SM again two NP parameters;

- (III) $C_{9,\mu}^{\text{NP}}$ and $C_{9,e}^{\text{NP}}$ varied in the range $[-4, 4]$, and C_7^{NP} varied in the range $[-0.5, 0.5]$, *i.e.* a scenario with three NP parameters;
- (IV) $C_{10,\mu}^{\text{NP}}$ and $C_{10,e}^{\text{NP}}$ varied in the range $[-4, 4]$, and C_7^{NP} varied in the range $[-0.5, 0.5]$, *i.e.* adding again to the SM three NP parameters;
- (V) $C_{9,\mu}^{\text{NP}} = -C_{10,\mu}^{\text{NP}}$ and $C_{9,e}^{\text{NP}} = -C_{10,e}^{\text{NP}}$ varied in the range $[-4, 4]$, and C_7^{NP} varied in the range $[-0.5, 0.5]$, *i.e.* a NP scenario again described by three different parameters.
- (VI) C_7^{NP} , $C_{9,\mu}^{\text{NP}}$, $C_{9,e}^{\text{NP}}$, $C_{10,\mu}^{\text{NP}}$ and $C_{10,e}^{\text{NP}}$ varied simultaneously in the respective ranges defined above, *i.e.* a NP scenario described by five different parameters.

We remark that while benchmarks (I) and (II) have been already studied in literature, none of the other cases has been analysed so far. In particular, scenarios (III) and (IV) allow one to study, for the first time, the interesting impact of a NP radiative dipole operator in combination with vector-like and axial-like LFUV effects generated by NP. Scenario (V) puts the correlation $C_9^{\text{NP}} = -C_{10}^{\text{NP}}$ under analysis, making room for possible hints of a $SU(2)_L$ preserving theory beyond the SM. As an additional interesting case to explore, we eventually generalize to the simultaneously nonvanishing of all the WCs in case (VI).

Another novelty in this study is that the six benchmarks defined above are studied for the first time under two different approaches in the estimate of QCD hadronic power corrections. A previous endeavour of some of the authors of Ref. [143] concerned a detailed treatment of hadronic contributions in the angular analysis of $B \rightarrow K^* \ell \ell$ [27, 30, 145]. The non-factorizable contributions, introduced in Eq. (3.309) and given by

$$h_\lambda(q^2) = \frac{\epsilon_\mu^*(\lambda)}{m_B^2} \int d^4y e^{iqy} \langle \bar{K}^* | T \{ j_{\text{em}}^{\text{had},\mu}(y) \mathcal{H}_{\text{eff}}^{\text{had}}(0) \} | \bar{B} \rangle, \quad (5.2)$$

are not fully calculable with known non-perturbative techniques. The sole estimate present in literature [146] was obtained by combining a LCSR calculation of the hadronic amplitude at $q^2 = 1 \text{ GeV}^2$ in the single soft gluon approximation, with a dispersion relation that is then used to extend the result to higher invariant masses. Although a remarkable computation in itself, it was pointed by its very authors that the adopted approximations and techniques impart large uncertainties to the result, some of which are not entirely under control. These concerns were also raised by the authors of Ref. [27], who decided to study how large the hadronic effects could be if one assumes that the LHCb data on the branching fractions and the angular distributions of these decay modes can be described within the SM. For that purpose, four hypotheses to the hadronic contributions were considered, with increasing theoretical input from the phenomenological analysis of Ref. [146]. The underlying functional form that was envisaged for the non-factorizable hadronic contribution is the truncated series

$$h_\lambda(q^2) = h_\lambda^{(0)} + \frac{q^2}{1 \text{ GeV}^2} h_\lambda^{(1)} + \frac{q^4}{1 \text{ GeV}^4} h_\lambda^{(2)}, \quad (5.3)$$

where the authors fitted for the complex, helicity-dependent, coefficients $h_\lambda^{(i)}$ ($i = 0, 1, 2$) using the data and the phenomenological model in Ref. [146]. Since h_0 enters the decay amplitude with an additional factor of $\sqrt{q^2}$ with respect to h_\pm , $h_0^{(2)}$ is neglected in the analysis. The dominant hadronic terms

correspond to the insertions of four-quark operators with charm, usually called *charm-loop* contributions:

$$h_\lambda(q^2)|_{c\bar{c}} = \frac{3}{2} \frac{\epsilon_\mu^*(\lambda)}{m_B^2} \int d^4y e^{iqy} \langle \bar{K}^* | T \{ [\bar{c}\gamma^\mu c](y) [C_1^c Q_1^c + C_2^c Q_2^c](0) \} | \bar{B} \rangle. \quad (5.4)$$

For convenience, the authors of Ref. [146] expressed these contributions as corrections to C_9 , which, in the absence of NP effects, would thus become

$$C_9 \longrightarrow C_9 + \Delta C_9(q^2). \quad (5.5)$$

They divide the decay amplitude of $B \rightarrow K^* \ell^+ \ell^-$ in three parts, each receiving its distinct charm-loop contribution. In turn, they decompose those $\Delta C_9^i(q^2)$ in two terms – one with the factorizable corrections, and one that encodes the non-factorizable charm-loop contributions:

$$\Delta C_9^i(q^2) = (3C_1 + C_2)g(m_c^2, q^2) + 2C_2 \tilde{g}_i(q^2). \quad (5.6)$$

The $\tilde{g}_{1,2,3}$ in the non-factorizable contributions to $\Delta C_9^i(q^2)$ are functions of combinations of h_λ , respectively, $h_-(q^2) - h_+(q^2)$, $h_-(q^2) + h_+(q^2)$, and $h_-(q^2) + h_+(q^2)$ together with $h_0(q^2)$ [27]. The full form of these relations, as well as the expression of the function $g(m_c^2, q^2)$, are provided in Appendix C.2.

For the present analysis, which requires a re-evaluation of the hadronic uncertainties, we proceed much in the same way and use the functional parameterization as given in Eq. (5.3). Yet, only two hadronic models are now considered: the first, corresponding to the most widely used assumption, relies completely on the phenomenological model in Ref. [146] below $q^2 < 4m_c^2$. The second is a more conservative approach, where one imposes the latter only in the large recoil region, at $q^2 \leq 1 \text{ GeV}^2$, while letting the data drive the hadronic contributions in the higher invariant mass region. The first approach will be referred to as phenomenological model driven (PMD), whereas the second is labelled as phenomenological and data driven (PDD). In our fit we vary the h_λ^i parameters over generous ranges, in accordance to the detailed discussions of Refs. [27, 30].

This global analysis requires one to address further decay modes, namely $B \rightarrow K\ell\ell$, $B_s \rightarrow \phi\ell\ell$ and $B_s \rightarrow \phi\gamma$. The decay $B \rightarrow K\ell\ell$ has been studied in detail in [39], where the authors show that the hadronic uncertainties are smaller than in $B \rightarrow K^*\ell\ell$. A comparison of the LCSR estimate of the soft gluon contribution and the QCDF estimate of the hard gluon contribution reveals that the soft gluon exchange is subdominant with respect to QCDF hard gluon exchange, which means that, although in principle the same concerns on the soft gluon contribution raised for $B \rightarrow K^*$ apply also for this mode, in practice the overall effect of soft gluons can be reasonably neglected. For this fit we include, therefore, only hard gluon exchange computed using the QCDF formalism in Ref. [147]. Barring the obvious difference in spectator quarks, the long distance contributions for $B_s \rightarrow \phi\ell\ell$ and $B_s \rightarrow \phi\gamma$ follow a similar theoretical derivation as, respectively, those for $B \rightarrow K^*\ell\ell$ and $B \rightarrow K^*\gamma$. Since no theoretical estimates of power corrections to the infinite mass limit are available for the $B_s \rightarrow \phi\ell\ell/\gamma$ decays, one has to rely on the ones for $B \rightarrow K^*\ell\ell/\gamma$ to get a handle on the long distance contributions: the spectator quark effects can come through the hard spectator scattering involving matrix elements of Q_2 , P_6 , and Q_{8g} computable in QCD factorization [147], which are included in our computations. We do not include, however, the sub-leading QCDF power corrections to spectator scattering involving Q_{8g} [148–150], and contributions

to weak spectator scattering involving Q_{sg} computed in LCSR [151–153]. The effect of the difference in all these spectator contributions is expected to be low, firstly because they are numerically small, secondly because the effect is proportional to the small flavour $SU(3)$ breaking. Different approaches in relating the long distance contributions in the $B \rightarrow K^* \ell \ell / \gamma$ channels to the ones in the $B \rightarrow \phi \ell \ell / \gamma$ channels have been used in the literature [41, 42, 154]. The distinguishing factor is the choice of the degree of correlation between the two channels: Ref [42] uses uncorrelated hadronic uncertainties, while Refs. [41, 154] have opted for the two contributions to be highly correlated, noting that the spectator contribution should be numerically small. Taking into account the insensitivity of the current data to such effects, this analysis follows the latter approach, by using the same value of power corrections in $B \rightarrow K^*$ and $B_s \rightarrow \phi$ amplitudes, even though this choice pertains to a quite oversimplifying and optimistic attitude. Again, a deeper look at this assumption, where one relaxes the correlation between the hadronic contributions in the two modes, is left to a subsequent work [142].

5.2 Experimental Information and Input Parameters

Regarding the information used in the global fit, we start by bringing attention to the fact that for the exclusive modes we make use only of measurements in the large recoil region. This choice harbours on the fact that the QCD long distance effects in the low recoil region are substantially different from the large recoil regime [155–158], and that it would require a dedicated analysis. For this fit, the following experimental information was considered:

- $B \rightarrow K^* \ell \ell$

For the $B \rightarrow K^* \mu \mu$ channel we use the LHCb measurements of CP-averaged angular observables extracted by means of the unbinned maximum likelihood fit, along with the provided correlation matrix [21]. Moreover, we employ the recent results for CP-averaged angular observables from ATLAS [32] and the ones measured by CMS [33, 159] as well.¹ Finally, we use the CP-averaged optimized angular observables recently measured by Belle [47].² Regarding the differential branching fractions, we use the recently updated measurements from LHCb [160] and the ones from CMS [159]. For the $B \rightarrow K^* e e$ channel we consider the LHCb results from Ref. [161], and the Belle results from Ref. [47]. The R_{K^*} observable is considered according to the recently presented measurements by LHCb in both the low- q^2 and central- q^2 bins [19]. As mentioned in Chapter 3, our theoretical predictions are computed in the helicity basis, the same framework being employed to study $B \rightarrow K^* \gamma$, $B_s \rightarrow \phi \mu \mu$, $B_s \rightarrow \phi \gamma$ and $B \rightarrow K \ell \ell$ channels. For the latter, we use the full set of form factors extrapolated from the lattice results, along with the provided correlation matrix [162]; for the remaining channels, we use the full set of form factors estimated combining LCSR and lattice

¹For all CMS data we use the 7, 8 TeV combined results, which can be found in <https://twiki.cern.ch/twiki/bin/view/CMSPublic/PhysicsResultsBPH13010>.

²Belle measures the $B^0 \rightarrow K^{*0} \mu \mu$ and $B^+ \rightarrow K^{*+} \mu \mu$ channels together, without providing the mixture ratio. On the theoretical side, one can use these measurements under the approximation that QCD power corrections decoupling the amplitudes of both channels are small. We have numerically checked that the impact of known QCD power corrections [147] is indeed at the percent level in the observables of interest.

results, along with the correlation matrices [163]. For the factorizable and non-factorizable QCD power corrections, we refer to the section above.

- $B \rightarrow K^*\gamma$

We include in our analysis the HFAG average for the branching fractions from Ref. [7].

- $B_s \rightarrow \phi\mu\mu$

We consider the LHCb CP-averaged angular observables and differential branching fractions measurements, along with the provided correlation matrix [38].

- $B_s \rightarrow \phi\gamma$

We use the LHCb measurement of the branching fraction from Ref. [164].

- $B \rightarrow K\ell\ell$

We employ the LHCb measurement of $B \rightarrow K\ell\ell$ differential branching fraction and R_K from Ref. [18].

- $B_s \rightarrow \mu\mu$

We consider the latest measurement from LHCb [165], and do not consider the measurement from CMS [166], which has the same central value as LHCb, but larger uncertainty. Moreover, we chose not to use results for $B_d \rightarrow \mu\mu$, since, so far, only upper bounds exist for this decay channel [165, 166].

- $B \rightarrow X_s\gamma$

We use the HFAG average from Ref. [7]. We perform our theoretical computation at NNLO in α_s and NLO in α_{em} , following Ref. [133] and references therein.

All the experimental data in the bullets above is fitted using the 16 real free parameters that characterize the non-factorizable power corrections – in accordance to Ref. [27] – along with the set of NP WCs necessary for each of the six scenarios devised in the previous section. To the hadronic parameters and the NP WCs, we assign flatly distributed priors in the relevant ranges, as mentioned when the scenarios were described. The remaining parameters used in the fit are listed in Table 5.1, where f_M is the usual decay constant of a meson M ; the Gegenbauer parameters, a_n , and λ_B are quantities present in the parametrization of light-cone distribution amplitudes of B decays [147]. The Gegenbauer parameters and λ_B have flat priors with half width reported in the third column; the remaining parameters have Gaussian priors. Meson masses, lepton masses, s -quark mass and electroweak couplings are fixed at their PDG value [167].

5.3 Results of the Global Fit

The results for the several scenarios of NP in WCs under consideration can be found in Fig. 5.1, and from Fig. 5.4 to Fig. 5.8, where the IC value for each model is also reported. The left green panels show the results for the PMD approach, whereas the right red panels show the results for the PDD

Parameters	Mean Value	Uncertainty	Reference
$\alpha_s(M_Z)$	0.1181	0.0009	[167, 168]
μ_W (GeV)	80.385	–	
m_t (GeV)	173.34	0.76	[169]
$m_c(m_c)$ (GeV)	1.28	0.02	[170]
$m_b(m_b)$ (GeV)	4.17	0.05	[171]
f_{B_s} (MeV)	226	5	[172]
f_{B_s}/f_{B_d}	1.204	0.016	[172]
$\Delta\Gamma_s/\Gamma_s$	0.129	0.009	[7]
λ	0.2250	0.0006	[84, 173]
A	0.829	0.012	[84, 173]
$\bar{\rho}$	0.132	0.018	[84, 173]
$\bar{\eta}$	0.348	0.012	[84, 173]
$f_{K^*,\parallel}$ (MeV)	204	7	[163]
$f_{K^*,\perp}(1\text{GeV})$ (MeV)	159	6	[163]
$f_{\phi,\parallel}$ (MeV)	233	4	[163]
$f_{\phi,\perp}(1\text{GeV})$ (MeV)	191	4	[163]
λ_B (MeV)	350	150	[174]
$a_1(\bar{K}^*)_{\perp,\parallel}$	0.04	0.03	[175]
$a_2(\bar{K}^*)_{\perp,\parallel}$	0.05	0.1	[176]
$a_2(\phi)_{\perp,\parallel}$	0.23	0.08	[177]
$a_1(K)$	0.06	0.03	[175]
$a_2(K)$	0.115	–	[135]

Table 5.1: Parameters used in the global analysis of $b \rightarrow s$ transitions.

one. In the 1D distributions we show the 16th, 50th and 84th percentile marked with dashed lines. In the correlation plots we show the 1, 2 and 3 σ contours in decreasing degrees of transparency. The blue square and lines identify the values of the NP WCs in the SM limit. The numbers at the bottom left corner of the 2D plots refer to the correlation. This graphical output is complemented by the information in Tables 5.2–5.3. In Tables 5.4–5.5, we report the results of the fit for observables of interest. An immediate observation that can be made is that all cases have comparable IC values, except cases **(IV)** and **(V)**, which are disfavoured in the PMD approach, while remaining viable scenarios in the PDD approach. The main difference between the two approaches is that angular observables, in particular P'_5 , call for a NP contribution from $C_{9,\mu}^{\text{NP}}$ in the PMD approach, whereas in the PDD approach they can be accommodated within the SM.

But let us discuss the various scenarios in more detail. For scenario **(I)**, presented in Fig. 5.1, the evidence for NP that comes out of the fit amounts to more than 5 σ in the PMD approach. For the PDD approach, however, the NP evidence gets significantly reduced, to roughly between 3 σ and 4 σ . This reduction in the significance can be explained by the larger hadronic uncertainties in the PDD approach, which weaken the constraining power of the angular observables on the NP WCs. We also performed

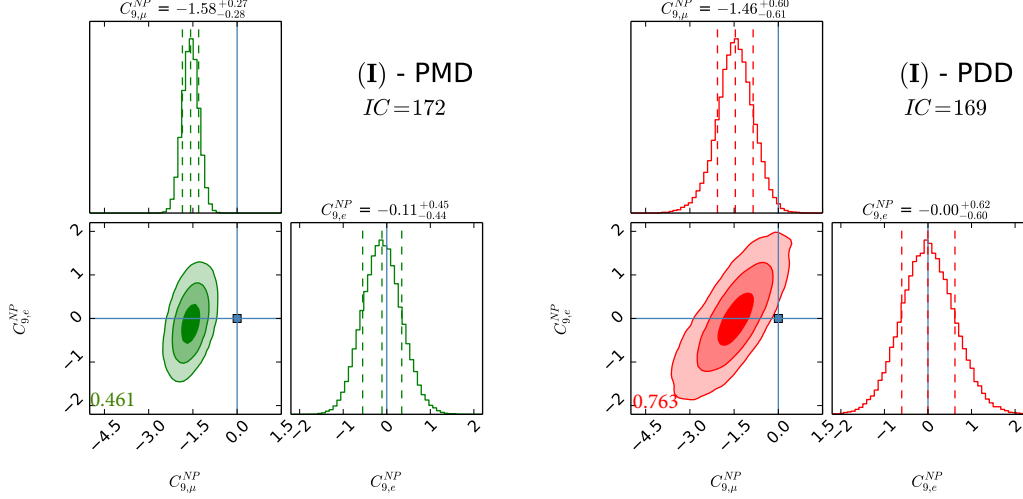


Figure 5.1: The two NP parameter fit using $C_{9,\mu}^{\text{NP}}$ and $C_{9,e}^{\text{NP}}$.

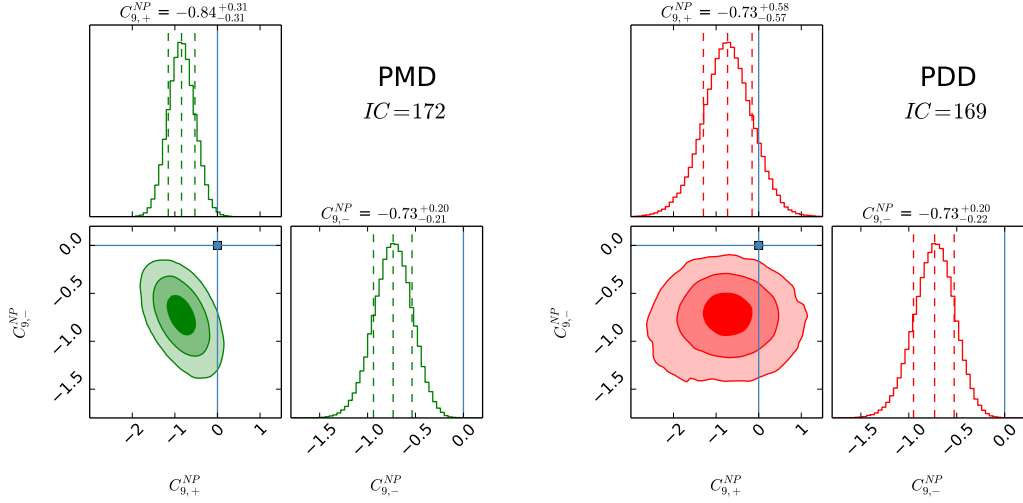


Figure 5.2: The two NP parameter fit using $C_{9,\mu}^{\text{NP}}$ and $C_{9,e}^{\text{NP}}$, given in the $C_{9,-}^{\text{NP}} - C_{9,+}^{\text{NP}}$ basis.

the fit in a basis where the hadronic contributions and the NP shifts can be disentangled in one of the coefficients,

$$C_{9,-} = \frac{C_{9,\mu} - C_{9,e}}{2} \longrightarrow C_{9,-} + C_{9,-}^{\text{NP}}, \quad (5.7)$$

$$C_{9,+} = \frac{C_{9,\mu} + C_{9,e}}{2} \longrightarrow C_{9,+} + C_{9,+}^{\text{NP}} + \Delta C_9, \quad (5.8)$$

with the resulting posteriors shown in Fig. 5.2. The fitted value of $C_{9,-}^{\text{NP}}$ does not depend on the chosen approach to treat the non-factorizable hadronic contributions, as can be seen from the individual histogram for that WC given in both cases. This means that, regardless of the way ΔC_9 is computed, there is indeed a deviation of approximately 3.5σ from the SM expectation for $C_{9,-}^{\text{NP}}$, which indicates, at this certainty level, first that $C_{9,\mu}^{\text{NP}}$ and $C_{9,e}^{\text{NP}}$ cannot be equal, and then that either of them is non-zero, or both are simultaneously non-zero. The choice of how to deal with the hadronic effects appears completely in the distribution of $C_{9,+}^{\text{NP}}$: whereas the PMD plot favours the case of a non-zero and dominating NP

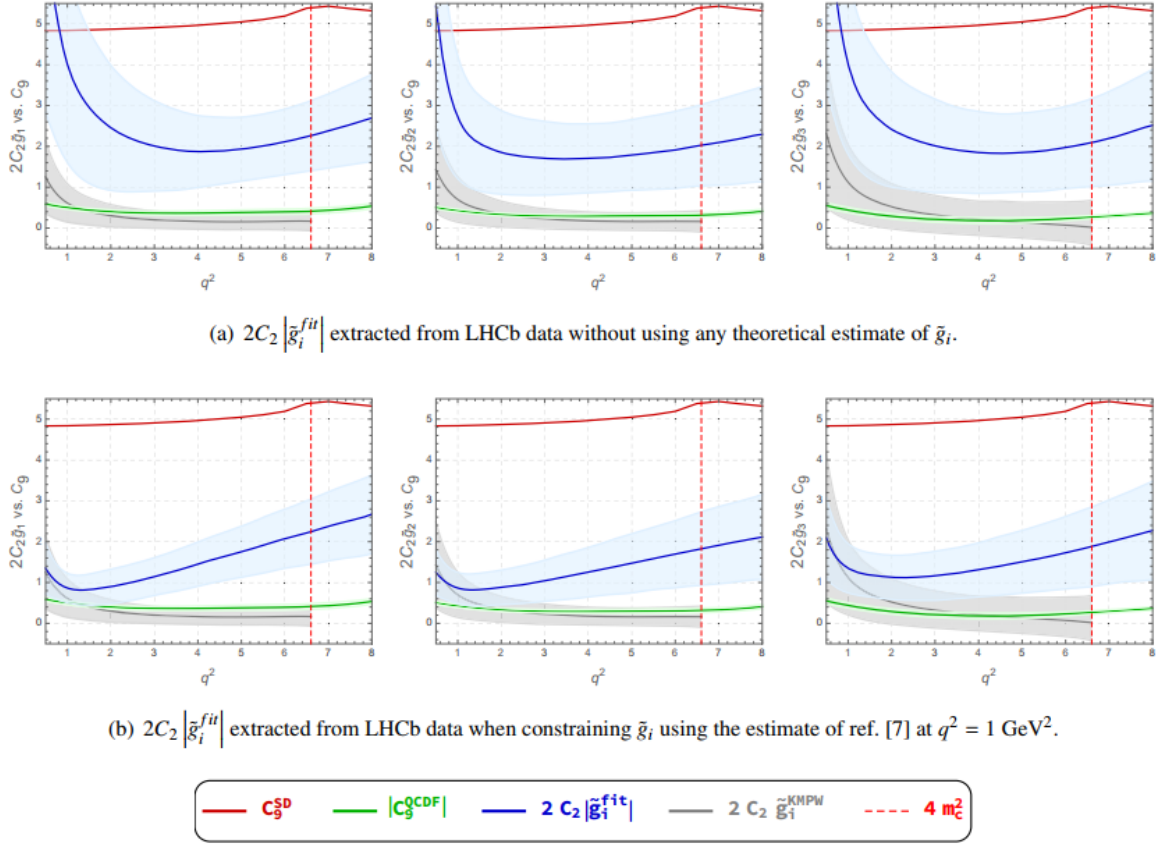


Figure 5.3: Comparison of $2C_2|\tilde{g}_i^{\text{fit}}|$ with the value of C_9 with perturbative charm-loop contributions included, C_9^{SD} , and the additional QCDF corrections, C_9^{QCDF} . KMPW denotes the estimate of Ref. [146]. (Taken from Ref. [145], ©2017 Elsevier B.V.; ref. [7] in that paper corresponds to Ref. [146] here.)

shift in $C_{9,\mu}$, the aforementioned larger uncertainty present in the PDD approach clearly shows in the histogram and 2D distribution on the right, and leaves more room for any case, as was also evident from the allowed regions at 3σ already shown in Fig. 5.1.

Another direction to possibly disentangle the charm-loop contribution to C_9 and some C_9^{NP} , which we feel couldn't go unmentioned, was put forward in Refs. [27, 30, 145]. There, the authors performed a fit to the functions \tilde{g}_i , with and without the theoretical estimate of Ref. [146]. The relevant portion of their results is quoted here, in Fig. 5.3. The main takeaway is that the precise extraction from data of the slope in the charm-loop contributions would constitute a unique access to the information of the size of the hadronic amplitudes, and thus provide a more reliable SM prediction, mandatory for unequivocal NP searches. While the current results are still non-conclusive, upcoming experimental data could shed some light on the issue. One comment must also be reserved to the size of the fitted corrections: even if they can amount to 5 – 6 times the size of the estimate from Ref. [146], and that of the QCDF corrections, mainly in the case where no theoretical input is used in the fit, and more pronounced near the charm resonances, it is apparent in the plots that they are always, nevertheless, smaller than the leading value of the coefficient. Here and there they get to be a $\mathcal{O}(50\% - 60\%)$ correction to C_9^{SD} , but no *leading order vs. sub-leading order* considerations are ever breached in the region of interest.

Concerning scenarios **(II)** and **(III)**, respectively in Fig. 5.4 and Fig. 5.5, we observe very similar

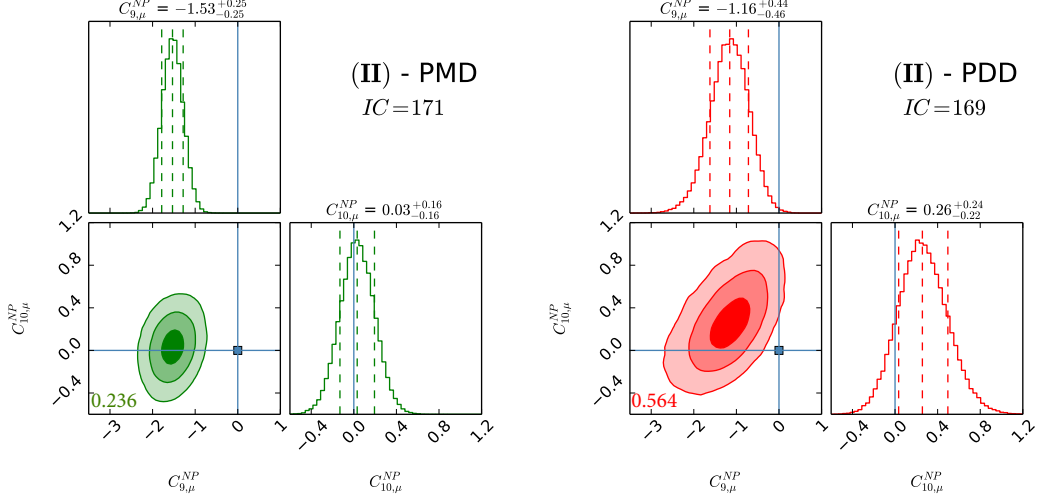


Figure 5.4: The two NP parameter fit using $C_{9,\mu}^{NP}$ and $C_{10,\mu}^{NP}$.

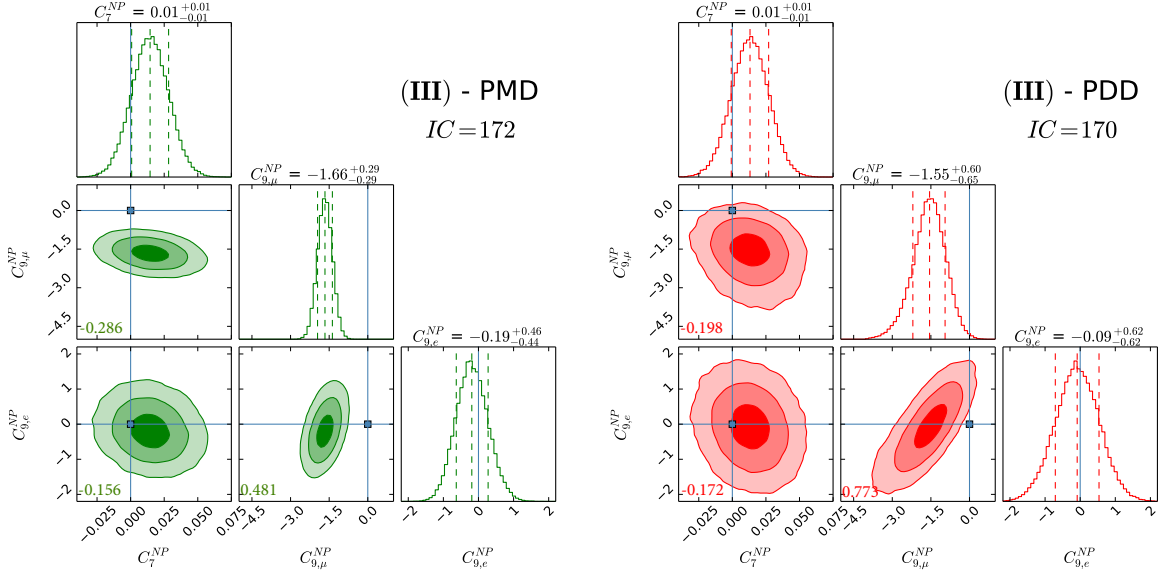


Figure 5.5: The three NP parameter fit using C_7^{NP} , $C_{9,\mu}^{NP}$, and $C_{9,e}^{NP}$.

evidences for NP as the ones obtained in **(I)**. Even with a third NP WC added, the fact that scenario **(III)** follows suit is because the effective coupling for the radiative dipole operator is very well constrained, especially from the inclusive $B \rightarrow X_s \gamma$ branching fraction. The reduction in the significance between approaches, PMD and PDD, can be explained for scenarios **(II)** and **(III)** with the same arguments already given above.

Regarding scenario **(IV)**, in which we vary the three NP parameters C_7^{NP} , $C_{10,\mu}^{NP}$ and $C_{10,e}^{NP}$, the model comparison between the PDD and PMD realization of this NP benchmark is quite informative: NP effects in the dipole operator and in the axial semileptonic currents cannot address at the same time R_{K,K^*} ratios and the P'_5 anomaly in a satisfactory way when we stick to small non-factorizable QCD power corrections; however, this is no longer true when we allow for a more conservative estimate of the hadronic uncertainties. In particular, the tension in the fit coming from the angular analysis of

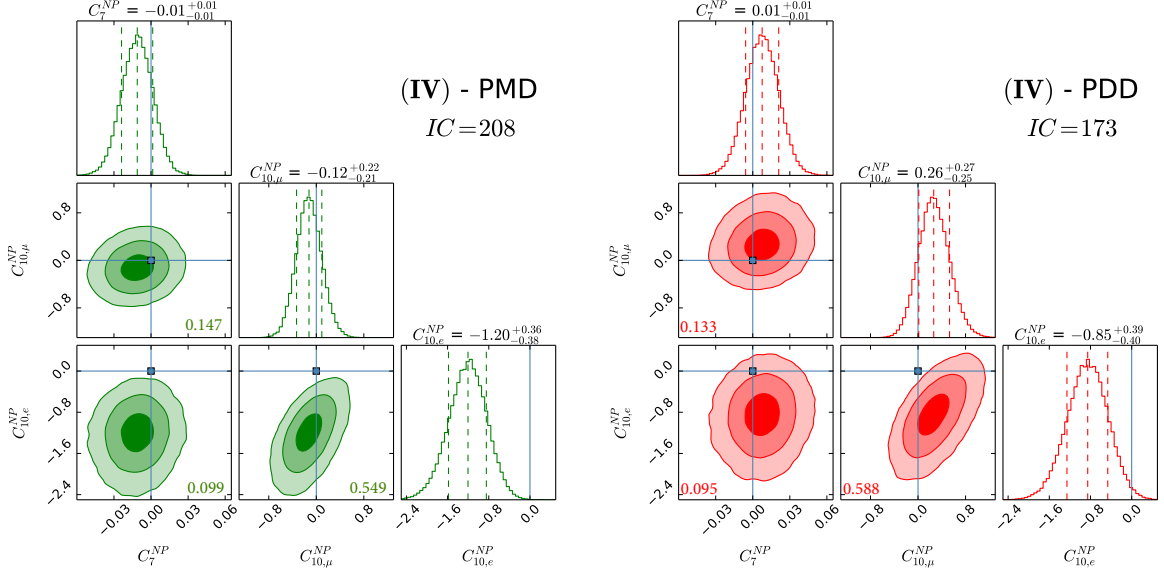


Figure 5.6: The three NP parameter fit using C_{10}^{NP} , $C_{10,\mu}^{\text{NP}}$, and $C_{10,e}^{\text{NP}}$.

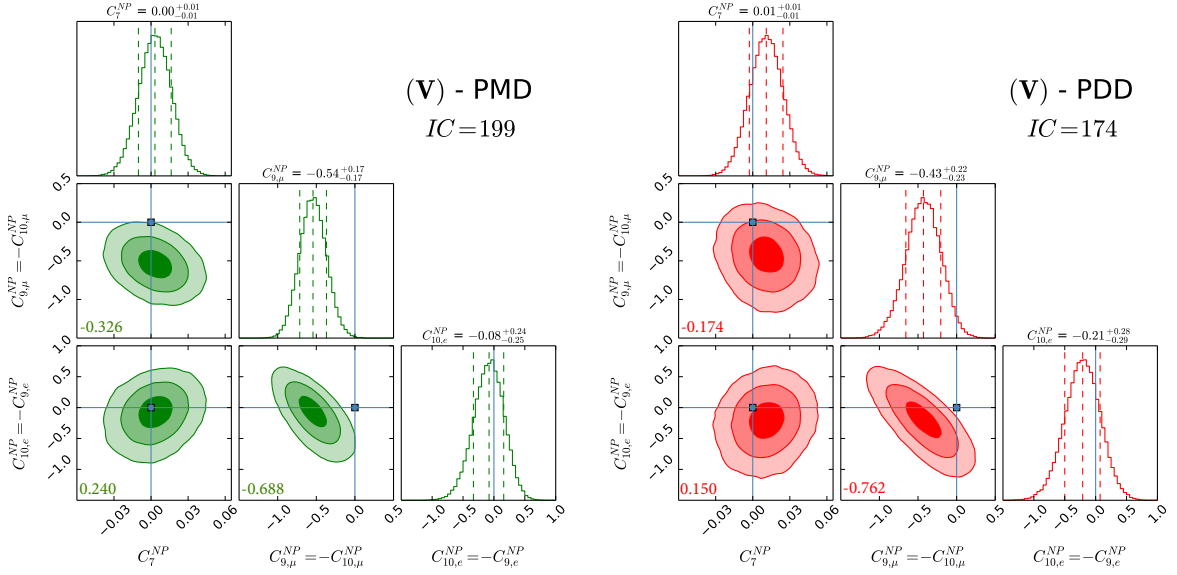


Figure 5.7: The three NP parameter fit using C_7^{NP} , $C_{9,\mu}^{\text{NP}}$, $C_{9,e}^{\text{NP}}$, and $C_{10,\mu,e}^{\text{NP}} = -C_{9,\mu,e}^{\text{NP}}$.

$B \rightarrow K^* \mu \mu$ can be now addressed by large QCD effects as given in Eq. (5.3), while a $C_{10,e}^{\text{NP}} \neq 0$ at about 3σ can successfully describe all the observational hints of LFUV shown by current measurements. This interesting possibility of *axial lepton-flavor violating NP* is not found in other global analyses [41–44], as it proceeds from the conservative treatment of hadronic uncertainties proposed in Ref. [27].

Concerning Tables 5.4–5.5, we would like to point out the pattern displayed by the transverse ratios $R_{K^*}^T$ and R_ϕ^T : cases (I)–(III) predict these values to be ~ 1 with a small error, while the remaining cases give different predictions with the central value ranging between ~ 0.7 and ~ 0.8 . Therefore, obtaining experimental information on transverse ratios may help in discerning between the different NP scenarios.

We then show results for scenario (V), in which we vary C_7^{NP} , $C_{9,\mu}^{\text{NP}}$, $C_{9,e}^{\text{NP}}$ and correlate the semileptonic vector and axial currents according to $C_{9,\mu}^{\text{NP}} = -C_{10,\mu}^{\text{NP}}$ and $C_{9,e}^{\text{NP}} = -C_{10,e}^{\text{NP}}$. In analogy to case (IV),

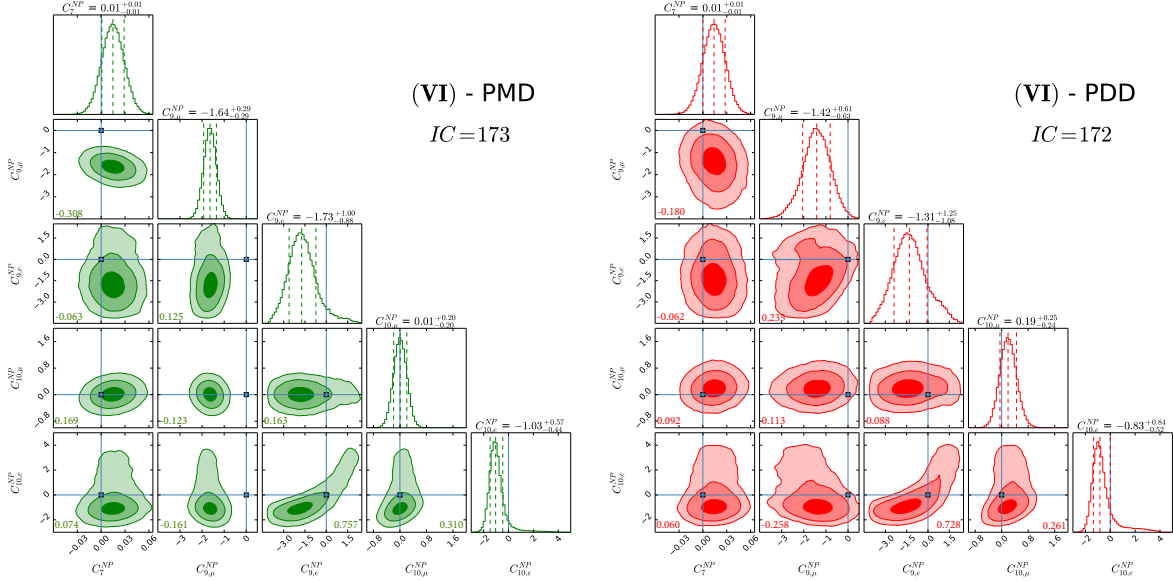


Figure 5.8: The five NP parameter fit using C_7^{NP} , $C_{9,\mu}^{\text{NP}}$, $C_{9,e}^{\text{NP}}$, $C_{10,\mu}^{\text{NP}}$, and $C_{10,e}^{\text{NP}}$.

only within the PDD approach we find for this NP benchmark a fairly good description of data, with $C_{9,\mu}^{\text{NP}} = -C_{10,\mu}^{\text{NP}}$ compatible with zero at $\sim 2\sigma$. Again, we are presented with the case where deviations in angular observables are addressed by large QCD power corrections, while LFUV is driven by semielectronic operators. Looking back at Tables 5.4–5.5, we note that for this scenario, as well as for (IV) and (VI), both transverse and longitudinal muon over electron ratios in the central- q^2 bin, namely $R_{K,K^*,\phi}^T$ and $R_{K,K^*,\phi}^L$, are characterized by similar central values.

We close our presentation with an analysis of scenario (VI) in which we float simultaneously all 5 NP WCs. As can be seen from Fig. 5.8, current measurements are informative enough to constrain, at the same time, all the NP WCs both in the PMD and PDD approaches. In particular, within the latter case, a nontrivial interplay among NP effects encoded both in $C_{9,\mu}^{\text{NP}}$ and $C_{10,e}^{\text{NP}}$, together with the hadronic contributions reported in Table 5.3, produces the weakest hint in favour of NP provided by our global analysis – sitting between 2σ and 3σ level – while allowing for a very good description of the entire data set, similar to the other cases. The power corrections we found are larger than those obtained in Ref. [146], but smaller than those required by the SM fit of $B \rightarrow K^* \mu \mu$ [27]. As discussed in detail in Refs. [30, 145], the size obtained for the power corrections is compatible with the naive power counting relative to the leading amplitude. We stress, once more, that a more optimistic attitude towards the estimate of QCD power corrections (PMD approach) leads to the a much stronger claim in favour of NP, at a statistical significance larger than 5σ .

In Tables 5.2–5.3 we report mean and standard deviation for the NP WCs and absolute values of h_λ for all the scenarios considered in the analysis. It is also relevant to observe that, once we switch on NP effects through $C_{9,\mu}^{\text{NP}}$ in order to attempt at simultaneously explaining observables such as R_{K,K^*} and P_5' in the PDD approach we find values for $|h_\lambda^{(1,2)}|$ compatible with zero at $\sim 1\sigma$. Conversely, if we set $C_{9,\mu}^{\text{NP}} = 0$ then a nonvanishing $|h_-^{(2)}|$ is needed to account for the angular observables, as found in Ref. [27], showing that one cannot disentangle hadronic uncertainties and NP in $B \rightarrow K^* \mu \mu$ at present.

Par.	(I)	(II)	(III)	(IV)	(V)	(VI)
C_7^{NP}	–	–	0.015 ± 0.014	-0.011 ± 0.013	0.003 ± 0.013	0.015 ± 0.014
$C_{9,\mu}^{\text{NP}}$	-1.58 ± 0.28	-1.53 ± 0.25	-1.66 ± 0.29	–	-0.54 ± 0.17	-1.64 ± 0.29
$C_{9,e}^{\text{NP}}$	-0.10 ± 0.45	–	-0.18 ± 0.46	–	0.09 ± 0.25	-1.6 ± 1.0
$C_{10,\mu}^{\text{NP}}$	–	0.03 ± 0.16	–	-0.12 ± 0.22	0.54 ± 0.17	0.009 ± 0.200
$C_{10,e}^{\text{NP}}$	–	–	–	-1.22 ± 0.37	-0.09 ± 0.25	-0.91 ± 0.76
$ h_0^{(0)} \cdot 10^4$	2.1 ± 1.2	2.0 ± 1.2	2.2 ± 1.3	1.8 ± 1.2	1.3 ± 1.0	2.0 ± 1.3
$ h_+^{(0)} \cdot 10^4$	0.079 ± 0.067	0.079 ± 0.067	0.076 ± 0.065	0.083 ± 0.069	0.086 ± 0.072	0.076 ± 0.064
$ h_-^{(0)} \cdot 10^4$	0.53 ± 0.19	0.54 ± 0.19	0.52 ± 0.19	0.56 ± 0.20	0.60 ± 0.21	0.52 ± 0.19
$ h_0^{(1)} \cdot 10^4$	0.30 ± 0.23	0.30 ± 0.22	0.30 ± 0.23	0.45 ± 0.26	0.32 ± 0.24	0.28 ± 0.22
$ h_+^{(1)} \cdot 10^4$	0.22 ± 0.20	0.22 ± 0.19	0.22 ± 0.19	0.21 ± 0.19	0.26 ± 0.22	0.22 ± 0.19
$ h_-^{(1)} \cdot 10^4$	0.23 ± 0.19	0.23 ± 0.19	0.23 ± 0.20	0.30 ± 0.21	0.32 ± 0.22	0.23 ± 0.19
$ h_+^{(2)} \cdot 10^4$	0.052 ± 0.045	0.053 ± 0.045	0.052 ± 0.044	0.046 ± 0.042	0.064 ± 0.053	0.050 ± 0.044
$ h_-^{(2)} \cdot 10^4$	0.046 ± 0.038	0.046 ± 0.039	0.046 ± 0.039	0.092 ± 0.050	0.070 ± 0.047	0.045 ± 0.038

Table 5.2: Results from the fit for WCs and hadronic contributions in the PMD approach, for each of the scenarios under study.

Par.	(I)	(II)	(III)	(IV)	(V)	(VI)
C_7^{NP}	–	–	0.013 ± 0.014	0.008 ± 0.014	0.011 ± 0.014	0.014 ± 0.014
$C_{9,\mu}^{\text{NP}}$	-1.47 ± 0.63	-1.17 ± 0.46	-1.58 ± 0.64	–	-0.43 ± 0.23	-1.43 ± 0.64
$C_{9,e}^{\text{NP}}$	0.007 ± 0.620	–	-0.08 ± 0.63	–	0.21 ± 0.29	-1.2 ± 1.2
$C_{10,\mu}^{\text{NP}}$	–	0.26 ± 0.23	–	0.27 ± 0.26	0.43 ± 0.23	0.20 ± 0.25
$C_{10,e}^{\text{NP}}$	–	–	–	-0.86 ± 0.4	-0.21 ± 0.29	-0.60 ± 0.99
$ h_0^{(0)} \cdot 10^4$	2.6 ± 1.6	2.3 ± 1.4	2.6 ± 1.6	1.7 ± 1.3	1.7 ± 1.3	2.6 ± 1.6
$ h_+^{(0)} \cdot 10^4$	0.075 ± 0.066	0.081 ± 0.070	0.077 ± 0.067	0.086 ± 0.075	0.087 ± 0.075	0.077 ± 0.067
$ h_-^{(0)} \cdot 10^4$	0.52 ± 0.21	0.55 ± 0.22	0.52 ± 0.21	0.60 ± 0.23	0.59 ± 0.23	0.53 ± 0.21
$ h_0^{(1)} \cdot 10^4$	0.40 ± 0.32	0.41 ± 0.34	0.39 ± 0.32	0.50 ± 0.36	0.46 ± 0.37	0.40 ± 0.33
$ h_+^{(1)} \cdot 10^4$	0.40 ± 0.29	0.42 ± 0.30	0.40 ± 0.29	0.39 ± 0.29	0.42 ± 0.30	0.41 ± 0.30
$ h_-^{(1)} \cdot 10^4$	0.47 ± 0.35	0.52 ± 0.38	0.48 ± 0.36	0.82 ± 0.46	0.73 ± 0.43	0.50 ± 0.37
$ h_+^{(2)} \cdot 10^4$	0.138 ± 0.087	0.160 ± 0.099	0.131 ± 0.086	0.139 ± 0.094	0.160 ± 0.100	0.145 ± 0.095
$ h_-^{(2)} \cdot 10^4$	0.112 ± 0.085	0.126 ± 0.098	0.111 ± 0.083	0.190 ± 0.100	0.170 ± 0.110	0.124 ± 0.094

Table 5.3: Results from the fit for WCs and hadronic contributions in the PDD approach, for each of the scenarios under study.

Obs.	Exp. value	(I)	(II)	(III)	(IV)	(V)	(VI)
$R_K[1,6]$	0.753 ± 0.090	0.722 ± 0.067	0.703 ± 0.047	0.722 ± 0.067	0.781 ± 0.055	0.740 ± 0.061	0.724 ± 0.067
$R_{K^*}[0.045,1.1]$	0.680 ± 0.093	0.885 ± 0.016	0.881 ± 0.016	0.885 ± 0.016	0.839 ± 0.024	0.858 ± 0.019	0.843 ± 0.030
$R_{K^*}[1.1,6]$	0.707 ± 0.102	0.803 ± 0.057	0.786 ± 0.049	0.802 ± 0.057	0.713 ± 0.065	0.740 ± 0.060	0.717 ± 0.067
$R_K^L[1.1,6]$	—	0.724 ± 0.067	0.705 ± 0.049	0.723 ± 0.067	0.722 ± 0.065	0.722 ± 0.063	0.723 ± 0.068
$R_{K^*}^T[1.1,6]$	—	1.053 ± 0.030	1.046 ± 0.069	1.050 ± 0.030	0.692 ± 0.067	0.794 ± 0.053	0.75 ± 0.25
$R_\phi[1.1,6]$	—	0.782 ± 0.060	0.764 ± 0.048	0.781 ± 0.060	0.720 ± 0.064	0.737 ± 0.061	0.717 ± 0.062
$R_\phi^L[1.1,6]$	—	0.723 ± 0.067	0.704 ± 0.049	0.722 ± 0.067	0.728 ± 0.064	0.723 ± 0.063	0.721 ± 0.067
$R_\phi^T[1.1,6]$	—	1.044 ± 0.032	1.038 ± 0.066	1.043 ± 0.033	0.691 ± 0.067	0.794 ± 0.053	0.75 ± 0.24
$P_5^{\text{LHCb}}[4,6]$	-0.301 ± 0.160	-0.423 ± 0.060	-0.427 ± 0.061	-0.420 ± 0.059	-0.556 ± 0.063	-0.587 ± 0.053	-0.431 ± 0.061
$P_5^{\text{LHCb}}[6,8]$	-0.505 ± 0.124	-0.602 ± 0.059	-0.607 ± 0.061	-0.598 ± 0.059	-0.677 ± 0.066	-0.704 ± 0.057	-0.61 ± 0.06
$P_5^{\text{ATLAS}}[4,6]$	-0.26 ± 0.39	-0.423 ± 0.060	-0.427 ± 0.061	-0.420 ± 0.059	-0.556 ± 0.063	-0.587 ± 0.053	-0.431 ± 0.061
$P_5^{\text{CMS}}[4,3,6]$	-0.955 ± 0.268	-0.442 ± 0.059	-0.447 ± 0.061	-0.440 ± 0.059	-0.572 ± 0.063	-0.603 ± 0.053	-0.451 ± 0.061
$P_5^{\text{CMS}}[6,8,68]$	-0.660 ± 0.220	-0.623 ± 0.060	-0.626 ± 0.061	-0.618 ± 0.059	-0.688 ± 0.067	-0.711 ± 0.058	-0.63 ± 0.06
$P_5^{\text{Belle}}[4,8]$	-0.025 ± 0.318	-0.520 ± 0.057	-0.524 ± 0.059	-0.516 ± 0.057	-0.620 ± 0.063	-0.649 ± 0.053	-0.528 ± 0.059
$P_{5,e}^{\text{Belle}}[4,8]$	-0.510 ± 0.272	-0.782 ± 0.054	-0.794 ± 0.039	-0.782 ± 0.054	-0.536 ± 0.063	-0.710 ± 0.044	-0.42 ± 0.23

Table 5.4: Experimental results (with symmetrized errors), and results from the fit for key observables in the PMD approach, for each of the scenarios under study.

Obs.	Exp. value	(I)	(II)	(III)	(IV)	(V)	(VI)
R_K [1,6]	0.753 ± 0.090	0.724 ± 0.068	0.714 ± 0.064	0.723 ± 0.067	0.775 ± 0.057	0.740 ± 0.062	0.719 ± 0.073
R_{K^*} [0.045,1.1]	0.680 ± 0.093	0.883 ± 0.017	0.873 ± 0.016	0.883 ± 0.017	0.842 ± 0.024	0.861 ± 0.019	0.847 ± 0.030
R_{K^*} [1.1,6]	0.707 ± 0.102	0.803 ± 0.059	0.777 ± 0.053	0.801 ± 0.059	0.714 ± 0.066	0.755 ± 0.059	0.722 ± 0.069
$R_{K^*}^L$ [1.1,6]	—	0.726 ± 0.070	0.719 ± 0.061	0.723 ± 0.070	0.726 ± 0.065	0.729 ± 0.063	0.719 ± 0.073
$R_{K^*}^T$ [1.1,6]	—	1.050 ± 0.033	0.959 ± 0.083	1.046 ± 0.034	0.688 ± 0.069	0.824 ± 0.049	0.8 ± 0.32
R_ϕ [1.1,6]	—	0.782 ± 0.062	0.761 ± 0.054	0.779 ± 0.062	0.722 ± 0.065	0.749 ± 0.060	0.718 ± 0.063
R_ϕ^L [1.1,6]	—	0.724 ± 0.070	0.716 ± 0.061	0.721 ± 0.070	0.731 ± 0.064	0.728 ± 0.063	0.716 ± 0.071
R_ϕ^T [1.1,6]	—	1.039 ± 0.036	0.955 ± 0.079	1.036 ± 0.036	0.693 ± 0.068	0.828 ± 0.049	0.79 ± 0.3
$P_{5[4,6]}^{\text{LHC}^b}$	-0.301 ± 0.160	-0.398 ± 0.066	-0.405 ± 0.068	-0.401 ± 0.066	-0.435 ± 0.065	-0.421 ± 0.068	-0.417 ± 0.068
$P_{5[6,8]}^{\text{LHC}^b}$	-0.505 ± 0.124	-0.536 ± 0.080	-0.521 ± 0.083	-0.539 ± 0.080	-0.521 ± 0.080	-0.508 ± 0.082	-0.545 ± 0.083
$P_{5[4,6]}^{\text{ATLAS}}$	-0.26 ± 0.39	-0.398 ± 0.066	-0.405 ± 0.068	-0.401 ± 0.066	-0.435 ± 0.065	-0.421 ± 0.068	-0.417 ± 0.068
$P_{5[4,3,6]}^{\text{CMS}}$	-0.955 ± 0.268	-0.414 ± 0.067	-0.420 ± 0.068	-0.417 ± 0.067	-0.447 ± 0.066	-0.434 ± 0.068	-0.433 ± 0.068
$P_{5[6,8,68]}^{\text{CMS}}$	-0.660 ± 0.220	-0.550 ± 0.083	-0.531 ± 0.086	-0.553 ± 0.083	-0.529 ± 0.084	-0.514 ± 0.085	-0.556 ± 0.086
$P_{5[4,8]}^{\text{Belle}}$	-0.025 ± 0.318	-0.472 ± 0.070	-0.467 ± 0.072	-0.475 ± 0.070	-0.481 ± 0.070	-0.467 ± 0.072	-0.486 ± 0.072
$P_{5,e^e[4,8]}^{\text{Belle}}$	-0.510 ± 0.272	-0.725 ± 0.075	-0.664 ± 0.095	-0.733 ± 0.075	-0.424 ± 0.063	-0.570 ± 0.066	-0.41 ± 0.22

Table 5.5: Experimental results (with symmetrized errors), and results from the fit for key observables in the PDD approach, for each of the scenarios under study.

Chapter 6

The Two Higgs Doublet Model

In this chapter we turn to the second target of our use of global analyses as means towards uncovering signs of NP in state-of-the-art experimental data, or, more appropriate to this second case, how such data still allows a particular direction for NP to go along. The model studied henceforth is the 2HDM, one of the simplest extensions to the SM compatible with $SU(2)_L \times U(1)_Y$, consisting in the addition of one scalar with the exact same quantum numbers of the one already present in the theory.

The parameter space and mass spectrum of the 2HDM is the subject of the following sections, first in its general form, then in the simplified Z_2 -symmetric case – the model we will analyse in the subsequent chapters. We finish this one with a section dedicated to the Coleman-Weinberg potential, the go-to one-loop effective potential when probing vacuum stability, both in the SM and the 2HDM.

6.1 The Higgs Basis and the Scalar Mass Terms

The 2HDM comprehends two doublets of $SU(2)_L$, both with hypercharge $Y = 1/2$:

$$\phi_1 = \begin{pmatrix} \varphi_1^+ \\ \varphi_1^0 \end{pmatrix}, \quad \phi_2 = \begin{pmatrix} \varphi_2^+ \\ \varphi_2^0 \end{pmatrix}. \quad (6.1)$$

The addition of another Higgs doublet has a considerable effect on the Higgs sector as defined in Eq. (2.5): one has now a kinetic term for each doublet, and the most general renormalizable, *i.e.* quartic, scalar potential can now be written as

$$\begin{aligned} V_H = & m_{11}^2 \phi_1^\dagger \phi_1 + m_{22}^2 \phi_2^\dagger \phi_2 - (m_{12}^2 \phi_1^\dagger \phi_2 + \text{h.c.}) \\ & + \frac{1}{2} \lambda_1 (\phi_1^\dagger \phi_1)^2 + \frac{1}{2} \lambda_2 (\phi_2^\dagger \phi_2)^2 + \lambda_3 (\phi_1^\dagger \phi_1) (\phi_2^\dagger \phi_2) + \lambda_4 (\phi_1^\dagger \phi_2) (\phi_2^\dagger \phi_1) \\ & + \left[\frac{1}{2} \lambda_5 (\phi_1^\dagger \phi_2)^2 + \lambda_6 (\phi_1^\dagger \phi_1) (\phi_1^\dagger \phi_2) + \lambda_7 (\phi_2^\dagger \phi_2) (\phi_1^\dagger \phi_2) + \text{h.c.} \right]. \end{aligned} \quad (6.2)$$

The parameters m_{12}^2 , λ_5 , λ_6 , and λ_7 are unprotected by the hermiticity of the potential and may thus be complex parameters. Due to the rephasing-invariance of the scalar sector, one of the complex phases can be rotated away, the number of parameters in a general 2HDM version of this sector counting to 13 parameters, almost seven times the number we had encountered in the SM.

After SSB both scalars acquire a VEV. The doublets can be parametrized linearly around the vacuum, as one does in the case of the SM,

$$\phi_1 = \begin{pmatrix} \varphi_1^+ \\ (v_1 + \rho_1 + i\eta_1)/\sqrt{2} \end{pmatrix}, \quad \phi_2 = \begin{pmatrix} \varphi_2^+ \\ (v_2 + \rho_2 + i\eta_2)/\sqrt{2} \end{pmatrix}, \quad (6.3)$$

where we have chosen the VEVs to be real. Demanding the vacuum solution to lie in a stationary point of V_H gives a set of relations between the VEVs and the parameters of the potential. These relations, the so-called *minimum conditions*, arise from the minimization of the potential,

$$\left. \frac{\partial V_H}{\partial \phi_i^\dagger} \right|_{\phi_i=v_i} = 0, \quad i = 1, 2, \quad (6.4)$$

$$\left. \frac{\partial V_H}{\partial \phi_i} \right|_{\phi_i=v_i} = 0, \quad i = 1, 2, \quad (6.5)$$

and allow us to trade m_{11}^2 and m_{22}^2 for v_1 and v_2 , and rephase away the imaginary part of m_{12}^2 :

$$m_{11}^2 = \frac{v_2}{v_1} \text{Re}(m_{12}^2) - \frac{1}{2} v_1^2 \lambda_1 - \frac{1}{2} v_2^2 [\lambda_3 + \lambda_4 + \text{Re}(\lambda_5)] - \frac{3}{2} v_1 v_2 \text{Re}(\lambda_6) - \frac{1}{2} \frac{v_2^3}{v_1} \text{Re}(\lambda_7), \quad (6.6)$$

$$m_{22}^2 = \frac{v_1}{v_2} \text{Re}(m_{12}^2) - \frac{1}{2} v_2^2 \lambda_2 - \frac{1}{2} v_1^2 [\lambda_3 + \lambda_4 + \text{Re}(\lambda_5)] - \frac{1}{2} \frac{v_1^3}{v_2} \text{Re}(\lambda_6) - \frac{3}{2} v_1 v_2 \text{Re}(\lambda_7), \quad (6.7)$$

$$\text{Im}(m_{12}^2) = \frac{1}{2} v_1 v_2 \text{Im}(\lambda_5) + \frac{1}{2} v_1^2 \text{Im}(\lambda_6) + \frac{1}{2} v_2^2 \text{Im}(\lambda_7). \quad (6.8)$$

Now, contrary to the case of the SM, in the 2HDM the doublets ϕ_i are not physical, *i.e.* the fields in this basis do not correspond to scalar mass eigenstates. This means that any unitary transformation of the doublets will produce the same physical predictions. One such transformation is of singular interest for it rotates the doublets to a particular basis where only one Higgs doublet acquires a VEV after SSB:

$$\begin{pmatrix} H_1 \\ H_2 \end{pmatrix} = \frac{1}{v} \begin{pmatrix} v_1 & v_2 \\ -v_2 & v_1 \end{pmatrix} \begin{pmatrix} \phi_1 \\ \phi_2 \end{pmatrix}, \quad (6.9)$$

where $v = \sqrt{v_1^2 + v_2^2}$. To emphasize the rotating character of this transformation, it is customary to introduce an angle β such that $\tan \beta = v_2/v_1$, so as to have instead

$$\begin{pmatrix} H_1 \\ H_2 \end{pmatrix} = \begin{pmatrix} \cos \beta & \sin \beta \\ -\sin \beta & \cos \beta \end{pmatrix} \begin{pmatrix} \phi_1 \\ \phi_2 \end{pmatrix}. \quad (6.10)$$

In this basis, commonly known as the *Higgs basis* and first introduced in Ref. [178], the vacuum state becomes

$$\langle H_1 \rangle_0 = \frac{1}{\sqrt{2}} \begin{pmatrix} 0 \\ v \end{pmatrix}, \quad \langle H_2 \rangle_0 = \begin{pmatrix} 0 \\ 0 \end{pmatrix}, \quad (6.11)$$

thus making it clear that only H_1 breaks $SU(2)_L \times U(1)_Y$, that one may take v as the VEV that outlines the electroweak scale, and that the parametrization of H_1 and H_2 around the vacuum can have the following form:

$$H_1 = \begin{pmatrix} G^+ \\ (v + S_1 + iG^0)/\sqrt{2} \end{pmatrix}, \quad H_2 = \begin{pmatrix} H^+ \\ (S_2 + iS_3)/\sqrt{2} \end{pmatrix}, \quad (6.12)$$

where G^+ and G^0 are the Goldstone bosons associated with the symmetry-breaking doublet.

The charged scalars mix only among themselves, and hence, in the Higgs basis, their mass terms come equal to

$$\mathcal{L}_{G^\pm, H^\pm} = - \begin{pmatrix} G^- & H^- \end{pmatrix} \begin{pmatrix} 0 & 0 \\ 0 & \frac{\text{Re}(m_{12}^2)}{\sin \beta \cos \beta} - \frac{v^2}{2} [\lambda_4 + \text{Re}(\lambda_5) + \cot \beta \text{Re}(\lambda_6) + \tan \beta \text{Re}(\lambda_7)] \end{pmatrix} \begin{pmatrix} G^+ \\ H^+ \end{pmatrix}, \quad (6.13)$$

which is often used to trade $\text{Re}(\lambda_5)$ for the mass of the charged Higgs:

$$\text{Re}(\lambda_5) = -\frac{2}{v^2} (M_{H^\pm}^2 - M^2) - \lambda_4 - \cot \beta \text{Re}(\lambda_6) - \tan \beta \text{Re}(\lambda_7), \quad (6.14)$$

where, for convenience, the parameter M^2 has been introduced, itself defined as

$$M^2 = \frac{\text{Re}(m_{12}^2)}{\sin \beta \cos \beta}. \quad (6.15)$$

Regarding the neutral sector, the rotation to the Higgs basis decouples the neutral Goldstone boson from the other three scalars, thus leaving a block diagonal mass matrix,

$$\mathcal{L}_{G^0, S_i} = -\frac{1}{2} \begin{pmatrix} S_1 & S_2 & G^0 & S_3 \end{pmatrix} \begin{pmatrix} M_{11}^2 & M_{12}^2 & 0 & M_{13}^2 \\ M_{12}^2 & M_{22}^2 & 0 & M_{23}^2 \\ 0 & 0 & 0 & 0 \\ M_{13}^2 & M_{23}^2 & 0 & M_{33}^2 \end{pmatrix} \begin{pmatrix} S_1 \\ S_2 \\ G^0 \\ S_3 \end{pmatrix}, \quad (6.16)$$

where we took advantage of the fact that the neutral mass terms compose a symmetric form [179], each independent entry of the associated matrix being

$$M_{11}^2 = s_{2\beta}^2 (M^2 - M_{H^\pm}^2) + v^2 \left[c_\beta^4 \lambda_1 + s_\beta^4 \lambda_2 + \frac{s_{2\beta}^2}{2} \lambda_3 + 2 s_\beta c_\beta^3 \text{Re}(\lambda_6) + 2 s_\beta^3 c_\beta \text{Re}(\lambda_7) \right], \quad (6.17)$$

$$M_{12}^2 = -\frac{s_{2\beta}}{4} \left\{ 4 c_{2\beta} (M_{H^\pm}^2 - M^2) + v^2 [\lambda_1 - \lambda_2 + c_{2\beta} (\lambda_1 + \lambda_2 - 2\lambda_3) + 2 s_{2\beta} \text{Re}(\lambda_6 - \lambda_7)] \right\}, \quad (6.18)$$

$$M_{13}^2 = -v^2 [s_\beta c_\beta \text{Im}(\lambda_5) + c_\beta^2 \text{Im}(\lambda_6) + s_\beta^2 \text{Im}(\lambda_7)], \quad (6.19)$$

$$M_{22}^2 = \frac{1}{2} \left\{ (1 + c_{4\beta}) M^2 + (1 - c_{4\beta}) M_{H^\pm}^2 + \frac{v^2}{4} (1 - c_{4\beta}) (\lambda_1 + \lambda_2 - 2\lambda_3) + v^2 \left[(4 s_\beta^3 c_\beta - t_\beta^{-1}) \text{Re}(\lambda_6) + (4 s_\beta c_\beta^3 - t_\beta) \text{Re}(\lambda_7) \right] \right\}, \quad (6.20)$$

$$M_{23}^2 = -\frac{v^2}{2} [c_{2\beta} \text{Im}(\lambda_5) - s_{2\beta} \text{Im}(\lambda_6 - \lambda_7)], \quad (6.21)$$

$$M_{33}^2 = 2 M_{H^\pm}^2 - M^2 + v^2 \lambda_4 + \frac{v^2}{2} (t_\beta^{-1} \lambda_6 + t_\beta \lambda_7), \quad (6.22)$$

with s_x, c_x, t_x standing as abbreviations for, respectively, $\sin x, \cos x, \tan x$. These expressions are, in turn, also often used to further change the parametrization of the model, by trading λ_{1-4} for $M_{11}^2, M_{12}^2, M_{22}^2, M_{33}^2$:

$$\lambda_1 = \frac{1}{v^2} [M_{11}^2 + t_\beta^2 (M_{22}^2 - M^2) - 2 t_\beta M_{12}^2] + \frac{1}{2} t_\beta [t_\beta^2 \text{Re}(\lambda_7) - 3 \text{Re}(\lambda_6)], \quad (6.23)$$

$$\lambda_2 = \frac{1}{v^2} [M_{11}^2 + t_\beta^{-2} (M_{22}^2 - M^2) + 2 t_\beta^{-1} M_{12}^2] + \frac{1}{2} t_\beta^{-1} [t_\beta^{-2} \text{Re}(\lambda_6) - 3 \text{Re}(\lambda_7)], \quad (6.24)$$

$$\lambda_3 = \frac{1}{v^2} (2 M_{H^\pm}^2 - M^2 + M_{11}^2 - M_{22}^2 + t_{2\beta}^{-1} M_{12}^2) - \frac{t_\beta^{-1}}{2} \text{Re}(\lambda_6) - \frac{t_\beta}{2} \text{Re}(\lambda_7), \quad (6.25)$$

$$\lambda_4 = \frac{1}{v^2} (M^2 - 2 M_{H^\pm}^2 + M_{33}^2) - \frac{t_\beta^{-1}}{2} \text{Re}(\lambda_6) - \frac{t_\beta}{2} \text{Re}(\lambda_7). \quad (6.26)$$

At this point, there is one final step we take for the sake of clarity. The remaining 3×3 mass matrix from Eq. (6.16) is a real symmetric matrix and therefore orthogonally diagonalizable. This means there is a matrix such that

$$R^T M_{S_i}^2 R = \text{diag}(m_1^2, m_2^2, m_3^2), \quad (6.27)$$

where $(M_{S_i}^2)_{ij} = M_{ij}^2$, and m_i^2 are the masses of the three physical neutral Higgs bosons. Being an orthogonal matrix, R can be parametrized as

$$R = \begin{pmatrix} R_{11} & R_{12} & R_{13} \\ R_{21} & R_{22} & R_{23} \\ R_{31} & R_{32} & R_{33} \end{pmatrix} \quad (6.28)$$

$$= \begin{pmatrix} c_{\alpha_1} c_{\alpha_2} & s_{\alpha_1} c_{\alpha_2} & -s_{\alpha_2} \\ c_{\alpha_1} s_{\alpha_2} s_{\alpha_3} - s_{\alpha_1} c_{\alpha_3} & s_{\alpha_1} s_{\alpha_2} s_{\alpha_3} + c_{\alpha_1} c_{\alpha_3} & c_{\alpha_2} s_{\alpha_3} \\ c_{\alpha_1} s_{\alpha_2} c_{\alpha_3} + s_{\alpha_1} s_{\alpha_3} & s_{\alpha_1} s_{\alpha_2} c_{\alpha_3} - c_{\alpha_1} s_{\alpha_3} & c_{\alpha_2} c_{\alpha_3} \end{pmatrix}. \quad (6.29)$$

This immediately allows us to consider $M_{ij}^2 \equiv M_{ij}^2(m_{1,2,3}^2, \alpha_{1,2,3})$, such functions being for the cases at hand:

$$M_{11}^2 = m_1^2 R_{11}^2 + m_2^2 R_{12}^2 + m_3^2 R_{13}^2, \quad (6.30)$$

$$M_{12}^2 = m_1^2 R_{11} R_{21} + m_2^2 R_{12} R_{22} + m_3^2 R_{13} R_{23}, \quad (6.31)$$

$$M_{22}^2 = m_1^2 R_{21}^2 + m_2^2 R_{22}^2 + m_3^2 R_{23}^2, \quad (6.32)$$

$$M_{33}^2 = m_1^2 R_{31}^2 + m_2^2 R_{32}^2 + m_3^2 R_{33}^2. \quad (6.33)$$

Moreover, using Eq. (6.27) and taking into account that the elements (1, 3) and (2, 3) of $M_{S_i}^2$ depend only on parameters that would naturally be input parameters of a general 2HDM (see Eq. (6.19) and Eq. (6.21)), we can make one final trade by writing m_2^2 and m_3^2 in terms of m_1^2 – which one may, without loss of generality, take to be the SM Higgs boson mass –, elements of R , the VEV v , the angle β , and $\text{Im}(\lambda_{5,6,7})$:

$$m_2^2 = \frac{1}{(R_{13}R_{22} - R_{12}R_{23})R_{32}} \left\{ m_1^2 (R_{11}R_{23} - R_{13}R_{21})R_{31} + \frac{v^2}{2} [\text{Im}(\lambda_5)(R_{23}s_{2\beta} - R_{13}c_{2\beta}) + 2\text{Im}(\lambda_6)(R_{23}c_{\beta}^2 + R_{13}s_{\beta}c_{\beta}) + 2\text{Im}(\lambda_7)(R_{23}s_{\beta}^2 - R_{13}s_{\beta}c_{\beta})] \right\}, \quad (6.34)$$

$$m_3^2 = \frac{1}{(R_{13}R_{22} - R_{12}R_{23})R_{33}} \left\{ m_1^2 (R_{12}R_{21} - R_{11}R_{22})R_{31} + \frac{v^2}{2} [\text{Im}(\lambda_5)(-R_{22}s_{2\beta} + R_{12}c_{2\beta}) - 2\text{Im}(\lambda_6)(R_{22}c_{\beta}^2 + R_{12}s_{\beta}c_{\beta}) - 2\text{Im}(\lambda_7)(R_{22}s_{\beta}^2 - R_{12}s_{\beta}c_{\beta})] \right\}. \quad (6.35)$$

At last, one reaches a point where one would have the model described by

$$v, \tan \beta, \alpha_{1,2,3}, m_1^2, M_{H^\pm}^2, \text{Re}(m_{12}^2), \text{Im}(\lambda_{5,6,7}), \text{Re}(\lambda_{6,7}), \quad (6.36)$$

counting a total of 13 independent parameters, just as we counted at the start of the section, and as should always be the total for any parametrization of a 2HDM with no symmetries imposed [180]. That

is not the case of the Z_2 -symmetric 2HDM, its softly-broken version introduced after we briefly take on the new couplings a second Higgs adds to the Yukawa sector.

6.2 The Yukawa Sector

The addition of another $SU(2)_L$ doublet with hypercharge $Y = 1/2$ also extends the Yukawa sector of the SM. The most general Yukawa Lagrangian in a 2HDM reads:

$$\mathcal{L}_Y = -\bar{Q}_L \left(Y_1^u \tilde{\phi}_1 + Y_2^u \tilde{\phi}_2 \right) u_R - \bar{Q}_L \left(Y_1^d \phi_1 + Y_2^d \phi_2 \right) d_R - \bar{L}_L \left(Y_1^\ell \phi_1 + Y_2^\ell \phi_2 \right) \ell_R + \text{h.c.} \quad (6.37)$$

After SSB, the scalar doublets acquire a VEV, generating, as in the case of the SM, fermion mass matrices which are then bi-diagonalized:

$$M_f = \frac{1}{\sqrt{2}} \left(v_1 Y_1^f + v_2 Y_2^f \right) \longrightarrow \frac{1}{\sqrt{2}} V^{f\dagger} \left(v_1 Y_1^f + v_2 Y_2^f \right) U^f, \quad \text{for } f = u, d, \ell. \quad (6.38)$$

By using the parametrization around the vacuum of Eq. (6.12), and expanding the resulting products of fields, it is straightforward to derive the fermion-scalar couplings in the 2HDM. Whereas in the SM the diagonalization of the mass matrices also diagonalizes the fermion-scalar couplings, in the 2HDM this is no longer necessarily true. One may easily illustrate this by switching once more to the Higgs basis. The β rotation of Eq. (6.10) yields

$$\begin{aligned} \mathcal{L}_Y = & -\bar{Q}_L \left[Y_1^u \left(\cos \beta \tilde{H}_1 - \sin \beta \tilde{H}_2 \right) + Y_2^u \left(\sin \beta \tilde{H}_1 + \cos \beta \tilde{H}_2 \right) \right] u_R \\ & -\bar{Q}_L \left[Y_1^d \left(\cos \beta H_1 - \sin \beta H_2 \right) + Y_2^d \left(\sin \beta H_1 + \cos \beta H_2 \right) \right] d_R \\ & -\bar{L}_L \left[Y_1^\ell \left(\cos \beta H_1 - \sin \beta H_2 \right) + Y_2^\ell \left(\sin \beta H_1 + \cos \beta H_2 \right) \right] \ell_R \\ & + \text{h.c.}, \end{aligned} \quad (6.39)$$

which, upon rearrangement and the identification that $v_1 = v \cos \beta$, $v_2 = v \sin \beta$, gives us the Yukawa Lagrangian expressed in the Higgs basis prior to the bi-diagonalization:

$$\mathcal{L}_Y = -\frac{\sqrt{2}}{v} \bar{Q}_L \left(M_u \tilde{H}_1 + N_u \tilde{H}_2 \right) u_R - \frac{\sqrt{2}}{v} \bar{Q}_L \left(M_d H_1 + N_d H_2 \right) d_R - \frac{\sqrt{2}}{v} \bar{L}_L \left(M_\ell H_1 + N_\ell H_2 \right) \ell_R + \text{h.c.}, \quad (6.40)$$

where

$$N_f = \frac{v}{\sqrt{2}} \left(-\sin \beta Y_1^f + \cos \beta Y_2^f \right), \quad \text{for } f = u, d, \ell. \quad (6.41)$$

Here the fact that only H_1 acquires a VEV is made even more significant, by making it the Higgs doublet which is associated with the mass matrices. The expansion in terms of the fields from the parametrization in Eq. (6.12) yields – again, in the absence of neutrino masses –

$$\begin{aligned} \mathcal{L}_Y = & -\bar{u}_L M_u u_R - \bar{d}_L M_d d_R - \bar{\ell}_L M_\ell \ell_R + \sqrt{2} \bar{d}_L \frac{M_u}{v} G^- u_R - \sqrt{2} \bar{u}_L \frac{M_d}{v} G^+ d_R \\ & - \sqrt{2} \bar{\nu}_L \frac{M_\ell}{v} G^+ \ell_R + \sqrt{2} \bar{d}_L \frac{N_u}{v} H^- u_R - \sqrt{2} \bar{u}_L \frac{N_d}{v} H^+ d_R - \sqrt{2} \bar{\nu}_L \frac{N_\ell}{v} H^+ \ell_R \\ & - \bar{u}_L \frac{M_u}{v} S_1 u_R - \bar{d}_L \frac{M_d}{v} S_1 d_R - \bar{\ell}_L \frac{M_\ell}{v} S_1 \ell_R - \bar{u}_L \frac{N_u}{v} S_2 u_R - \bar{d}_L \frac{N_d}{v} S_2 d_R \\ & - \bar{\ell}_L \frac{N_\ell}{v} S_2 \ell_R + i \bar{u}_L \frac{N_u}{v} S_3 u_R - i \bar{d}_L \frac{N_d}{v} S_3 d_R - i \bar{\ell}_L \frac{N_\ell}{v} S_3 \ell_R + \text{h.c.} \end{aligned} \quad (6.42)$$

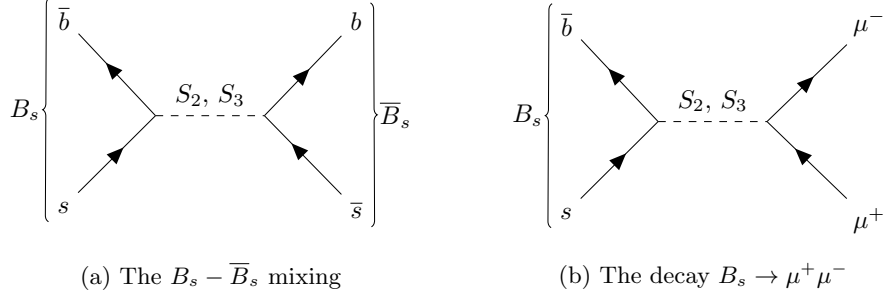


Figure 6.1: Example of tree-level FCNCs mediated by neutral scalars. The currents mediated by actual neutral scalar mass eigenstates come via rotations that include S_2 and S_3 , the unphysical states associated with the non-diagonal matrices N^f .

By rotating the fermions to their mass eigenstates, the N_f matrices also transform according to

$$N_f \longrightarrow N'_f = V^{f\dagger} N_f U^f, \quad \text{for } f = u, d, \ell. \quad (6.43)$$

and, dropping the primes for simplicity, one has in the Higgs basis together with the fermion mass basis:

$$\begin{aligned}
\mathcal{L}_Y = & - \left(1 + \frac{S_1}{v} \right) (\bar{u} M_u u + \bar{d} M_d d + \bar{\ell} M_\ell \ell) \\
& + \sqrt{2} \frac{G^+}{v} [\bar{u} (M_u V P_L - V M_d P_R) d - \bar{\nu} M_\ell P_R \ell] \\
& + \sqrt{2} \frac{G^-}{v} [\bar{d} (V^\dagger M_u P_R - M_d V^\dagger P_L) u - \bar{\ell} M_\ell P_L \nu] \\
& + i \frac{G^0}{v} (\bar{u} M_u \gamma_5 u - \bar{d} M_d \gamma_5 d - \bar{\ell} M_\ell \gamma_5 \ell) \\
& + \sqrt{2} \frac{H^+}{v} [\bar{u} (N_u^\dagger V P_L - V N_d P_R) d - \bar{\nu} N_\ell P_R \ell] \\
& + \sqrt{2} \frac{H^-}{v} [\bar{d} (V^\dagger N_u P_R - N_d^\dagger V^\dagger P_L) u - \bar{\ell} N_\ell^\dagger P_L \nu] \\
& - \frac{S_2}{v} [\bar{u} (N_u P_R + N_u^\dagger P_L) u + \bar{d} (N_d P_R + N_d^\dagger P_L) d + \bar{\ell} (N_\ell P_R + N_\ell^\dagger P_L) \ell] \\
& + i \frac{S_3}{v} [\bar{u} (N_u P_R - N_u^\dagger P_L) u - \bar{d} (N_d P_R - N_d^\dagger P_L) d - \bar{\ell} (N_\ell P_R - N_\ell^\dagger P_L) \ell].
\end{aligned} \quad (6.44)$$

While the matrices M_f are diagonal, real and positive by definition, the matrices N_f are not necessarily so – they are, in general, completely arbitrary and complex. This leads to the Yukawa interactions with the neutral scalars not being diagonal, thus opening the possibility for having FCNCs at tree level in a generic 2HDM. This is a major departure from the SM.

6.3 The 2HDM with a Softly-broken Z_2 Symmetry

One could say that the tree-level FCNC problem is the defining predicament of the 2HDM. However sizable as NP contributions may be, as we saw in the $b \rightarrow s$ transition in Chapter 5, it seems reasonable that contributions at tree-level order would be sizable enough to exceed the experimental bounds for this type of phenomena – *e.g.* the oscillations in the neutral meson systems, or the leptonic decays of neutral mesons, examples of which can be found in Fig. 6.1. For this reason, ever since the introduction of the

model, many have been the proposed mechanisms to get rid of these tree-level FCNCs, regardless of how viable models with these currents may still be.

An instant look back at Eq. (6.44) and the $S_{2,3}$ terms, tells us that if, say, $N_f \propto M_f$, the diagonalization of mass terms would also diagonalize the other neutral Yukawa couplings, thus leaving the theory free of the pernicious tree-level currents. This is precisely the idea behind the *Aligned 2HDM* [181]. The proportionality coefficients are, in general, complex and, therefore, possible new sources for CP violation, one of the main attractions of this model. The alignment is, however, *ad hoc*: the relations may be imposed at whichever scale and are, in principle, not radiatively stable [182]. There have been, nevertheless, efforts to provide a UV completion to this model [183], to find a symmetry-based justification for the alignment hypothesis [184, 185], and it has even been noted that the loop correction may comply with Minimal Flavour Violation [186–188].

If, on the other hand, one looks at Eq. (6.39), it is clear that another way to achieve flavour-conservation, again by only having one matrix per flavour, would be to make the matrices coupling to H_2 the same as those H_1 couples to, which, barring judicious choices of β , comes down to making those matrices either Y_1^f or Y_2^f , for each $f = u, d, \ell$, and never a combination of both. In other words, *if all fermions of a given charge and helicity transform according to the same irreducible representation of $SU(2)$, correspond to the same value of T_3 , and if a basis exists in which they receive their contributions in the mass matrix from a single source*, the absence of FCNCs at tree-level is guaranteed [50]. This is the condition for Natural Flavour Conservation (NFC), which was formalized simultaneously by Glashow and Weinberg [189], and Paschos [190]. In the 2HDM, NFC may be achieved by imposing discrete or continuous symmetries; with a Z_2 , the simplest discrete symmetry that yields NFC, there are four different possibilities, usually called types I, II, X (or *lepton-specific*), and Y (or *flipped*) [191].

6.3.1 Types I, II, X, Y

By convention, one fixes the couplings of up-quarks only to Y_2^u , *i.e.* only to ϕ_2 . From Eq. (6.37), one can easily construct the following transformation assignments which define the four types of the Z_2 -symmetric 2HDM:

- **type I:** $\phi_1 \rightarrow -\phi_1$

All fermions acquire their mass terms from their couplings to ϕ_2 .

- **type II:** $\phi_1 \rightarrow -\phi_1$, $d_R \rightarrow -d_R$, $\ell_R \rightarrow -\ell_R$

Up-quarks acquire their mass terms from their couplings to ϕ_2 ;

Down-quarks and charged leptons acquire their mass terms from their couplings to ϕ_1 .

- **type X:** $\phi_1 \rightarrow -\phi_1$, $\ell_R \rightarrow -\ell_R$

Quarks acquire their mass terms from their couplings to ϕ_2 ;

Charged leptons acquire their mass terms from their couplings to ϕ_1 .

- **type Y:** $\phi_1 \rightarrow -\phi_1$, $d_R \rightarrow -d_R$

Up-quarks and charged leptons acquire their mass terms from their couplings to ϕ_2 ;

Down-quarks acquire their mass terms from their couplings to ϕ_1 .

Regardless of one's choice, the impact of a Z_2 on the scalar sector is uniform, since all types share the same Higgs doublets' charge assignments. With

$$\phi_1 \rightarrow -\phi_1, \quad \phi_2 \rightarrow \phi_2, \quad (6.45)$$

it follows automatically from Eq. (6.2) that

$$m_{12}^2 = \lambda_6 = \lambda_7 = 0. \quad (6.46)$$

Because one has the freedom to rephase the remaining parameter unprotected by hermiticity, the imaginary part of λ_5 can also be put to zero. Thus, on top of freeing the theory from possibly dangerous FCNCs, and any CP violation associated with complex and non-diagonal Yukawa matrices, we have obtained a scalar potential that is CP-conserving as well. Additionally, because one of the main motivations for 2HDMs is the Higgs sector of the MSSM, one tends to mimic the soft-breaking of supersymmetry and the mixed bilinear term that originates there¹: one introduces the soft-breaking of Z_2 by bringing back m_{12}^2 , still keeping it real to preserve the CP properties of the model. The potential in Eq. (6.2) becomes, in a softly-broken Z_2 -symmetric 2HDM (which, for simplicity, we will henceforth refer to simply as *the* 2HDM):

$$\begin{aligned} V_H = & m_{11}^2 \phi_1^\dagger \phi_1 + m_{22}^2 \phi_2^\dagger \phi_2 - m_{12}^2 (\phi_1^\dagger \phi_2 + \phi_2^\dagger \phi_1) + \frac{1}{2} \lambda_1 (\phi_1^\dagger \phi_1)^2 + \frac{1}{2} \lambda_2 (\phi_2^\dagger \phi_2)^2 \\ & + \lambda_3 (\phi_1^\dagger \phi_1) (\phi_2^\dagger \phi_2) + \lambda_4 (\phi_1^\dagger \phi_2) (\phi_2^\dagger \phi_1) + \frac{1}{2} \lambda_5 \left[(\phi_1^\dagger \phi_2)^2 + (\phi_2^\dagger \phi_1)^2 \right]. \end{aligned} \quad (6.47)$$

We have now 8 independent real parameters in V_H . As before, we would like to inspect the mass spectrum of the scalar sector and, *en route*, define a better set of input parameters for the numerical analysis ahead. The minimum conditions have reduced to two. One may still use the trivially modified conditions in Eqs. (6.6) and (6.7) to trade m_{11}^2 and m_{22}^2 for v and $\tan \beta$. The square of the charged Higgs mass becomes

$$M_{H^\pm}^2 = M^2 - \frac{v^2}{2} (\lambda_4 + \lambda_5), \quad (6.48)$$

and we write again λ_5 in terms of it. Regarding the neutral scalars, the situation has changed considerably. Looking at Eqs. (6.17)–(6.22), it is clear that

$$M_{13}^2 = M_{23}^2 = 0, \quad (6.49)$$

and that, from Eq. (6.16), S_3 has decoupled from $S_{1,2}$, and is a mass eigenstate with

$$M_{33}^2 = 2 M_{H^\pm}^2 - M^2 + v^2 \lambda_4. \quad (6.50)$$

Since CP is conserved, CP itself is defined in the mass basis: this physical pseudoscalar is a CP-odd state, which, by convention, one calls the A boson. Setting $M_A^2 = M_{33}^2$, the relations in Eqs. (6.23)–(6.26) have the new form:

$$\lambda_1 = \frac{1}{v^2} \left[M_{11}^2 + t_\beta^2 (M_{22}^2 - M^2) - 2 t_\beta M_{12}^2 \right], \quad (6.51)$$

$$\lambda_2 = \frac{1}{v^2} \left[M_{11}^2 + t_\beta^{-2} (M_{22}^2 - M^2) + 2 t_\beta^{-1} M_{12}^2 \right], \quad (6.52)$$

$$\lambda_3 = \frac{1}{v^2} \left(2 M_{H^\pm}^2 - M^2 + M_{11}^2 - M_{22}^2 + t_{2\beta}^{-1} M_{12}^2 \right), \quad (6.53)$$

$$\lambda_4 = \frac{1}{v^2} (M^2 - 2 M_{H^\pm}^2 + M_A^2). \quad (6.54)$$

¹See, for example, Ref. [192] for a comprehensive review of Higgs bosons in the MSSM.

In turn, the CP-even mass eigenstates are obtained after the diagonalization of the remaining 2×2 block in Eq. (6.16). By convention, these neutral scalars are denoted h and H , and it is also conventional to take $M_h < M_H$. Instead of three mixing angles, only one is needed now, and, following Ref. [191], we write

$$\begin{pmatrix} H \\ h \end{pmatrix} = R(\alpha) \begin{pmatrix} \rho_1 \\ \rho_2 \end{pmatrix}, \quad (6.55)$$

where $\rho_{1,2}$ are the fields in the original basis, and

$$R(x) = \begin{pmatrix} \cos x & \sin x \\ -\sin x & \cos x \end{pmatrix}. \quad (6.56)$$

In terms of the fields from the Higgs basis, this is simply

$$\begin{pmatrix} H \\ h \end{pmatrix} = R(\alpha) R^T(\beta) \begin{pmatrix} S_1 \\ S_2 \end{pmatrix} = R^T(\beta - \alpha) \begin{pmatrix} S_1 \\ S_2 \end{pmatrix} = \begin{pmatrix} c_{\beta-\alpha} & -s_{\beta-\alpha} \\ s_{\beta-\alpha} & c_{\beta-\alpha} \end{pmatrix} \begin{pmatrix} S_1 \\ S_2 \end{pmatrix}. \quad (6.57)$$

One takes this rotation to get – in agreement with, for example, Ref. [180] –

$$M_{11}^2 = M_h^2 s_{\beta-\alpha}^2 + M_H^2 c_{\beta-\alpha}^2, \quad (6.58)$$

$$M_{22}^2 = M_h^2 s_{\beta-\alpha}^2 + M_H^2 s_{\beta-\alpha}^2, \quad (6.59)$$

$$M_{12}^2 = (M_h^2 - M_H^2) c_{\beta-\alpha} s_{\beta-\alpha}, \quad (6.60)$$

reaching a point where one would have a 2HDM described by

$$v, \tan \beta, \beta - \alpha, M_{H^\pm}^2, M_h^2, M_H^2, M_A^2, m_{12}^2, \quad (6.61)$$

counting a total of 8 independent parameters, just as we counted above.

The Yukawa sector is quite straightforward. If one is working with, say, the 2HDM of type II, the charge assignments amount to taking in Eq. (6.37)

$$Y_1^u \longrightarrow 0, \quad (6.62)$$

$$Y_2^n \longrightarrow 0, \quad \text{for } n = d, \ell. \quad (6.63)$$

From Eq. (6.39), one sees that M_f , the matrices associated with H_1 , are

$$M_u = \frac{v}{\sqrt{2}} \sin \beta Y_2^u, \quad (6.64)$$

$$M_n = \frac{v}{\sqrt{2}} \cos \beta Y_1^n, \quad \text{for } n = d, \ell, \quad (6.65)$$

and that N_f , the matrices associated with H_2 , are

$$N_u = \frac{v}{\sqrt{2}} \cos \beta Y_2^u = \cot \beta M_u, \quad (6.66)$$

$$N_n = -\frac{v}{\sqrt{2}} \sin \beta Y_1^n = -\tan \beta M_n, \quad \text{for } n = d, \ell. \quad (6.67)$$

Whereas the mass terms are, by construction, stable under these redefinitions, the fermion-scalar couplings in Eq. (6.44) have gained the following shape:

$$\begin{aligned}
\mathcal{L}_Y^{2\text{HDM}} = & -\frac{S_1}{v} (\bar{u} M_u u + \bar{d} M_d d + \bar{\ell} M_\ell \ell) \\
& -\frac{S_2}{v} [\bar{u} (\cot \beta M_u) u - \bar{d} (\tan \beta M_d) d - \bar{\ell} (\tan \beta M_\ell) \ell] \\
& + i \frac{A}{v} [\bar{u} (\cot \beta M_u \gamma_5) u + \bar{d} (\tan \beta M_d \gamma_5) d + \bar{\ell} (\tan \beta M_\ell \gamma_5) \ell] \\
& + \sqrt{2} \frac{H^+}{v} [\bar{u} (\cot \beta M_u V P_L + \tan \beta V M_d P_R) d + \bar{\nu} (\tan \beta M_\ell P_R) \ell] \\
& + \sqrt{2} \frac{H^-}{v} [\bar{d} (\cot \beta V^\dagger M_u P_R + \tan \beta M_d V^\dagger P_L) u + \bar{\ell} (\tan \beta M_\ell P_L) \nu].
\end{aligned} \tag{6.68}$$

Using Eq. (6.57), the first two lines in the equation above can be rewritten, this time in terms of the mass eigenstates of the CP-even scalars:

$$-\frac{h}{v} (\bar{u} \xi_h^u M_u u + \bar{n} \xi_h^n M_n n) - \frac{H}{v} (\bar{u} \xi_H^u M_u u + \bar{n} \xi_H^n M_n n), \tag{6.69}$$

where

$$\xi_h^u = s_{\beta-\alpha} + c_{\beta-\alpha} \cot \beta = \frac{\cos \alpha}{\sin \beta}, \tag{6.70}$$

$$\xi_h^n = s_{\beta-\alpha} - c_{\beta-\alpha} \tan \beta = -\frac{\sin \alpha}{\cos \beta}, \quad \text{for } n = d, \ell, \tag{6.71}$$

$$\xi_H^u = c_{\beta-\alpha} - s_{\beta-\alpha} \cot \beta = \frac{\sin \alpha}{\sin \beta}, \tag{6.72}$$

$$\xi_H^n = c_{\beta-\alpha} + s_{\beta-\alpha} \tan \beta = \frac{\cos \alpha}{\cos \beta}, \quad \text{for } n = d, \ell. \tag{6.73}$$

If, finally, one defines further ξ coefficients for A ,

$$\xi_A^u = \cot \beta, \tag{6.74}$$

$$\xi_A^n = \tan \beta, \quad \text{for } n = d, \ell, \tag{6.75}$$

and taking advantage of the fact that the coefficients $\xi_{H^\pm}^f$ would always be equal, one may put $\mathcal{L}_Y^{2\text{HDM}}$ in a condensed notation, introduced by Aoki *et al.* [191]:

$$\begin{aligned}
\mathcal{L}_Y^{2\text{HDM}} = & -\sum_{f=d,u,\ell} \frac{m_f}{v} \left(\xi_h^f \bar{f} f h + \xi_H^f \bar{f} f H - i \xi_A^f \bar{f} \gamma_5 f A \right) \\
& + \left[\frac{\sqrt{2}}{v} V_{ud} \bar{u} (m_u \xi_A^u P_L + m_d \xi_A^d P_R) d H^+ + \frac{\sqrt{2}}{v} \bar{\nu}_\ell (m_\ell \xi_A^\ell P_R) \ell H^+ + \text{h.c.} \right],
\end{aligned} \tag{6.76}$$

where all matrix multiplications have been fleshed out, and u , d , and ℓ stand, respectively, for each individual up-type quark, down-type quark, and charged lepton, the sum over which is implicit.

Proceeding accordingly for the other three types of 2HDM, one arrives at the coefficients that characterize the Yukawa Lagrangian for each type, collected in Table 6.1.

6.4 The Coleman-Weinberg Potential

The vacuum structure of a model and its relation with SSB have, at tree-level, a geometrical meaning: the vacuum states sit at the bottom of the deepest well in the potential surface, producing a breakdown of

	Type I	Type II	Type X	Type Y
ξ_h^u	$\cos \alpha / \sin \beta$	$\cos \alpha / \sin \beta$	$\cos \alpha / \sin \beta$	$\cos \alpha / \sin \beta$
ξ_h^d	$\cos \alpha / \sin \beta$	$-\sin \alpha / \cos \beta$	$\cos \alpha / \sin \beta$	$-\sin \alpha / \cos \beta$
ξ_h^ℓ	$\cos \alpha / \sin \beta$	$-\sin \alpha / \cos \beta$	$-\sin \alpha / \cos \beta$	$\cos \alpha / \sin \beta$
ξ_H^u	$\sin \alpha / \sin \beta$	$\sin \alpha / \sin \beta$	$\sin \alpha / \sin \beta$	$\sin \alpha / \sin \beta$
ξ_H^d	$\sin \alpha / \sin \beta$	$\cos \alpha / \cos \beta$	$\sin \alpha / \sin \beta$	$\cos \alpha / \cos \beta$
ξ_H^ℓ	$\sin \alpha / \sin \beta$	$\cos \alpha / \cos \beta$	$\cos \alpha / \cos \beta$	$\sin \alpha / \sin \beta$
ξ_A^u	$\cot \beta$	$\cot \beta$	$\cot \beta$	$\cot \beta$
ξ_A^d	$-\cot \beta$	$\tan \beta$	$-\cot \beta$	$\tan \beta$
ξ_A^ℓ	$-\cot \beta$	$\tan \beta$	$\tan \beta$	$-\cot \beta$

Table 6.1: Yukawa couplings of up-type quarks, down-type quarks, and charged leptons to the neutral scalars h , H , and A . The coefficients of the charged Higgs are equal to those of the pseudoscalar.

the theory's symmetry in the case of a non-null VEV. This was the scenario we encountered in the SM, in Chapter 2, and in the sections above for the 2HDM. This geometrical picture may, however, be somewhat obscured by the complexity that comes with corrections beyond the leading order. Take statistical mechanics, for example: at zero temperature, the thermodynamic ground state is the state of lowest energy; when thermal fluctuations are considered, on the other hand, the natural statistical quantities of the internal energy are no longer good descriptors of the system, and one no longer necessarily finds a minimum at the preferred thermodynamic state [193]. Nevertheless, a generalization of the principle of minimum energy is at hand, the geometrical picture being recovered if one minimizes the Gibbs free energy instead. Here we follow Peskin and Schroeder [194], and start by writing the Helmholtz free energy, $F(H)$, of a magnetic system:

$$Z(H) = e^{-\beta F(H)} = \int \mathcal{D}s \exp \left[-\beta \int dx (\mathcal{H}[s] - Hs(x)) \right], \quad (6.77)$$

where H is an external magnetic field, $\mathcal{H}[s]$ is the spin energy density, $s(x)$ is the local spin field, and $\beta = (kT)^{-1}$. The magnetization of the system is found by differentiating F at a fixed temperature,

$$\begin{aligned} -\frac{\partial F}{\partial H} &= \frac{1}{\beta} \frac{\partial}{\partial H} \ln Z \\ &= \frac{1}{Z} \int dx \int \mathcal{D}s s(x) \exp \left[-\beta \int dx (\mathcal{H}[s] - Hs(x)) \right] \\ &= \int dx \langle s(x) \rangle \equiv M, \end{aligned} \quad (6.78)$$

and defining the Gibbs free energy as a Legendre transform of F ,

$$G = F + MH, \quad (6.79)$$

we obtain:

$$\frac{\partial G}{\partial M} = \frac{\partial F}{\partial H} \frac{\partial H}{\partial M} + M \frac{\partial H}{\partial M} + H = H. \quad (6.80)$$

If the external field H is zero, $G(M)$ reaches a minimum for the given value of M .

One has to find a quantity in QFT which (analogously to G) gives a picture of the preferred vacuum (thermodynamic) state that is geometrical and, at the same time, includes all effects of quantum (thermal) fluctuations. Let us introduce a quantum scalar field ϕ , and an external source $J(x)$. We define an energy functional $W[J]$ by

$$Z[J] = e^{iW[J]} = \int \mathcal{D}\phi \exp \left[i \int d^4x (\mathcal{L}[\phi] + J(x)\phi) \right], \quad (6.81)$$

where $W[J]$ is playing the part of the Helmholtz free energy. As in the previous example, we take a derivative of the functional with respect to the external source,

$$\begin{aligned} \frac{\delta}{\delta J(x)} W[J] &= -i \frac{\delta}{\delta J(x)} \ln Z[J] \\ &= \frac{\int \mathcal{D}\phi \phi(x) \exp \left[i \int d^4x (\mathcal{L} + J\phi) \right]}{\int \mathcal{D}\phi \exp \left[i \int d^4x (\mathcal{L} + J\phi) \right]} \\ &= \langle \phi(x) \rangle_J \equiv \phi_{\text{cl}}(x), \end{aligned} \quad (6.82)$$

arriving at a quantity we call the *classical field*, which is related to the quantum field $\phi(x)$ much in the same way the magnetization M was related with $s(x)$. The QFT version of the Gibbs free energy is, then, a functional of the classical field, defined as the Legendre transform of $W[J]$:

$$\Gamma[\phi_{\text{cl}}] = W[J] - \int d^4x J(x)\phi_{\text{cl}}(x). \quad (6.83)$$

This object is known as the *effective action*, and it is trivial to derive that

$$\frac{\delta}{\delta \phi_{\text{cl}}(x)} \Gamma[\phi_{\text{cl}}] = -J(x), \quad (6.84)$$

in complete analogy with Eq. (6.80). If the external source is set to zero, the functional derivative of the effective action is zero. Moreover, since Γ is, just like G , an extensive quantity, it is proportional to the volume of the spacetime region over which the functional integral is taken. Thus, we write:

$$\Gamma[\phi_{\text{cl}}] = -(VT) \cdot V_{\text{eff}}(\phi_{\text{cl}}), \quad (6.85)$$

where T is the time extent of the integration region, V is its three-dimensional volume, and V_{eff} , the *effective potential*, is exactly what we ordered – a function of the classical field that satisfies

$$\frac{\partial}{\partial \phi_{\text{cl}}} V_{\text{eff}}(\phi_{\text{cl}}) = 0. \quad (6.86)$$

6.4.1 One-loop Effective Potentials

Taking two functional derivatives of $W[J]$ with respect to the external source gets us

$$\frac{\delta^2}{\delta J(x)\delta J(y)} W[J] = i \langle \phi(x)\phi(y) \rangle_J, \quad (6.87)$$

where, for simplicity, we have omitted the state in the matrix element. Using Eq. (6.82), we also have

$$\frac{\delta^2}{\delta J(x)\delta J(y)} W[J] = \frac{\delta}{\delta J(x)} \phi_{\text{cl}}, \quad (6.88)$$

which, taking into account Eq. (6.84), gives in turn:

$$\frac{\delta^2}{\delta \phi_{\text{cl}}(x)\delta \phi_{\text{cl}}(y)} \Gamma[\phi_{\text{cl}}] = -\frac{\delta}{\delta \phi_{\text{cl}}(x)} J(y) = i \left(\langle \phi(x)\phi(y) \rangle_J \right)^{-1}. \quad (6.89)$$

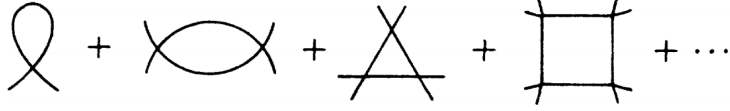


Figure 6.2: The one-loop diagrams which contribute to V_{CW} in the $\lambda\phi^4$ model.

(Figure taken from Ref. [195], ©1973 American Physical Society)

For the field configuration where ϕ_{cl} is given by the true expectation value of ϕ , *i.e.* when $J = 0$ and the effective action is minimized, this is nothing but the inverse of the two point function of scalar theory,

$$\frac{\delta^2}{\delta\phi_{\text{cl}}(x)\delta\phi_{\text{cl}}(y)}\Gamma[\phi_{\text{cl}}] \equiv iG(x, y)^{-1}. \quad (6.90)$$

It can be shown, if we go on to take up to the n -th order derivative, that the effective action can be written as a series that generates all 1PI Green's functions with $i = 1, \dots, n$ external legs. Denoting $\Gamma^{(n)}(x_1, \dots, x_n)$ as the sum of all 1PI Feynman diagrams with n external legs,

$$\Gamma[\phi_{\text{cl}}] = \sum_n \frac{1}{n!} \int d^4x_1 \dots d^4x_n \Gamma^{(n)}(x_1, \dots, x_n) \phi_{\text{cl}}(x_1) \dots \phi_{\text{cl}}(x_n), \quad (6.91)$$

and, evaluating the spacetime integrals, it is not difficult to make out that V_{eff} reads

$$V_{\text{eff}} = - \sum_n \frac{1}{n!} \Gamma^{(n)}(0, \dots, 0) \phi_{\text{cl}}(x)^n. \quad (6.92)$$

In their foundational paper [195], Sidney Coleman and Erik Weinberg advocated for a loop expansion of the effective potential, instead of the expansion in powers of the coupling constant, and that is indeed the common practice, which we also adhere to in this work. In tree-level approximation, the effective potential is just the ordinary potential, V_H , whereas the one-loop contributions compose what is known as the *Coleman-Weinberg potential*. Adding the necessary set of counterterms to treat the divergences introduced by the loop corrections, we define

$$V_{\text{eff}}^{(1)} = V_H + V_{\text{CW}}^{(1)} + \delta V. \quad (6.93)$$

Let us work out V_{CW} for the simple $\lambda\phi^4$ single scalar theory. The tree-level effective potential is given by the scalar potential with the quantum field replaced by its classical counterpart:

$$V_H = \frac{1}{2}m^2\phi_{\text{cl}}^2 + \frac{\lambda}{4!}\phi_{\text{cl}}^4. \quad (6.94)$$

Since we only have even powers of ϕ_{cl} , no diagrams with odd external legs are generated, meaning $V_{\text{CW}}^{(1)}$ is a sum of the one-loop diagrams with an even number of external legs; these are the polygon diagrams that are represented in Fig. 6.2. Thus we obtain

$$V_{\text{CW}}^{(1)} = i \sum_{n=1}^{\infty} \int \frac{d^4k}{(2\pi)^4} \frac{1}{2n} \left(\frac{\frac{1}{2}\lambda\phi_{\text{cl}}^2}{k^2 - m^2 + i\varepsilon} \right)^n, \quad (6.95)$$

where $1/2n$ is a combinatorial factor that accounts for rotations and reflections of the n -sided polygon, and for the swapping of external legs, replacing the factor $1/n!$ in that process. Performing the usual Wick rotation into Euclidean space, $k^2 \rightarrow -k_0^2 - \vec{k}^2 = -k_E^2$, dropping the 'E' for simplicity, summing the series,

$$\ln(1+x) = - \sum_{n=1}^{\infty} \frac{(-1)^n x^n}{n} \quad (6.96)$$

and also dropping $i\varepsilon$, one has

$$\begin{aligned} V_{\text{CW}}^{(1)} &= \frac{1}{2} \int \frac{d^4 k}{(2\pi)^4} \ln \left(1 + \frac{\frac{1}{2} \lambda \phi_{\text{cl}}^2}{k^2 + m^2} \right) \\ &= \frac{1}{2} \int \frac{d^4 k}{(2\pi)^4} \left[\ln \left(k^2 + m^2 + \frac{1}{2} \lambda \phi_{\text{cl}}^2 \right) - \ln(k^2 + m^2) \right]. \end{aligned} \quad (6.97)$$

This integral has an ultraviolet divergence and needs to be regularized if one wants to evaluate it. The second term does not depend on the field: it will, therefore, merely give a constant contribution to the effective potential, which we can neglect without loss of generality. If one differentiates what remains with respect to ϕ_{cl} , one obtains

$$\frac{\partial}{\partial \phi_{\text{cl}}} V_{\text{CW}}^{(1)} = \frac{1}{2} \frac{\partial m_{\text{eff}}^2}{\partial \phi_{\text{cl}}} \int \frac{d^4 k}{(2\pi)^4} \frac{1}{k^2 + m_{\text{eff}}^2}, \quad (6.98)$$

where we have introduced

$$m_{\text{eff}}^2 \equiv m_{\text{eff}}^2(\phi_{\text{cl}}) = m^2 + \frac{1}{2} \lambda \phi_{\text{cl}}^2. \quad (6.99)$$

This integral in momentum has the typical shape of the expressions we commonly evaluate using dimensional regularization. Recalling that in D dimensions

$$\int \frac{d^4 k}{(2\pi)^4} \longrightarrow \mu^{4-D} \int \frac{d^D k}{(2\pi)^D}, \quad (6.100)$$

and that we define $4 - D = 2\epsilon$, we get:

$$\begin{aligned} \frac{\partial}{\partial \phi_{\text{cl}}} V_{\text{CW}}^{(1)} &= \frac{1}{2} \frac{\partial m_{\text{eff}}^2}{\partial \phi_{\text{cl}}} \left[\frac{\mu^{2\epsilon}}{(4\pi)^{2-\epsilon}} \frac{\Gamma(\epsilon)}{\epsilon - 1} (m_{\text{eff}}^2)^{1-\epsilon} \right] \\ &= \frac{1}{2} \frac{\partial m_{\text{eff}}^2}{\partial \phi_{\text{cl}}} \left[-\frac{m_{\text{eff}}^2}{(4\pi)^2} \left(\ln \left(\frac{4\pi \mu^2}{m_{\text{eff}}^2} \right) + 1 + \frac{1}{\epsilon} - \gamma_E + \mathcal{O}(\epsilon) \right) \right] \\ &= \frac{m_{\text{eff}}^2}{32\pi^2} \frac{\partial m_{\text{eff}}^2}{\partial \phi_{\text{cl}}} \left[\ln \left(\frac{m_{\text{eff}}^2}{\tilde{\mu}^2} \right) - 1 - \frac{1}{\epsilon} + \mathcal{O}(\epsilon) \right], \end{aligned} \quad (6.101)$$

where $\tilde{\mu}^2 = 4\pi\mu^2 e^{-\gamma_E}$. To integrate back over the field, we simply have to make a change of variables,

$$m_{\text{eff}}^2 = \tilde{\mu}^2 x, \quad \frac{\partial m_{\text{eff}}^2}{\partial \phi_{\text{cl}}} d\phi_{\text{cl}} = \tilde{\mu}^2 dx, \quad (6.102)$$

such that

$$\int dx x [\ln x + b] = \frac{x^2}{2} \left[\ln x + b - \frac{1}{2} \right], \quad (6.103)$$

yields, in our case:

$$V_{\text{CW}}^{(1)} = \frac{m_{\text{eff}}^4}{64\pi^2} \left[\ln \left(\frac{m_{\text{eff}}^2}{\tilde{\mu}^2} \right) - \frac{3}{2} - \frac{1}{\epsilon} \right]. \quad (6.104)$$

The parameter we introduced above as m_{eff}^2 can be viewed as a field-dependent effective mass, hence the reason we wrote it with the moniker ‘eff’, and is the main driver of the one-loop corrections to the tree-level potential.

6.4.2 Field-dependent Effective Mass Terms

Proceeding much in the same way, only now to include diagrams with external scalar legs and a gauge boson in the loop, we will get the following contribution:

$$V_{\text{CW}}^{(1)} = 3 \frac{m_{\text{eff},B}^4}{64\pi^2} \left[\ln \left(\frac{m_{\text{eff},B}^2}{\tilde{\mu}^2} \right) - \frac{5}{6} - \frac{1}{\epsilon} \right]. \quad (6.105)$$

	h	H	A	H^\pm	G^0	G^\pm	Z_μ	W_μ^\pm	t	b	τ
N_i	1	1	1	2	1	2	3	6	-12	-12	-4
C_i	3/2	3/2	3/2	3/2	3/2	3/2	5/6	5/6	3/2	3/2	3/2

Table 6.2: The values of the constants in Eq. (6.107) for each of the relevant particles in the 2HDM.

For a fermionic loop, on the other hand, the result would be

$$V_{\text{CW}}^{(1)} = -4 \frac{m_{\text{eff},F}^4}{64\pi^2} \left[\ln \left(\frac{m_{\text{eff},F}^2}{\tilde{\mu}^2} \right) - \frac{3}{2} - \frac{1}{\epsilon} \right]. \quad (6.106)$$

Bringing back the “master formula” in Eq. (6.93), a given choice of δV translates to a different renormalization scheme. The authors of Ref. [195], for example, demanded that the second and fourth derivatives of the effective potential produced, respectively, the mass and coupling constant of the scalar. In the $\overline{\text{MS}}$ scheme, which we employ in this work, the counterterms are chosen in such a way that the divergent term with ϵ is cancelled, and $\tilde{\mu}^2$ is simply μ . So, for a model that has neutral scalar fields h, H, A , charged scalars H^\pm , Goldstone bosons G^0, G^\pm , massive gauge bosons Z_μ, W_μ^\pm , third generation fermions t, b , and third generation charged lepton τ , one writes the total Coleman-Weinberg potential as a sum over the contributions of each mass eigenstate:

$$V_{\text{CW}}^{(1)} = \sum_i \frac{N_i}{64\pi^2} M_i^4(\phi) \left[\ln \left(\frac{M_i^2(\phi)}{\mu^2} \right) - C_i \right], \quad (6.107)$$

where, for economy of notation, a generic effective mass is now $M_i^2(\phi)$, and, taking into account the number of colours and the mass degeneracy of charged bosons, the constants N_i and C_i are as given in Table 6.2. It should be noted that the Goldstone bosons, while not massive themselves, can have an effective mass term and, therefore, their contributions must be included. Also worth of note is the fact that, in the $\overline{\text{MS}}$ scheme, one is left with a dependence on the renormalization scale μ in the logarithms. However, up to higher order effects, the masses and VEVs should not depend on this scale, and, as long as it still renders the loop expansion meaningful, it can be chosen to take the value of a natural scale of the model. In order to have all fractions in the logarithms close to 1, μ should be of the order of the physical masses; thus, we choose the closest natural scale around those values, the electroweak scale:

$$\mu \sim v = 246 \text{ GeV}. \quad (6.108)$$

What are, then, the effective mass terms in the 2HDM? First, we rewrite the Higgs doublets in Eq. (6.12), which are in the convenient basis where only H_1 is associated with mass generation, this time parametrized with the fields of the Z_2 -symmetric model

$$H_1 = \begin{pmatrix} G^+ \\ [v + S_1(h, H) + iG^0]/\sqrt{2} \end{pmatrix}, \quad H_2 = \begin{pmatrix} H^+ \\ [S_2(h, H) + iA]/\sqrt{2} \end{pmatrix}, \quad (6.109)$$

where $S_{1,2}(h, H)$ follow from the rotation with $\beta - \alpha$ from Eq. (6.57). The fields on which the effective masses depend on represent the possibility that beyond tree-level the quantum fields above may acquire themselves non-null VEVs, thus shifting our vacuum configuration towards another stationary point.

Numerically speaking, these classical fields are simply variables that are surveyed computationally in order to minimize the effective potential. If we keep the Goldstone bosons from having a classical counterpart, for they are not physical fields, and do not allow the charged Higgs to possibly get a VEV, *i.e.* charge-breaking minima, the effective mass terms will be functions of h , H , and A :

$$M_i^2(\phi) \equiv M_i^2(h, H, A). \quad (6.110)$$

Since the kinetic terms of the doublets are invariant under basis transformations, the effective masses of the gauge bosons come from the kinetic term of H_1 , and are thus given by their interactions with $v + S_1$:

$$M_Z^2(\phi) = \frac{g^2}{4} [v + S_1(h, H)]^2, \quad (6.111)$$

$$M_{W^\pm}^2(\phi) = \frac{g^2 + g'^2}{4} [v + S_1(h, H)]^2. \quad (6.112)$$

Regarding the fermions, let us write the top mass in terms of its Yukawa coupling:

$$m_t = \frac{v}{\sqrt{2}} \sin \beta (Y_2^u)_{33} = \frac{v}{\sqrt{2}} y_t, \quad (6.113)$$

denoting the bottom and tau masses as well by

$$m_n = \frac{v}{\sqrt{2}} y_n, \quad \text{for } n = b, \tau, \quad (6.114)$$

so that the differences between types I, II, X, and Y are encoded inside SM-like Yukawas. With this prescription, the relevant terms for fermion effective masses – the actual mass term plus the first line of Eq. (6.76) – are given by

$$\mathcal{L}_{\text{eff.mass}} = - \sum_{f=t,b,\tau} \frac{y_f}{\sqrt{2}} \bar{f} \left(v + \xi_h^f h + \xi_H^f H - i \xi_A^f \gamma_5 A \right) f, \quad (6.115)$$

the squared effective masses being, therefore

$$M_f^2(\phi) = \frac{y_f^2}{2} \left[\left(v + \xi_h^f h + \xi_H^f H \right)^2 + \xi_A^{f2} A^2 \right], \quad \text{for } f = t, b, \tau. \quad (6.116)$$

For the scalars, we must go back to the tree-level potential and consider both quadratic and, so as to account for the field-dependence, quartic terms. With V_H as in Eq. (6.47), expanded in terms of the fields in Eq. (6.109), and with the parametrization changed to that of Eq. (6.47), the mass of H^\pm would simply be

$$M_{H^\pm}^2 = \frac{\partial^2 V_H}{\partial H^{\pm 2}} \quad (6.117)$$

evaluated at the VEV of the doublets, *i.e.* setting all fields to zero after differentiation. By keeping all couplings, one has to trace the definition of this mass further back, to Eq. (6.13), where it was but the surviving eigenvalue of a mass matrix

$$\mathcal{M}_{G^\pm, H^\pm}^2 = \begin{pmatrix} \frac{\partial^2 V_H}{\partial G^{\pm 2}} & \frac{\partial^2 V_H}{\partial G^\pm \partial H^\pm} \\ \frac{\partial^2 V_H}{\partial G^\pm \partial H^\pm} & \frac{\partial^2 V_H}{\partial H^{\pm 2}} \end{pmatrix}. \quad (6.118)$$

In keeping all terms with h, H, A after taking the derivatives, one achieves the *effectivization* of the masses above, $\mathcal{M}_{G^\pm, H^\pm}^2 \rightarrow \mathcal{M}_{G^\pm, H^\pm}^2(\phi)$, the contributions to the sum over mass eigenstates of Eq. (6.107) being simply the eigenvalues

$$M_{G^\pm, H^\pm}^2(\phi) = \frac{1}{2} \left[\mathcal{M}_{11}^2 + \mathcal{M}_{22}^2 \pm \sqrt{(\mathcal{M}_{11}^2 - \mathcal{M}_{22}^2)^2 + 4|\mathcal{M}_{12}^2|^2} \right]. \quad (6.119)$$

By the same token, the effective masses of neutral scalar must be obtained from matrices of second derivatives as well. Respecting the fact that with a Z_2 symmetry the physical fields are also CP eigenstates, the CP-even scalars contribute via the eigenvalues

$$M_{h, H}^2(\phi) = \frac{1}{2} \left[\mathcal{M}_{11}^2 + \mathcal{M}_{22}^2 \pm \sqrt{(\mathcal{M}_{11}^2 - \mathcal{M}_{22}^2)^2 + (\mathcal{M}_{12}^2)^2} \right] \quad (6.120)$$

of an effective mass matrix

$$\mathcal{M}_{h, H}^2(\phi) = \begin{pmatrix} \left. \frac{\partial^2 V_H}{\partial S_1^2} \right|_{S_{1,2}(h, H)} & \left. \frac{\partial^2 V_H}{\partial S_1 \partial S_2} \right|_{S_{1,2}(h, H)} \\ \left. \frac{\partial^2 V_H}{\partial S_1 \partial S_2} \right|_{S_{1,2}(h, H)} & \left. \frac{\partial^2 V_H}{\partial S_2^2} \right|_{S_{1,2}(h, H)} \end{pmatrix}, \quad (6.121)$$

whereas for the pseudoscalars the 2×2 mass terms are

$$\mathcal{M}_{G^0, A}^2(\phi) = \begin{pmatrix} \frac{\partial^2 V_H}{\partial G^{02}} & \frac{\partial^2 V_H}{\partial G^0 \partial A} \\ \frac{\partial^2 V_H}{\partial G^0 \partial A} & \frac{\partial^2 V_H}{\partial A^2} \end{pmatrix}, \quad (6.122)$$

with the eigenvalues $M_{G^0, A}^2(\phi)$ following the same same formula as $M_{h, H}^2(\phi)$. Since the expressions for all these terms are large, and are mere algebraic manipulations of all the information we have been presenting above, they can be provided upon request in the form of a `Mathematica` package.

Chapter 7

Vacuum Stability and Other Constraints

An unconstrained 2HDM is a model whose theoretical self-consistency is left to chance, and whose parameter space is allowed to produce observables inconsistent with experimental data. Demanding that the 2HDM is a well-behaved model will lead to several bounds within which our parameters can be deemed reasonable with a given level of confidence. In this chapter, we go through the constraints we will impose in the numerical analysis, focusing on the issue of the stability of the vacuum at one-loop level.

7.1 Positivity, or: Boundedness from Below

The vacuum we live in should be a stable vacuum, one that hasn't decayed within the present age of the universe. What are the necessary sufficient conditions to guarantee stability? A very first step towards a stable vacuum is to require that, in very least, the scalar potential should be bounded from below, *i.e.* that its parameters are such that they ensure that in no direction in field space the potential tends to minus infinity. To see how this constraint, usually termed positivity, translates into bounds on our parameters, we consider here a different notation for the potential. This notation emphasizes the fact that the scalar potential has field bilinears $\phi_a^\dagger \phi_b$ as its building blocks, and can be traced back to the work of Velhinho *et al.* [196], subsequent refinements of the formalism being those of Refs. [197–200].

If one arranges the bilinears that compose the 2HDM potential into the following Hermitian matrix:

$$R := \begin{pmatrix} \phi_1^\dagger \phi_1 & \phi_2^\dagger \phi_1 \\ \phi_1^\dagger \phi_2 & \phi_2^\dagger \phi_2 \end{pmatrix}, \quad (7.1)$$

and exploiting the completeness of the Pauli matrices together with the identity matrix to write R by its decomposition

$$R_{ij} = \phi_j^\dagger \phi_i = \frac{1}{2} (r^0 \delta_{ij} + r^a \sigma_{ij}^a), \quad (7.2)$$

where δ_{ij} is the Kroenecker delta, and σ^a ($a = 1, 2, 3$) are the Pauli matrices, one can derive a 4-vector

r^μ by inverting Eq. (7.2):

$$r^\mu = (r^0, r^1, r^2, r^3) = \begin{pmatrix} \phi_1^\dagger \phi_1 + \phi_2^\dagger \phi_2 \\ \phi_1^\dagger \phi_2 + \phi_2^\dagger \phi_1 \\ i(\phi_2^\dagger \phi_1 - \phi_1^\dagger \phi_2) \\ \phi_1^\dagger \phi_1 - \phi_2^\dagger \phi_2 \end{pmatrix}. \quad (7.3)$$

The scalar potential of the 2HDM is thus written in allusion to a Minkowski space, and with standard Minkowski space conventions, in the form:

$$V_H = -M_\mu r^\mu + \frac{1}{2} \Lambda_{\mu\nu} r^\mu r^\nu, \quad (7.4)$$

where, in our Z_2 -symmetric case, it is easy to show that the covariant vector M_μ and the tensor $\Lambda_{\mu\nu}$ are given by

$$M_\mu = -\frac{1}{2} (m_{11}^2 + m_{22}^2, -2m_{12}^2, 0, m_{11}^2 - m_{22}^2) \quad (7.5)$$

$$\Lambda_{\mu\nu} = \frac{1}{2} \begin{pmatrix} (\lambda_1 + \lambda_2)/2 + \lambda_3 & 0 & 0 & (\lambda_1 - \lambda_2)/2 \\ 0 & \lambda_4 + \lambda_5 & 0 & 0 \\ 0 & 0 & \lambda_4 - \lambda_5 & 0 \\ (\lambda_1 - \lambda_2)/2 & 0 & 0 & (\lambda_1 + \lambda_2)/2 + \lambda_3 \end{pmatrix}. \quad (7.6)$$

It has been proved [199, 201] that, in this language, the positivity constraint amounts to requiring that, being $\Lambda_0, \Lambda_1, \Lambda_2, \Lambda_3$ the eigenvalues of the mixed Λ_μ^ν :

- All eigenvalues must be real;
- $\Lambda_0 > 0$;
- $\Lambda_0 > \{\Lambda_1, \Lambda_2, \Lambda_3\}$.

This is a *strong* requirement of boundedness from below, for it demands the quartic sector of the potential, V_4 , to be strictly positive for all $\phi_i \rightarrow \infty$, discarding possibly interesting models where V_4 is asymptotically zero in those directions. Such a *marginal* positivity constraint, namely $V_4 \geq 0$, would demand, however, an inspection of the quadratic sector in those points, so as to guarantee $V_2 \geq 0$ when $V_4 \rightarrow 0$. The usual positivity conditions in terms of the quartic couplings of the scalar potential can be obtained from the bullets above by diagonalizing $\Lambda_\mu^\nu = g^{\nu\alpha} \Lambda_{\mu\alpha}$ – the same entries as the tensor $\Lambda_{\mu\nu}$, but with second, third, and fourth columns multiplied by minus 1. If we rescale the doublets as

$$\phi_1 \longrightarrow q \phi_1, \quad \phi_2 \longrightarrow q^{-1} \phi_2, \quad \text{with } q = \left(\frac{\lambda_2}{\lambda_1} \right)^{1/8} \quad (7.7)$$

we observe the following transformation of the parameters

$$m_{11}^2 \longrightarrow q^2 m_{11}^2, \quad m_{22}^2 \longrightarrow q^{-2} m_{22}^2, \quad \lambda_1 \longrightarrow \sqrt{\lambda_1 \lambda_2}, \quad \lambda_2 \longrightarrow \sqrt{\lambda_1 \lambda_2}. \quad (7.8)$$

From Eq. (7.6), it is immediate to check that this transformation indeed diagonalizes the covariant tensor,

the eigenvalues of the mixed one thus being

$$\Lambda_0 = \frac{1}{2}(\sqrt{\lambda_1\lambda_2} + \lambda_3), \quad (7.9)$$

$$\Lambda_1 = -\frac{1}{2}(\lambda_4 + \lambda_5), \quad (7.10)$$

$$\Lambda_2 = \frac{1}{2}(\lambda_5 - \lambda_4), \quad (7.11)$$

$$\Lambda_3 = \frac{1}{2}(\lambda_3 - \sqrt{\lambda_1\lambda_2}). \quad (7.12)$$

Imposing the bulleted conditions on these expressions, the demand of positivity comes equal to

$$\lambda_1 > 0, \quad \lambda_2 > 0, \quad \lambda_3 > -\sqrt{\lambda_1\lambda_2}, \quad \lambda_3 + \lambda_4 - |\lambda_5| > -\sqrt{\lambda_1\lambda_2}. \quad (7.13)$$

7.2 The Tree-level Global Minimum

After making sure that our potential respects positivity, one can ensure that the vacuum we live in is stable if it is the global minimum of the potential, *i.e.* if we reside in the lowest, stablest configuration possible. With a Z_2 symmetry, the electroweak vacuum has real VEVs, this type of vacua being usually categorized as *natural* vacua. The absolute stability of a natural vacuum depends, at tree-level, on the category the extra vacuum falls upon [202, 203]: if the value of the potential at a minimum corresponding to a natural vacuum is V_N , and V_{CB} is the value for a charge-breaking vacuum configuration,

$$\langle\phi_1\rangle_{CB} = \frac{1}{\sqrt{2}} \begin{pmatrix} 0 \\ v'_1 \end{pmatrix}, \quad \langle\phi_2\rangle_{CB} = \frac{1}{\sqrt{2}} \begin{pmatrix} \alpha \\ v'_2 \end{pmatrix}, \quad (7.14)$$

it has been shown that the natural minimum sits always at a deepest stationary point, $V_{CB} - V_N > 0$; if it is a vacuum with an unremovable complex phase and, therefore, spontaneously CP-violating,

$$\langle\phi_1\rangle_{CP} = \frac{1}{\sqrt{2}} \begin{pmatrix} 0 \\ v'_1 \end{pmatrix}, \quad \langle\phi_2\rangle_{CP} = \frac{1}{\sqrt{2}} \begin{pmatrix} 0 \\ v'_2 e^{i\theta} \end{pmatrix}, \quad (7.15)$$

it has been shown that a coexisting natural minimum will always be lower, $V_{CP} - V_N > 0$; if, however, there exists a second minimum which is also categorized as natural, with VEVs $\{v'_1, v'_2\}$, their squared sum falling either above or below the square of the electroweak scale, the authors of Ref. [201] have shown that the conclusion on whether our vacuum or this one is the global minimum will depend on the precise value of these VEVs:

$$V_{N'} - V_N = \frac{m_{12}^2}{4v_1v_2} \left(1 - \frac{v_1v_2}{v'_1v'_2}\right) (v_1v'_2 - v_2v'_1)^2. \quad (7.16)$$

Also in Ref. [201], it was demonstrated that it is possible, nevertheless, to devise a discriminant that signals if a vacuum of a CP-conserving model sits, indeed, at the global minimum. Using the Minkowski-like formalism we defined above, the authors concluded that such vacuum, with VEVs $\{v_1 = v \cos \beta, v_2 = v \sin \beta\}$, is the global minimum of the potential if and only if, for intermediate discriminants $D_1 = \hat{M}_1 \hat{r}^1$ and $D_3 = \hat{M}_3 \hat{r}^3$,

$$D = D_1 D_3 > 0, \quad (7.17)$$

where \hat{r}_i and \hat{M}_i are, respectively, the i -th elements of the 4-vectors from Eq. (7.3) and Eq. (7.5), evaluated in the basis where Λ_μ^ν is diagonal. That basis is the basis where the doublets are rescaled according to Eq. (7.7), from whence it follows that, for the Z_2 -symmetric 2HDM,

$$D_1 = v^2 \sin \beta \cos \beta m_{12}^2, \quad (7.18)$$

$$D_3 = v^2 q^2 \cos^2 \beta (\tan^2 \beta - q^{-4}) (m_{11}^2 - q^{-4} m_{22}^2). \quad (7.19)$$

Introducing a parameter k , defined as

$$k^2 \equiv \left[\left(\frac{\lambda_1}{\lambda_2} \right)^{1/4} \right]^2 = q^{-4}, \quad (7.20)$$

one gets for the multiplication:

$$D_1 D_3 = \frac{v^4 k^{-2}}{4} \cos^3 \beta \sin \beta m_{12}^2 (\tan \beta - k) (\tan \beta + k) (m_{11}^2 - k^2 m_{22}^2), \quad (7.21)$$

and, recalling that β is taken in the first quadrant, one may remove the terms that are positive by definition and write the global minimum condition with a simplified discriminant: our vacuum is the global minimum of the potential if and only if

$$D = m_{12}^2 (\tan \beta - k) (m_{11}^2 - k^2 m_{22}^2) > 0. \quad (7.22)$$

If one imposes this discriminant to be verified, together with the positivity conditions turned on, one is sure to have a resulting range of the parameter space where stability is respected and our vacuum is the true vacuum of nature. This is however, as we've been stressing here and there throughout this chapter, only true at tree level. This discriminant was derived by minimizing the tree-level potential, and we know from the previous chapter that there is an object whose minimization provides better information on the stationary points of the potential with loop corrections – the effective potential. In fact, the corrections arriving from the Coleman-Weinberg term in $V_{\text{eff}}^{(1)}$ may modify completely the shape of the potential sheet, which, in the worst case scenario for the tree-level analysis, may include the introduction of new minima or the lowering of existing ones into the status of the true global minimum; they may even turn a gauge symmetric vacuum into a radiatively breaking one [195, 204]. Furthermore, the very positivity conditions may lead to inaccurate conclusions of boundedness from below when loop corrections are considered: these too were derived inspecting only the behaviour of V_H in the infinite directions of field space. It may happen that we sit in a point where one of the quartic couplings are near a turning point, *e.g.* λ_1 or λ_2 near zero, and the loop-induced terms may provide the necessary nudge to unmask an unbounded potential. By running the quartic couplings with their RGEs, and thus RGE-improving the scalar potential, one may, nevertheless, rescue the positivity conditions – as long as one remains within the perturbative regime, where replacing tree-level couplings by running couplings in a tree-level potential can still be considered a good approximation.

7.3 Vacuum Decay in Field Theory

How does one proceed when the stability constraint is to be imposed on the loop corrected potential? First of all, for the one-loop effective potential there is no device in the vein of the tree-level discriminant

we found in the previous section. What remains to be done is to minimize $V_{\text{eff}}^{(1)}$ ‘by hand’, and assert which vacuum corresponds to the lowest minimum. Such a state we call a *true vacuum*; a minimum sitting above the global minimum is referred to as a *false vacuum*. The plethora of minima of the 2HDM can be quite complex, an analytical solution being too involved to be practical: the tree-level potential and the Coleman-Weinberg potential, with its field-dependent masses, need to be simultaneously minimized, thus, assuming vacua to be either natural or CP-violating, a system of first derivatives with respect to h, H, A gets easily out of hand. Several computer programs exist which use homotopy continuation methods to find all the stationary points of a polynomial systems, among these one can cite `HOM4PS-2.0` [205], or `Bertini` [206]. This means we can use a polynomial solver for the tree-level potential, get all the stationary points (maxima, minima, and saddle points), and take these as starting points for a gradient-based numerical minimizer (`MINUIT` [207] or later versions in C++; in Python the `iminuit` package,¹ for example) that does inspect the whole expression of $V_{\text{eff}}^{(1)}$. This is the course taken by the first section of `Vevacious` [208].

After computing all the minima of the loop-corrected potential, an interesting situation, or, as Barroso *et al.* put it [209], a *panic* situation, happens when our vacuum is not the global minimum and may, therefore, decay into the actual true vacuum. At first glance, such a model would be deemed unstable. If, however, one computes the tunnelling rate between our state and that of the deepest minimum, and that rate comes out to be larger than the age of the universe, our vacuum would have been stable at least up until now, notwithstanding the fact that the fate of the universe would have to be left uncertain. One ground state with a lifetime larger than the age of the universe must be accepted as valid, this situation being labelled one of metastability.

7.3.1 Instantons in Particle Mechanics

To compute the decay rate of the electroweak vacuum in the situations it is a false vacuum, one must introduce the concept of vacuum decay in field theory. This is described by the semiclassical formalism whose groundwork is found in the seminal papers of Sidney Coleman and Curtis Callan [210, 211]. This is the formalism that underlies the physics of bubble nucleation and instantons, and it is not our intention to give here a thorough account of these subjects.² Our aim is to rather give a reasonable description of the ingredients relevant to the calculation of the tunnelling between a false vacuum and the true vacuum.

Let us start with simple particle mechanics. Our intuition for tunnelling comes from Quantum Mechanics, and Coleman even goes as far as to say that *every child knows that the amplitude for transmissions obeys the WKB formula* [204]:

$$|T(E)| = \exp \left[-\frac{1}{\hbar} \int_a^b dx \sqrt{2(V-E)} \right] (1 + \mathcal{O}(\hbar)), \quad (7.23)$$

where E is the energy of the state, a and b are the classical turning points in the potential barrier, and the factors of \hbar were left explicit to lay bare the semiclassical nature of this approximation. For a particle

¹One can find the code and all the documentation from <http://iminuit.readthedocs.io/en/latest/>.

²The interested reader is pointed to the compiled Erice lectures of Sidney Coleman [204], or a recent review by Andreassen, Farhi, Frost, and Schwartz [212], and references therein.

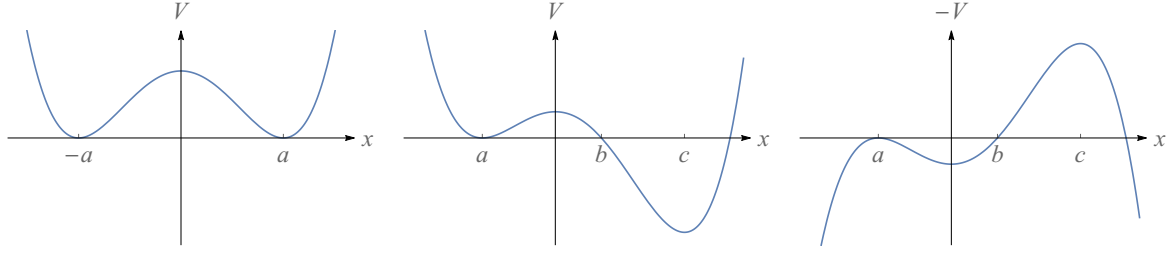


Figure 7.1: Illustrations of, respectively, a symmetric double-well potential, a double-well with a false and a true vacuum, and the inverted potential of the skewed case.

in, say, a well, hitting the barrier at a rate A , and each time tunnelling with a probability given by the transmission amplitude, one expects the decay rate to take the form

$$\Gamma \sim A |T(E)|^2 = A e^{-B/\hbar} (1 + \mathcal{O}(\hbar)). \quad (7.24)$$

In order to find the analogous of the WKB approximation in QFT, one should investigate the transition between two states in the path integral formulation. For an interaction with duration T , starting at x_i and finishing at x_f ,

$$Z \equiv \langle x_f | e^{-HT/\hbar} | x_i \rangle = \int \mathcal{D}x e^{-S_E[x]/\hbar}. \quad (7.25)$$

The measure $\mathcal{D}x$ denotes the “sum over histories”, *i.e.* the integration over all possible paths with boundary conditions $x(-T/2) = x_i$, and $x(T/2) = x_f$; in turn, $S_E[x]$ is the Euclidean action (imaginary time), and for a spinless particle with unit mass it is

$$S_E[x] = \int_{-T/2}^{T/2} dt \left[\frac{1}{2} \left(\frac{dx}{dt} \right)^2 + V(x) \right]. \quad (7.26)$$

In the semiclassical limit (small \hbar), the path integral is dominated by the stationary points of the action: denoting one such point by \bar{x} , the functional derivative of S_E ,

$$\frac{\delta S_E}{\delta \bar{x}} = -\frac{d^2 \bar{x}}{dt^2} + V'(\bar{x}) = 0, \quad (7.27)$$

comes to describe the equations of motion of a unit mass particle moving in a potential *minus* V , whence it follows that

$$E = \frac{1}{2} \left(\frac{d\bar{x}}{dt} \right)^2 - V(x) \quad (7.28)$$

is a constant of the motion of a given stationary \bar{x} .

Now, let us imagine that the particle is in a symmetric double-well potential as illustrated in the left panel of Fig. 7.1. The inverted potential consists of two hills, at $\pm a$, and a valley between them. Two trivial stationary paths are those where the particle remains fixed in either of the hilltops. To evaluate the corresponding amplitudes, one may take advantage of the usual expansion in energy eigenstates,

$$\langle x_f | e^{-HT/\hbar} | x_i \rangle = \sum_n e^{-E_n T/\hbar} \langle x_f | n \rangle \langle n | x_i \rangle, \quad (7.29)$$

whose leading term for large T keeps the energy and wave function of the lowest-lying energy eigenstate. Since, to a good approximation, the static particle is in the ground-state of a harmonic oscillator, we

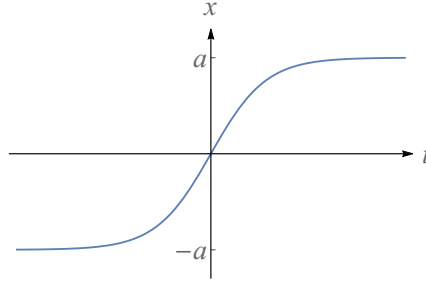


Figure 7.2: The shape of an instanton in the symmetric double-well potential.

simply have

$$E_0 = \frac{1}{2} \hbar \omega (1 + \mathcal{O}(\hbar)), \quad (7.30)$$

whereas for large T and a Gaussian intermediate state $|0\rangle$ we get

$$\langle \pm a | e^{-HT/\hbar} | \pm a \rangle = \left(\frac{\omega}{\pi \hbar} \right)^{1/2} e^{-\omega T/2} (1 + \mathcal{O}(\hbar)), \quad (7.31)$$

where we have introduced ω defined by: $\omega^2 = V(\pm a)$. There is, however, another, potentially interesting, solution: one where the particle starts at the top of the $-a$ hill at $-T/2$, rolls down through the valley, and moves up towards the a hilltop, where it stops at $T/2$. Since we are interested in the large T limit, we consider the form of the solution where the particle sits at the top of the hills at plus and minus infinity. In this case, the constant of the motion E is actually zero, which yields

$$\frac{dx}{dt} = \sqrt{2V}, \quad (7.32)$$

or, equivalently,

$$t = t_0 + \int_0^x dy \frac{1}{\sqrt{2V(y)}}, \quad (7.33)$$

where t_0 is the time at which x vanishes – zero for this symmetric motion. This object, sketched in Fig. 7.2, is called an *instanton*: ‘instant-’ because it is a mathematical structure in Euclidean time, narrowly centered in t_0 (’t Hooft even suggested the name *Euclidean-gauge soliton* [213]); ‘-on’ because it is a particle-like solution of classical field theories (Polyakov suggested the name *pseudoparticle* [214, 215], still used in some literature). The inverse transition, from a to $-a$, is called an *anti-instanton*. The action of an (anti-)instanton, S_0 , is easily derived from Eq. (7.32):

$$S_0 = \int dt \left[\frac{1}{2} \left(\frac{dx}{dt} \right)^2 + V \right] = \int dt \left(\frac{dx}{dt} \right)^2 = \int_{-a}^a dx \sqrt{2V}, \quad (7.34)$$

and we are starting to see the signs of a possible WKB-like expression.

To compute $\langle a | e^{-HT/\hbar} | -a \rangle$, we must sum over all possible paths, which translates to the sum over a sequence of n instantons and anti-instantons distributed between $-a$ and a , and centered at each t_n with $-T/2 < t_1 < t_2 < \dots < t_n < T/2$. Moreover, this distribution is actually not arbitrary: since we want to start at $-a$ and move forward with an instanton, followed by an anti-instanton, followed by an instanton, so on and so forth, ending at a with another instanton, n must be an odd number. Likewise, to start at $-a$ and finish back at $-a$, one must have an even number of motions. If one considers that

- each small time interval containing an (anti-)instanton provides a correction K to the harmonic-oscillator matrix-element,
- the total action is the sum of n (anti-)instanton actions, $S_E = n S_0$,
- time integration is done over the locations of centers t_n , all adding up to $T^n/n!$,

one gets

$$\langle a|e^{-HT/\hbar}| - a \rangle = \left(\frac{\omega}{\pi\hbar}\right)^{1/2} e^{-\omega T/2} \sum_{\text{odd } n} \frac{(K e^{-S_0/\hbar} T)^n}{n!} (1 + \mathcal{O}(\hbar)), \quad (7.35)$$

while to end back at $-a$ one has the same expression, but summing instead over even n 's. The calculation of both sums is trivial, and it produces:

$$\langle \pm a|e^{-HT/\hbar}| - a \rangle = \left(\frac{\omega}{\pi\hbar}\right)^{1/2} e^{-\omega T/2} \frac{1}{2} \left[\exp\left(K e^{-S_0/\hbar} T\right) \mp \exp\left(-K e^{-S_0/\hbar} T\right) \right] (1 + \mathcal{O}(\hbar)), \quad (7.36)$$

which, recalling the expansion in energy eigenstates of Eq. (7.29), means this system comprises two ground-states with energies

$$E_{\pm} = \left[\frac{1}{2} \hbar\omega \pm \hbar K e^{-S_0/\hbar} \right] (1 + \mathcal{O}(\hbar)), \quad (7.37)$$

where it is clear that each eigenstate is, in first approximation, a harmonic-oscillator eigenstate centered at the bottom of each well, with the degeneracy of the two states broken by a term proportional to a barrier penetration factor $e^{-S_0/\hbar}$.

We are, of course, interested in a more asymmetrical configuration. Going back to Fig. 7.1, we want to focus not in the double well on the left, but rather in the skewed version of that potential, in the center panel, where a false vacuum and a true vacuum coexist. The inverse is shown in the right panel, and one may observe there that now, besides the static solution at a , another stationary path also starting in the false vacuum is one where the particle rolls down towards the valley, but, without the necessary energy to go up to c , it simply bounces off the classical turning point in the barrier, at b , and returns to the top of the hill at a . This motion is, accordingly, called the *bounce*. Denoting the action of the bounce by B , and taking into account that in this case there is no restriction to an even or odd number of bounces, meaning the exponential series that we found for the potential well must be summed in its entirety, we obtain

$$\langle a|e^{-HT/\hbar}|a \rangle = \left(\frac{\omega}{\pi\hbar}\right)^{1/2} e^{-\omega T/2} \exp\left(K e^{-B/\hbar} T\right), \quad (7.38)$$

and ground state energy eigenvalue is

$$E_0 = \frac{1}{2} \hbar\omega \pm \hbar K e^{-B/\hbar}, \quad (7.39)$$

where the factors of $(1 + \mathcal{O}(\hbar))$ are omitted and implied. An argument could be made that these calculations have generated a correction to the static energy that may be small compared with \hbar^2 terms which have been neglected; furthermore, the very state we are trying to compute, should not appear in the spectrum of the Hamiltonian, for it has a barrier penetration term that renders it unstable and, therefore, not an eigenstate of real energy. That is, however, the very fact that makes this exactly what we wanted to derive: the second term may indeed be small compared to higher-order terms, but, given this is an unstable state, its energy must have an imaginary part, and this should be its leading contribution:

$$\text{Im}(E_0) \equiv \frac{\Gamma}{2} \sim \hbar |K| e^{-B/\hbar}. \quad (7.40)$$

7.3.2 The $O(4)$ Bounce Formalism

The decay of the false vacuum has a homologous process in thermodynamics, which has been used ever since Ref. [210] to shed light on the qualitative features of this type of phenomena. One can imagine the central potential in Fig. 7.1 to be a plot describing the nucleation in the boiling of a superheated liquid: the false vacuum corresponds to the superheated fluid phase, the true vacuum is the vapour phase, both being minima of the free energy as a function of density. Here and there, bubbles appear in the liquid due to thermodynamic fluctuations; for a small bubble, the increase in volume energy that occurs with the materialization of the bubble is compensated with the loss in surface energy, causing the bubble to diminish back to nothing; at one point, however, a large enough bubble may be formed such that it is energetically favourable for it to expand, and thus drive the conversion of liquid to vapour phase until it encompasses the whole system (or coalesce with other expanding bubbles and together take on what remains of the fluid). Since the probability per unit time that such a critical bubble will form in a given system is proportional to the latter's volume, the quantity one is after is, in fact, a decay probability per unit time per unit volume: Γ/\mathcal{V} .

In field theory, one changes thermodynamic fluctuations to quantum fluctuations, with bubbles of true vacuum expanding within a false stationary state of nature, converting the vacuum configuration of the universe in their stride. Denoting the bounce as a field ϕ_b , its Euclidean action being

$$B \equiv S_E[\phi_b] = \int d^4x \left[\frac{1}{2} (\partial_\mu \phi_b)^2 + V(\phi_b) \right], \quad (7.41)$$

where $x_0 \rightarrow ix_0$, Eq. (7.40) tells us that we can write, to leading order in \hbar , and returning to natural units,

$$\frac{\Gamma}{\mathcal{V}} = A e^{-B}. \quad (7.42)$$

The prefactor A is formally given by a ratio of two functional determinants [211]. Their evaluation is, however, too cumbersome for most field theories of interest, so much so that usually it is more practical to simply estimate the prefactor by dimensional analysis: A has dimensions of $[\text{mass}]^4$ and is, therefore, expected to be of the order of a characteristic mass of the theory [216–218]:

$$A \sim \eta M^4, \quad (7.43)$$

where η is a dimensionless number of order unity. Indeed, taking, as we did for the Coleman-Weinberg potential, the natural mass scale of the theory to be v , and citing a Hubble constant converted to natural units from the values of Refs. [219, 220]:

- $A \sim (246 \text{ GeV})^4$,
- $H_0 \sim 9 \times 10^{-42} \text{ GeV}$,

we find that a metastable universe, where a false vacuum must respect

$$\frac{\Gamma}{\mathcal{V}} \lesssim H_0^4, \quad (7.44)$$

implies that

$$B \gtrsim -\ln\left(\frac{H_0^4}{A}\right) \simeq 400.067. \quad (7.45)$$

This means that, as soon as we compute the action of the bounce, our assessment of metastability of the 2HDM comes down a simple imposition of this inequality.

Fleshing out the Euclidean nature of the action by separating the time and spatial derivatives in Eq. (7.41), one has

$$B = \int dt d^3x \left[\frac{1}{2} \left(\frac{\partial \phi_b}{\partial t} \right)^2 + \frac{1}{2} (\nabla \phi_b)^2 + V(\phi_b) \right]. \quad (7.46)$$

The Euclidean equation of motion of the bounce is thus

$$\left(\frac{\partial^2}{\partial t^2} + \nabla^2 \right) \phi_b = V'(\phi_b), \quad (7.47)$$

where the prime denotes differentiation with respect to ϕ_b . The bounce is defined by its motion, which can be translated into the following boundary conditions:

$$\frac{\partial \phi_b}{\partial t}(0, x) = 0, \quad (7.48)$$

and,

$$\lim_{t \rightarrow \pm\infty} \phi_b(t, x) = \phi_{\text{fv}} \quad (7.49)$$

where ϕ_{fv} is the value of the local minimum that corresponds to the false vacuum. In turn, it is easy to see that, in order for the B integral to be finite, it is necessary that ϕ_b takes a finite value also at spatial infinities; to be consistent with the description of false vacuum decay as a bubble of true vacuum that appears somewhere, with false vacuum undisturbed outside and far from the bubble, that value should, in fact, be ϕ_{fv} :

$$\lim_{|x| \rightarrow \infty} \phi_b(t, x) = \phi_{\text{fv}}. \quad (7.50)$$

Defining $r = \sqrt{t^2 + \sum x_i^2}$, these conditions hint at a radius-dependent, $O(4)$ -invariant bounce, whose boundary conditions at infinity would combine into a single equation:

$$\lim_{r \rightarrow \infty} \phi_b(r) = \phi_{\text{fv}}. \quad (7.51)$$

This reasonable guess that ϕ_b might only depend on the distance from a point in Euclidean space was, indeed, developed into a proof that an $O(4)$ -invariant bounce always exist, and that its action is always smaller than that of an $O(4)$ -noninvariant bounce [221].³ For an $O(4)$ -invariant bounce, the first boundary condition becomes

$$\left. \frac{d\phi_b}{dr} \right|_{r=0} = 0, \quad (7.52)$$

the equation of motion turns into

$$\frac{d^2 \phi_b}{dr^2} + \frac{3}{r} \frac{d\phi_b}{dr} = V'(\phi_b), \quad (7.53)$$

and the Euclidean action is

$$B = 2\pi^2 \int_0^\infty dr r^3 \left[\frac{1}{2} \left(\frac{d\phi_b}{dr} \right)^2 + V(\phi_b) \right]. \quad (7.54)$$

Generalization to our problem with more than one field is straightforward: with the three fields of the 2HDM – h , H , A – in one-to-one correspondence with three ϕ_i , such that we denote the multi-dimensional

³We refrain from providing here that proof, offering the following quote from Coleman as an excuse: “*The rigor of our proof is matched only by its tedium; I would not lecture on it to my worst enemy*” [204].

bounce by $\vec{\phi}_b = (\phi_1, \phi_2, \phi_3)$, the equation of motion becomes a system of coupled ordinary differential equations:

$$\frac{d^2\phi_i}{dr^2} + \frac{3}{r} \frac{d\phi_i}{dr} = \frac{\partial V(\vec{\phi}_b)}{\partial \phi_i}. \quad (7.55)$$

A trivial vectorization of the boundary conditions and the expression of B ensues. It is worth recalling that $V(\vec{\phi}_b)$ is to be identified with the one-loop effective potential of Eq. (6.93).

7.3.3 Numerical Solutions of Tunnelling Rates

Finding the solution of the tunnelling rate between vacua comprehends finding the solution to the bounce equation of motion. In its $1D$ form, an equation like Eq. (7.53) can be seen as representing a particle that moves in the inverted potential $-V(\phi)$ under the influence of a velocity-dependent friction term. Exact analytical solutions to this kind of motion are not easy to get, even though for certain approximations, such as that of a bubble with a thin-wall separating the two regimes, or for some special potentials, such as the case of *quartic bounces* produced by the single-field $\lambda\phi^4$ theory, exact solutions can be found in literature [222–225].

For generic, realistic cases, one must resort to finding numerical solutions to the bounce equation of motion. This is, however, not without its difficulties. A straightforward method to solve Eq. (7.53) would be the traditional shooting method, where the boundary condition in Eq. (7.52) is imposed together with an initial guess at zero, $\phi_b(0) = \phi_0$, which is then iteratively optimized until the solution produces the other boundary condition, in Eq. (7.51) – too large or too small values of ϕ_0 cause the particle to overshoot or undershoot ϕ_{fv} at large r . Each step of this method requires the determination of the solution at the center of the bubble, where the friction term is divergent: if not treated carefully, like expanding the potential around ϕ_0 as suggested in Ref. [212], the particle cannot start rolling from $r = 0$ without a numerical singularity. Additionally, a simple shooting method may be plagued by instabilities associated with faster descending (or ascending in the upside-down potential) modes that can drive the solution away from the mode we are after. This can be avoided by a multi-shooting scheme, where one shoots over small ranges of r , integrating only in *microscopic* intervals between each ϕ_n and ϕ_{n+1} , and choosing enough intermediate r_n points so as to ensure that the unstable modes do not overcome the final *macroscopic* field evolution. An efficient implementation of such a numerical procedure has been recently put forward [226], and is available as a Mathematica package called **AnyBubble**. Although this program works for any number of fields, it becomes slow when the system of coupled equations of motion becomes too complex, taking a time in the order of seconds to compute bounce and action for potentials with 3 fields, minutes even for 4 fields and more. Because of this speed issue, the same authors have even proposed in their subsequent work an approximation of the tunnelling for large multi-dimensional field spaces based on transitions between minima via $1D$ paths through the saddle points of the potential [227].

Another numerical method that tackles vacuum decay with multiple fields is the one proposed and implemented in **CosmoTransitions** [228]. The idea behind it is quite simple: one starts with an initial guess that assumes as well that the tunnelling occurs on a $1D$ path in field space, $\vec{\phi}_{\text{guess}} = \vec{\phi}_b(s)$, where s

parametrizes the path. If s is chosen in such a way that $\left|\frac{d\vec{\phi}_b}{ds}\right| = 1$, the equations of motion in Eq. (7.55), which can be split into a part parallel to the path and a part perpendicular to it, take the form:

$$\frac{d^2 s}{dr^2} + \frac{3}{r} \frac{ds}{dr} = \frac{\partial}{\partial s} V(\vec{\phi}_b(s)), \quad (7.56)$$

$$\frac{d^2 \vec{\phi}_b}{ds^2} \left(\frac{ds}{dr}\right)^2 = \nabla_{\perp} V(\vec{\phi}_b), \quad (7.57)$$

where $\nabla_{\perp} V$ denotes the components of the gradient of the potential that are perpendicular to s . Using again the particle analogy, the equation parallel to the path describes the forces only concerned with the speed of the particle along its motion. The other equation, on the other hand, does not affect directly the kinematics of the particle: it can be seen as describing the normal force,

$$N = \frac{d^2 \vec{\phi}_b}{ds^2} \left(\frac{ds}{dr}\right)^2 - \nabla_{\perp} V(\vec{\phi}_b), \quad (7.58)$$

that the path exerts to keep the particle from falling off of it. The equation parallel to s is an usual one-dimensional equation of motion and can be solved with a shooting method. With this at hand, and taking into account that these solutions must also be solutions of the equality that renders the normal force null, **CosmoTransitions** consists in the method of iterative path deformations in the direction of field space which converges towards $N = 0$.

CosmoTransitions is available as a Python package, and, due to its multiple field capabilities, comprises one of the sectors inside of **Vevacious**. It is also our choice of vacuum decay calculator, used in the analysis detailed in the following chapter.

7.4 Further Theoretical Constrains

Before presenting our results for the analysis of vacuum stability in the 2HDM at the loop level, let us touch upon the other constraints that we imposed on this model. Apart from positivity and stability, the list of theoretical constraints must also include unitarity and perturbativity.

7.4.1 Unitarity

As was already mentioned at the very start of Chapter 2, unitarity is nothing but the conservation of probability in physical amplitudes. One of the implications of this is the requirement that the S-matrix is a unitary matrix, and good visualization of such condition at play is the *optical theorem*, which can be stated in its general form as⁴

$$\mathcal{A}(i \rightarrow f) - \mathcal{A}^*(f \rightarrow i) = i \sum_X \int d\Pi_X (2\pi)^4 \delta^4(p_i - p_X) \mathcal{A}(i \rightarrow X) \mathcal{A}^*(f \rightarrow X), \quad (7.59)$$

where the sum is over single- and multi-particle states $|X\rangle$ which define the completeness of the Hilbert space,

$$\sum_X \int d\Pi_X |X\rangle \langle X| = 1, \quad (7.60)$$

⁴We follow here Ref. [66].

and

$$d\Pi_X = \prod_{j \in X} \frac{d^3 p_j}{(2\pi)^3} \frac{1}{2E_j}. \quad (7.61)$$

For a two-particle state $|\Phi\rangle$, and considering the process $\Phi \rightarrow \Phi$ in the center-of-mass frame, one can write the optical theorem in its more familiar form:

$$\text{Im}(\mathcal{A}(\Phi \rightarrow \Phi)) = 2E_{\text{CM}} |\vec{p}_i| \sum_X \sigma_{\text{tot}}(\Phi \rightarrow X), \quad (7.62)$$

which says that the imaginary part of the forward scattering amplitude is proportional to the total scattering cross section.

The total cross section of a $2 \rightarrow 2$ elastic scattering process is a well-known result, which is for two particles ϕ_a and ϕ_b :

$$\sigma_{\text{tot}}(\phi_a \phi_b \rightarrow \phi_a \phi_b) = \frac{1}{32\pi E_{\text{CM}}^2} \int d\cos\theta |\mathcal{A}(\theta)|^2 \quad (7.63)$$

where θ is the usual scattering angle. Moreover, one may make use of the formalism of the partial wave expansion to express the amplitude as

$$\mathcal{A}(\theta) = 16\pi \sum_{j=0}^{\infty} (2j+1) a_j P_j(\cos\theta), \quad (7.64)$$

where j is the quantum number of the angular momentum, and $P_j(\cos\theta)$ are the Legendre Polynomials which satisfy $P_j(1) = 1$ and

$$\int_{-1}^1 d\cos\theta P_j(\cos\theta) P_k(\cos\theta) = \frac{2\delta_{jk}}{2j+1}. \quad (7.65)$$

This brings the total cross section of the $\phi_a \phi_b \rightarrow \phi_a \phi_b$ scattering to be

$$\sigma_{\text{tot}}(\phi_a \phi_b \rightarrow \phi_a \phi_b) = \frac{32\pi}{E_{\text{CM}}^2} \sum_{j=0}^{\infty} (2j+1) |a_j|^2, \quad (7.66)$$

and, going back to Eq. (7.62), the imaginary part of the amplitude at $\theta = 0$ is simply

$$\text{Im}(\mathcal{A}(\phi_a \phi_b \rightarrow \phi_a \phi_b | \theta = 0)) = 16\pi \sum_{j=0}^{\infty} (2j+1) \text{Im}(a_j). \quad (7.67)$$

Taking the high energy limit, in which each particle mass can be neglected and $|\vec{p}_{a,b}| = E_{\text{CM}}/2$, and considering that

$$\sum_X \sigma_{\text{tot}}(\phi_a \phi_b \rightarrow X) \geq \sigma_{\text{tot}}(\phi_a \phi_b \rightarrow \phi_a \phi_b), \quad (7.68)$$

we can finally convey the optical theorem in terms of a *partial wave unitarity bound*:

$$\text{Im}(a_j) \geq |a_j|^2. \quad (7.69)$$

In the Argand plane, the equality relation corresponds to a circle centered at $i/2$, with a radius of $1/2$, such that it becomes apparent that partial wave unitarity can be translated into the following bounds:

$$|a_j| \leq 1, \quad 0 \leq \text{Im}(a_j) \leq 1, \quad |\text{Re}(a_j)| \leq \frac{1}{2}. \quad (7.70)$$

On a 2HDM, the partial wave amplitudes a_j are the eigenvalues of a matrix \mathbf{a}_j , since each quartic coupling of the scalar potential induces scatterings with all combinations of the four doublets in initial

Y	τ	Z_2 -even	Z_2 -odd
0	0	$\frac{1}{\sqrt{2}}(\phi_1^\dagger\phi_1)$	$\frac{1}{\sqrt{2}}(\phi_1^\dagger\phi_2)$
		$\frac{1}{\sqrt{2}}(\phi_2^\dagger\phi_2)$	$\frac{1}{\sqrt{2}}(\phi_2^\dagger\phi_1)$
0	1	$\frac{1}{\sqrt{2}}(\phi_1^\dagger\tau^k\phi_1)$	$\frac{1}{\sqrt{2}}(\phi_1^\dagger\tau^k\phi_2)$
		$\frac{1}{\sqrt{2}}(\phi_2^\dagger\tau^k\phi_2)$	$\frac{1}{\sqrt{2}}(\phi_2^\dagger\tau^k\phi_1)$
1	0	—	$\frac{1}{\sqrt{2}}(\tilde{\phi}_1\phi_2)$
1	1	$\frac{1}{2}(\tilde{\phi}_1\tau^k\phi_1)$	$\frac{1}{\sqrt{2}}(\tilde{\phi}_1\tau^k\phi_2)$
		$\frac{1}{2}(\tilde{\phi}_2\tau^k\phi_2)$	

Table 7.1: Two-particle states for $2 \rightarrow 2$ scattering in a 2HDM. The Z_2 -even, $Y = 1$, $\tau = 0$ states are identically zero.

and final states, each doublet being itself an $SU(2)_L$ vector with a neutral and a charged component. In the high energy limit, $E_{\text{CM}} \gg |\lambda_i|v^2 \gg M_W^2$, the $SU(2)_L \times U(1)_Y$ symmetry is manifest, meaning that the electroweak generators are unbroken, which itself implies that weak isospin, τ , and hypercharge, Y , are conserved in $2 \rightarrow 2$ scattering processes at tree level. This prompted the authors of Refs. [229, 230] to write the two-particle states in a basis with definite isospin and hypercharge, such that the LO of \mathbf{a}_j breaks down in blocks. Also at tree-level, and for the energies of interest for the unitarity analysis, the only non-trivial partial wave is the $j = 0$ wave, and so one only considers \mathbf{a}_0 .

These blocks \mathbf{a}_0 can be further divided into smaller blocks by noting that, at tree-level, Z_2 -even and -odd states do not mix. Recalling that we consider Higgs doublets with $Y = 1/2$, the total hypercharge of a state with two Higgs fields can be $Y = \{-1, 0, 1\}$. Regarding the weak isospin, it relates to the completeness of Pauli matrices together with the identity matrix, such that states with $\tau = 1$ can be classified according to the τ^k matrix, $k = \{1, 2, 3\}$, present in that block. We collect the possible states for $2 \rightarrow 2$ scattering in Table 7.1, where the states with $Y = -1$ can be obtained from those with $Y = 1$ by charge conjugation. In the basis where τ^1 and τ^2 are replaced with τ^+ and τ^- , and dropping the $j = 0$ index for simplicity, each block of the partial wave amplitude can thus be labelled as $\mathbf{a}_{Y\tau(\pm)}^{Z_2}$; omitting the eigenvalues that are identically zero, one has at LO [231]:⁵

$$-16\pi a_{01\pm}^{\text{even,LO}} = \frac{1}{2} \left(\lambda_1 + \lambda_2 \pm \sqrt{(\lambda_1 - \lambda_2)^2 + 4\lambda_4^2} \right), \quad (7.71)$$

$$-16\pi a_{01\pm}^{\text{odd,LO}} = \lambda_3 \pm \lambda_5, \quad (7.72)$$

$$-16\pi a_{11\pm}^{\text{even,LO}} = \frac{1}{2} \left(\lambda_1 + \lambda_2 \pm \sqrt{(\lambda_1 - \lambda_2)^2 + 4\lambda_5^2} \right), \quad (7.73)$$

$$-16\pi a_{11}^{\text{odd,LO}} = \lambda_3 + \lambda_4, \quad (7.74)$$

$$-16\pi a_{00\pm}^{\text{even,LO}} = \frac{1}{2} \left(3\lambda_1 + 3\lambda_2 \pm \sqrt{(3\lambda_1 - 3\lambda_2)^2 + 4(2\lambda_3 + \lambda_4)^2} \right), \quad (7.75)$$

$$-16\pi a_{00\pm}^{\text{odd,LO}} = \lambda_3 + 2\lambda_4 \pm 3\lambda_5, \quad (7.76)$$

$$-16\pi a_{10}^{\text{odd,LO}} = \lambda_3 - \lambda_4. \quad (7.77)$$

The one-loop corrections to the partial wave amplitude were recently computed in Ref. [231]. Although,

⁵These eigenvalues are related to the ones defined in [230] by $a_{Y\tau(\pm)}^{Z_2} = -32\pi^2 \Lambda_{Y\tau(\mp)}^{Z_2}$.

in general, the loop-corrections do not respect the block diagonal structure of \mathbf{a}_0 at tree-level, the authors of that reference have shown that this structure is only broken by numerically negligible wavefunction corrections. As such, the one-loop eigenvalues come to be [231, 232]:

$$32\pi a_{00\pm}^{\text{even,NLO}} = B_1 + B_2 \pm \sqrt{(B_1 - B_2)^2 + 4B_3^2}, \quad (7.78)$$

$$32\pi a_{00\pm}^{\text{odd,NLO}} = 2B_4 \pm 2B_6, \quad (7.79)$$

$$32\pi a_{01\pm}^{\text{even,NLO}} = B_7 + B_8 \pm \sqrt{(B_7 - B_8)^2 + 4B_9^2}, \quad (7.80)$$

$$32\pi a_{01\pm}^{\text{odd,NLO}} = 2B_{13} \pm 2B_{15}, \quad (7.81)$$

$$32\pi a_{10}^{\text{odd,NLO}} = 2B_{19}, \quad (7.82)$$

$$32\pi a_{11\pm}^{\text{even,NLO}} = B_{20} + B_{21} \pm \sqrt{(B_{20} - B_{21})^2 + 4B_{22}^2}, \quad (7.83)$$

$$32\pi a_{11}^{\text{odd,NLO}} = 2B_{30}, \quad (7.84)$$

where each block-diagonal element B_n is given in Eq. (B.n) from Ref. [231]. The condition of unitarity is fulfilled if all eigenvalues

$$a_{Y\tau(\pm)}^{Z_2} = a_{Y\tau(\pm)}^{Z_2,\text{LO}} + a_{Y\tau(\pm)}^{Z_2,\text{NLO}} \quad (7.85)$$

respect Eq. (7.70).

7.4.2 Perturbativity

Another condition required is that all our perturbative expansions are indeed valid expansions. What one means by this is that, in the case of unitarity, the higher order corrections should not exceed in magnitude the LO terms. Thus, perturbative unitarity is achieved by demanding that [231]

$$R'_1 \equiv \frac{|a_{Y\tau(\pm)}^{Z_2,\text{NLO}}|}{|a_{Y\tau(\pm)}^{Z_2,\text{LO}}|} < 1. \quad (7.86)$$

To avoid the exclusion of points with accidentally small LO contributions – such as a small $a_{10}^{\text{odd,LO}}$ by the mere fact that $\lambda_3 \approx \lambda_4$, whereas the NLO contribution has a dependence on other quartic couplings – we follow Ref. [232] in using R'_1 only in cases where $|a_{Y\tau(\pm)}^{Z_2,\text{LO}}| \gtrsim 1/(16\pi)$.

Other perturbative series that are made to be stable are the running quartic couplings λ_i with which we impose the positivity constraint. Here, the perturbative criterion consists in demanding that they do not exceed 4π in the range of scales over which the renormalization group evolution is performed.

7.5 Experimental Constraints

We finish this chapter with an exposition of the experimental information we use to constrain the parameter space of the 2HDM. A first word goes to the signal strengths of Higgs decays, which need to comply with LHC data if the boson discovered by ATLAS and CMS is allowed to be part of an extended Higgs sector. Similar to this is the lack of direct observation of the heavy scalars, which comes in the form of exclusion limits in searches of $X \rightarrow H/A \rightarrow Y$ processes and their mass ranges. In the present analysis we do not use this information, but take nevertheless advantage of the conclusions of Ref. [233]

to fix the value of $\beta - \alpha$ in Type-II, shown there to be heavily constrained due to h signal strengths, to $\pi/2$: this removes one parameter from the fit and, consequently, improves the Markov Chain Monte Carlo convergence.

7.5.1 Oblique Parameters

Being an extension of the scalar sector of the SM, a strong constraint on a 2HDM is that the new heavy degrees of freedom contribute to electroweak precision observables through virtual loops only. The dominant NP effects can thus be parametrized by three variables which absorb the radiative corrections produced by new contributions to the vacuum polarization of the vector bosons. These are known as *oblique parameters*, and a popular parametrization used in literature is the one by Peskin and Takeuchi, where the parameters are S , T , and U [234]. The high precision of the electroweak observables allows to constrain the parameter space of NP models that produce contributions to S , T , U .

The contributions to S , T , U in the 2HDM have long been available in literature [235–237], and their collected expressions can be found in Eqs. (21)–(23) of Ref. [238]. Mentioned there and worth of mention here is the fact that the 2HDM oblique corrections do not depend on the type of the model, since the four types differ in the Yukawa sector only, and Yukawa couplings do not enter the oblique parameters at one-loop order.

7.5.2 Flavour Observables

Of the plethora of flavour observables with various levels of significance for the 2HDM [239], we use two of the observables most relevant for multi-Higgs analyses: the aforementioned branching fraction of the radiative decay $B \rightarrow X_s \gamma$, and the mass difference of the B_s system. For the weak radiative B-meson decays, we take once more Ref. [133] and references therein. To provide here some explanation of how the 2HDM contributes to the branching fraction, let us start by noting that the leading additions to the transition within SM come via the exchange of a charged Higgs boson instead of the W in the radiative penguin from Fig. 3.4. Quoting from Ref. [133], contributions from physics beyond the SM are parametrized as changes to the WCs $C_{7,8}$, which in turn produce a shift in the branching fraction:

$$\text{BR}(B \rightarrow X_s \gamma) = \text{BR}^{\text{[SM]}}(B \rightarrow X_s \gamma) + \alpha_7 \Delta C_7 + \alpha_8 \Delta C_8. \quad (7.87)$$

This is a linearized expression, where $\alpha_{7,8}$ are coefficients of the linearization. It assumes that quadratic terms in $\Delta C_{7,8}$ can be neglected when they enter with $\mathcal{O}(1)$ coefficients into the branching fraction. If that is not the case, a detailed analysis of the QCD corrections of the NP model is necessary. Such endeavour has been pursued in the 2HDM, where, for Type-II, corrections to $\Delta C_{7,8}$ are known at NLO [240–242] and NNLO [243].

Regarding $B_s - \bar{B}_s$ mixing, it is a $\Delta F = 2$ process which we did not discuss in our sections dedicated to $b \rightarrow s$ transitions. Nevertheless, and in complete similarity with the radiative decay, the LO 2HDM contributions arrive via the exchange of charged Higgs bosons, here in box diagrams like the one from Fig. 3.4, with the leptonic line replaced by the suitable quarks. If the SM loop function is S_{WW} , then

the difference between the heavy and light mass eigenstates of this system in the 2HDM can be written as [239, 244]:

$$\Delta m_s = \frac{G_F^2}{24\pi^2} |\lambda_t|^2 \eta_B m_B m_t^2 f_{B_s}^2 B_{B_s} (S_{WW} + S_{WH} + S_{HH}), \quad (7.88)$$

where η_B is the SM QCD correction, ~ 0.55 at NLO [85], and B_{B_s} is the bag parameter. The loop functions, which correspond respectively to the replacement of none, one, or both W lines with a charged Higgs, are given in Eqs. (21)–(23) of Ref. [239].

Of course other flavour observables should be used in a global analysis. Of those, worth of mention is the leptonic decay $B_s \rightarrow \mu^+ \mu^-$, which receives tree-level contributions in the general 2HDM, and, with FCNCs absent when the Z_2 symmetry is imposed, can still get sizeable contributions from the heavy scalars – mainly from boxes with, again, W bosons replaced with H^\pm . The impact this observable has on the 2HDM can be seen for example, in the recent analysis of Ref. [245]. On the $\tan \beta$ -charged Higgs mass plane, as shown there, this impact concerns, for Type-II, the region of large $\tan \beta$ and low $M_{H^\pm}^2$. Since this region is already heavily constrained by the radiative $b \rightarrow s$ transition [246], this also pointed out by the authors of Ref. [245], and by the theoretical constraints, the inclusion of $B_s \rightarrow \mu^+ \mu^-$ is, for now, redundant and can be left out.

Chapter 8

On the Metastability of the 2HDM

We have finally arrived at the chapter which concerns the results of the second global analysis we set out to perform. Without further ado, we will recapitulate the procedure of the analysis. After an exposition of the values of the inputs and observables we use in the fits, we present our numerical results. Closing remarks and a discussion of the thesis as a whole is then left for a final chapter of conclusions.

8.1 Procedure and Samples

We use this section not to restate what has already been said in terms of the necessary steps that lead to a computation of tunnelling rates, but rather to clarify the order in which everything is put together, and the different scenarios that will be considered. In the first global analysis we resorted to `HEPfit` alone to do all the calculations. In going beyond the leading order in stability, however, we sought the aid of publicly available third-party software, since we deemed it would be unpractical to build from scratch a homotopy continuation algorithm in `HEPfit`, and the implementation of a C++ calculator of decay rates would have been too time consuming. As software goes, therefore, we are, for now, using `HEPfit`, followed by a Python script of our own making, which incorporates `HOM4PS-2`, `iminuit` and `CosmoTransitions`. It should come as no surprise that such a convoluted configuration was the source of many problems in the numerics of this analysis, not least because of the limited control (or even lack of control, in the case of `HOM4PS-2`) one always has over third-party software. Dividing the analysis in steps that correspond to the software being used at that stage, we can describe the procedure as follows:

1. We start in `HEPfit`, where we generate with a Markov Chain Monte Carlo sets of points which comply with a given combination of imposed constraints. These combinations characterize the sampling being made, the samples we consider here being:
 - **PT**: A global minimum condition is never imposed in the `HEPfit` runs, since it would remove the points that we want to see being saved by the calculation of metastability. A study of potentials unbounded from below being rescued by the loop corrections was done in Ref. [62]. In this thesis, on the other hand, we can rather focus on the impact of constraints the author of that reference did not have at hand, meaning we want to start with potentials that are

already bounded from below. The RGE-improved positivity conditions together with the perturbativity of the quartic couplings (P) will thus be present in every sampling. This first category consists then of how the other theoretical constraints (T), namely NLO unitarity and the R'_1 condition, influence the stability of the model.

- **PE**: For this scenario, the output points respect both positivity and the the current bounds on the experimental observables (E) we consider in this work. Given these constraints impact heavily the charged sector, this scenario allows one to see how bounds on that sector are related to bounds on instability and metastability.
 - **PTE**: The final type of sampling we do with `HEPfit` corresponds to the global analysis, where all of the constraints above – positivity, the other theoretical constrains, and the experimental constraints – are simultaneously turned on.
2. With sets of already good points (up to the issue of stability), we move on to the steps comprised in our Python script. Passing first through `HOM4PS-2`, one computes and collects all the extrema of the tree-level potential characterized by the parameter values of each point. As such, the question of tree-level stability can be addressed immediately at this point.
 3. All the extrema computed in the previous step are then used as starting points to `iminuit`, which will obtain all the minima towards which the tree-level maxima, minima and saddle points roll, when the loop corrections from the Coleman-Weinberg potential are also taken into account. At this point, one can finally evaluate if the effective potential contains, or not, lower vacua than the one we attribute to our universe.
 4. For the vacua that are lower than the electroweak vacuum, we move further down in our script and call `CosmoTransitions` to compute the action of the bounce. As explained in the previous chapter, for values lower than 400 that configuration would produce an unstable vacuum, for values above that threshold the point under scrutiny would at least allow for a decay long enough that our universe would have been stable up until now.

The points from each sample, **PT**, **PE**, or **PTE**, are classified with the new information, and can then be colour-coded according to the type of universe with which they are associated. We provide the resulting 2D scatter plots two sections bellow.

8.2 Inputs and Experimental Values

The 2HDM with a softly-broken Z_2 symmetry is described by 8 parameters, which we have chosen to be those in Eq. (6.61). Since the VEV and the Higgs mass can be fixed to their observed values, one usually deals with 6 parameters, all given as inputs with generous flat priors. We will be working in Type-II only, given its interest and ubiquity in literature, to take advantage of the order of precision reached in flavour for this type of 2HDM, and also due to the limited time we had after all our issues related with software had been solved. Moreover, as we alluded to in Chapter 7, we will be making use

Parameter	$\tan\beta$	m_H, m_A, m_{H^\pm}	m_{12}^2
Range	[0.25; 100]	[130; 1100] GeV	$[-1; 7] \times 10^5 \text{ GeV}^2$

Table 8.1: Priors on the 2HDM parameters.

Parameters	Mean Value	Uncertainty	Reference
m_τ (MeV)	1776.86	0.12	[80]
B_{B_s}	0.888	0.040	[170]
A	0.825	0.010	[248]
$\bar{\rho}$	0.145	0.015	[248]
$\bar{\eta}$	0.350	0.013	[248]

Table 8.2: Parameters used in the global analysis.

Observable	Value	Correlation matrix		
S	0.09 ± 0.10	1	0.86	-0.56
T	0.11 ± 0.12	0.86	1	-0.84
U	-0.01 ± 0.09	-0.56	-0.84	1

Table 8.3: S, T, U values and correlations from Ref. [247].

Observable	Value	Reference
Δm_{B_s}	$17.757 \pm 0.021 \text{ ps}^{-1}$	[249]
$\text{BR}(\bar{B} \rightarrow X_s \gamma)$	$(3.43 \pm 0.21 \pm 0.07) \times 10^{-4}$	[249]

Table 8.4: Flavour observables used in the fits.

of the results of Ref. [233] for $\beta - \alpha$ in Type-II, which permits us to fix it at $\pi/2$, yielding a scalar sector fully described by 5 2HDM parameters:

$$\tan\beta, M_{H^\pm}^2, M_H^2, M_A^2, m_{12}^2. \quad (8.1)$$

The priors we give to these parameters are shown in Table 8.1. Further parameters being used in the fits, chiefly quark masses and the parameters present in the formulas of flavour observables, can be consulted in Table 5.1; the ones we add or update for this analysis are provided in Table 8.2.

Regarding the experimental information itself, needed for the **PE** and **PTE** fits, we report the S, T, U values from Ref. [247] in Table 8.3, where the correlation matrix computed by those authors is also provided. The values of the flavour observables considered here are given in Table 8.4.

8.3 Numerical Results

Let us start with the case of **PT** sampling. We collect in Fig. 8.1 the combinations of quartic couplings which have produced a potential stable, unstable, or metastable at the one-loop level, the colours that

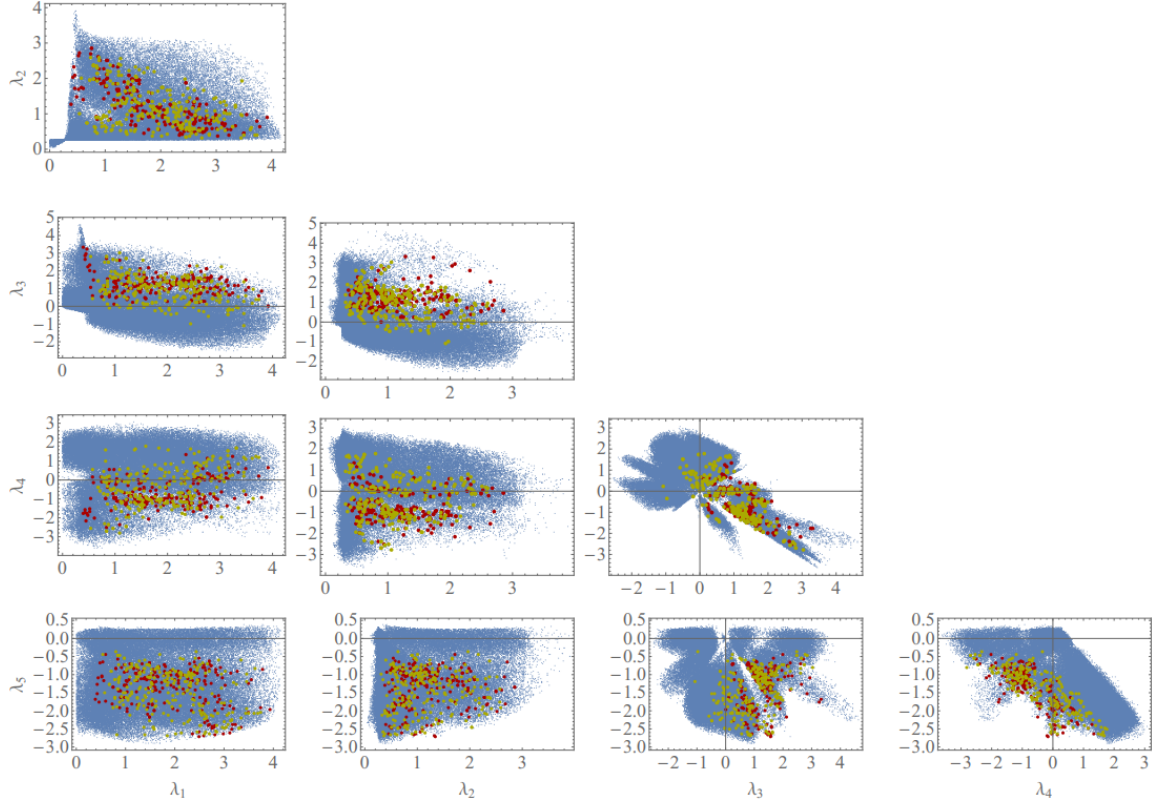


Figure 8.1: Scatter plots of stability for case **PT**, projected in the $\lambda_i - \lambda_j$ planes. The colour-coding is the following: blue points represent potentials completely stable at the one-loop level, red points correspond to unstable potentials at the one-loop level, and yellow points stand for potentials with metastability at the one-loop level.

represent each option being explained in the caption of that same figure. A general assessment that can be made is that, obviously, instability and metastability are bundled together, for a small change in one parameter or another can be sufficient to make the true vacuum move a little bit lower or higher, to make the tunnelling rate go a little above or below the metastability threshold. In terms of identifying a clear region of instability/metastability, these planes in parameter space may show some hints of an organizing principle, but there is always a big overlap with a region of absolutely stable points. The quartic coupling 2D plots with NLO perturbative unitarity imposed had already been computed in Ref. [232], and here, even though with lower statistics and without a definition of the 1σ , 2σ , 3σ regions, we manage to find more or less the same shape, and we get the same bounds on the size of the couplings, *i.e.* a constraint that they must be smaller than at least ~ 5 in magnitude. We get a bigger tendency for $\lambda_5 < 0$, a tendency that is, of course, followed by the red and yellow points. The strongest hint is that instability or metastability would occur for $\lambda_3 > 0$, which can be seen in the planes with λ_1 and λ_2 , and also in the $\lambda_3 - \lambda_4$ plane, this one also showing a slight preference for the red/yellow points to sit in the legs with negative λ_4 , which could be argued that is also discernible in the tendency for these points to be in the region closer to the third quadrant of the $\lambda_4 - \lambda_5$ plot.

If one looks in other directions of parameter space, it becomes apparent that the hints in the $\lambda_i - \lambda_j$ planes were mainly due to correlations between observables. This because in Fig. 8.2 we find a clear

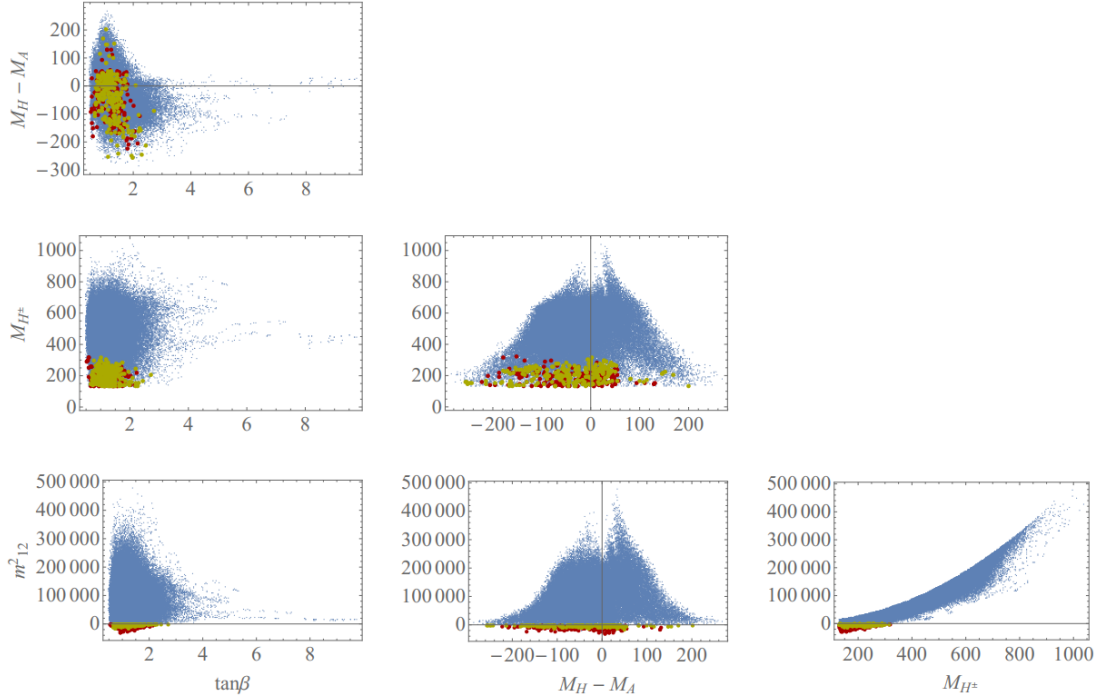


Figure 8.2: Scatter plots of stability for case **PT**, projected in planes with $\tan\beta$, $M_H - M_A$, M_{H^\pm} , and m_{12}^2 . For the colour-coding see the caption of Fig. 8.1.

indication that instability/metastability at the one-loop level happens for $m_{12}^2 < 0$, a behaviour mimicked by the lower values of the correlated parameter M_{H^\pm} . The interpretation of this is twofold: first, it makes us go back to Eq. (7.22), where the discriminant to ensure the global minimum condition at tree-level was heavily dependent on the sign of m_{12}^2 ; one could infer that, with perturbativity imposed, our Coleman-Weinberg terms should be small and thus mere corrections to the issue of instability, which would then always come from the existence of extra minima already at tree-level. On a similar footing, this could be the result of the known difficulty in finding extra minima with MINUIT, since we are rolling down the steepest directions of the effective potential sheet with the tree-level extrema as starting points, and there is no guarantee that this will find us the extra minima created by the loop corrections, beyond the extra minima that might already exist in the leading order. In fact, our code never finds extra minima at the one-loop level when there were none beyond the EW minimum at tree-level. Moreover, and pointed out by the authors of *Vevacious*,¹ homotopy continuation algorithms compute, in principle, all the extrema of the tree-level potential, however, because of finite-precision and finite-step-size issues, an algorithm like *HOM4PS-2* will sometimes miss some extrema.

Either way, for this analysis, it looks like everything comes down to identifying the problematic regions of m_{12}^2 . Would this mean that one might advocate the implementation of the tree-level condition and the matter of stability would be solved? Not really. Loop-corrections and the calculation of the tunnelling rate are, nevertheless, able to save many points with negative m_{12}^2 that would otherwise be deemed unstable and removed from the parameter space. This can be seen in the plots of Fig. 8.3, where green points, made stable by the Coleman-Weinberg terms, and the blue region, made metastable after the

¹See the README file that comes with their software, available at <https://github.com/benoleary/Vevacious>.

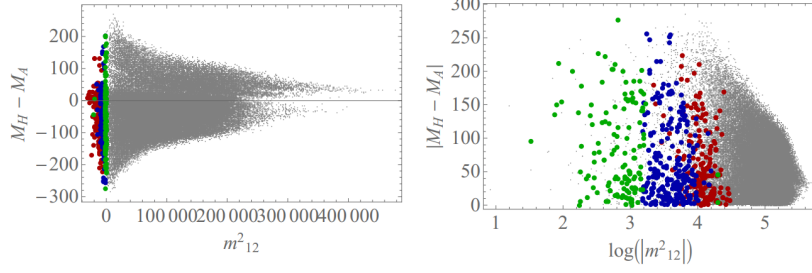


Figure 8.3: Points misidentified as unstable in a **PT** sample, rescued by loop-corrections and the calculation of the tunnelling rate: green points become stable at the one-loop level, blue points become metastable, red points remain unstable; grey points are stable at both levels.

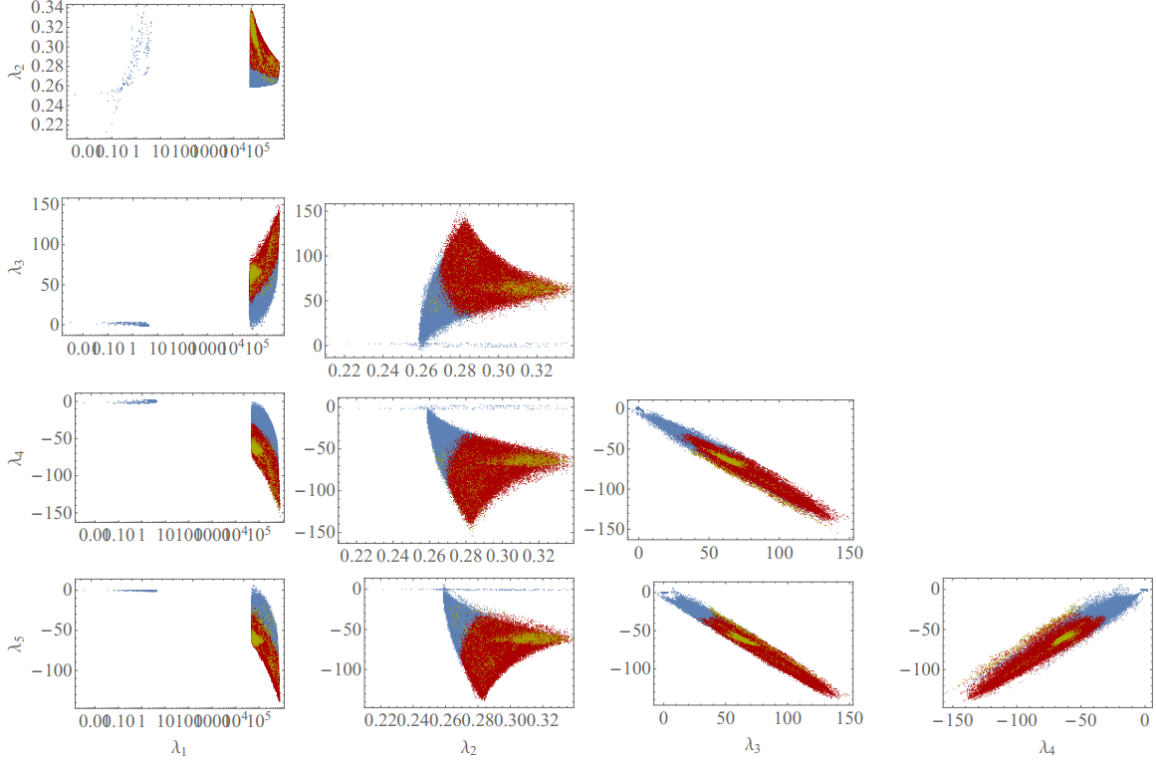


Figure 8.4: Scatter plots of stability for case **PE**, projected in the $\lambda_i - \lambda_j$ planes. For the colour-coding see the caption of Fig. 8.1.

calculation of the decay rates with **CosmoTransitions**, would have been eliminated together with the red band. In the second panel, it is visible how the coloured regions from the left panel really break into phases of stability dependent on the size of m_{12}^2 .

Regarding the **PE** scenario, we present the same plots we did for **PT**, with exactly the same colour labelling as used before. In Fig. 8.4, we show the regions that are allowed when electroweak precision observables and flavour observables are switched on, and perturbative unitarity is no longer being demanded. This last detail explains the regions of very large quartic coupling that are now available. Indeed, for these regions, we can see that instability and metastability became very well pronounced. Still, we chose a log scale for λ_1 in order to make clear that, although the Markov Chains have preferred the mode with very large λ 's, and therefore many points that are unstable or metastable at the one-loop level, the

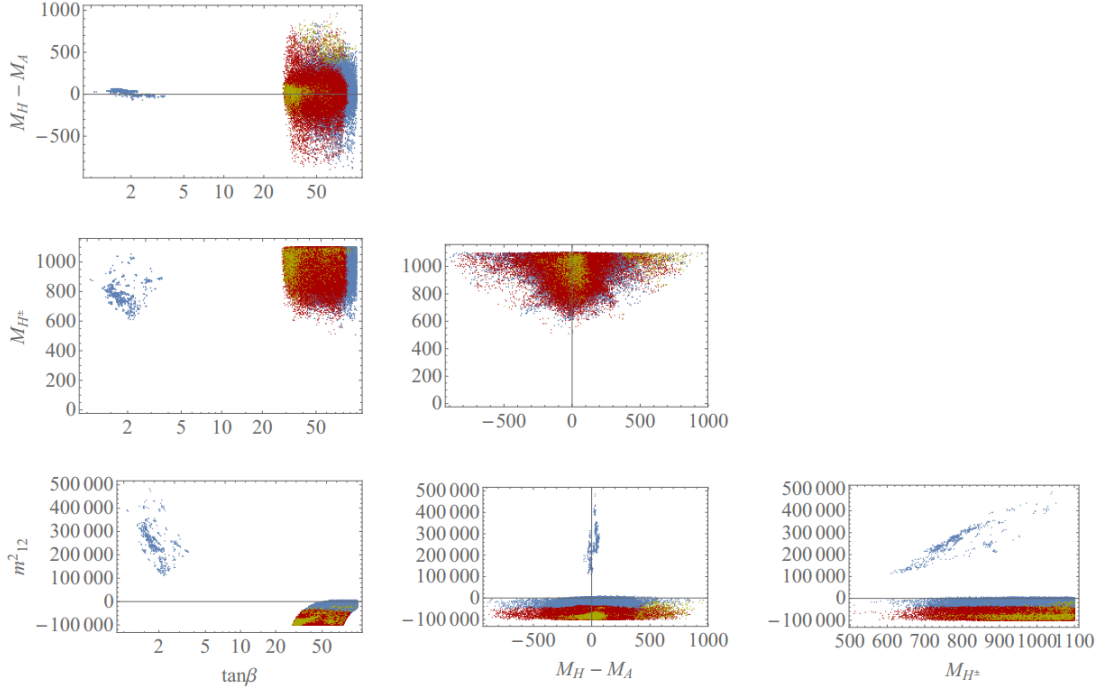


Figure 8.5: Scatter plots of stability for case **PE**, projected in planes with $\tan\beta$, $M_H - M_A$, M_{H^\pm} , and m_{12}^2 . For the colour-coding see the caption of Fig. 8.1.

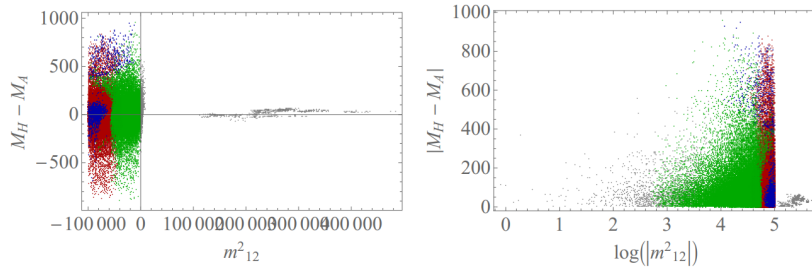


Figure 8.6: Points misidentified as unstable in a **PE** sample, rescued by loop-corrections and the calculation of the tunnelling rate: for the colour-coding see the caption of Fig. 8.3.

mode with small couplings we found in the presence of unitarity is still there, and it is completely stable.

The same can be said for the planes with $\tan\beta$, $M_H - M_A$, M_{H^\pm} , and m_{12}^2 , found in Fig. 8.5. There, we chose a log scale to present $\tan\beta$ as well, and, by doing so, we find the sources of the bi-modal distributions: in the $\tan\beta - m_{12}^2$ plane, there is a solution which fits the experimental observables with small $\tan\beta$ and positive m_{12}^2 , and there is also a solution with large $\tan\beta$ and negative m_{12}^2 , expected from the expressions of flavour observables in the 2HDM, namely where by pushing $\tan\beta$ to very large values you can make the NP contributions to $B_s - \bar{B}_s$ mixing as small as you want and always be within a fitting parameter space, whereas in $\tan\beta - M_{H^\pm}$ we can discern in the large $\tan\beta$ mode a truncated piece of the profile of the renowned exclusion region from $b \rightarrow s\gamma$, that indeed corresponds to the red/yellow region we find in the panel below, for negative m_{12}^2 . This to say that it is again this parameter which is dominating the determination of stable or unstable potentials, appearing in other planes by its correlation with the other parameters. Furthermore, we can make our case for the usage of the effective potentials and the

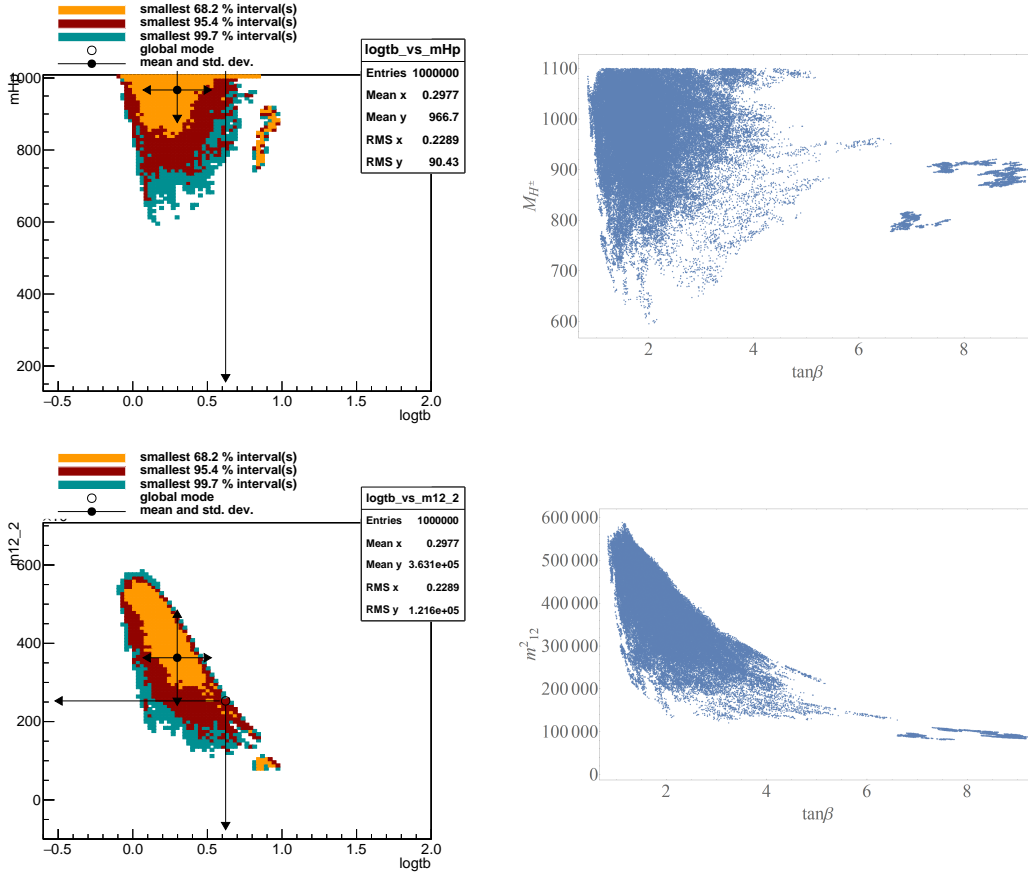


Figure 8.7: Example of output histograms from `HEPfit` and stability points for **PTE**.

evaluation of tunnelling rates: we observe a large portion of points that would be labelled unstable, but are stable because of loop-corrections, or even metastable, for the cases where the decay from our vacuum to the true vacuum would not have happened within the age of universe. In Fig. 8.6, these points are shown, respectively, in green and blue for the case of the **PE** fit.

For the global analysis, **PTE**, when we include simultaneously all constraints, one can guess the results even before computing them. In fact, because NLO unitarity will pick the small quartic couplings and will favour the mode with small $\tan \beta$, and given the experimental constraints curtail negative values of m_{12}^2 in that mode, it is easy to infer that, for the configuration of software and algorithms we have used in this analysis, there will be no region of either instability, or metastability. And indeed that is what we get when we perform our runs. Since it would be redundant to plot again the blue regions of quartic couplings from the **PT** scenario, we simply provide in Fig. 8.7 the relevant planes, those with $\tan \beta$, M_{H^\pm} , and m_{12}^2 , presenting both the histograms that come out of `HEPfit` – which we note have $\log(\tan \beta)$ instead of $\tan \beta$ – and the corresponding scatter plots that we obtain after passing the points through the one-loop treatment of our Python script. Regardless of what has caused m_{12}^2 to dominate our findings and make the issue of stability/instability here so tree-level-like, we can finish this chapter with the reasonable message that performing global analyses can take care of some unattended problems of a given model: in our example, positivity, unitarity, and experimental constraints turned out to impose what a global minimum condition would.

Chapter 9

Conclusions

It is a long established fact that the SM, although remarkable in itself, is not the “final theory”. The lack of NP signals from past and ongoing experiments as launched us on a quest to reach better and better levels of precision in both experimental observations and theoretical calculations. Inspired by this Precision Era that is being lived in particle physics, we perform in this thesis two global analyses. On a general note, we can say that global analyses prove to be worthwhile endeavours in the pursuit of NP, allowing for the combination of a variety of constraints, direct and indirect, theoretical and experimental, both on the parameter space of a given model or in a model-independent way. Our work was mainly concerned with the development and usage of `HEPfit` [48]. While the implementation of a coherent $\Delta F = 1$ effective Hamiltonian with both QCD and QED corrections was included in this thesis, there are indeed modules of the code which received participation of the student and were left out for future employment: these consist of the entire inclusive sector of semileptonic $b \rightarrow s$ transitions, and the module for general 2HDMs.

Our first global analysis was a study of $b \rightarrow s$ transitions, where so-called flavour anomalies, deviations from SM predictions, keep appearing in many decay channels. The global analysis consisted on performing fits to model-independent shifts to the WC that contribute to radiative and (semi)leptonic decays of B mesons. We critically examined several NP scenarios in order to possibly explain the growing pattern of the B anomalies, recently enriched by the measurement of R_{K^*} by LHCb [19]. The analysis was carried out in an effective field theory framework, describing the non-factorizable power corrections by means of 16 free parameters, this done in accordance with the previous procedure of Ref. [27]. These fits were performed here using two different approaches to the hadronic contributions: the first approach, labelled PMD, relies completely on the phenomenological model from Ref. [146] and corresponds to the choice that is more widely used in literature; the second one, labelled PDD, imposes the result of Ref. [146] only at $q^2 \leq 1$, allowing the current data to drive the hadronic contributions in the higher invariant mass region.

Regarding the NP contributions, six different benchmark scenarios were considered, distinguished by the respective combination of NP WCs employed in the fits: scenario **(I)** allows for $C_{9,\mu}^{\text{NP}}$ and $C_{9,e}^{\text{NP}}$; scenario **(II)** considers the scenario with $C_{9,\mu}^{\text{NP}}$ and $C_{10,\mu}^{\text{NP}}$; case **(III)** studies NP effects coming as C_7^{NP} ,

$C_{9,\mu}^{\text{NP}}$ and $C_{9,e}^{\text{NP}}$; case **(IV)** is the same as the case **(III)**, but with C_{10}^{NP} instead of C_9^{NP} ; case **(V)** studies the possibility described in case **(III)**, with $C_{10,\mu}^{\text{NP}} = -C_{9,\mu}^{\text{NP}}$ and $C_{10,e}^{\text{NP}} = -C_{9,e}^{\text{NP}}$ enforced; finally, case **(VI)** considers the general case with all the five NP WCs being allowed to float independently. Our main results are collected in Figs. 5.1–5.8, supported by the information in Tables 5.2–5.5.

By means of comparing the IC of each fit, we have found that all the considered cases are on the same footing except for scenarios **(IV)** and **(V)**. These are strongly disfavoured in the PMD approach, as there is no $C_{9,\mu}^{\text{NP}}$ in case **(IV)** to account for the deviation in P'_5 , while in case **(V)** $C_{9,\mu}^{\text{NP}}$ is constrained by its correlation with $C_{10,\mu}^{\text{NP}}$ and the measured value of $\text{BR}(B_s \rightarrow \mu\mu)$. Overall, from our analysis it is possible to identify two classes of viable NP scenarios:

- The widely studied $C_{9,\mu}^{\text{NP}} \neq 0$ scenario, as we find a remarkable $\gtrsim 5\sigma$ evidence in favour of $C_{9,\mu}^{\text{NP}} \neq 0$ in the PMD approach. One must point that it is indeed nontrivial that a single NP WC can explain all the present anomalies in $b \rightarrow s$ transitions [9, 40–44]. In the more conservative PDD approach, however, the significance of a nonvanishing $C_{9,\mu}^{\text{NP}}$ drops to about 3σ , driven mainly by the LFUV observables.
- An alternative scenario with nonvanishing $C_{10,e}^{\text{NP}}$, which emerges in the presence of large hadronic corrections to the infinite mass limit, namely our PDD approach. To our knowledge, a NP electronic axial current has not been studied in the literature, since it does not provide a satisfactory description of the angular observables within the commonly used PMD approach. As we have noted, the present theoretical status of power correction calculations is not robust enough, thus making it impossible to discard this interesting NP scenario until the hadronic sector is fully under control.

In the most general fit we performed, that of scenario **(VI)**, one confirms in the PDD approach that both classes above are viable, even though a slight preference for $C_{9,\mu}^{\text{NP}} \neq 0$ is found. More data are needed to disentangle NP shifts from charm-loop contributions, and, in case the flavour anomalies persist, to assess what kind of NP scenario is realized in Nature. Channels such as the inclusive semileptonic decay $B \rightarrow X_s \ell^+ \ell^-$, or the semileptonic baryon decay $\Lambda_b \rightarrow \Lambda \ell^+ \ell^-$, could be the providers of that definitive constraint which will point us in the right direction; these are among the processes that will be studied in the eagerly awaited Belle II experiment, expected to begin taking data early next year, and set to fuel the following years of B physics together with LHCb.

We then permitted ourselves a second venture, consisting in the analysis of metastability in the 2HDM with a softly-broken Z_2 symmetry. In more detail, this was a first attempt at a study of the issue of stability of the scalar potential at the one-loop level, in the context of a global analysis, imposing many theoretical and experimental constraints. For this we devised three scenarios, corresponding to the constraints used in the preliminary fit performed in **HEPfit**: the first one, **PT**, provides a set of points that comply with positivity, NLO perturbative unitarity, and perturbativity of the 2HDM quartic couplings; the second, **PE**, trades perturbative unitarity for experimental constraints, which comprise electroweak precision observables, and two flavour observables, the mass difference in $B_s - \bar{B}_s$ mixing and the branching fraction of $B \rightarrow X_s \gamma$. Although we do not use Higgs signal strengths, we employ a recent result from Ref. [233] and fix $\beta - \alpha = \pi/2$ in Type-II; the third and final fit, **PTE**, corresponds

to the simultaneous imposition of the constraints from **PT** and **PE**.

Stability at the one-loop level is assessed by making use of the effective one-loop Hamiltonian with Coleman-Weinberg contributions. Metastability, on the other hand, is evaluated by computing the vacuum tunnelling rate in the $O(4)$ bounce formalism. For the **PT** scenario we found theory to favour a region with small $\tan\beta$, and with just a few metastable or unstable points, due to a small region where m_{12}^2 is allowed to be negative. This preponderance for the sign of m_{12}^2 to dictate the stability of the potential was also found for **PE**, where a bigger region of $m_{12}^2 < 0$ and large $\tan\beta$ is also allowed, yielding huge sectors of instability all over the parameter space. In both cases, however, we observed that either by loop corrections, or by decay rates being larger than the age of the universe, a considerable amount of points were always being rescued from what would be a classification of instability and removal from the accepted regions of parameters. This goes along the lines of the rates of misidentification put forward by Ref. [62]. **PE** produces a bi-modal distribution, and for the mode with small $\tan\beta$ these constraints cut out any possibility of having negative values for m_{12}^2 . This means that when both sets of constraints are put together, the Markov Chain Monte Carlo of **HEPfit** results in a sample with $m_{12}^2 > 0$, such that the last global fit finds absolutely nothing but stability in both the tree- and the one-loop level.

To say that **PTE** resolves completely the issue of vacuum stability in the 2HDM would be a long claim, and we are certainly not prepared to make it. First, because it seems highly unlikely that one parameter would control the stability of the one-loop effective potential. More so because this parameter corresponds exactly to parameter whose signal has an immediate impact on the discriminant of the tree-level global minimum condition. In our chapter of results we alluded to the possibility that in the perturbative regime the existence of extra minima in the potential could be bound to the tree-level sheet, with loop corrections merely adjusting the relative depth of each minimum. The most probable scenario, however, may be that we are falling prey of our own configuration to try to find all possible minima of the one-loop potential: even assuming that the homotopy continuation algorithm is finding all the tree-level extrema, one can never say for certain that giving those values as starting points to the numerical minimizer will roll us down into all the extra minima that can be created with the inclusion of the Coleman-Weinberg terms. The authors of **Vevacious** [208], for example, try to solve this by rolling in the direction of steepest descent and rolling in the exact opposite direction as well. Another option, which we want to implement in our scripts next, is to use the tree-level extrema as starting points – which, mind, did not get us any new minima when there was none initially – and to have also a generator of randoms throwing a few starting values and see where they might lead us. Neither this or **Vevacious**' solution is a guarantee of success, but either, or both, can be a path towards the improvement of our results.

On a final note, we point to the fact that current analyses of loop vacuum stability in the softly-broken Z_2 -symmetric 2HDM [62], or the Inert Doublet Model [60, 61], have been performed mainly with scatter plots, as we did in this thesis. With a tool as powerful as **HEPfit**, and given the modular nature of the project, it is natural to set a goal that in the near future we will implement successfully homotopy continuation and vacuum tunnelling calculation in the code, in order to have a full Bayesian analysis, with proper Markov Chain Monte Carlo and proper posterior histograms, so as to have stability as a means to an end, and not the other way around.

Appendix A

Beta Functions

A.1 Coefficients of the QCD Beta Function

The coefficients of Eq. 3.41 are given by [99, 100]:

$$\beta_0 = \frac{11}{3}C_A - \frac{4}{3}T_F n_f, \quad (\text{A.1})$$

$$\beta_1 = \frac{34}{3}C_A^2 - \frac{20}{3}C_A T_F n_f - 4C_F T_F n_f, \quad (\text{A.2})$$

$$\beta_2 = \frac{2857}{54}C_A^3 - \frac{1415}{27}C_A^2 T_F n_f + \frac{158}{27}C_A T_F^2 n_f^2 + \frac{44}{9}C_F T_F^2 n_f^2 - \frac{205}{9}C_F C_A T_F n_f + 2C_F^2 T_F n_f, \quad (\text{A.3})$$

$$\begin{aligned} \beta_3 = & C_A C_F T_F^2 n_f^2 \left(\frac{17152}{243} + \frac{448}{9}\zeta_3 \right) + C_A C_F^2 T_F n_f \left(-\frac{4204}{27} + \frac{352}{9}\zeta_3 \right) + \frac{424}{243}C_A T_F^3 n_f^3 \\ & + C_A^2 C_F T_F n_f \left(\frac{7073}{243} - \frac{656}{9}\zeta_3 \right) + C_A^2 T_F^2 n_f^2 \left(\frac{7930}{81} + \frac{224}{9}\zeta_3 \right) + \frac{1232}{243}C_F T_F^3 n_f^3 \\ & + C_A^3 T_F n_f \left(-\frac{39143}{81} + \frac{136}{3}\zeta_3 \right) + C_A^4 \left(\frac{150653}{486} - \frac{44}{9}\zeta_3 \right) + C_F^2 T_F^2 n_f^2 \left(\frac{1352}{27} - \frac{704}{9}\zeta_3 \right) \\ & + 46C_F^3 T_F n_f + n_f \frac{N_c(N_c^2 + 6)}{48} \left(\frac{512}{9} - \frac{1664}{3}\zeta_3 \right) + n_f^2 \frac{N_c^4 - 6N_c^2 + 18}{96N_c^2} \left(-\frac{704}{9} + \frac{512}{3}\zeta_3 \right) \\ & + \frac{N_c^2(N_c^2 + 36)}{24} \left(-\frac{80}{9} + \frac{704}{3}\zeta_3 \right), \end{aligned} \quad (\text{A.4})$$

where, for an $SU(N)$ group:

$$T_F = \frac{1}{2}, \quad C_F = \frac{N_c^2 - 1}{2N_c}, \quad C_A = N_c. \quad (\text{A.5})$$

A.2 Coefficients of Beta Functions with QED Corrections

We provide here the coefficients needed for the QCD and QED renormalization group evolution championed in Ref. [109]:

$$\begin{aligned} \beta_{01}^s &= -4T_F \overline{Q^2}, & \beta_{11}^s &= (4C_F - 8C_A) T_F \overline{Q^2}, & \beta_{02}^s &= \frac{11}{3}T_F \overline{Q^2} \beta_{00}^e + 2t_F \overline{Q^4}, \\ \beta_{00}^e &= \frac{4}{3} \left(\overline{Q^2} N_c + 3Q_\ell^2 \right), & \beta_{10}^e &= 4 \left(\overline{Q^4} N_c + 3Q_\ell^4 \right), & \beta_{01}^e &= 4C_F N_c \overline{Q^2}, \end{aligned} \quad (\text{A.6})$$

where

$$\overline{Q^n} = n_u Q_u^n + n_d Q_d^n. \quad (\text{A.7})$$

Appendix B

Loop Functions

B.1 Functions Used in M Matchings

The loop functions and power expansions present in the matching conditions for the M block can be read from Ref. [115]:

$$\begin{aligned}
C_{7,\text{loop}}^{t,(3)}(x) = & L_t \left[\frac{-592x^5 - 22x^4 + 12814x^3 - 6376x^2 + 512x}{27(x-1)^5} \text{Li}_2 \left(1 - \frac{1}{x} \right) \right. \\
& + \frac{-26838x^5 + 25938x^4 + 627367x^3 - 331956x^2 + 16989x - 460}{729(x-1)^6} \ln x \\
& \left. + \frac{34400x^5 + 276644x^4 - 2668324x^3 + 1694437x^2 - 323354x + 53077}{2187(x-1)^5} \right] \\
& + L_t^2 \left[\frac{-63x^5 + 532x^4 + 2089x^3 - 1118x^2}{9(x-1)^6} \ln x \right. \\
& \left. + \frac{1186x^5 - 2705x^4 - 24791x^3 - 16099x^2 + 19229x - 2740}{162(x-1)^5} \right], \tag{B.1}
\end{aligned}$$

where $L_t = \ln \frac{\mu_W^2}{m_t^2}$.

$$\begin{aligned}
C_{7,M_W}^{c,(3)}(z) \simeq & 1.525 - 0.1165z + 0.01975z \ln z + 0.06283z^2 + 0.005349z^2 \ln z + 0.01005z^2 \ln^2 z \\
& - 0.04202z^3 + 0.01535z^3 \ln z - 0.00329z^3 \ln^2 z + 0.002372z^4 - 0.0007910z^4 \ln z + \mathcal{O}(z^5), \tag{B.2}
\end{aligned}$$

where $z = \frac{1}{x}$.

$$\begin{aligned}
C_{7,m_t}^{t,(3)}(z) \simeq & 12.06 + 12.93z + 3.013z \ln z + 96.71z^2 + 52.73z^2 \ln z + 147.9z^3 + 187.7z^3 \ln z \\
& - 144.9z^4 + 236.1z^4 \ln z + \mathcal{O}(z^5). \tag{B.3}
\end{aligned}$$

$$\begin{aligned}
C_{8,\text{loop}}^{t,(3)} = & L_t \left[\frac{-148x^5 + 1052x^4 - 4811x^3 - 3520x^2 - 61x}{18(x-1)^5} \text{Li}_2 \left(1 - \frac{1}{x} \right) \right. \\
& + \frac{-15984x^5 + 152379x^4 - 1358060x^3 - 1201653x^2 - 74190x + 9188}{1944(x-1)^6} \ln x \\
& + \left. \frac{109669x^5 - 1112675x^4 + 6239377x^3 + 8967623x^2 + 768722x - 42796}{11664(x-1)^5} \right] \\
& + L_t^2 \left[\frac{-139x^4 - 2938x^3 - 2683x^2}{12(x-1)^6} \ln x \right. \\
& + \left. \frac{1295x^5 - 7009x^4 + 29495x^3 + 64513x^2 + 17458x - 2072}{216(x-1)^5} \right], \tag{B.4}
\end{aligned}$$

$$\begin{aligned}
C_{8,M_W}^{c,(3)}(z) \simeq & -1.870 + 0.1010z - 0.1218z \ln z + 0.1045z^2 - 0.03748z^2 \ln z + 0.01151z^2 \ln^2 z \\
& - 0.01023z^3 + 0.004342z^3 \ln z + 0.0003031z^3 \ln^2 z - 0.001537z^4 + 0.0007532z^4 \ln z + \mathcal{O}(z^5), \tag{B.5}
\end{aligned}$$

$$\begin{aligned}
C_{8,m_t}^{t,(3)}(z) \simeq & -0.8954 - 7.043z - 98.34z^2 - 46.21z^2 \ln z - 127.1z^3 - 181.6z^3 \ln z + 535.8z^4 \\
& - 76.76z^4 \ln z + \mathcal{O}(z^5). \tag{B.6}
\end{aligned}$$

B.2 Functions Used in L Matchings

Regarding the auxiliary functions from the large- m_t expansion of Ref. [116] for the L block, one has:

$$\begin{aligned}
\tau_b^{(2)}(x) = & 9 - \frac{13}{4}x - 2x^2 - \frac{x}{4}(19 + 6x) \ln x - \frac{x^2}{4}(7 - 6x) \ln^2 x - \left(\frac{1}{4} + \frac{7}{2}x^2 - 3x^3 \right) \frac{\pi^2}{6} \\
& + \left(\frac{x}{2} - 2 \right) \sqrt{x} g(x) + (x-1)^2 \left(4x - \frac{7}{4} \right) \text{Li}_2(1-x) - \left(x^3 - \frac{33}{4}x^2 + 18x - 7 \right) f(x); \tag{B.7}
\end{aligned}$$

$$\Delta_t(\mu, x) = 18 \ln \frac{\mu}{m_t} + 11 - \frac{x}{2} + \frac{x(x-6)}{2} \ln x + \frac{x-4}{2} \sqrt{x} g(x). \tag{B.8}$$

In the functions above,

$$g(x) = \begin{cases} 2\sqrt{4-x} \arccos \sqrt{x/4} & \text{for } 0 \leq x \leq 4, \\ \sqrt{x-4} \ln \left(\frac{1-\sqrt{1-4/x}}{1+\sqrt{1-4/x}} \right) & \text{for } x \geq 4, \end{cases} \tag{B.9}$$

and

$$f(x) = \int_0^1 dt \left[\text{Li}_2(1-r(t,x)) + \frac{r(t,x)}{r(t,x)-1} \ln r(t,x) \right], \quad \text{with } r(t,x) = \frac{1+(x-1)t}{t(1-t)}. \tag{B.10}$$

Appendix C

Form Factors

C.1 Form Factors in the Transversality Basis

The $B \rightarrow V$ form factors are, in the transversality basis and with the parametrization of Ref. [24]:

$$\langle V(k, \lambda) | \bar{q} \gamma_\mu b | B(p) \rangle = \epsilon_{\mu\nu\rho\sigma} \epsilon_\lambda^{*\nu} p^\rho k^\sigma \frac{2}{m_B + m_V} V(q^2), \quad (\text{C.1})$$

$$\begin{aligned} \langle V(k, \lambda) | \bar{q} \gamma_\mu \gamma_5 b | B(p) \rangle &= i(\epsilon_\lambda^* \cdot q) \frac{q_\mu}{q^2} 2 m_V A_0(q^2) \\ &+ i(m_B + m_V) \left(\epsilon_\lambda^{*\mu} - \frac{(\epsilon_\lambda^* \cdot q) q^\mu}{q^2} \right) A_1(q^2) \\ &- i(\epsilon_\lambda^* \cdot q) \left(\frac{(2p - q)^\mu}{m_B + m_V} - (m_B - m_V) \frac{q^\mu}{q^2} \right) A_2(q^2), \end{aligned} \quad (\text{C.2})$$

$$q^\nu \langle V(k, \lambda) | \bar{q} \sigma_{\mu\nu} b | B(p) \rangle = 2 i \epsilon_{\mu\nu\rho\sigma} \epsilon_\lambda^{*\nu} p^\rho k^\sigma T_1(q^2), \quad (\text{C.3})$$

$$\begin{aligned} q^\nu \langle V(k, \lambda) | \bar{q} \sigma_{\mu\nu} \gamma_5 b | B(p) \rangle &= (\epsilon_{\lambda;\mu}^* (m_B^2 - m_V^2) - (\epsilon^* \cdot q) (2p - q)_\mu) T_2(q^2) \\ &+ (\epsilon^* \cdot q) \left(q_\mu - \frac{q^2}{m_B^2 - m_V^2} (2p - q)_\mu \right) T_3(q^2). \end{aligned} \quad (\text{C.4})$$

Furthermore, from partially conserved axial current,

$$i \langle V(k, \lambda) | \bar{q} \gamma_5 b | B(p) \rangle = \frac{2 m_V}{m_b + m_q} (\epsilon^* \cdot q) A_0(q^2), \quad (\text{C.5})$$

$$\langle V(k, \lambda) | \bar{q} P_{L,R} b | B(p) \rangle = \mp i \frac{m_V}{m_b + m_q} (\epsilon^* \cdot q) A_0(q^2). \quad (\text{C.6})$$

Upon the rescaling the helicity-0 form factors as

$$\begin{aligned} V_0(q^2) &= \frac{2 m_B \sqrt{q^2}}{\lambda^{1/2}} \tilde{V}_{L0}(q^2), \\ T_0(q^2) &= \frac{2 m_B^3}{\sqrt{q^2} \lambda^{1/2}} \tilde{T}_{L0}(q^2), \\ S(q^2) &= -\frac{2 m_B (m_b + m_s)}{\lambda^{1/2}} \tilde{S}_L(q^2), \end{aligned} \quad (\text{C.7})$$

where $\lambda = 4m_B^2 |\vec{k}|^2$ and $S_R = -S_L$, and defining as well

$$V_\pm(q^2) \equiv \tilde{V}_{L\pm}(q^2), \quad (\text{C.8})$$

$$T_\pm(q^2) \equiv \tilde{T}_{L\pm}(q^2), \quad (\text{C.9})$$

the seven helicity basis form factors can be related with those written in the traditional basis:

$$V_{\pm}(q^2) = \frac{1}{2} \left[\left(1 + \frac{m_V}{m_B} \right) A_1(q^2) \mp \frac{\lambda^{1/2}}{m_B(m_B + m_V)} V(q^2) \right], \quad (\text{C.10})$$

$$V_0(q^2) = \frac{1}{2m_V\lambda^{1/2}(m_B + m_V)} \left[(m_B + m_V)^2(m_B^2 - q^2 - m_V^2)A_1(q^2) - \lambda A_2(q^2) \right], \quad (\text{C.11})$$

$$T_{\pm}(q^2) = \frac{m_B^2 - m_V^2}{2m_B^2} T_2(q^2) \mp \frac{\lambda^{1/2}}{2m_B^2} T_1(q^2), \quad (\text{C.12})$$

$$T_0(q^2) = \frac{m_B}{2m_V\lambda^{1/2}} \left[(m_B^2 + 3m_V^2 - q^2)T_2(q^2) - \frac{\lambda}{(m_B^2 - m_V^2)} T_3(q^2) \right], \quad (\text{C.13})$$

$$S(q^2) = A_0(q^2). \quad (\text{C.14})$$

C.2 Auxiliary Functions in Charm-loop Contributions

The $\tilde{g}_i(q^2)$ in Eq. (5.6) are related to $h_{\lambda}(q^2)$ as follows [27]:

$$\tilde{g}_1 = -\frac{1}{2C_1} \frac{16m_B^3(m_B + m_{K^*})\pi^2}{\sqrt{\lambda(q^2)}V(q^2)q^2} (h_-(q^2) - h_+(q^2)), \quad (\text{C.15})$$

$$\tilde{g}_2 = -\frac{1}{2C_1} \frac{16m_B^3\pi^2}{(m_B + m_{K^*})A_1(q^2)q^2} (h_-(q^2) + h_+(q^2)), \quad (\text{C.16})$$

$$\tilde{g}_3 = \frac{1}{2C_1} \left[\frac{64\pi^2 m_B^3 m_{K^*} \sqrt{q^2} (m_B + m_{K^*})}{\lambda(q^2) A_2(q^2) q^2} h_0(q^2) - \frac{16m_B^3\pi^2(m_B + m_{K^*})(m_B^2 - q^2 - m_{K^*}^2)}{\lambda(q^2) A_2(q^2) q^2} (h_-(q^2) + h_+(q^2)) \right]. \quad (\text{C.17})$$

The charm-loop coefficient function $g(m_c^2, q^2)$ is given by [146]:

$$g(m_c^2, q^2) = -\frac{8}{9} \ln \left(\frac{m_c}{m_b} \right) + \frac{8}{27} + \frac{4}{9} y(q^2) - \frac{4}{9} [2 + y(q^2)] \sqrt{y(q^2) - 1} \arctan \left[\frac{1}{\sqrt{y(q^2) - 1}} \right] \quad (\text{C.18})$$

where $y(q^2) = 4m_c^2/q^2$.

Acknowledgements

First and foremost, I thank my advisor, Marco Ciuchini, who has been a source of guidance and support ever since I knocked on his office door on a sunny September day, after I had finished my *prova scritta* to get admitted to Roma Tre. I am grateful for everything I have learned with him about particle physics and the very scientific world, for the sense of true partnership I have always felt in our long and laborious afternoon meetings, for his calmness and belief in me, even when this thesis was extending way beyond all healthy deadlines.

My work was embedded in the ambitious project that is the development of `HEPfit` and, as such, I am also indebted to Luca Silvestrini and Enrico Franco, for being an integral part of the great work environment we have in code meetings, paper meetings, and other office discussions. I am thankful for all the cheerful and newsy lunches when I am at Sapienza, and the subsequent Italian coffee ritual, in which I never participate!

A special word must go to Mauro Valli, Ayan Paul, and Marco Fedele, for the marathon they ran to allow the delivery of all of our Easter eggs on time and with plenty of flavour to satiate (some of) the current New Physics hunger.

On the two Higgs side of `HEPfit`, I could not have asked for better collaborators than Debtosh Chowdhury and Otto Eberhardt. Whether general or Z_2 -symmetric, our research has not been easy, yet from them I know I can always expect encouragement, clarifying answers, and engaging conversations about different cultures, history, football, cinema, or TV.

Finally, I could not finish this section without acknowledging Richard Feynman and Bertrand Russell, for lifelong inspiration, overall entertainment, and for keeping me company in my many commutes around Rome.

Bibliography

- [1] UA1 collaboration, G. Arnison et al., *Experimental Observation of Isolated Large Transverse Energy Electrons with Associated Missing Energy at $s^{*}(1/2) = 540\text{-GeV}$* , *Phys. Lett.* **122B** (1983) 103–116.
- [2] UA2 collaboration, M. Banner et al., *Observation of Single Isolated Electrons of High Transverse Momentum in Events with Missing Transverse Energy at the CERN anti-p p Collider*, *Phys. Lett.* **122B** (1983) 476–485.
- [3] UA1 collaboration, G. Arnison et al., *Experimental Observation of Lepton Pairs of Invariant Mass Around $95\text{-GeV}/c^{*2}$ at the CERN SPS Collider*, *Phys. Lett.* **126B** (1983) 398–410.
- [4] UA2 collaboration, P. Bagnaia et al., *Evidence for $Z^0 \rightarrow e^+ e^-$ at the CERN anti-p p Collider*, *Phys. Lett.* **129B** (1983) 130–140.
- [5] ATLAS collaboration, G. Aad et al., *Observation of a new particle in the search for the Standard Model Higgs boson with the ATLAS detector at the LHC*, *Phys. Lett.* **B716** (2012) 1–29, [1207.7214].
- [6] CMS collaboration, S. Chatrchyan et al., *Observation of a new boson at a mass of 125 GeV with the CMS experiment at the LHC*, *Phys. Lett.* **B716** (2012) 30–61, [1207.7235].
- [7] Y. Amhis et al., *Averages of b-hadron, c-hadron, and τ -lepton properties as of summer 2016*, 1612.07233.
- [8] A. J. Buras, *Climbing NLO and NNLO Summits of Weak Decays*, 1102.5650.
- [9] F. Beaujean, C. Bobeth and D. van Dyk, *Comprehensive Bayesian analysis of rare (semi)leptonic and radiative B decays*, *Eur. Phys. J.* **C74** (2014) 2897, [1310.2478].
- [10] T. Blake, G. Lanfranchi and D. M. Straub, *Rare B Decays as Tests of the Standard Model*, *Prog. Part. Nucl. Phys.* **92** (2017) 50–91, [1606.00916].
- [11] S. L. Glashow, J. Iliopoulos and L. Maiani, *Weak Interactions with Lepton-Hadron Symmetry*, *Phys. Rev.* **D2** (1970) 1285–1292.
- [12] LHCb collaboration, R. Aaij et al., *Differential branching fraction and angular analysis of the decay $B^0 \rightarrow K^{*0} \mu^+ \mu^-$* , *JHEP* **08** (2013) 131, [1304.6325].

- [13] LHCb collaboration, T. L. Collaboration, *Angular analysis of the $B^0 \rightarrow K^{*0} \mu^+ \mu^-$ decay*, .
- [14] J. Matias, F. Mescia, M. Ramon and J. Virto, *Complete Anatomy of $\bar{B}_d^- \rightarrow \bar{K}^{*0} (- \rightarrow K\pi) l^+ l^-$ and its angular distribution*, *JHEP* **04** (2012) 104, [1202.4266].
- [15] S. Descotes-Genon, J. Matias, M. Ramon and J. Virto, *Implications from clean observables for the binned analysis of $B^- \rightarrow K^* \mu^+ \mu^-$ at large recoil*, *JHEP* **01** (2013) 048, [1207.2753].
- [16] S. Descotes-Genon, T. Hurth, J. Matias and J. Virto, *Optimizing the basis of $B \rightarrow K^* l l$ observables in the full kinematic range*, *JHEP* **05** (2013) 137, [1303.5794].
- [17] J. Matias and N. Serra, *Symmetry relations between angular observables in $B^0 \rightarrow K^* \mu^+ \mu^-$ and the LHCb P'_5 anomaly*, *Phys. Rev.* **D90** (2014) 034002, [1402.6855].
- [18] LHCb collaboration, R. Aaij et al., *Test of lepton universality using $B^+ \rightarrow K^+ \ell^+ \ell^-$ decays*, *Phys. Rev. Lett.* **113** (2014) 151601, [1406.6482].
- [19] LHCb collaboration, R. Aaij et al., *Test of lepton universality with $B^0 \rightarrow K^{*0} \ell^+ \ell^-$ decays*, *JHEP* **08** (2017) 055, [1705.05802].
- [20] LHCb collaboration, R. Aaij et al., *Measurement of Form-Factor-Independent Observables in the Decay $B^0 \rightarrow K^{*0} \mu^+ \mu^-$* , *Phys. Rev. Lett.* **111** (2013) 191801, [1308.1707].
- [21] LHCb collaboration, R. Aaij et al., *Angular analysis of the $B^0 \rightarrow K^{*0} \mu^+ \mu^-$ decay using 3 fb^{-1} of integrated luminosity*, *JHEP* **02** (2016) 104, [1512.04442].
- [22] BELLE collaboration, A. Abdesselam et al., *Angular analysis of $B^0 \rightarrow K^*(892)^0 \ell^+ \ell^-$* , in *Proceedings, LHCSki 2016 - A First Discussion of 13 TeV Results: Obergurgl, Austria, April 10-15, 2016*, 1604.04042.
- [23] S. Descotes-Genon, L. Hofer, J. Matias and J. Virto, *On the impact of power corrections in the prediction of $B \rightarrow K^* \mu^+ \mu^-$ observables*, *JHEP* **12** (2014) 125, [1407.8526].
- [24] S. Jäger and J. Martin Camalich, *On $B \rightarrow V \ell \ell$ at small dilepton invariant mass, power corrections, and new physics*, *JHEP* **05** (2013) 043, [1212.2263].
- [25] S. Jager and J. Martin Camalich, *Reassessing the discovery potential of the $B \rightarrow K^* \ell^+ \ell^-$ decays in the large-recoil region: SM challenges and BSM opportunities*, *Phys. Rev.* **D93** (2016) 014028, [1412.3183].
- [26] J. Lyon and R. Zwicky, *Resonances gone topsy turvy - the charm of QCD or new physics in $b \rightarrow s \ell^+ \ell^-$?*, 1406.0566.
- [27] M. Ciuchini, M. Fedele, E. Franco, S. Mishima, A. Paul, L. Silvestrini and M. Valli, *$B \rightarrow K^* \ell^+ \ell^-$ decays at large recoil in the Standard Model: a theoretical reappraisal*, *JHEP* **06** (2016) 116, [1512.07157].

- [28] T. Hurth, F. Mahmoudi and S. Neshatpour, *On the anomalies in the latest LHCb data*, *Nucl. Phys.* **B909** (2016) 737–777, [1603.00865].
- [29] J. Martin Camalich, *Hadronic uncertainties in semileptonic B decays*, *PoS BEAUTY2016* (2016) 037.
- [30] M. Ciuchini, M. Fedele, E. Franco, S. Mishima, A. Paul, L. Silvestrini and M. Valli, *$B \rightarrow K^* \ell^+ \ell^-$ in the Standard Model: Elaborations and Interpretations*, *PoS ICHEP2016* (2016) 584, [1611.04338].
- [31] B. Capdevila, S. Descotes-Genon, L. Hofer and J. Matias, *Hadronic uncertainties in $B \rightarrow K^* \mu^+ \mu^-$: a state-of-the-art analysis*, *JHEP* **04** (2017) 016, [1701.08672].
- [32] ATLAS collaboration, *Angular analysis of $B_d^0 \rightarrow K^* \mu^+ \mu^-$ decays in pp collisions at $\sqrt{s} = 8$ TeV with the ATLAS detector*, *ATLAS-CONF-2017-023* (2017) .
- [33] CMS collaboration, *Measurement of the P_1 and P'_5 angular parameters of the decay $B^0 \rightarrow K^{*0} \mu^+ \mu^-$ in proton-proton collisions at $\sqrt{s} = 8$ TeV*, *CMS-PAS-BPH-15-008* (2017) .
- [34] G. Hiller and F. Kruger, *More model-independent analysis of $b \rightarrow s$ processes*, *Phys. Rev.* **D69** (2004) 074020, [hep-ph/0310219].
- [35] M. Bordone, G. Isidori and A. Pattori, *On the Standard Model predictions for R_K and R_{K^*}* , *Eur. Phys. J.* **C76** (2016) 440, [1605.07633].
- [36] LHCb collaboration, R. Aaij et al., *Differential branching fractions and isospin asymmetries of $B \rightarrow K^{(*)} \mu^+ \mu^-$ decays*, *JHEP* **06** (2014) 133, [1403.8044].
- [37] LHCb collaboration, R. Aaij et al., *Measurement of the phase difference between short- and long-distance amplitudes in the $B^+ \rightarrow K^+ \mu^+ \mu^-$ decay*, *Eur. Phys. J.* **C77** (2017) 161, [1612.06764].
- [38] LHCb collaboration, R. Aaij et al., *Angular analysis and differential branching fraction of the decay $B_s^0 \rightarrow \phi \mu^+ \mu^-$* , *JHEP* **09** (2015) 179, [1506.08777].
- [39] A. Khodjamirian, T. Mannel and Y. M. Wang, *$B \rightarrow K \ell^+ \ell^-$ decay at large hadronic recoil*, *JHEP* **02** (2013) 010, [1211.0234].
- [40] T. Hurth and F. Mahmoudi, *On the LHCb anomaly in $B \rightarrow K^* \ell^+ \ell^-$* , *JHEP* **04** (2014) 097, [1312.5267].
- [41] W. Altmannshofer and D. M. Straub, *New physics in $b \rightarrow s$ transitions after LHC run 1*, *Eur. Phys. J.* **C75** (2015) 382, [1411.3161].
- [42] S. Descotes-Genon, L. Hofer, J. Matias and J. Virto, *Global analysis of $b \rightarrow s \ell \ell$ anomalies*, *JHEP* **06** (2016) 092, [1510.04239].

- [43] V. G. Chobanova, T. Hurth, F. Mahmoudi, D. Martinez Santos and S. Neshatpour, *Large hadronic power corrections or new physics in the rare decay $B \rightarrow K^* \mu^+ \mu^-$?*, *JHEP* **07** (2017) 025, [[1702.02234](#)].
- [44] W. Altmannshofer, C. Niehoff, P. Stangl and D. M. Straub, *Status of the $B \rightarrow K^* \mu^+ \mu^-$ anomaly after Moriond 2017*, *Eur. Phys. J.* **C77** (2017) 377, [[1703.09189](#)].
- [45] B. Capdevila, S. Descotes-Genon, J. Matias and J. Virto, *Assessing lepton-flavour non-universality from $B \rightarrow K^* \ell \ell$ angular analyses*, *JHEP* **10** (2016) 075, [[1605.03156](#)].
- [46] N. Serra, R. Silva Coutinho and D. van Dyk, *Measuring the breaking of lepton flavor universality in $B \rightarrow K^* \ell^+ \ell^-$* , *Phys. Rev.* **D95** (2017) 035029, [[1610.08761](#)].
- [47] BELLE collaboration, S. Wehle et al., *Lepton-Flavor-Dependent Angular Analysis of $B \rightarrow K^* \ell^+ \ell^-$* , *Phys. Rev. Lett.* **118** (2017) 111801, [[1612.05014](#)].
- [48] HEPFIT collaboration, *HEPfit: a Code for the Combination of Indirect and Direct Constraints on High Energy Physics Models*, <http://hepfit.roma1.infn.it/>.
- [49] T. D. Lee, *A Theory of Spontaneous T Violation*, *Phys. Rev.* **D8** (1973) 1226–1239.
- [50] G. C. Branco, P. M. Ferreira, L. Lavoura, M. N. Rebelo, M. Sher and J. P. Silva, *Theory and phenomenology of two-Higgs-doublet models*, *Phys. Rept.* **516** (2012) 1–102, [[1106.0034](#)].
- [51] M. Gell-Mann, *The interpretation of the new particles as displaced charge multiplets*, *Nuovo Cim.* **4** (1956) 848–866.
- [52] G. Degrandi, S. Di Vita, J. Elias-Miro, J. R. Espinosa, G. F. Giudice, G. Isidori and A. Strumia, *Higgs mass and vacuum stability in the Standard Model at NNLO*, *JHEP* **08** (2012) 098, [[1205.6497](#)].
- [53] D. Buttazzo, G. Degrandi, P. P. Giardino, G. F. Giudice, F. Sala, A. Salvio and A. Strumia, *Investigating the near-criticality of the Higgs boson*, *JHEP* **12** (2013) 089, [[1307.3536](#)].
- [54] J. E. Camargo-Molina, B. O’Leary, W. Porod and F. Staub, *Stability of the CMSSM against sfermion VEVs*, *JHEP* **12** (2013) 103, [[1309.7212](#)].
- [55] J. E. Camargo-Molina, B. Garbrecht, B. O’Leary, W. Porod and F. Staub, *Constraining the Natural MSSM through tunneling to color-breaking vacua at zero and non-zero temperature*, *Phys. Lett.* **B737** (2014) 156–161, [[1405.7376](#)].
- [56] U. Chattopadhyay and A. Dey, *Exploring MSSM for Charge and Color Breaking and Other Constraints in the Context of Higgs@125 GeV*, *JHEP* **11** (2014) 161, [[1409.0611](#)].
- [57] W. G. Hollik, *A new view on vacuum stability in the MSSM*, *JHEP* **08** (2016) 126, [[1606.08356](#)].
- [58] J. Beuria, U. Chattopadhyay, A. Datta and A. Dey, *Exploring viable vacua of the Z_3 -symmetric NMSSM*, *JHEP* **04** (2017) 024, [[1612.06803](#)].

- [59] M. E. Krauss, T. Opferkuch and F. Staub, *Spontaneous Charge Breaking in the NMSSM - Dangerous or not?*, *Eur. Phys. J.* **C77** (2017) 331, [1703.05329].
- [60] P. M. Ferreira and B. Swiezevska, *One-loop contributions to neutral minima in the inert doublet model*, *JHEP* **04** (2016) 099, [1511.02879].
- [61] B. Swiezevska, *Inert scalars and vacuum metastability around the electroweak scale*, *JHEP* **07** (2015) 118, [1503.07078].
- [62] F. Staub, *Reopen parameter regions in Two-Higgs Doublet Models*, 1705.03677.
- [63] G. 't Hooft, *Renormalization of Massless Yang-Mills Fields*, *Nucl. Phys.* **B33** (1971) 173–199.
- [64] G. 't Hooft, *Renormalizable Lagrangians for Massive Yang-Mills Fields*, *Nucl. Phys.* **B35** (1971) 167–188.
- [65] S. Weinberg, *A Model of Leptons*, *Phys. Rev. Lett.* **19** (1967) 1264–1266.
- [66] M. D. Schwartz, *Quantum Field Theory and the Standard Model*. Cambridge University Press, New York (NY), USA, 2014.
- [67] F. Englert and R. Brout, *Broken Symmetry and the Mass of Gauge Vector Mesons*, *Phys. Rev. Lett.* **13** (1964) 321–323.
- [68] P. W. Higgs, *Broken Symmetries and the Masses of Gauge Bosons*, *Phys. Rev. Lett.* **13** (1964) 508–509.
- [69] G. S. Guralnik, C. R. Hagen and T. W. B. Kibble, *Global Conservation Laws and Massless Particles*, *Phys. Rev. Lett.* **13** (1964) 585–587.
- [70] P. W. Higgs, *Spontaneous Symmetry Breakdown without Massless Bosons*, *Phys. Rev.* **145** (1966) 1156–1163.
- [71] J. Goldstone, *Field Theories with Superconductor Solutions*, *Nuovo Cim.* **19** (1961) 154–164.
- [72] J. Goldstone, A. Salam and S. Weinberg, *Broken Symmetries*, *Phys. Rev.* **127** (1962) 965–970.
- [73] R. P. Feynman and M. Gell-Mann, *Theory of Fermi interaction*, *Phys. Rev.* **109** (1958) 193–198.
- [74] E. C. G. Sudarshan and R. E. Marshak, *Chirality invariance and the universal Fermi interaction*, *Phys. Rev.* **109** (1958) 1860–1860.
- [75] C. Giunti and C. W. Kim, *Fundamentals of Neutrino Physics and Astrophysics*. Oxford University Press, Oxford, U.K., 2007.
- [76] G. Altarelli and F. Feruglio, *Discrete Flavor Symmetries and Models of Neutrino Mixing*, *Rev. Mod. Phys.* **82** (2010) 2701–2729, [1002.0211].
- [77] G. C. Branco, R. G. Felipe and F. R. Joaquim, *Leptonic CP Violation*, *Rev. Mod. Phys.* **84** (2012) 515–565, [1111.5332].

- [78] N. Cabibbo, *Unitary Symmetry and Leptonic Decays*, *Phys. Rev. Lett.* **10** (1963) 531–533.
- [79] M. Kobayashi and T. Maskawa, *CP Violation in the Renormalizable Theory of Weak Interaction*, *Prog. Theor. Phys.* **49** (1973) 652–657.
- [80] PARTICLE DATA GROUP collaboration, C. Patrignani et al., *Review of Particle Physics*, *Chin. Phys.* **C40** (2016) 100001.
- [81] L. Wolfenstein, *Parametrization of the Kobayashi-Maskawa Matrix*, *Phys. Rev. Lett.* **51** (1983) 1945.
- [82] G. C. Branco, L. Lavoura and J. P. Silva, *CP Violation*, in *Int. Ser. Monogr. Phys.*, vol. 103. Oxford University Press, Oxford, U.K., 1999.
- [83] C. Jarlskog, *Commutator of the Quark Mass Matrices in the Standard Electroweak Model and a Measure of Maximal CP Violation*, *Phys. Rev. Lett.* **55** (1985) 1039.
- [84] UTFIT collaboration, online update at <http://www.utfit.org/UTfit/>.
- [85] G. Buchalla, A. J. Buras and M. E. Lautenbacher, *Weak decays beyond leading logarithms*, *Rev. Mod. Phys.* **68** (1996) 1125–1144, [[hep-ph/9512380](https://arxiv.org/abs/hep-ph/9512380)].
- [86] A. J. Buras, *Weak Hamiltonian, CP violation and rare decays*, in *Probing the standard model of particle interactions. Proceedings, Summer School in Theoretical Physics, NATO Advanced Study Institute, 68th session, Les Houches, France, July 28-September 5, 1997. Pt. 1, 2*, pp. 281–539, 1998, [hep-ph/9806471](https://arxiv.org/abs/hep-ph/9806471).
- [87] K. G. Wilson, *Nonlagrangian models of current algebra*, *Phys. Rev.* **179** (1969) 1499–1512.
- [88] W. Zimmermann, *Composite operators in the perturbation theory of renormalizable interactions*, *Annals Phys.* **77** (1973) 536–569.
- [89] K. G. Wilson and W. Zimmermann, *Operator product expansions and composite field operators in the general framework of quantum field theory*, *Commun. Math. Phys.* **24** (1972) 87–106.
- [90] G. 't Hooft and M. J. G. Veltman, *Regularization and Renormalization of Gauge Fields*, *Nucl. Phys.* **B44** (1972) 189–213.
- [91] P. Breitenlohner and D. Maison, *Dimensional Renormalization and the Action Principle*, *Commun. Math. Phys.* **52** (1977) 11–38.
- [92] W. A. Bardeen, A. J. Buras, D. W. Duke and T. Muta, *Deep Inelastic Scattering Beyond the Leading Order in Asymptotically Free Gauge Theories*, *Phys. Rev.* **D18** (1978) 3998.
- [93] A. J. Buras and P. H. Weisz, *QCD Nonleading Corrections to Weak Decays in Dimensional Regularization and 't Hooft-Veltman Schemes*, *Nucl. Phys.* **B333** (1990) 66–99.
- [94] M. J. Dugan and B. Grinstein, *On the vanishing of evanescent operators*, *Phys. Lett.* **B256** (1991) 239–244.

- [95] S. Herrlich and U. Nierste, *Evanescent operators, scheme dependences and double insertions*, *Nucl. Phys.* **B455** (1995) 39–58, [[hep-ph/9412375](#)].
- [96] E. Witten, *Short Distance Analysis of Weak Interactions*, *Nucl. Phys.* **B122** (1977) 109–143.
- [97] L. P. Kadanoff, *Scaling laws for Ising models near $T(c)$* , *Physics* **2** (1966) 263–272.
- [98] K. G. Wilson, *Renormalization group and critical phenomena. 1. Renormalization group and the Kadanoff scaling picture*, *Phys. Rev.* **B4** (1971) 3174–3183.
- [99] T. van Ritbergen, J. A. M. Vermaseren and S. A. Larin, *The Four loop beta function in quantum chromodynamics*, *Phys. Lett.* **B400** (1997) 379–384, [[hep-ph/9701390](#)].
- [100] M. Czakon, *The Four-loop QCD beta-function and anomalous dimensions*, *Nucl. Phys.* **B710** (2005) 485–498, [[hep-ph/0411261](#)].
- [101] M. Antonelli et al., *Flavor Physics in the Quark Sector*, *Phys. Rept.* **494** (2010) 197–414, [[0907.5386](#)].
- [102] T. Hurth and M. Nakao, *Radiative and Electroweak Penguin Decays of B Mesons*, *Ann. Rev. Nucl. Part. Sci.* **60** (2010) 645–677, [[1005.1224](#)].
- [103] K. G. Chetyrkin, M. Misiak and M. Munz, *Weak radiative B meson decay beyond leading logarithms*, *Phys. Lett.* **B400** (1997) 206–219, [[hep-ph/9612313](#)].
- [104] K. G. Chetyrkin, M. Misiak and M. Munz, $|\Delta F| = 1$ *nonleptonic effective Hamiltonian in a simpler scheme*, *Nucl. Phys.* **B520** (1998) 279–297, [[hep-ph/9711280](#)].
- [105] G. Buchalla, A. J. Buras and M. K. Harlander, *The Anatomy of Epsilon-prime / Epsilon in the Standard Model*, *Nucl. Phys.* **B337** (1990) 313–362.
- [106] C. Bobeth, P. Gambino, M. Gorbahn and U. Haisch, *Complete NNLO QCD analysis of anti-B $\rightarrow X(s) l^+ l^-$ and higher order electroweak effects*, *JHEP* **04** (2004) 071, [[hep-ph/0312090](#)].
- [107] T. Inami and C. S. Lim, *Effects of Superheavy Quarks and Leptons in Low-Energy Weak Processes $k(L) \rightarrow \mu \text{ anti-}\mu$, $K^+ \rightarrow \pi^+$ Neutrino anti-neutrino and $K^0 \leftrightarrow \text{anti-}K^0$* , *Prog. Theor. Phys.* **65** (1981) 297.
- [108] C. Bobeth, M. Misiak and J. Urban, *Photonic penguins at two loops and m_t dependence of $BR[B \rightarrow X_s l^+ l^-]$* , *Nucl. Phys.* **B574** (2000) 291–330, [[hep-ph/9910220](#)].
- [109] T. Huber, E. Lunghi, M. Misiak and D. Wyler, *Electromagnetic logarithms in $\bar{B} \rightarrow X_s l^+ l^-$* , *Nucl. Phys.* **B740** (2006) 105–137, [[hep-ph/0512066](#)].
- [110] P. Gambino and U. Haisch, *Complete electroweak matching for radiative B decays*, *JHEP* **10** (2001) 020, [[hep-ph/0109058](#)].
- [111] A. J. Buras, P. Gambino and U. A. Haisch, *Electroweak penguin contributions to nonleptonic $\Delta F = 1$ decays at NNLO*, *Nucl. Phys.* **B570** (2000) 117–154, [[hep-ph/9911250](#)].

- [112] A. J. Buras, M. Misiak, M. Munz and S. Pokorski, *Theoretical uncertainties and phenomenological aspects of $B \rightarrow X(s)$ gamma decay*, *Nucl. Phys.* **B424** (1994) 374–398, [[hep-ph/9311345](#)].
- [113] M. Misiak, *QCD corrected effective Hamiltonian for the $b \rightarrow s$ gamma decay*, *Phys. Lett.* **B269** (1991) 161–168.
- [114] M. Ciuchini, E. Franco, G. Martinelli, L. Reina and L. Silvestrini, *Scheme independence of the effective Hamiltonian for $b \rightarrow s$ gamma and $b \rightarrow s g$ decays*, *Phys. Lett.* **B316** (1993) 127–136, [[hep-ph/9307364](#)].
- [115] M. Misiak and M. Steinhauser, *Three loop matching of the dipole operators for $b \rightarrow s\gamma$ and $b \rightarrow sg$* , *Nucl. Phys.* **B683** (2004) 277–305, [[hep-ph/0401041](#)].
- [116] G. Buchalla and A. J. Buras, *Two loop large m_t electroweak corrections to $K \rightarrow \pi\nu\bar{\nu}$ for arbitrary Higgs boson mass*, *Phys. Rev.* **D57** (1998) 216–223, [[hep-ph/9707243](#)].
- [117] C. Bobeth, M. Gorbahn and E. Stamou, *Electroweak Corrections to $B_{s,d} \rightarrow \ell^+\ell^-$* , *Phys. Rev.* **D89** (2014) 034023, [[1311.1348](#)].
- [118] A. J. Buras, M. Jamin and M. E. Lautenbacher, *Two loop anomalous dimension matrix for Delta $S = 1$ weak nonleptonic decays. 2. $O(\alpha_s)$* , *Nucl. Phys.* **B400** (1993) 75–102, [[hep-ph/9211321](#)].
- [119] A. J. Buras, M. Jamin, M. E. Lautenbacher and P. H. Weisz, *Two loop anomalous dimension matrix for $\Delta S = 1$ weak nonleptonic decays I: $O(\alpha_s^2)$* , *Nucl. Phys.* **B400** (1993) 37–74, [[hep-ph/9211304](#)].
- [120] M. Ciuchini, E. Franco, G. Martinelli and L. Reina, *The Delta $S = 1$ effective Hamiltonian including next-to-leading order QCD and QED corrections*, *Nucl. Phys.* **B415** (1994) 403–462, [[hep-ph/9304257](#)].
- [121] M. Gorbahn and U. Haisch, *Effective Hamiltonian for non-leptonic $|\Delta F| = 1$ decays at NNLO in QCD*, *Nucl. Phys.* **B713** (2005) 291–332, [[hep-ph/0411071](#)].
- [122] M. Czakon, U. Haisch and M. Misiak, *Four-Loop Anomalous Dimensions for Radiative Flavour-Changing Decays*, *JHEP* **03** (2007) 008, [[hep-ph/0612329](#)].
- [123] K. Baranowski and M. Misiak, *The $O(\alpha_s)$ correction to $BR[B \rightarrow X(s)\gamma]$* , *Phys. Lett.* **B483** (2000) 410–416, [[hep-ph/9907427](#)].
- [124] M. Gorbahn, U. Haisch and M. Misiak, *Three-loop mixing of dipole operators*, *Phys. Rev. Lett.* **95** (2005) 102004, [[hep-ph/0504194](#)].
- [125] BELLE collaboration, T. Saito et al., *Measurement of the $\bar{B} \rightarrow X_s\gamma$ Branching Fraction with a Sum of Exclusive Decays*, *Phys. Rev.* **D91** (2015) 052004, [[1411.7198](#)].

- [126] BELLE collaboration, A. Abdesselam et al., *Measurement of the inclusive $B \rightarrow X_{s+d}\gamma$ branching fraction, photon energy spectrum and HQE parameters*, in *Proceedings, 38th International Conference on High Energy Physics (ICHEP 2016): Chicago, IL, USA, August 3-10, 2016*, 1608.02344.
- [127] BABAR collaboration, J. P. Lees et al., *Precision Measurement of the $B \rightarrow X_s\gamma$ Photon Energy Spectrum, Branching Fraction, and Direct CP Asymmetry $A_{CP}(B \rightarrow X_{s+d}\gamma)$* , *Phys. Rev. Lett.* **109** (2012) 191801, [1207.2690].
- [128] LHCb collaboration, R. Aaij et al., *Differential branching fraction and angular analysis of $\Lambda_b^0 \rightarrow \Lambda\mu^+\mu^-$ decays*, *JHEP* **06** (2015) 115, [1503.07138].
- [129] F. Kruger and J. Matias, *Probing new physics via the transverse amplitudes of $B^0 \rightarrow K^{*0}(\rightarrow K^-\pi^+)l^+l^-$ at large recoil*, *Phys. Rev.* **D71** (2005) 094009, [hep-ph/0502060].
- [130] W. Altmannshofer, P. Ball, A. Bharucha, A. J. Buras, D. M. Straub and M. Wick, *Symmetries and Asymmetries of $B \rightarrow K^*\mu^+\mu^-$ Decays in the Standard Model and Beyond*, *JHEP* **01** (2009) 019, [0811.1214].
- [131] S. Descotes-Genon, J. Matias and J. Virto, *Understanding the $B \rightarrow K^*\mu^+\mu^-$ Anomaly*, *Phys. Rev.* **D88** (2013) 074002, [1307.5683].
- [132] C. Bobeth, M. Gorbahn, T. Hermann, M. Misiak, E. Stamou and M. Steinhauser, *$B_{s,d} \rightarrow l^+l^-$ in the Standard Model with Reduced Theoretical Uncertainty*, *Phys. Rev. Lett.* **112** (2014) 101801, [1311.0903].
- [133] M. Misiak et al., *Updated NNLO QCD predictions for the weak radiative B-meson decays*, *Phys. Rev. Lett.* **114** (2015) 221801, [1503.01789].
- [134] P. Ball and R. Zwicky, *$B_{d,s} \rightarrow \rho, \omega, K^*, \phi$ decay form-factors from light-cone sum rules revisited*, *Phys. Rev.* **D71** (2005) 014029, [hep-ph/0412079].
- [135] P. Ball and R. Zwicky, *New results on $B \rightarrow \pi, K, \eta$ decay formfactors from light-cone sum rules*, *Phys. Rev.* **D71** (2005) 014015, [hep-ph/0406232].
- [136] G. D'Agostini, *Bayesian reasoning in high-energy physics: Principles and applications*, in *CERN Yellow Reports: Monographs*. CERN-99-03, CERN-YELLOW-99-03, Geneva, Switzerland, 1999.
- [137] A. Caldwell, D. Kollar and K. Kroninger, *BAT: The Bayesian Analysis Toolkit*, *Comput. Phys. Commun.* **180** (2009) 2197–2209, [0808.2552].
- [138] N. Metropolis, A. W. Rosenbluth, M. N. Rosenbluth, A. H. Teller and E. Teller, *Equation of state calculations by fast computing machines*, *J. Chem. Phys.* **21** (1953) 1087–1092.
- [139] A. Gelman and D. B. Rubin, *Inference from Iterative Simulation Using Multiple Sequences*, *Statist. Sci.* **7** (1992) 457–472.

- [140] T. Ando, *Predictive bayesian model selection, American Journal of Mathematical and Management Sciences* **31** (2011) 13–38.
- [141] A. Gelman, J. B. Carlin, H. S. Stern and D. B. Rubin, *Bayesian data analysis, in Texts in Statistical Science Series*. Chapman & Hall / CRC, Boca Raton (FL), USA, 2004.
- [142] M. Ciuchini, A. M. Coutinho, M. Fedele, E. Franco, A. Paul, L. Silvestrini and M. Valli, *in preparation* .
- [143] M. Ciuchini, A. M. Coutinho, M. Fedele, E. Franco, A. Paul, L. Silvestrini and M. Valli, *On Flavourful Easter eggs for New Physics hunger and Lepton Flavour Universality violation, Eur. Phys. J.* **C77** (2017) 688, [1704.05447].
- [144] J. Aebischer, A. Crivellin, M. Fael and C. Greub, *Matching of gauge invariant dimension-six operators for $b \rightarrow s$ and $b \rightarrow c$ transitions, JHEP* **05** (2016) 037, [1512.02830].
- [145] M. Ciuchini, M. Fedele, E. Franco, S. Mishima, A. Paul, L. Silvestrini and M. Valli, *Knowns and Unknowns in the Predictions for $B \rightarrow K^* \mu^+ \mu^-$, Nucl. Part. Phys. Proc.* **285-286** (2017) 45–49.
- [146] A. Khodjamirian, T. Mannel, A. A. Pivovarov and Y. M. Wang, *Charm-loop effect in $B \rightarrow K^{(*)} \ell^+ \ell^-$ and $B \rightarrow K^* \gamma$, JHEP* **09** (2010) 089, [1006.4945].
- [147] M. Beneke, T. Feldmann and D. Seidel, *Systematic approach to exclusive $B \rightarrow V l^+ l^-$, $V \gamma$ decays, Nucl. Phys.* **B612** (2001) 25–58, [hep-ph/0106067].
- [148] A. L. Kagan and M. Neubert, *Isospin breaking in $B \rightarrow K^* \gamma$ decays, Phys. Lett.* **B539** (2002) 227–234, [hep-ph/0110078].
- [149] T. Feldmann and J. Matias, *Forward backward and isospin asymmetry for $B \rightarrow K^* l^+ l^-$ decay in the standard model and in supersymmetry, JHEP* **01** (2003) 074, [hep-ph/0212158].
- [150] M. Beneke, T. Feldmann and D. Seidel, *Exclusive radiative and electroweak $b \rightarrow d$ and $b \rightarrow s$ penguin decays at NLO, Eur. Phys. J.* **C41** (2005) 173–188, [hep-ph/0412400].
- [151] P. Ball, G. W. Jones and R. Zwicky, *$B \rightarrow V \gamma$ beyond QCD factorisation, Phys. Rev.* **D75** (2007) 054004, [hep-ph/0612081].
- [152] M. Dimou, J. Lyon and R. Zwicky, *Exclusive Chromomagnetism in heavy-to-light FCNCs, Phys. Rev.* **D87** (2013) 074008, [1212.2242].
- [153] J. Lyon and R. Zwicky, *Isospin asymmetries in $B \rightarrow (K^*, \rho) \gamma / l^+ l^-$ and $B \rightarrow K l^+ l^-$ in and beyond the standard model, Phys. Rev.* **D88** (2013) 094004, [1305.4797].
- [154] A. Paul and D. M. Straub, *Constraints on new physics from radiative B decays, JHEP* **04** (2017) 027, [1608.02556].
- [155] B. Grinstein and D. Pirjol, *Exclusive rare $B \rightarrow K^* \ell^+ \ell^-$ decays at low recoil: Controlling the long-distance effects, Phys. Rev.* **D70** (2004) 114005, [hep-ph/0404250].

- [156] C. Bobeth, G. Hiller and D. van Dyk, *The Benefits of $\bar{B}^- \rightarrow \bar{K}^* l^+ l^-$ Decays at Low Recoil*, *JHEP* **07** (2010) 098, [1006.5013].
- [157] M. Beylich, G. Buchalla and T. Feldmann, *Theory of $B \rightarrow K^{(*)} l^+ l^-$ decays at high q^2 : OPE and quark-hadron duality*, *Eur. Phys. J.* **C71** (2011) 1635, [1101.5118].
- [158] C. Bobeth, G. Hiller and D. van Dyk, *More Benefits of Semileptonic Rare B Decays at Low Recoil: CP Violation*, *JHEP* **07** (2011) 067, [1105.0376].
- [159] CMS collaboration, V. Khachatryan et al., *Angular analysis of the decay $B^0 \rightarrow K^{*0} \mu^+ \mu^-$ from pp collisions at $\sqrt{s} = 8$ TeV*, *Phys. Lett.* **B753** (2016) 424–448, [1507.08126].
- [160] LHCb collaboration, R. Aaij et al., *Measurements of the S-wave fraction in $B^0 \rightarrow K^+ \pi^- \mu^+ \mu^-$ decays and the $B^0 \rightarrow K^*(892)^0 \mu^+ \mu^-$ differential branching fraction*, *JHEP* **11** (2016) 047, [1606.04731].
- [161] LHCb collaboration, R. Aaij et al., *Angular analysis of the $B^0 \rightarrow K^{*0} e^+ e^-$ decay in the low- q^2 region*, *JHEP* **04** (2015) 064, [1501.03038].
- [162] J. A. Bailey et al., *$B \rightarrow Kl^{+l^-}$ decay form factors from three-flavor lattice QCD*, *Phys. Rev.* **D93** (2016) 025026, [1509.06235].
- [163] A. Bharucha, D. M. Straub and R. Zwicky, *$B \rightarrow V l^+ l^-$ in the Standard Model from light-cone sum rules*, *JHEP* **08** (2016) 098, [1503.05534].
- [164] LHCb collaboration, R. Aaij et al., *Measurement of the ratio of branching fractions $BR(B_0 \rightarrow K^{*0} \gamma)/BR(B_{s0} \rightarrow \phi \gamma)$ and the direct CP asymmetry in $B_0 \rightarrow K^{*0} \gamma$* , *Nucl. Phys.* **B867** (2013) 1–18, [1209.0313].
- [165] LHCb collaboration, R. Aaij et al., *Measurement of the $B_s^0 \rightarrow \mu^+ \mu^-$ branching fraction and effective lifetime and search for $B^0 \rightarrow \mu^+ \mu^-$ decays*, *Phys. Rev. Lett.* **118** (2017) 191801, [1703.05747].
- [166] CMS collaboration, S. Chatrchyan et al., *Measurement of the $B(s)$ to $mu^+ mu^-$ branching fraction and search for $B0$ to $mu^+ mu^-$ with the CMS Experiment*, *Phys. Rev. Lett.* **111** (2013) 101804, [1307.5025].
- [167] PARTICLE DATA GROUP collaboration, K. A. Olive et al., *Review of Particle Physics*, *Chin. Phys.* **C38** (2014) 090001.
- [168] J. de Blas, M. Ciuchini, E. Franco, S. Mishima, M. Pierini, L. Reina and L. Silvestrini, *Electroweak precision observables and Higgs-boson signal strengths in the Standard Model and beyond: present and future*, *JHEP* **12** (2016) 135, [1608.01509].
- [169] ATLAS, CDF, CMS, D0 collaboration, *First combination of Tevatron and LHC measurements of the top-quark mass*, 1403.4427.

- [170] V. Lubicz. private communication.
- [171] F. Sanfilippo, *Quark Masses from Lattice QCD*, *PoS LATTICE2014* (2015) 014, [1505.02794].
- [172] S. Aoki et al., *Review of lattice results concerning low-energy particle physics*, *Eur. Phys. J.* **C74** (2014) 2890, [1310.8555].
- [173] UTFIT collaboration, M. Bona et al., *The Unitarity Triangle Fit in the Standard Model and Hadronic Parameters from Lattice QCD: A Reappraisal after the Measurements of Delta $m(s)$ and $BR(B \rightarrow \tau \nu(\tau))$* , *JHEP* **10** (2006) 081, [hep-ph/0606167].
- [174] S. W. Bosch and G. Buchalla, *The Radiative decays $B \rightarrow V\gamma$ at next-to-leading order in QCD*, *Nucl. Phys.* **B621** (2002) 459–478, [hep-ph/0106081].
- [175] P. Ball and R. Zwicky, *$SU(3)$ breaking of leading-twist K and K^* distribution amplitudes: A Reprise*, *Phys. Lett.* **B633** (2006) 289–297, [hep-ph/0510338].
- [176] P. Ball and R. Zwicky, *$|V_{td}/V_{ts}|$ from $B \rightarrow V\gamma$* , *JHEP* **04** (2006) 046, [hep-ph/0603232].
- [177] P. Ball and G. W. Jones, *Twist-3 distribution amplitudes of K^* and ϕ mesons*, *JHEP* **03** (2007) 069, [hep-ph/0702100].
- [178] L. Lavoura and J. P. Silva, *Fundamental CP violating quantities in a $SU(2) \times U(1)$ model with many Higgs doublets*, *Phys. Rev.* **D50** (1994) 4619–4624, [hep-ph/9404276].
- [179] L. T. Magalhães, *Álgebra Linear como Introdução a Matemática Aplicada*. Texto Editores, Lisbon, Portugal, 1989.
- [180] S. Kanemura and K. Yagyu, *Unitarity bound in the most general two Higgs doublet model*, *Phys. Lett.* **B751** (2015) 289–296, [1509.06060].
- [181] A. Pich and P. Tuzon, *Yukawa Alignment in the Two-Higgs-Doublet Model*, *Phys. Rev.* **D80** (2009) 091702, [0908.1554].
- [182] P. M. Ferreira, L. Lavoura and J. P. Silva, *Renormalization-group constraints on Yukawa alignment in multi-Higgs-doublet models*, *Phys. Lett.* **B688** (2010) 341–344, [1001.2561].
- [183] H. Serodio, *Yukawa Alignment in a Multi Higgs Doublet Model: An effective approach*, *Phys. Lett.* **B700** (2011) 133–138, [1104.2545].
- [184] I. de Medeiros Varzielas, *Family symmetries and alignment in multi-Higgs doublet models*, *Phys. Lett.* **B701** (2011) 597–600, [1104.2601].
- [185] F. J. Botella, G. C. Branco, A. M. Coutinho, M. N. Rebelo and J. I. Silva-Marcos, *Natural Quasi-Alignment with two Higgs Doublets and RGE Stability*, *Eur. Phys. J.* **C75** (2015) 286, [1501.07435].
- [186] A. J. Buras, M. V. Carlucci, S. Gori and G. Isidori, *Higgs-mediated FCNCs: Natural Flavour Conservation vs. Minimal Flavour Violation*, *JHEP* **10** (2010) 009, [1005.5310].

- [187] C. B. Braeuninger, A. Ibarra and C. Simonetto, *Radiatively induced flavour violation in the general two-Higgs doublet model with Yukawa alignment*, *Phys. Lett.* **B692** (2010) 189–195, [1005.5706].
- [188] M. Jung, A. Pich and P. Tuzon, *Charged-Higgs phenomenology in the Aligned two-Higgs-doublet model*, *JHEP* **11** (2010) 003, [1006.0470].
- [189] S. L. Glashow and S. Weinberg, *Natural Conservation Laws for Neutral Currents*, *Phys. Rev.* **D15** (1977) 1958.
- [190] E. A. Paschos, *Diagonal Neutral Currents*, *Phys. Rev.* **D15** (1977) 1966.
- [191] M. Aoki, S. Kanemura, K. Tsumura and K. Yagyu, *Models of Yukawa interaction in the two Higgs doublet model, and their collider phenomenology*, *Phys. Rev.* **D80** (2009) 015017, [0902.4665].
- [192] A. Djouadi, *The Anatomy of electro-weak symmetry breaking. II. The Higgs bosons in the minimal supersymmetric model*, *Phys. Rept.* **459** (2008) 1–241, [hep-ph/0503173].
- [193] W. Greiner, L. Neise and H. Stöcker, *Thermodynamics and Statistical Mechanics*. Springer-Verlag, New York (NY), USA, 1995.
- [194] M. E. Peskin and D. V. Schroeder, *An Introduction to Quantum Field Theory*. Addison-Wesley, Boulder (CO), USA, 1995.
- [195] S. R. Coleman and E. J. Weinberg, *Radiative Corrections as the Origin of Spontaneous Symmetry Breaking*, *Phys. Rev.* **D7** (1973) 1888–1910.
- [196] J. Velhinho, R. Santos and A. Barroso, *Tree level vacuum stability in two Higgs doublet models*, *Phys. Lett.* **B322** (1994) 213–218.
- [197] F. Nagel, *New aspects of gauge-boson couplings and the Higgs sector*, Ph.D. thesis, Heidelberg U., 2004.
- [198] M. Maniatis, A. von Manteuffel, O. Nachtmann and F. Nagel, *Stability and symmetry breaking in the general two-Higgs-doublet model*, *Eur. Phys. J.* **C48** (2006) 805–823, [hep-ph/0605184].
- [199] I. P. Ivanov, *Minkowski space structure of the Higgs potential in 2HDM*, *Phys. Rev.* **D75** (2007) 035001, [hep-ph/0609018].
- [200] I. P. Ivanov, *Minkowski space structure of the Higgs potential in 2HDM. II. Minima, symmetries, and topology*, *Phys. Rev.* **D77** (2008) 015017, [0710.3490].
- [201] A. Barroso, P. M. Ferreira, I. P. Ivanov and R. Santos, *Metastability bounds on the two Higgs doublet model*, *JHEP* **06** (2013) 045, [1303.5098].
- [202] P. M. Ferreira, R. Santos and A. Barroso, *Stability of the tree-level vacuum in two Higgs doublet models against charge or CP spontaneous violation*, *Phys. Lett.* **B603** (2004) 219–229, [hep-ph/0406231].

- [203] A. Barroso, P. M. Ferreira and R. Santos, *Charge and CP symmetry breaking in two Higgs doublet models*, *Phys. Lett.* **B632** (2006) 684–687, [[hep-ph/0507224](#)].
- [204] S. Coleman, *Aspects of Symmetry: Selected Erice Lectures*. Cambridge University Press, Cambridge, U.K., 1985.
- [205] T. L. Lee, T. Y. Li and C. H. Tsai, *HOM4PS-2.0: a software package for solving polynomial systems by the polyhedral homotopy continuation method*, *Computing* **83** (2008) 109–133.
- [206] D. J. Bates, J. D. Hauenstein, A. J. Sommese and C. W. Wampler, *Bertini: Software for Numerical Algebraic Geometry*. Available at bertini.nd.edu with permanent doi: dx.doi.org/10.7274/R0H41PB5.
- [207] F. James and M. Roos, *Minuit: A System for Function Minimization and Analysis of the Parameter Errors and Correlations*, *Comput. Phys. Commun.* **10** (1975) 343–367.
- [208] J. E. Camargo-Molina, B. O’Leary, W. Porod and F. Staub, **Vevacious: A Tool For Finding The Global Minima Of One-Loop Effective Potentials With Many Scalars**, *Eur. Phys. J.* **C73** (2013) 2588, [[1307.1477](#)].
- [209] A. Barroso, P. M. Ferreira, I. P. Ivanov, R. Santos and J. P. Silva, *Evading death by vacuum*, *Eur. Phys. J.* **C73** (2013) 2537, [[1211.6119](#)].
- [210] S. R. Coleman, *The Fate of the False Vacuum. 1. Semiclassical Theory*, *Phys. Rev.* **D15** (1977) 2929–2936.
- [211] C. G. Callan, Jr. and S. R. Coleman, *The Fate of the False Vacuum. 2. First Quantum Corrections*, *Phys. Rev.* **D16** (1977) 1762–1768.
- [212] A. Andreassen, D. Farhi, W. Frost and M. D. Schwartz, *Precision decay rate calculations in quantum field theory*, *Phys. Rev.* **D95** (2017) 085011, [[1604.06090](#)].
- [213] G. ’t Hooft, *Symmetry Breaking Through Bell-Jackiw Anomalies*, *Phys. Rev. Lett.* **37** (1976) 8–11.
- [214] A. M. Polyakov, *Compact Gauge Fields and the Infrared Catastrophe*, *Phys. Lett.* **59B** (1975) 82–84.
- [215] A. A. Belavin, A. M. Polyakov, A. S. Schwartz and Yu. S. Tyupkin, *Pseudoparticle Solutions of the Yang-Mills Equations*, *Phys. Lett.* **59B** (1975) 85–87.
- [216] A. H. Guth and E. J. Weinberg, *Cosmological Consequences of a First Order Phase Transition in the SU(5) Grand Unified Model*, *Phys. Rev.* **D23** (1981) 876.
- [217] A. W. Wipf, *Tunnel Determinants*, *Nucl. Phys.* **B269** (1986) 24–44.
- [218] E. J. Weinberg, *Vacuum decay in theories with symmetry breaking by radiative corrections*, *Phys. Rev.* **D47** (1993) 4614–4627, [[hep-ph/9211314](#)].

- [219] PLANCK collaboration, P. A. R. Ade et al., *Planck 2015 results. XIII. Cosmological parameters*, *Astron. Astrophys.* **594** (2016) A13, [1502.01589].
- [220] V. Bonvin et al., *H0LiCOW – V. New COSMOGRAIL time delays of HE 0435-1223: H_0 to 3.8 per cent precision from strong lensing in a flat Λ CDM model*, *Mon. Not. Roy. Astron. Soc.* **465** (2017) 4914–4930, [1607.01790].
- [221] S. R. Coleman, V. Glaser and A. Martin, *Action Minima Among Solutions to a Class of Euclidean Scalar Field Equations*, *Commun. Math. Phys.* **58** (1978) 211.
- [222] A. Ferraz de Camargo, R. C. Shellard and G. C. Marques, *Vacuum Decay in a Soluble Model*, *Phys. Rev.* **D29** (1984) 1147.
- [223] K.-M. Lee and E. J. Weinberg, *Tunneling without Barriers*, *Nucl. Phys.* **B267** (1986) 181–202.
- [224] K. Dutta, C. Hector, P. M. Vaudrevange and A. Westphal, *More Exact Tunneling Solutions in Scalar Field Theory*, *Phys. Lett.* **B708** (2012) 309–313, [1110.2380].
- [225] A. Aravind, B. S. DiNunno, D. Lorshbough and S. Paban, *Analyzing multifield tunneling with exact bounce solutions*, *Phys. Rev.* **D91** (2015) 025026, [1412.3160].
- [226] A. Masoumi, K. D. Olum and B. Shlaer, *Efficient numerical solution to vacuum decay with many fields*, *JCAP* **1701** (2017) 051, [1610.06594].
- [227] A. Masoumi, K. D. Olum and J. M. Wachter, *Approximating tunneling rates in multi-dimensional field spaces*, 1702.00356.
- [228] C. L. Wainwright, *CosmoTransitions: Computing Cosmological Phase Transition Temperatures and Bubble Profiles with Multiple Fields*, *Comput. Phys. Commun.* **183** (2012) 2006–2013, [1109.4189].
- [229] I. F. Ginzburg and I. P. Ivanov, *Tree level unitarity constraints in the 2HDM with CP violation*, hep-ph/0312374.
- [230] I. F. Ginzburg and I. P. Ivanov, *Tree-level unitarity constraints in the most general 2HDM*, *Phys. Rev.* **D72** (2005) 115010, [hep-ph/0508020].
- [231] B. Grinstein, C. W. Murphy and P. Uttayarat, *One-loop corrections to the perturbative unitarity bounds in the CP-conserving two-Higgs doublet model with a softly broken \mathbb{Z}_2 symmetry*, *JHEP* **06** (2016) 070, [1512.04567].
- [232] V. Cacchio, D. Chowdhury, O. Eberhardt and C. W. Murphy, *Next-to-leading order unitarity fits in Two-Higgs-Doublet models with soft \mathbb{Z}_2 breaking*, *JHEP* **11** (2016) 026, [1609.01290].
- [233] D. Chowdhury and O. Eberhardt, *Update of Global Two-Higgs-Doublet Model Fits*, 1711.02095.
- [234] M. E. Peskin and T. Takeuchi, *Estimation of oblique electroweak corrections*, *Phys. Rev.* **D46** (1992) 381–409.

- [235] C. D. Froggatt, R. G. Moorhouse and I. G. Knowles, *Leading radiative corrections in two scalar doublet models*, *Phys. Rev.* **D45** (1992) 2471–2481.
- [236] H. E. Haber, *Introductory low-energy supersymmetry*, in *Proceedings, Theoretical Advanced Study Institute (TASI 92): From Black Holes and Strings to Particles: Boulder, USA, June 1-26, 1992*, pp. 589–686, 1993, [hep-ph/9306207](#).
- [237] H. E. Haber and H. E. Logan, *Radiative corrections to the $Z b$ anti- b vertex and constraints on extended Higgs sectors*, *Phys. Rev.* **D62** (2000) 015011, [[hep-ph/9909335](#)].
- [238] M. Baak, M. Goebel, J. Haller, A. Hoecker, D. Ludwig, K. Moenig, M. Schott et al., *Updated Status of the Global Electroweak Fit and Constraints on New Physics*, *Eur. Phys. J.* **C72** (2012) 2003, [[1107.0975](#)].
- [239] O. Deschamps, S. Descotes-Genon, S. Monteil, V. Niess, S. T’Jampens and V. Tisserand, *The Two Higgs Doublet of Type II facing flavour physics data*, *Phys. Rev.* **D82** (2010) 073012, [[0907.5135](#)].
- [240] M. Ciuchini, G. Degrossi, P. Gambino and G. F. Giudice, *Next-to-leading QCD corrections to $B \rightarrow X_s \gamma$: Standard model and two Higgs doublet model*, *Nucl. Phys.* **B527** (1998) 21–43, [[hep-ph/9710335](#)].
- [241] F. Borzumati and C. Greub, *2HDMs predictions for anti- $B \rightarrow X(s) \gamma$ in NLO QCD*, *Phys. Rev.* **D58** (1998) 074004, [[hep-ph/9802391](#)].
- [242] F. Borzumati and C. Greub, *Two Higgs doublet model predictions for anti- $B \rightarrow X(s) \gamma$ in NLO QCD: Addendum*, *Phys. Rev.* **D59** (1999) 057501, [[hep-ph/9809438](#)].
- [243] T. Hermann, M. Misiak and M. Steinhauser, *$\bar{B} \rightarrow X_s \gamma$ in the Two Higgs Doublet Model up to Next-to-Next-to-Leading Order in QCD*, *JHEP* **11** (2012) 036, [[1208.2788](#)].
- [244] C. Q. Geng and J. N. Ng, *Charged Higgs Effect in $B(d)0 - \bar{B}(d)0$ Mixing, $K \rightarrow \pi$ Neutrino Anti-neutrino Decay and Rare Decays of B Mesons*, *Phys. Rev.* **D38** (1988) 2857.
- [245] P. Arnan, D. Becirevic, F. Mescia and O. Sumensari, *Two Higgs doublet models and $b \rightarrow s$ exclusive decays*, *Eur. Phys. J.* **C77** (2017) 796, [[1703.03426](#)].
- [246] M. Misiak and M. Steinhauser, *Weak radiative decays of the B meson and bounds on M_{H^\pm} in the Two-Higgs-Doublet Model*, *Eur. Phys. J.* **C77** (2017) 201, [[1702.04571](#)].
- [247] J. de Blas, M. Ciuchini, E. Franco, S. Mishima, M. Pierini, L. Reina and L. Silvestrini, *The Global Electroweak and Higgs Fits in the LHC era*, in *5th Large Hadron Collider Physics Conference (LHCP 2017)*, 2017, [1710.05402](#).
- [248] UTFIT collaboration, private communication; see also the talk by Luca Silvestrini at the 2017 edition of *Implications of LHCb measurements and future prospects*.
- [249] HEAVY FLAVOR AVERAGING GROUP (HFAG) collaboration, Y. Amhis et al., *Averages of b -hadron, c -hadron, and τ -lepton properties as of summer 2014*, [1412.7515](#).